**Faculty of Science and Engineering**
**Department of Chemical Engineering**

# Multi-scale modelling of biomass pyrolysis process

**Abhishek Sharma**

**This thesis is presented for the Degree of**
**Doctor of Philosophy**
**of**
**Curtin University**

**March 2014**

# Declaration

To the best of my knowledge and belief this thesis contains no material previously published by any other person except where due acknowledgment has been made.

This thesis contains no material which has been accepted for the award of any other degree or diploma in any university.

Signature : …….

Date : ……...

# Author's Biography

Abhishek Sharma holds a Bachelor of Engineering degree in Chemical Engineering from Malaviya National Institute of Technology in India. Before joining Curtin University in 2010, he worked as a Process Engineer in Engineers India Limited in India. Over the past 3 years, he has worked for developing the challenging units such as Thermodynamics and Process Synthesis and Design in Chemical Engineering Department. His major research interests are in the fields of bio-fuels, process design and development and reactive multi-phase Computational Fluid Dynamics (CFD) modelling.

Journal Publications:

1. Sharma, A., Pareek, V. & Zhang, D. (2012). *Multi-scale modeling of biomass pyrolysis processes.* Proceedings of the 22nd European Symposium on Computer Aided Process Engineering, London, UK, 1133-1137.

2. Sharma, A., Pareek, V., Wang, S., Zhang, Z., Yang, H. & Zhang, D. (2014). *A phenomenological model of the mechanisms of lignocellulosic biomass pyrolysis processes*. Computers and Chemical Engineering, 60(0), 231-241.

3. Sharma, A., Pareek, V., Wang, S., Yang, H. & Zhang, D. (2014). *CFD modelling of mixing/segregation behaviour of biomass and biochar particles in a bubbling fluidized bed.* Chemical Engineering Science, 106(0), 264-274.

4. Sharma, A., Pareek, V., Wang, S., Yang, H. & Zhang, D. (2014). M*ulti-fluid reactive modelling of fluidized bed pyrolysis process*. Chemical Engineering Science. *Submitted.*

5. Sharma, A., Pareek, V. & Zhang, D. (2014). *Biomass Pyrolysis – A review of modelling, process parameters and catalytic studies.* Renewable and Sustainable Energy Reviews. *Submitted.*

Conferences and Workshops:

1. Sharma, A., Pareek, V. & Zhang, D. (2012). *Multi-scale modeling of biomass pyrolysis processes.* Proceedings of the 22nd European Symposium on Computer Aided Process Engineering, London, UK, 1133-1137.

2. Sharma, A., Pareek, V., Utikar, R., Wang, S., Yang, H. & Zhang, D. (2012). *A CFD modelling study of multi-phase flow behavior of biomass and biochar particles in a bubbling fluidized bed.* Ninth International Conference on CFD in the Minerals and Process Industries, Melbourne, Australia.

3. Sharma, A., Pareek, V., Wang, S., Yang, H. & Zhang, D. (2013). *CFD modelling study of biomass pyrolysis using biochar bed in a fluidized bed reactor*. 9th World Congress of Chemical Engineering, Seoul, Korea.

4. Sharma, A., Pareek, V., Wang, S., Yang, H. & Zhang, D. (2014). *CFD modelling of biomass pyrolysis in a bubbling fluidized bed reactor*. Chemeca 14, Perth, Australia.

# Abstract

Biomass as a form of energy source may be utilised in two different ways: directly by burning the biomass and indirectly by converting it into solid, liquid or gaseous fuels. Pyrolysis is an indirect conversion method, and can be described in simpler terms as a thermal decomposition of biomass in the absence of oxygen to produce an array of solid, liquid and gas products, namely biochar (carbonaceous residue), tar (bio-oil) and non-condensable gases (fuel gas), which can then be converted to a wide range of fuels, solvents and chemicals. However, pyrolysis of biomass is a complex chemical process with several operational and environmental challenges. Consequently, this process has been widely investigated in order to understand the mechanisms and kinetics of pyrolysis at different scales, viz. particle level, multi-phase reacting flow, product distribution and reactor performance, process integration and control. However, there are a number of uncertainties in current biomass pyrolysis models, especially in their ability of optimising process conditions to achieve desired product yields and distribution. Hence, considerably more research is required to develop accurate models of biomass pyrolysis.

In this study, a set of models has been developed to understand different scales of pyrolysis process. Firstly, a phenomenological model has been developed for examining the particle scale degradation of biomass. This model explicitly accounts for the kinetic mechanism of the pyrolysis process in the presence of biochar by considering a combined impact of various parameters such as particle shrinkage and drying during the conversion process. The model was then used to study the effect of operating parameters such as particle size and moisture content on the pyrolysis time. It was found that for the particles less than 1 mm in size, a uniform temperature throughout the particle was predicted, thus leading to higher conversion rates in comparison to those in the larger particles. On the other hand, any increase in the moisture content led to considerable decrease in the rate of biomass conversion.

However, the phenomenological model cannot account for the reactor hydrodynamics. Therefore, a CFD model has been developed to study the mixing/segregation behaviour of biomass with other solid phases such as biochar in a bubbling fluidized bed. This model was then used to study the effect of parameters such as superficial gas velocity and particle size on the bed hydrodynamics. It was

found that on increasing the superficial gas velocity, the bubbles size increased which led to better mixing of biomass and biochar particles. While the biochar particle size had a significant impact, the biomass particle size had only little impact on the distribution of biomass particles in the bed.

Finally, integrating the phenomenological and CFD models formulated a reactive multi-phase model. This multi-scale model was then used for analysing the pyrolysis of biomass in the presence of biochar in a bubbling fluidized bed. The effect of operating parameters such as superficial gas velocity and reactor temperature on the product yields was also analysed using this model. It was found that higher reactor temperature (around 800°C) favours the catalytic cracking of tar into non-condensable gases and biochar. However, the effect of superficial gas velocity was not significant on the catalytic cracking reactions. Although the integrated model was capable of predicting the hydrodynamics and products formation inside the bubbling fluidized bed reactor, there is still a need to conduct lab-scale experiments for accurate estimation of kinetic parameters for biomass pyrolysis in the presence of biochar.

## Acknowledgement

First and foremost, I like to thank my supervisor Prof. Vishnu Pareek for providing the opportunity to work under his guidance. He has provided immense support in dealing with technical and non-technical issues during the whole period. While working with him, I have gained significant experience in the area of research, design and development. Furthermore, the high level of encouragement and motivation from his end has really helped me in achieving the research goals and developing the professional attributes.

I offer my sincerest gratitude to my associate-supervisor Prof. Dongke Zhang from University of Western Australia for providing deep insights in the area of biofuels with inputs on PhD thesis and journal publications. I also like to thank my co-supervisor Shaobin Wang and thesis chairperson Prof. Ming Ang for their valuable support and guidance during this period.

I further like to thank Dr. Ranjeet Utikar, as without his technical assistance, it would be really difficult to conduct the research work in a given amount of time. He has given plenty of inputs in terms of modelling and simulation techniques for efficient and timely completion of the research activities.

In administrative staff, I want to thank Ms Tammy Atkins and Ms Jann Bolton for helping me with all kind of official issues while staying in the University. There were many colleagues who made my stay comfortable while working in here; I particularly like to thank Mr. Harisinh Parmar, as he supported me professionally as well as personally for completing this thesis.

And most of all, I like to thank my wife Laghima Sharma and parents for their vast moral support during this whole period.

Financial support from the Australian Research Council (ARC) under the ARC Linkage (LP100200135) and Discovery (DP110103699) schemes is also highly acknowledged.

# Table of Contents

# List of Figures

# List of Tables

# Nomenclature

| | |
|---|---|
| A | Pre-exponential factor ($s^{-1}$) |
| $C_p$ | Specific heat (J/kg-°C) |
| $D$ | Diffusivity ($m^2/s$) |
| E | Activation energy (J/kgmol) |
| $M$ | Molecular weight (kg/kmol) |
| $P$ | Particle pressure (atm) |
| $r_p$ | Particle radius/half-thickness (m) |
| $T$ | Temperature (°C) |
| u | Gas inlet velocity (m/s) |
| $u_{mf}$ | Minimum fluidization velocity (m/s) |
| $v$ | Vapour velocity (m/s) |
| $V$ | Particle volume ($m^3$) |

*Greek Letters*

| | |
|---|---|
| $\alpha$ | Volume fraction |
| $\beta$ | Permeability ($m^2$) |
| $\varepsilon$ | Voidage/porosity |
| $k$ | Thermal conductivity (W/m-°C) |
| $\rho$ | Density ($kg/m^3$) |
| $\mu$ | Viscosity (kg/m-s) |
| $\theta$ | Granular temperature |
| $\phi$ | Specularity coefficient |

*Subscript*

| | |
|---|---|
| B | Biomass |
| C | Char/Biochar |
| G | Non-condensable gases |

| | |
|---|---|
| T1 | Primary tar |
| T2 | Secondary tar |
| $g$ | Gas-mixture phase |
| $v$ | Vapour phase |
| $s$ | Solid phase |

*Abbreviations*

| | |
|---|---|
| BFB | Bubbling Fluidized Bed |
| CFB | Circulating Fluidized Bed |
| CFD | Computational Fluid Dynamics |
| CPD | Chemical Percolation Devolatilization |
| CSSTR | Continuous Self Stirred Tank Reactor |
| DAE | Distributed Activation Energy |
| DBM | Discrete Bubble Model |
| DDPM | Dense Discrete Phase Model |
| DEM | Discrete Element Method |
| DPM | Discrete Particle Model |
| EE | Eulerian- Eulerian |
| EL | Eulerian-Lagrangian |
| FBR | Fluidized Bed Reactor |
| FSP | Fiber Saturation Point |
| PAH | Poly-aromatic Hydrocarbon |
| PFR | Plug Flow Reactor |
| TFM | Two Fluid Model |
| TGA | Thermo Gravimetric Analyser |
| UDF | User Defined Function |

# Chapter 1 Introduction

Owing to their possible effect on the global warming, there is a worldwide drive for reducing reliance on fossil fuels, which contribute about 98% of carbon emissions (Demirbaş, 2006). Also, there is a shift from non-renewable energy sources to bio-energy (bio-fuels) due to continuous depletion of fossil fuels. Furthermore, since biofuels are derived from biomass, they significantly decrease emissions of harmful gases such as $SO_x$ and $NO_x$ (Zhang et al., 2007). Examples of commonly used biomass include plant matter such as forest residues (dead trees, branches and tree stumps), yard clippings, wood chips and municipal solid waste. The benefit of using biomass arises due to its renewable nature and ability to re-utilize the emitted greenhouse gas ($CO_2$). With increasing usage of the biomass-derived fuels as a result of their low carbon footprints, biofuels are currently estimated to contribute around 13% of the world's energy supply (Demirbas et al., 2009).

## 1.1. Background

Biomass conversion to bioenergy is carried out using various thermo-chemical and bio-chemical processes as shown in Figure 1.1. Thermo-chemical processes use heat energy and chemical catalysts for the decomposition of biomass into high value energy products. On the other hand, bio-chemical processes use enzymes and micro-organisms to convert biomass into desirable energy products.

In the direct *combustion* of biomass, the primary product is thermal energy, which may be used as the energy source for production of electricity, or for combined heat and power (CHP) production. Biomass *gasification* is used for production of bio-fuels such as “green” gasoline and also electrical energy. *Pyrolysis* is used for production of bio-fuels, chemicals and charcoal with electricity and CHP generation using turbines, engines and boilers. *Hydrothermal liquefaction* is used for direct conversion of biomass into crude oil for application in heat and power generation. The focus of this study would be on the thermo-chemical conversion of biomass using pyrolysis process. Refer the work of other researchers such as Saxena et al. (2009) and Zhang et al. (2010) for details of the bio-chemical conversion and other thermo-chemical processes respectively.

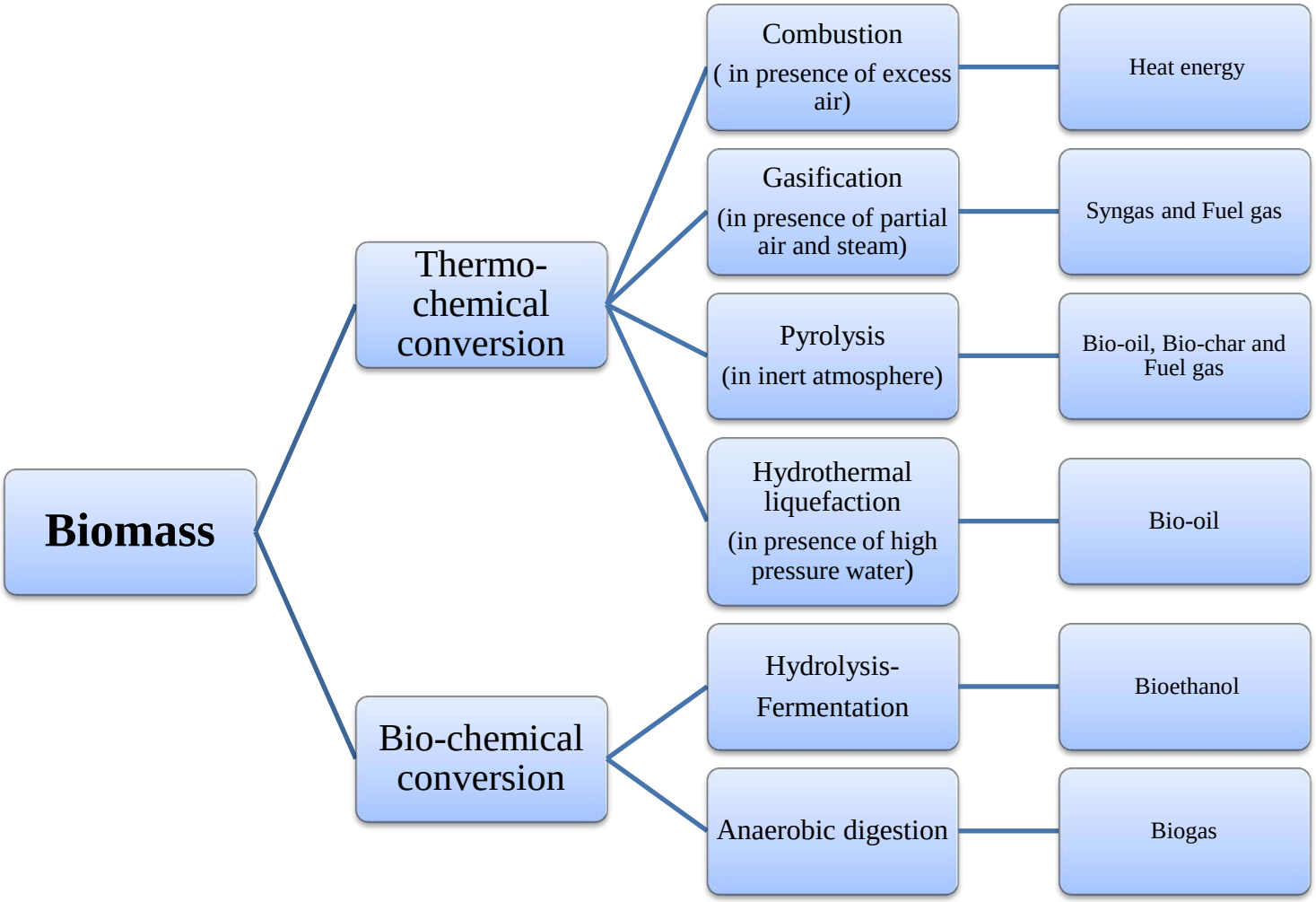


**Figure 1.1:** Biomass to bioenergy conversion processes.

As shown in Figure 1.1, pyrolysis is a thermo-chemical decomposition processes in which organic material such as biomass is converted into a carbon-rich solid and volatile matter by heating in the absence of oxygen (Demirbas and Arin, 2002). The solid product of this process is known as biochar or char, and is generally high in carbon content. The volatile fraction of this process is partly condensed to give a liquid fraction called tar or bio-oil along with a mixture of the non-condensable gases. The bio-oil is stored and further used for energy production. The gases can be utilized for providing heat energy to the pyrolysis reactor. The overall process for biomass pyrolysis is shown in Figure 1.2. The pyrolysis products are formed from both primary decomposition of the solid biomass as well as secondary reactions of volatile condensable organic products into low-molecular weight gases, secondary tar and char (Di Blasi, 2008). One of the significant benefits of the pyrolysis process is that it can be conducted at temperatures lower (normally in range of 400-700°C) than those required in gasification (>700°C) (Ruiz et al., 2013) and combustion (>900°C) (Demirbas, 2004) processes. It has been found that the presence of metallic compounds in biomass causes further reduction in decomposition temperature during pyrolysis process (Raveendran et al., 1995). The pressure requirement is also much lower in pyrolysis process (1-2 atm) as compared to hydrothermal liquefaction (100-250 atm) (Toor et al., 2011) of biomass to generate bio-oil.

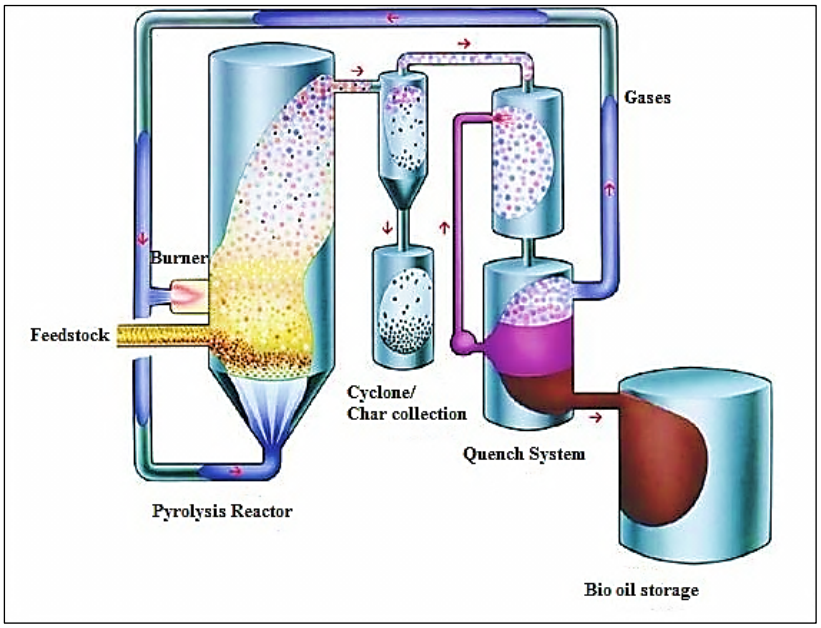


**Figure 1.2:** Biomass pyrolysis process for production and separation of gas, liquid and solid products (http://blogs.princeton.edu).

The pyrolysis process is dependent on several operational parameters such as the feedstock and reactor conditions which lead to formation of products in different proportions and also affect the pyrolysis rate and product quality. A significant amount of experimental and modelling research (Agarwal et al., 1984; Heidenreich et al., 1999b; Heidenreich et al., 1999a; Shen et al., 2000; Yip et al., 2007) has been conducted in order to understand the effect of different parameters on the efficient pyrolysis of coal at an industrial scale. The potential of biomass for generating a range of high value products by pyrolysis process also promoted research in this area. Biomass has composition similar to coal, but varies in content of constituents such as holocellulose and lignin, which highly affects the degradation mechanism. Also, there are differences in the density and structure (like fibrosity) of coal and biomass, which mandates different operating conditions such as solid residence time, temperature, etc. This raises the need for studying the effect of operating parameters on the biomass pyrolysis. Therefore, fundamental (Sreekanth and Kolar, 2009; Lu et al., 2010; Park et al., 2010; Peters, 2011) and CFD (Papadikis et al., 2009c; Gerber et al., 2010; Xue et al., 2011) modelling studies have been conducted for analysing the biomass decomposition according to the physical and chemical processes as shown in Figure 1.3

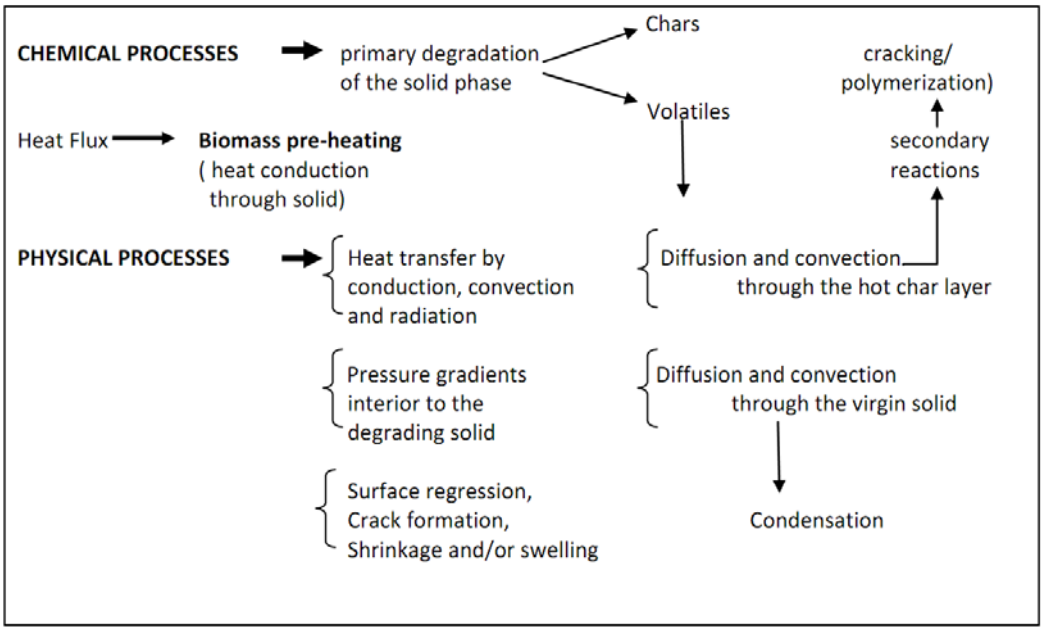


**Figure 1.3:** Schematic diagram of chemical and physical processes inside biomass particle during pyrolysis (Di Blasi, 1993b).

However, there is still lack of an integrated multi-scale model that can explain the combined effect of the process parameters on biomass conversion time and product yield, and can also analyse the hydrodynamic behaviour of different phases in larger scale reactors. Furthermore, the effect of biochar catalytic activity on the cracking of heavy compounds such as tar has not been fully understood. Only a few studies have been reported for examining change in the product quality and distribution due to tar cracking reactions in the presence of biochar as a catalyst (Boroson et al., 1989a; Abu El-Rub et al., 2008). However, there is a compelling need for understanding the impact of biochar on *in-situ* cracking of tarry compounds into other forms of products. This leads to a need of formulating a multi-scale model for analysing different scales of a pyrolysis proces.

## 1.2. Scope and Objectives

This thesis focuses on the multi-scale modelling of biomass pyrolysis process. The main aims of this research are to study the fundamentals of thermo-chemical degradation of biomass particles in an inert gas environment, examine the behaviour of biomass particles with other phases in the reactor and formulate a reactor scale model for biomass pyrolysis in the presence of sand and biochar particles bed. The specific objectives are as follows:

1. Develop a phenomenological model by incorporating combined impact of process parameters such as drying and change in thermo-physical properties of biomass during pyrolysis. This model includes the kinetic mechanism of primary decomposition of biomass with secondary tar cracking reactions in the presence of biochar.
2. Analyse the effect of operating parameters such as the particle size and reactor temperature on the biomass conversion time.
3. Formulate a CFD model to study the hydrodynamics of biomass particles in the presence of other solid phases such as biochar particles.
4. Examine the effect of process parameters such as superficial gas velocity, particle size and density, and modelling parameters such as the wall boundary conditions and coefficient of restitution on the mixing/segregation of different solid phases in the bed.

5. Develop a multi-scale CFD model for analysing biomass pyrolysis in a fluidized bed reactor. This model combines the phenomenological model with the hydrodynamics model for studying the biomass decomposition in the presence of biochar.
6. Analyse the effect of operating parameters such as reactor temperature and biochar bed height on the product yield.

## 1.3. Thesis Structure

The work conducted as part of this thesis has been reported in form of the following chapters.

**Chapter 1**

An introduction to the biomass pyrolysis process has been given in this chapter with focus on the research objectives of this study.

**Chapter 2**

In this chapter, the literature review of the kinetic, particle and reactor scale modelling of biomass pyrolysis process using fundamental as well as CFD approaches have been presented. The effect of various operating parameters such as particle size and reactor temperature on the pyrolysis process has been discussed. The impact of different catalysts on the products yield during tar cracking reactions has also been reviewed.

This chapter further discusses the methodology for carrying out the current research work. It includes the approach used for generating a multi-scale model for biomass pyrolysis in a bubbling fluidized bed.

**Chapter 3**

In this chapter, a particle- scale phenomenological model for biomass pyrolysis in presence of biochar has been developed. This model includes the combined impact of different process parameters such as the particle shrinkage and drying. The simulations were conducted using MATLAB, and the results were used to examine the effect of process parameters such as particle size and moisture content on the biomass conversion time.

**Chapter 4**

In this chapter, a multi-phase CFD model has been used to study the mixing/segregation behaviour of biomass and biochar particles in the bubbling fluidized bed. The effect of process parameters such as particle density and modelling parameters such as the coefficient of restitution on bed hydrodynamics has been analysed.

**Chapter 5**

In this chapter, a multi-phase CFD model has been used to study the biomass pyrolysis in a bubbling fluidized bed reactor. This multi-scale model is used for studying the effect of operating parameters such as reactor temperature and particle size on the product yield in presence of inert sand as well as catalytically active biochar particles.

**Chapter 6**

This chapter concludes the thesis with emphasis on the discussion based on the modelling and simulation results of the previous chapters. It also focuses on the recommendations related to future work based on the new knowledge gaps found in previous chapters.

The structure followed for completion of this thesis is given in Figure 1.4.

**Figure 1.4:** Thesis Map

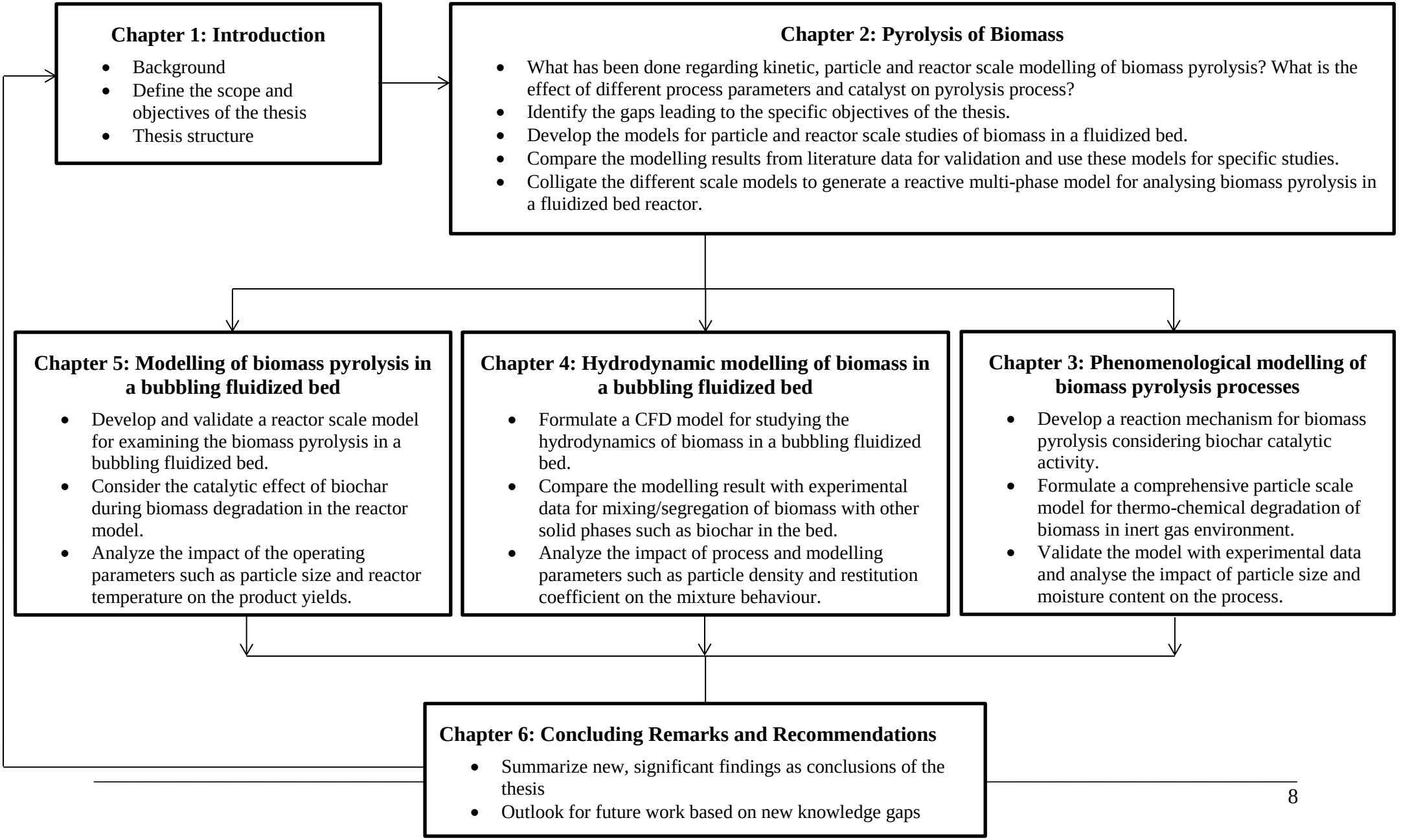
Chapter 1: Introduction
Background
Define the scope and objectives of the thesis
Thesis structure
Chapter 2: Pyrolysis of Biomass
What has been done regarding kinetic, particle and reactor scale modelling of biomass pyrolysis? What is the effect of different process parameters and catalyst on pyrolysis process?
Identify the gaps leading to the specific objectives of the thesis.
Develop the models for particle and reactor scale studies of biomass in a fluidized bed.
Compare the modelling results from literature data for validation and use these models for specific studies.
Colligate the different scale models to generate a reactive multi-phase model for analysing biomass pyrolysis in a fluidized bed reactor.
Chapter 5: Modelling of biomass pyrolysis in a bubbling fluidized bed
Develop and validate a reactor scale model for examining the biomass pyrolysis in a bubbling fluidized bed.
Consider the catalytic effect of biochar during biomass degradation in the reactor model.
Analyze the impact of the operating parameters such as particle size and reactor temperature on the product yields.
Chapter 4: Hydrodynamic modelling of biomass in a bubbling fluidized bed
Formulate a CFD model for studying the hydrodynamics of biomass in a bubbling fluidized bed.
Compare the modelling result with experimental data for mixing/segregation of biomass with other solid phases such as biochar in the bed.
Analyze the impact of process and modelling parameters such as particle density and restitution coefficient on the mixture behaviour.
Chapter 3: Phenomenological modelling of biomass pyrolysis processes
Develop a reaction mechanism for biomass pyrolysis considering biochar catalytic activity.
Formulate a comprehensive particle scale model for thermo-chemical degradation of biomass in inert gas environment.
Validate the model with experimental data and analyse the impact of particle size and moisture content on the process.
Chapter 6: Concluding Remarks and Recommendations
Summarize new, significant findings as conclusions of the thesis
Outlook for future work based on new knowledge gaps

# Chapter 2 Pyrolysis of Biomass

The thermo-chemical decomposition of biomass can be carried out in a number of ways such as pyrolysis, gasification and combustion, by varying the operating conditions such as vapour residence time, heating rate and reactor configuration for converting it into useful forms of energy. Pyrolysis leads to the formation of a range of products in form of gas and liquid compounds. The solid by-product of biomass pyrolysis – the biochar – has also found application in carbon emission reduction and carbon sequestration via soil management systems (Lehmann et al., 2006). On the other hand, hydrothermal liquefaction of biomass focuses on generation of liquid fuel only. With this, gasification mainly focuses on production of fuel gas and other gaseous products such as syngas which found major application in Fischer- Tropsch processes for producing liquid transportation fuels, while combustion leads to production of heat energy. Hence, it is clear that the pyrolysis process offers much broader opportunities for converting biomass into useful chemicals than any of the other thermal conversion processes.

## 2.1. Biomass Composition and its Implication on Pyrolysis

A biomass is any mixture of hydrocarbon material consisting of carbon, hydrogen, oxygen with small contents of sulphur and nitrogen. Some biomass types also carry significant proportions of inorganic species. Biomass resources include various natural and derived materials, such as woody and herbaceous species, wood wastes, bagasse, agricultural and industrial residues, waste paper, municipal solid waste, sawdust, bio-solids, grass, waste from food processing, animal wastes, aquatic plants and algae, etc.(Yaman, 2004).

Biomass is generally composed of three main groups of natural polymeric materials: cellulose (around 50% on dry basis), hemicellulose (10-30% in woods and 20-40% in herbaceous biomass on dry basis) and lignin (20-40% in woods and 10-40% in herbaceous biomass on dry basis). Other typical components are grouped as extractives (generally smaller organic molecules or polymers like protein, acids, salts) and minerals (Yaman, 2004) (inorganic compounds like alkali metals mainly potassium, calcium, sodium, silicon, phosphorus and magnesium and also chlorine in herbaceous biomass (Zabaniotou, 1999)). The concentrations of these extractives

varies from less than 1% in woods to 15% in herbaceous biomass feedstock and up to 25 % in agricultural residues (Fitz et al., 1996).

The pyrolysis process for biomass degradation may be broadly classified into two major categories depending on the operating conditions. The first of these processes is “fast pyrolysis”, which is characterized by high heating rates and short vapour residence times. This generally requires a feedstock consisting of small particles with the process having a provision to remove the vapours quickly to avoid further contact with the hot solid particles. There are a number of different reactor configurations for fast pyrolysis including ablative systems, fluidized beds, stirred or moving beds and vacuum pyrolysis systems (Brownsort, 2009). Figure 2.1 shows a fast pyrolysis fluidized bed reactor. It normally operates at moderate temperatures of around 500°C. On the other hand, “slow pyrolysis” is characterised by a gentle heating of relatively larger solid particle for longer vapour residence times, and usually a lower temperature than fast pyrolysis, typically 400°C. At industrial scales, large retorts (batch or continuous), agitated drum kilns, rotary kilns and screw pyrolyzers are used for processing of feed at given conditions (Brownsort, 2009). Figure 2.2 shows a screw pyrolyzer for slow pyrolysis.

The variation in operating conditions will also affect the product yields of gas, tar and char during the decomposition of biomass. A typical comparison of product yields on dry basis by Brown (2009) for different operating modes is given in Table 2.1.

**Table 2.1:** Product yield for different types of thermal degradation processes (Brown, 2009).

| Mode | Conditions | Liquid | Char | Gas |
|---|---|---|---|---|
| Fast | Temperature ~ 500°C, short vapor residence time ~ 1 s | 75% | 12% | 13% |
| Moderate | Temperature ~ 500°C, moderate vapor residence time ~ 10-20 s | 50% | 20% | 30% |
| Slow | Temperature ~ 500°C, very long vapor residence time ~ 5-30 min | 30% | 35% | 35% |
| Gasification | Temperature > 750°C, moderate vapor residence time ~ 10-20 s | 5% | 10% | 85% |

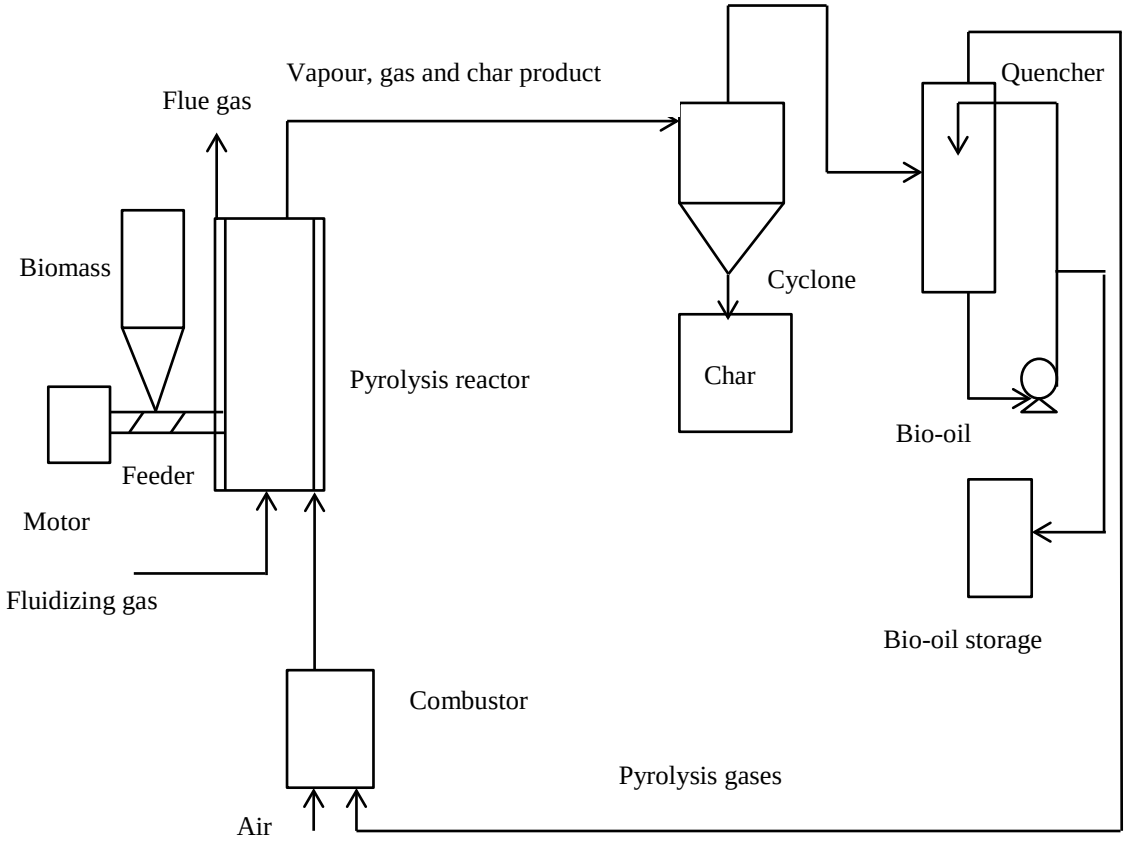


**Figure 2.1:** Schematic of a fast pyrolysis fluidized bed reactor configuration (Brown, 2003).

The biomass degradation leads to production of a range of products via different thermo-chemical processes. Pyrolysis is one of the major processes for converting biomass resources to petroleum-grade products. The fuel gas produced in the process is utilized for getting solvents such as acetone and methanol, hydrocarbons and electricity. The bio-oil produced is utilized for getting different chemicals such as levoglucosan and acetic acid, upgraded motor fuel and electricity. Also, the char produced may be used as either a slurry fuel, a soil improving agent or as the activated carbon in industrial applications (Balat et al., 2009).

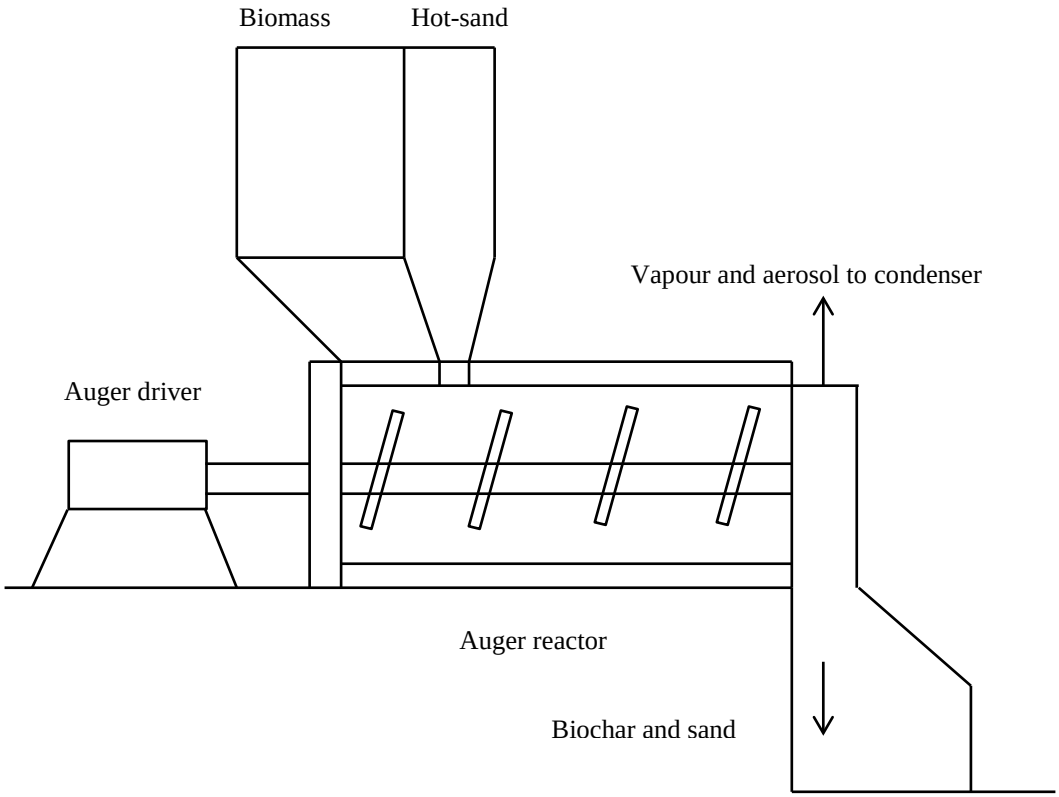


**Figure 2.2:** Schematic of a slow pyrolysis screw reactor with heating medium (Brown, 2003).

## 2.2. Modelling of pyrolysis processes

Due to increasing use of biomass for production of gaseous and liquid products via pyrolysis, significant research has been reported on developing numerical models of the process to better understand this process. Most of the research efforts have been on understanding the reaction kinetics of the pyrolysis process. Some studies have also been conducted for reactor design and modelling using particle scale models with due consideration to other mechanisms such as secondary cracking reactions occurring simultaneously in the reactor. For developing economic and efficient pyrolysis reactors, much better understanding of transport phenomena inside the reactor as well as the reaction kinetics of pyrolysis process is required.

### 2.2.1. Kinetic model

A kinetic or reaction model simulates the different type of reactions occurring during degradation of biomass by application of thermal energy. These models are divided

into two categories, i.e., lumped and distributed models, based on the reaction mechanism of the pyrolysis process.

In lumped models, different reaction products and individual components of biomass are lumped into three classes that are gas, tar and char. Depending on this, different kinetic schemes have been proposed for primary degradation of biomass as well as secondary decomposition of volatile products (mainly tar or higher molecular weight hydrocarbons) of the pyrolysis process. The lumped models are further divided for studying individual components as well as single homogeneous species decomposition of biomass.

The specific models were provided for decomposition of major components of biomass that are cellulose, hemicellulose and lignin. Bradbury et al. (1979) proposed a three reaction model for pyrolysis of cellulose at low pressure, also known as Broido-Shafizadeh model as it was developed by modifying the original Broido model (Broido and Nelson, 1975) for cellulosic pyrolysis. The Broido model stipulated that the dehydration reactions occur at low temperatures (around 220°C) causing formation of anhydrocellulose which further converts to char and gas exothermically, while depolymerization reactions occur at higher temperatures (around 280°C) causing formation of levoglucosan which leads to formation of volatile tars endothermically. In this model (Bradbury et al., 1979), it was assumed that an “initiation reaction” leads to formation of “active cellulose” which subsequently decomposes by two competitive first-order reactions, one yielding volatiles and the other char and a gaseous fraction. It was found that the active cellulose formation i.e. activation of cellulose macromolecules was due to intermediate physical and chemical changes before they had undergone rapid thermal degradation to form gases, char and low molecular weight volatile products. Agrawal (1988) studied a three- reaction scheme for pyrolysis of cellulose based on two aspects: low pressure and high temperature favours cracking reactions of active cellulose to gases, while low temperature favours cross-linking and aromatization of active cellulose into char. Therefore, according to this model, the formation of gas, tar and char may not be entirely linked and the variation in percentage of volatile products and char with operating conditions can be predicted. Diebold (1994) proposed a multi-step global kinetic model for two-char forming steps, as well as the

formation of depolymerized or active cellulose, primary vapours, secondary gases and secondary tars (see Figure 2.3).

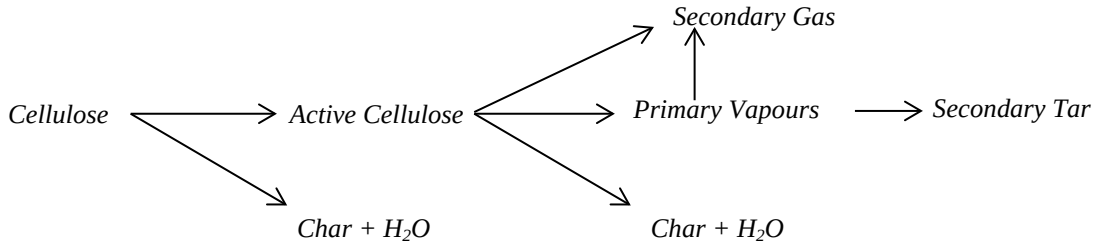


**Figure 2.3:** Primary and secondary decomposition of cellulose (Diebold, 1994).

According to this model (Diebold, 1994), dehydration and chain cleavage (decarboxylation) of primary cellulose and active cellulose led to formation of char, water and carbon oxides, while vaporization of active cellulose led to formation of primary vapours which further undergo cleavage, dehydration, decarboxylation and decarbonylation reactions to form secondary gas (CO, $H_2$ ,$CO_2$ , $CH_4$ and higher olefins) and secondary tar (phenolic or polycyclic aromatic tars). Gronli et al.(1999) conducted a kinetic analysis of cellulose pyrolysis for evaluation of kinetic parameters using thermogravimetic experimental techniques at two different heating rates (5°C/min and 40°C/min). The activation energy and the pre-exponential factor calculated for the cellulose decomposition was 244 kJ/mol and $1.06x10^{19}$ $s^{-1}$, respectively. Recently, Lin et al. (2009) studied the mechanism of conversion of cellulose into levoglucosan and anhydrosugar polymers, which further undergo series of reactions such as polymerization, dehydration and condensation for formation of gases and char. However, the proposed reaction pathway contradicted the scheme given by Diebold (1994) in terms of energy requirement and product formation. The kinetic model (Lin et al., 2009) with thermal lag was used to measure the dynamics of cellulose pyrolysis, which led to calculation of first order reaction rate for the process.

Di Blasi and Lanzetta (1997) proposed a model describing the kinetics of isothermal decomposition of hemicellulose (or xylan) in inert atmosphere using a two-stage mechanism.


**Figure 2.4:** Overall decomposition of hemicellulose (Di Blasi and Lanzetta, 1997).

In this model (see Figure 2.4), A is hemicellulose (or xylan), B is intermediate reaction product with a reduced degree of polymerization, and V1 and V2 are volatiles formed during reactions. The activation energy and pre-exponential factor for first order primary degradation were calculated as 76.5 kJ/mol and $3.62 \times 10^5$ $s^{-1}$, respectively; and for first order secondary degradation were 54.8 kJ/mol and $3.83 \times 10^2$ $s^{-1}$, respectively.

Antal (1982) proposed a semi-global, multi- pathway model for primary lignin pyrolysis (see Figure 2.5).

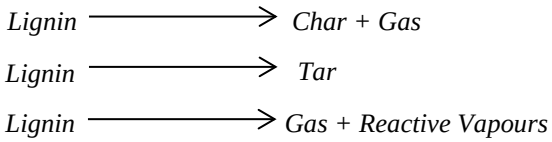


**Figure 2.5:** Overall degradation of lignin (Antal, 1982).

According to this model (Antal, 1982), at low temperatures (below 500°C), dehydration reactions led to formation of char and gas, while at higher temperatures (above 500°C), lignin monomers were formed which may led to secondary degradation and condensation reactions; at very high heating rates, lignin resulted into formation of gas and reactive vapours that probably led to formation of secondary char by condensation. Caballero et al.(1995) studied the kinetics for thermal degradation of lignin as a function of distribution of solid decomposition, which led to estimation of different activation energies and pre-exponential factors with variation in temperature. Recently, Adam et al. (2013) developed a lumped model for primary and secondary pyrolysis of Kraft lignin and analysed the formation of gas, tar and solid products at different temperatures in a fluidized bed reactor. This model was further used to study the cracking of tar with different retention times in a catalytic reactor.

Different kinetic models (Shafizadeh and Chin Peter P, 1977; Thurner and Mann, 1981; Font et al., 1990; Samolada and Vasalos, 1991; Di Blasi and Branca, 2001) have been proposed by considering biomass as a homogeneous species. In these models, only the primary thermo-chemical degradation of biomass has been studied, keeping negligible effect of secondary tar decomposition reactions on product yields. Shafizadeh and Chin Peter P (1977) model discussed the detailed chemistry of formation of char, liquid and gaseous products from wood pyrolysis by decomposition of cellulose, hemicellulose and lignin. Shafizadeh and Chin Peter P (1977) found that the hemicellulose component is the least stable and decomposes at 225-325°C (325-375°C for cellulose and 250-500°C for lignin). It was also concluded that cellulose and hemicellulose components provide the volatile pyrolysis products, while lignin predominantly forms a charred residue. However, the studies of Yang et al. (2007a) showed that lignin has a higher temperature range (160-900°C) for decomposition, and the main gaseous products ($CO_2$, CO and $CH_4$) and organics formed by pyrolysis of cellulose, hemicellulose and lignin were the same with different yields for each component. Thurner and Mann (1981) studied a model for investigating the kinetics of wood pyrolysis and identifying the composition of pyrolysis products. Based on the experimental analysis with oak sawdust in temperature range of 300-400$^0$C in isothermal tube furnace, it was found that gas consists mainly of $CO_2$, CO, $O_2$ and C3+ compounds with trace amounts of $CH_4$, $C_2H_4$, and $C_2H_2$, and tar consists mainly of levoglucosan. The activation energies for first order reactions leading to formation of gas, tar and char via wood were calculated as 88.6 kJ/mol, 112.7 kJ/mol and 106.5 kJ/mol, respectively; and the pre-exponential factors for these reactions were estimated as $1.43x10^5$, $4.12x10^6$ and $7.4x10^5$ $s^{-1}$, respectively.

Font et al.(1990) studied the kinetics of biomass using almond shells in both fluidized bed reactor (400-460°C) and pyroprobe (460-605°C). This model also considered the conversion of primary reaction tar into secondary gases and liquids. The kinetic constants for gas and tar production included both primary and secondary decomposition reactions. The activation energy for overall decomposition was 108 kJ/mol and pre-exponential factor was $1.88x10^6$ $s^{-1}$. The activation energies for gas, tar and char forming reactions in fluidized bed reactor were 156, 148 and 61

kJ/mol, respectively; and pre-exponential factors for these reactions were $6.803x10^8$, $8.23x10^8$ and $2.91x10^2$ $s^{-1}$, respectively.

Samolada and Vasalos (1991) analysed the biomass thermal decomposition kinetics using fir wood in a fluidized bed reactor (400-500°C). The authors had considered the first order degradation of wood using two kinetic models: simple first order kinetic model and simple first order kinetic model assuming an ultimate yield of each product at infinite reaction time. It was found that simple first order kinetics can be used to describe the evolution of total volatiles and gases, and kinetic model with infinite reaction time assumption is better than the other model. The activation energies for total volatiles and gas evolution reactions were estimated as 56.48 and 94.49 kJ/mol, respectively; and pre-exponential factors as 136.04 and $2.38x\ 10^4$ $s^{-1}$, respectively.

Di Blasi and Branca (2001) studied the kinetics of isothermal primary degradation of beech wood in temperature range of 300-435°C in both Thermo Gravimetric Analyser (TGA) and laboratory scale reactor. The authors calculated the first order reaction rates with activation energies of 141.2, 111.7, 148 and 152.7 kJ/mol for overall, char, gas and tar forming reactions, respectively; the pre-exponential factors for these reactions were $4.38x10^9$, $3.27x10^6$, $4.38x10^9$and $1.08x10^{10}$ $s^{-1}$, respectively. Based on the results, it was found that variation in the product yields and kinetic rates is mainly because of the effect of different heating rates, operating temperatures and experimental setups.

The models were also proposed by considering biomass as a heterogeneous mixture of different components. In these models, the negligible effect of secondary tar degradation mechanism on product yields was considered. A number of studies were performed for calculating the kinetic parameters for devolatalization of pseudo-components (mainly considering three component mechanism for cellulose, hemicellulose and lignin) of various biomass species in different temperature and heating rate ranges using thermo gravimetric techniques and non-linear least squares algorithm (Orfão et al., 1999; Grønli et al., 2002; Manyà et al., 2002; Mészáros et al., 2004; Branca et al., 2005). Few models (Alves and Figueiredo, 1988; Koufopanos et al., 1989; Miller and Bellan, 1997; Ranzi et al., 2008) were proposed for considering multi-component decomposition mechanism of biomass pyrolysis. Branca and Di

Blasi (2003) studied the multi-step reaction mechanism of isothermal wood degradation. The experiments were performed using beech wood in temperature range of 255-435°C and a kinetic model was proposed considering degradation of extractives, hemicellulose, cellulose and lignin in three reaction zones: (I) extractives and most reactive fractions of hemicellulose, (II) cellulose and part of lignin and hemicellulose and (III) lignin and small fractions of other two constituents.

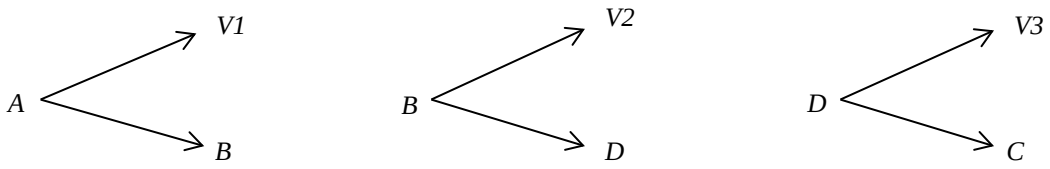


**Figure 2.6:** Multi-component mechanism of biomass decomposition (Branca and Di Blasi, 2003).

As per this model (see Figure 2.6), A is wood, B and D are intermediate solid-phase reaction products, and V1, V2 and V3 are volatiles generated in three stages. C is final charred residue. The authors (Branca and Di Blasi, 2003) found that the first and third reaction zone kinetic constants (activation energies of 76 and 44 kJ/mol, respectively) were in good agreement with studies in both isothermal and dynamic conditions, whereas the second reaction zone kinetic constants (activation energy of 143 kJ/mol) were in good agreement with isothermal analysis, but not with dynamic conditions (activation energy of 195-213 kJ/mol). Radmanesh et al.(2006) proposed a three-independent parallel reaction model for complete devolatilization of biomass components using thermogravimetry and gas chromatography techniques and analysed the effect of heating rate on yield of gases and tars.

The models (Liden et al., 1988; Boroson et al., 1989b; Koufopanos et al., 1991) have been used for studying the homogeneous decomposition of tar produced by primary degradation of biomass. The decomposition of tar in vapour phase, both inside the particle and in reactor environment has been considered. Liden et al. (1988) proposed a kinetic model for production of organic liquids from flash pyrolysis of wood (see Figure 2.7).

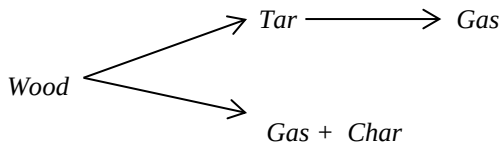


**Figure 2.7:** Primary and secondary decomposition of wood (Liden et al., 1988).

In this scheme (Liden et al., 1988), it was assumed that the wood decomposes according to two parallel reactions yielding gas with char and liquid tar which further decomposes by secondary homogeneous reactions. The combined activation energy for first order decomposition of wood was calculated as 183.3 kJ/mol and pre-exponential factor of $10^{13}$ $s^{-1}$. The activation energy of first order secondary decomposition reaction was given as 107.5 kJ/mol with a pre-exponential factor of $4.28x10^{6}$ $s^{-1}$. It was analysed that at 500°C, the tar yield is almost independent of gas residence time, whereas at 600°C, the tar yield decreases with increasing gas residence time. It was also observed that wood particles have a longer residence time at lower temperatures because of lower decomposition rate. Boroson et al. (1989b) had offered a kinetic scheme for secondary reactions of condensable vapours through vapour phase homogeneous cracking (extra-particle cracking) in temperature range of 500-800°C, with residence times of 0.9-2.2 seconds in a tubular reactor. The authors (Boroson et al., 1989b) studied this scheme with single first -order reaction model using primary degradation kinetic parameters from Nunn et al. (1985), and also with distributed activation energy model using parameters from curve-fitting of product yield data. The activation energy of first order secondary reaction was calculated as 93.3 kJ/mol with pre-exponential factor of $10^{5}$ $s^{-1}$. It was found that the major tar conversion product is CO and the distributed activation energy model is better than single reaction model in terms of tar conversion behaviour over a broader range of residence times and temperatures.

Koufopanos et al.(1991) model included the kinetic scheme for primary and secondary reactions describing pyrolysis of small particles of main biomass components that are cellulose, hemicellulose and lignin by summing up their individual reaction rates.

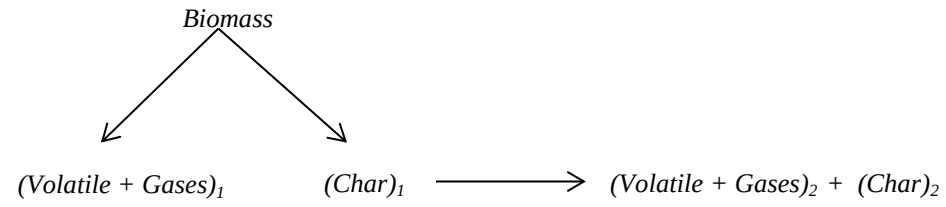


**Figure 2.8:** Combined mechanism for primary and secondary decomposition of biomass (Koufopanos et al., 1991).

This model (see Figure 2.8) indicated that the biomass decomposes to volatiles, gases and char; the volatiles and gases may further react with char to produce volatiles, gases and char of different compositions. Srivastava et al. (1996) modified this kinetic mechanism (Koufopanos et al., 1991) for detailed study of order of reactions during biomass pyrolysis. According to their study (Srivastava et al., 1996), initial decomposition of biomass has either $0^{th}$ order or $1^{st}$ order of reaction, while the secondary decomposition has $1.5^{th}$ order of reaction. It was found that pyrolysis is faster for $0^{th}$ order of reaction and final pyrolysis temperature is higher for $1^{st}$ order of reaction because time and temperature have a linear relationship. Fagbemi et al. (2001) studied the thermal cracking of tar in the temperature range of 400 to 900°C in a quartz tube reactor for residence time of 0 to 4 seconds. It was found that with increase in temperature, the gas volume also increases, but heating value of gas stabilises above 700°C. It was further stated that decrease in $CO_2$ concentration with temperature was due to simultaneous increase in CO (heterogeneous $CO_2$-solid reactions) and $H_2$ (dehydrogenation of C2, C3) concentration. According to their study (Fagbemi et al., 2001), the quantity of tar reached a maximum value at about 500°C, and then dropped with increasing temperatures due to secondary tar cracking reactions, leading to formation of larger amount of gas with higher energetic content. From experimental studies, the activation energy for the reaction was given as 23.4 kJ/mol and pre-exponential factor as 4.34 $s^{-1}$. Morf et al.(2002) analysed the homogeneous secondary cracking of tar produced by pyrolyis of wood chips (fir and spruce, 10-40 mm diameter) in the temperature range of 500 to 1000°C in tubular reactor with isothermal space times below 0.2 second. According to their study (Morf et al., 2002), the tar cracking results in production of gases like CO, $CH_4$ and $H_2$ for temperatures greater than 650°C, and also favours the conversion of primary tar (mainly oxygenates such as

acetol) into secondary (mono-aromatics such as phenols) and tertiary tar compounds (poly-aromatics such as napthalene) at higher temperatures. The homogeneous conversion was assumed with plug flow behaviour in tubular reactor and defined with a first-order kinetic reaction having activation energy of 76.6 kJ/mol and pre-exponential factor of $4x10^4$ $s^{-1}$. It was concluded from the model as well as experimental findings that in temperature range up to 600°C, the secondary tar reactions occur to a very low level and increase considerably with increasing temperatures up to 1000°C. Baumlin et al. (2005) worked to overcome the problems associated with assumptions of considering plug flow behaviour for secondary cracking reactions of pyrolysis vapours, leading to inappropriate study of reaction temperatures and gas residence times (Rath and Staudinger, 2001; Morf et al., 2002). The authors (Baumlin et al., 2005) studied the cracking of biomass pyrolysis vapours in a continuous self-stirred tank reactor (CSSTR) instead of plug flow reactor (PFR), for mean gas residence times between 0.29 and 0.49 seconds and temperatures ranging from 563 to 1030°C. For the global cracking behaviour of biomass pyrolysis derived vapours, the kinetic constants were calculated with activation energy of 59 kJ/mol and pre-exponential factor of 1930 $s^{-1}$. It was also concluded that with increasing temperatures, there is an increase in mole fractions of $H_2$ and $CH_4$, with corresponding decrease in that of $CO_2$, keeping CO as nearly constant. Park et al. (2010) studied the kinetics of wood pyrolysis considering both primary and secondary decomposition reactions. According to this model (Park et al., 2010), wood primarily decomposes to gas, tar and an intermediate solid. Tar further decomposes to give gas and char with increase in temperature, while intermediate solid converts to char only.

As compared to homogeneous cracking, the heterogeneous cracking of tar on char matrix in presence of inert metals or minerals has not been discussed in detail in literature. Few studies have been performed for analysing the effect of char on tar decomposition reactions (Boroson et al., 1989a; Morf, 2001; Abu El-Rub, 2008). Boroson et al. (1989a) conducted the experiments in temperature range of 400-600°C and space time from 2.5 to 100 milliseconds in fixed char beds. Based on the study, it was concluded that there was conversion of some amount (around 35%) of total tar (considerably aromatic in nature) on char surfaces, causing formation of

gases (such as CO and $CO_2$) and some amount of additional char (or coke). Morf (2001) studied the heterogeneous cracking of tars on a fixed char bed with space time less than 0.4 seconds and temperature in range of 450- 960°C. It was found that the increase in concentration of non-condensable gases is higher as compared to homogeneous cracking in the same temperature range. The major conclusion was regarding the effect of char on conversion processes of primary, secondary and tertiary tar, according to which, there is shift in thermal behaviour of tar compounds towards lower temperatures as compared to homogeneous reactions. However, no kinetic scheme was proposed for these heterogeneous cracking reactions (Boroson et al., 1989a; Morf, 2001). Abu El-Rub (2008) studied the catalytic activity of biomass chars for tar reduction in gasifier product stream. The experimental studies were conducted with a fixed char bed in temperature range of 700-900°C, with gas residence time of 0.3 second and an atmosphere of $CO_2$ and steam. Based on these experiments, a kinetic model was proposed for conversion of a single tar component, i.e. napthalene, with activation energy of 61 kJ/mol and pre-exponential factor of $10^4$ $s^{-1}$. It was concluded that during the process, tar molecules adsorb on char particle active sites to convert into gases and coke (deposit on char surfaces) according to gasification and polymerization reactions, respectively.

The distributed models are different from lumped models in terms of their application in pyrolysis process. In these models, it is considered that the pyrolysis products are formed by an infinite number of independent parallel reactions having different activation energies given using Gaussian distribution function. Chen et al. (1998) model was based on a coal pyrolysis model known as FG-DVC (Functional Group- Depolymerization, Vaporization, Cross-linking) for examining the biomass pyrolysis. The FG-DVC model combines a Functional Group (FG) model for gas evolution and a statistical Depolymerization, Vaporization and Cross-linking (DVC) model for tar and char formation. The results of this model were not quite satisfactory when compared to experimental yields and composition of pyrolysis products (Chen et al., 1998). This is due to the fact that the model had not included the impact of secondary reactions, heating rate and mineral effect on kinetics of biomass pyrolysis.

Niksa (2000) reaction scheme (see Figure 2.9) was based on the depolymerization of a mixture of chain macromolecules into fragments that volatilize into tar, partially decompose into gases, or recombine with the nascent char matrix. This reaction model for biomass devolatilization is also known as bio-FLASCHAIN (bio-FC) and was earlier used for coal devolatilization. However, this mechanism is much more difficult to implement because of substantial gaps in the supporting database required for validating this model.

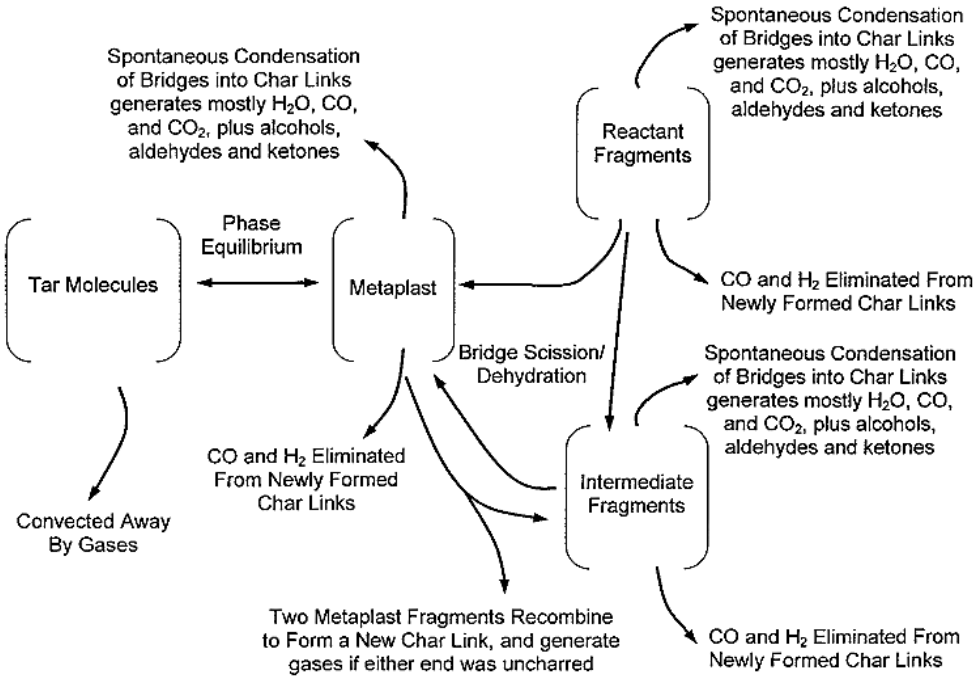


**Figure 2.9:** Reaction mechanism in bio-FLASHCHAIN (Niksa, 2000).

The Chemical Percolation Devolatilization (CPD) model (Shen and Zhang, 2001; Sheng and Azevedo, 2002), was an extension of coal CPD model for three main biomass components, i.e., cellulose, hemicellulose (with extractives) and lignin, on basis of their chemical structure and behaviour during transformation under different mechanisms. For this model (Sheng and Azevedo, 2002), it was considered that the structure of biomass components (cellulose as a linear molecular chain, hemicellulose as a linear chain with more branched and shorter chains, and lignin as a molecular chain cross-linked to form a simple network) is more similar to a chain rather than the macromolecular network of low rank coals. Using the structural parameters (coordinate number, initial fraction of intact bridges, average molecular weight per cluster and molecular weight per side chain) and fitted kinetic parameters,

the model was validated using experimental data for devolatilization of cellulose, hemicellulose and lignin. Some deviation was found with the experimental data because of not properly considering the secondary decomposition of tar clusters to yield light gases in the model.

Rostami et al.(2004) presented a new model based on distributed activation energy mechanism for biomass pyrolysis. The model assumed that the reactions kinetics is represented by a set of independent and parallel reactions, with the same pre-exponential factor and a continuous distribution of activation energies. This model was applied to study pyroylsis of cellulose, charcoal and a tobacco sample. Few other mechanisms were proposed for understanding thermo-chemical decomposition of different biomass samples using distributed models (Becidan et al., 2007; Sonobe and Worasuwannarak, 2008; Várhegyi et al., 2010). These studies utilized the thermogravimetric analysis for model validation with experimental data. The non-linear least squares algorithm used in these models (Becidan et al., 2007; Sonobe and Worasuwannarak, 2008; Várhegyi et al., 2010) for calculation of the model parameters was based on mass loss rate of biomass samples with respect to temperature or time, such as shown in Figure 2.10.

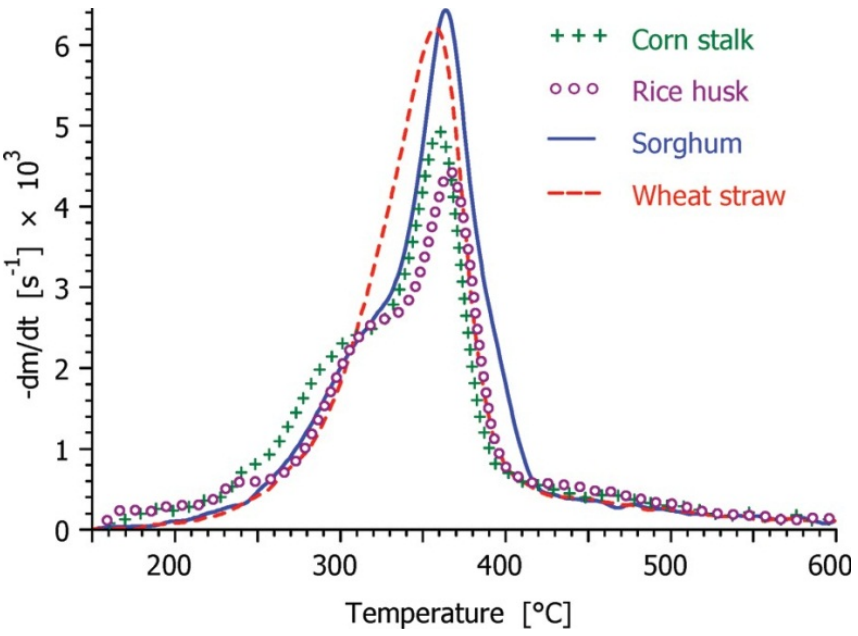


**Figure 2.10:** Mass loss rate curves for different biomass samples (Heating rate = $40^0$C/min) (Várhegyi et al., 2010).

### 2.2.2. Particle model

In the kinetic models discussed above, it was assumed that the degradation of biomass takes place either at very slow heating rates for avoiding spatial gradients of temperature or at very high heating rates for avoiding initial heating period. Both the schemes were utilized for studying the static degradation of biomass i.e. degradation taking place isothermally during pyrolysis process. However, both the mechanisms have some drawbacks. In former case, the weight loss cannot be neglected during heating period and interpretation of this data is not possible. In latter case, the results are affected by heat transfer limitations because accurate control of sample temperature is not possible. Therefore, these reaction models have to be further coupled with transport equations for studying the overall thermo-chemical degradation process including heat and mass transfer effects.

Different particle models (Kung, 1972; Kansa et al., 1977; Pyle and Zaror, 1984) have been proposed by modifying the Bamford Model (Bamford et al., 1946) to understand the physical and chemical processes during pyrolysis of different types of biomass. Within the solid, the main heat transfer process before thermal decomposition is conduction. Once decomposition begins, the efflux of volatiles may lead to convective heat transfer from the hotter solid closer to the surface inhibiting the transfer of heat by conduction into the solid. The porous structure also plays a fundamental role in this process. The effect of convective heat transfer between pyrolysis gases and solid, and enthalpy changes associated with reaction and with phase changes during heat transfer to the solid are also important (Kanury and Blackshear, 1970; Roberts, 1971).

In majority of these models, the basic assumptions for understanding the overall process were:

1. A global Arrhenius pyrolysis mechanism with regard to biomass consumption.
2. Local thermal equilibrium between solid and volatiles.
3. The ideal gas law applied.
4. Darcy flow considered inside the porous medium.

Kung (1972) studied the particle decomposition with some assumptions such as negligible secondary catalytic chemical reactions between the volatiles and hot char.

This model included the effect of heat convection by outward flowing volatiles, which is an important aspect of the physics of pyrolysis. Kansa et al. (1977) proposed a 1-dimensional (1-D) model of charring pyrolysis including porous and permeable structural effects on the volatile flow. The model comparison with experimental data for maple wood indicated good agreement at low surface heating rates (0.022 J $mm^{-2}$ $sec^{-1}$), but poor at fire level heat fluxes (0.084 J $mm^{-2}$ $sec^{-1}$). At high heat fluxes, it appeared that both structural changes and secondary pyrolysis reactions are important. According to the model of Pyle and Zaror (1984), the relative importance of internal and external heat transfer and of the intrinsic (first order) pyrolysis kinetics were determined from the Biot number and one of two pyrolysis numbers. The effect of secondary pyrolysis, i.e., decomposition of volatiles in presence of char was not taken into account in this model. It was found that under low temperature conditions (380 to 500°C), internal convection is unimportant. Chan et al. (1985) aimed a model to predict single particle devolatilization rates and product compositions on the basis of fundamental physical and chemical principles. The authors assumed quasi-steady approximation and negligible accumulation of volatiles. This model incorporated the secondary reactions of tar decomposition in pyrolysis reaction kinetics scheme. It was analysed that mass transfer by diffusion is negligible in comparison with hydrodynamic flow for active devolatilization. It was also concluded that over the range of pyrolysis onset (227°C) to the highest observed temperatures (827°C), the heat and mass transfer properties of the wood change due to explicit temperature effects by less than an order of magnitude. Koufopanos et al. (1991) model assumed that heat is transmitted inside the solid by conduction only and effect of radiation from pore walls and transmission through gas phase inside the particle pores is negligible. Particle shrinkage effects and convective mass transfer inside the particle was neglected. According to this study, pyrolysis is endothermic at low conversion rates, but exothermic at high conversion rates. It was analysed that for particles smaller than 1 mm, the effect of internal heat transfer is negligible and process is mainly controlled by primary reactions and external heat transfer. It was also found that secondary reactions are responsible for carbon enrichment of final residue.

Di Blasi (1996a) proposed an advanced model based on an earlier defined model (Di Blasi, 1993a), for including the effect of particle shrinkage on pyrolysis. The model considered the formation of chars, tars and gases through mechanisms including both primary reactions of the virgin biomass degradation and secondary reactions of the primary tar to gas and repolymerized char. Some assumptions such as negligible moisture content and no condensation of tar species inside the particle were taken into account. The model results showed that particle shrinkage affects both the primary and secondary reaction paths due to different heat transfer conditions interior to particle and to reduced volatile residence times, respectively. A 2-dimensional (2-D) model was studied by Di Blasi (1998) for examining anisotropic behaviour of biomass. Based on the results, it was concluded that the process is faster with higher volatiles yield for 2-D configuration as compared to 1-D configuration.

Janse et al. (2000) described the relevant physical and chemical processes inside a single particle which are dominating the product distribution and conversion times of wood particles for flash pyrolysis conditions. The effect of out-flowing pyrolysis vapours and of sign/size of reaction heat was also included. The authors (Janse et al., 2000) examined that the spherical particle has shortest conversion time due to higher surface/volume ratio and conversion time of a particle may increase up to 40% due to the cooling effect of out flowing vapours. It was found that the detailed knowledge of internal mass transport phenomena in fast/flash pyrolysis modelling is not required, while accurate details of reaction kinetics and heat transfer is important.

Bryden and Hagge (2003) model included the detailed analysis of pyrolysis of a moist, shrinking biomass particle. In this model, the combined impact of both moisture (Bryden et al., 2002) and particle shrinkage (Hagge and Bryden, 2002) on pyrolysis times and product yields were taken into account. The negligible recondensation of tar in cooler core of solid matrix due to pressure peak of moisture wave flowing out of particle was assumed. However, the effect of shrinkage due to char was considered, and not due to volume occupied by volatiles as used in Di Blasi (1996a) model. It was concluded that pyrolysis can be divided into three regimes-thermally thin, thermally thick and thermal wave; and the combined impact of shrinkage and moisture content is mostly there in thermal wave regime. Galgano and

Di Blasi (2004) modelled the radiative decomposition of 40 mm thick moist (between 0 to 47% moisture content) beech wood particle using shrinking unreacted-core model (Galgano and Di Blasi, 2003). The progress of degradation of moist wood particle is shown in Figure 2.11. As per the model (Galgano and Di Blasi, 2004), the drying stage comprised of three zones in the particle domain, i.e., moist core, dry wood and char layer; after moisture evaporation, only char and dry wood were left. Based on the analysis, it was found that the wood drying and conversion times are linearly dependent on initial moisture content.

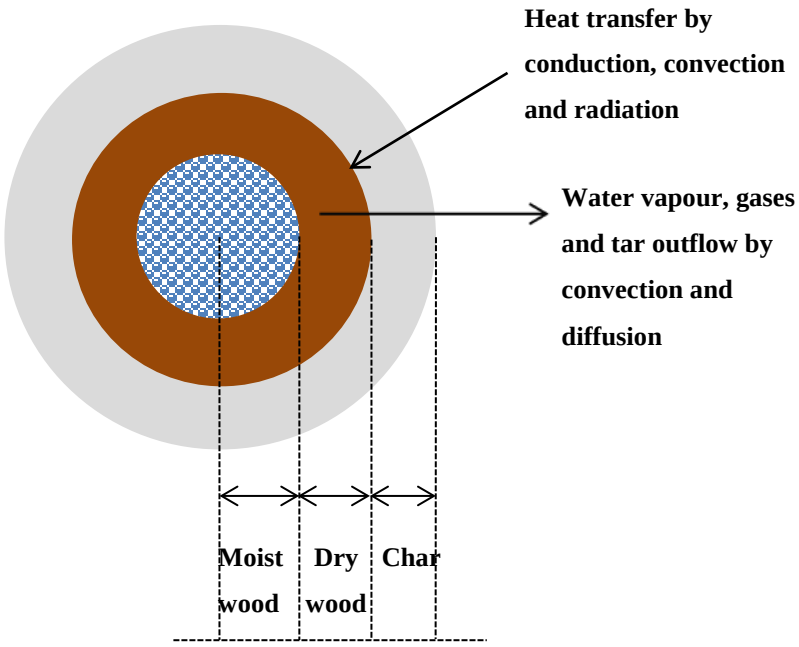


**Figure 2.11:** Schematic for showing decomposition progress in a moist wood particle (cross section of the particle) (adapted and modified from Galgano and Di Blasi (2004)).

Babu and Chaurasia (2004a) proposed a model for examining the impact of shrinkage on particle size, pyrolysis time, products yield, specific heat capacity and Biot number. According to the authors (Babu and Chaurasia, 2004a), lower possible values of shrinkage factor were more realistic and provided better model predictions as compared to higher values given by Di Blasi (1996a). The shrinkage of the particle favoured the attainment of larger yields of volatiles and gases produced by primary reactions at the expense of other two products. Yuen et al. (2007) formulated a 3-D model for pyrolysis of wet wood by incorporating the anisotropic properties of wood and internal convection of gases with a single kinetic reaction for

the overall devolatilization process. However, the model did not provide accurate results when compared to experiments due to insufficient reactions considered for primary wood decomposition and secondary tar reactions. Some other simplified models (Sadhukhan et al., 2008; Damartzis et al., 2009) for degradation of biomass considering heat transfer with primary and secondary chemical reactions were developed and compared with experimental data conducted in a single particle reactor.

Sreekanth and Kolar (2009) provided a 2-D model for the thermal decomposition of a single wood particle in a fluidized bed reactor (FBR). This model considered the effect of anisotropy, temperature, density and moisture content on pyrolysis process. The comparison was made with 1–D anisotropic models with respect to the propagation of a temperature and drying front within the particle. Park et al. (2010) studied the degradation mechanism of wood for analysing the effect of endo/exothermicity of the reactions occurring during the process and of pressure generation on particle structure. The model didn't account for particle shrinkage and diffusive flux for gaseous species. It was suggested that at high temperatures, thick wood particle may split due to a combination of high internal pressure and weakened structure. Lu et al. (2010) model analysed the effect of particle shape and size on rate of biomass devolatilization. It was assumed that particle aspect ratios and shapes do not change during devolatilization. The effect of particle shrinkage and moisture content were not taken into account in this model. The authors (Lu et al., 2010) contradicted the results of Janse et al.(2000) by stating that spherical particles have slower rate of heat and mass transfer as compared to other aspherical particles of the same volume/mass (see Figure 2.12). It was also concluded that conversion time for spherical particles is high (almost twice) as compared to aspherical particles for large size and aspect ratio, and produce less volatile yields relative to other shapes. Peters (2011) developed a model for analysing the pyrolysis rate of different biomass samples such as spruce, beech, casuarina, pine wood, cellulose and lignin for different heating rates and particle geometries with a one-step kinetic model as well as by including the secondary tar reactions. However, this model also not included the effect of particle shrinkage and drying during pyrolysis.

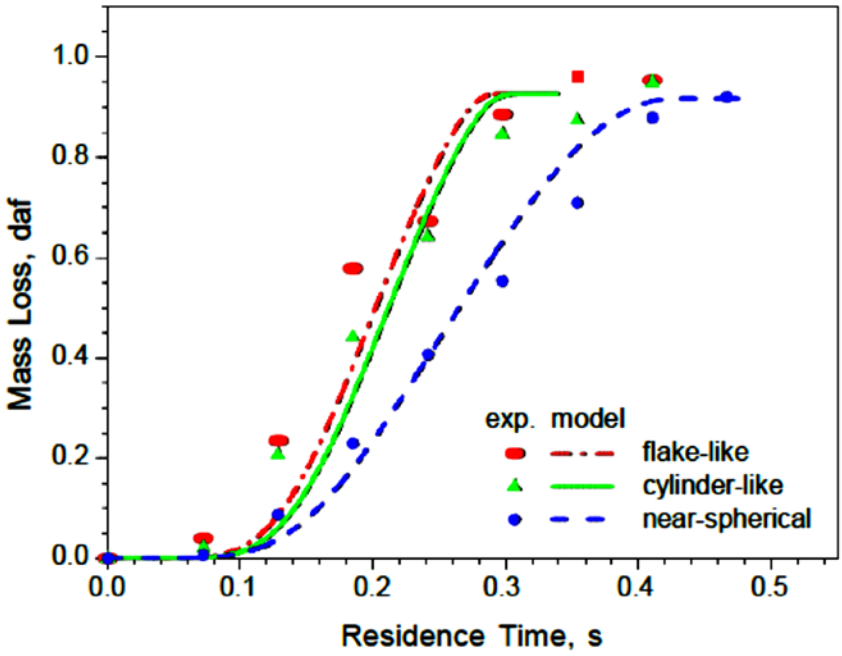


**Figure 2.12:** Mass loss (daf or dry ash free basis) profile for sawdust particles with different shapes and similar mass/volume (Reactor temperature = 1352°C, Gas temperature = 1037°C, equivalent particle diameter = 0.32 mm) (Lu et al., 2010).

### 2.2.3. Reactor model

The single particle models are used for reactor modelling and design taking extra-particle processes into account, such as the effect of residence time of the gas phase and the solid phase on primary decomposition and secondary tar cracking mechanism inside the reactor. Fundamental as well as CFD models have been studied for biomass pyrolysis in various reactor configurations for analysing the effect of process parameters on the reactor hydrodynamics and the product yields.

For slow or conventional pyrolysis, rotary kiln (Klose and Wiest, 1999) and fixed bed (Yang et al., 2007b) reactor configurations were studied. Di Blasi et al. (2004) proposed a 2-D mathematical model for pyrolysis of wheat straw in a convective heated pyrolyzer considering as a fixed bed reactor due to long residence time of solids and high solid to gas density. This model was used to show that for solid residence times of around 100 seconds, the highest conversion of straw is about 60%. The effect of the gas temperature and the solid residence time on the conversion level has also been evaluated. Yang et al. (2007b) examined segregated solid wastes in a packed-bed pyrolyzer for analysing the final yields of gas, tar and char in the temperature range of 350-700$^0$C and heating rate around 10°C/min.

According to this study, production of char, tar and gas yields vary between 21-34%, 34-46% and 23-43%, respectively. It was also concluded that final quantity of char is 30-100% more in packed bed pyrolyzer as compared to TGA studies due to tar cracking and repolymerization, both inside the pyrolyzing particles and on activated outer surface of other particles.

For fast pyrolysis, the FBR is a very prominent option for effective heat and mass transfer during the process. Some simplified models for studying the devolatilization of biomass in fluidized bed environment have been proposed (De Diego et al., 2002; Jand and Foscolo, 2005; Saastamoinen, 2006). The biomass fast pyrolysis modelling and experimental studies have also been performed in rotating cone (Wagenaar et al., 1994) and entrained flow reactor (Brown et al., 2001).

Difelice et al. (1999) applied the devolatilization model of a single biomass particle in a FBR. The important aspects considered for fitting the particle model into FBR were heat transfer rate, effect of fluidization quality of gas produced by devolatilization process, and mixing/segregation behaviour of biomass and bed particles. The volatiles consisted mainly of permanent gases, with negligible tar production for temperatures greater than 427°C. It was found that biomass particles float or sink depending on the bulk density of bed particles, and based on this, the feeding point for biomass is finalized. Di Blasi (2000) proposed a model for pyrolysis of cellulose and wood (Di Blasi, 2002) in a FBR. For this study, a single particle model (Di Blasi, 1996b) was coupled with an external heat transfer model (Agarwal, 1991), and also the effect of bed hydrodynamics on particle conversion was considered. The single particle and reactor model results were compared with experimental studies for gas, tar and char yields (see Figure 2.13). It was found that at high bed temperatures, the activity of secondary reactions is not negligible in freeboard zone, and the volatile residence time is smaller than as calculated using bubble velocity of two-phase theory, due to net flux addition by fast devolatilization rate.

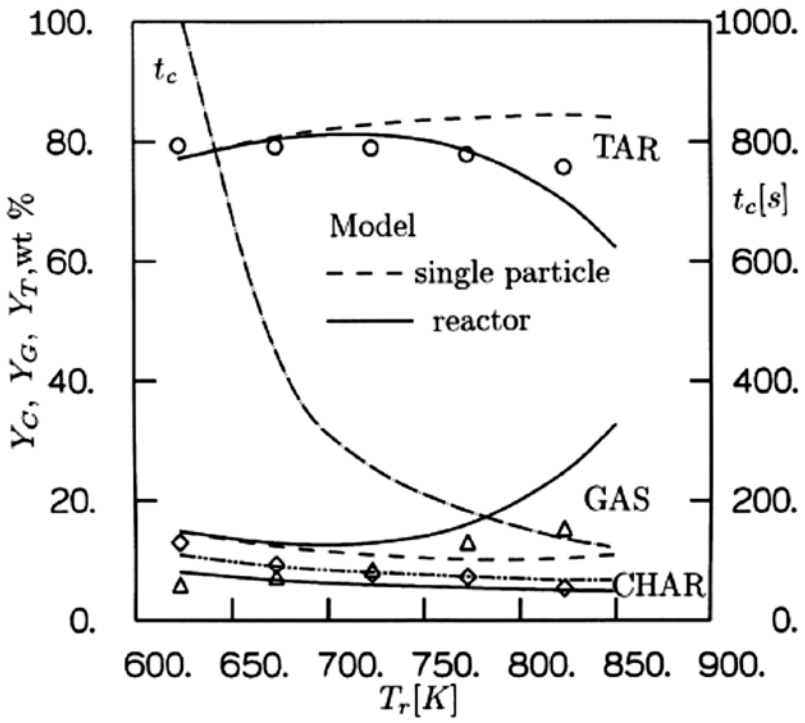


**Figure 2.13:** Particle and reactor model results comparison (for yield of gas ($Y_G$), tar ($Y_T$) and char ($Y_C$); reactor temperature = $T_r$ in Kelvin; volatiles residence time = $t_c$ in seconds) with experimental data (Di Blasi, 2000).

Luo et al. (2005) discussed flash pyrolysis of wood and the effect of main operational parameters on product distribution in a FBR. For this study, the secondary tar cracking was considered homogeneously in gas phase, both inside the particle as well as in reactor environment, and heterogeneously inside the particle only. According to modelling and experimental results (Luo et al., 2004), maximum bio-oil production occurs at dense bed temperature of around 500°C. It was determined that wood particle should be of moderate size because fine particles are carried easily by gas flow leading to short residence time and incomplete decomposition, whereas larger size reduces bio-oil production due to slower heating rates. Kaushal and Abedi (2010) developed a 1-D model for biomass pyrolysis using a two- step kinetic model with the two-phase hydrodynamic model (bubble and emulsion phase) in a FBR. It was found that the cracking and gas phase reactions are important at temperatures higher than 500°C; and the bed hydrodynamic and mass transfer governs the pyrolysis rate at these higher temperatures.

In last few years, CFD modelling has proven its utility as a powerful tool for evaluating the reactor performance for different kinds of processes, instead of going

for expensive experimental analysis. Multi-phase CFD modelling is broadly divided as Euler- Euler and Euler-Lagrangian approaches. Different models based on these categories are shown in Figure 2.14, with their type of interactions and industrial scale utilization given in Table 2.2.

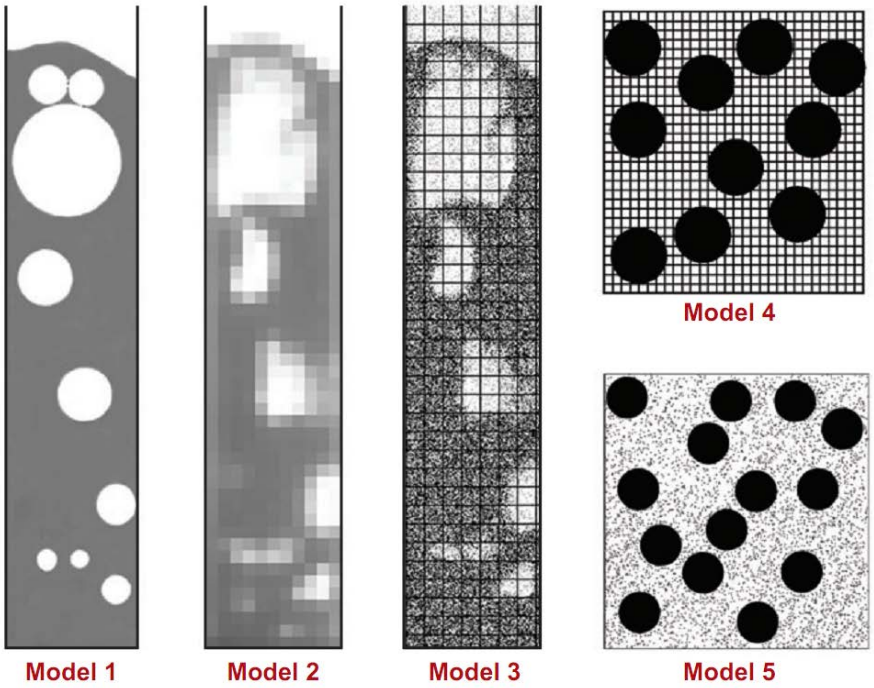


**Figure 2.14:** Graphical representation of different CFD models (van der Hoef et al., 2008).

**Table 2.2:** Description of different CFD models (van der Hoef et al., 2008).

| Name | Gas phase | Solid phase | Gas-solid coupling | Scale |
|---|---|---|---|---|
| Discrete bubble model (Model 1) | Lagrangian | Eulerian | Drag closures for bubbles | Industrial (10 m) |
| Two-fluid model (Model 2) | Eulerian | Eulerian | Gas-solid drag closures | Engineering (1 m) |
| Unresolved discrete particle model (Model 3) | Eulerian (unresolved) | Lagrangian | Gas-particle drag closures | Laboratory (0.1 m) |
| Resolved discrete particle model (Model 4) | Eulerian (resolved) | Lagrangian | Boundary condition at particle surface | Laboratory (0.01 m) |
| Molecular dynamics (Model 5) | Lagrangian | Lagrangian | Elastic collisions at particle surface | Mesoscopic (<0.001 m) |

Out of these models, mainly first three types (Model 1-3) have been utilized for real gas-solid fluidized bed studies. And for fluidized bed studies, mainly Euler-Euler such as Two-Fluid Model (TFM) (Pain et al., 2002) and Euler-Lagrangian such as Discrete Particle Model (DPM) (Kafui et al., 2002) have been discussed with current computational capabilities. Discrete Bubble Model (DBM) (Bokkers et al., 2006) is still in its early stages of development and has not been discussed in detail in the literature. Euler-Euler modelling approach considers different phases (gas-solid, gas-liquid, liquid-solid) as inter-penetrating continuum, with each phase occupying a volume fraction inside the reactor. Conservation equations are derived for each phase based on Navier- Stokes relationships, while some additional closure laws are required to describe particle phase constitutive relations, such as those given by kinetic theory of granular flows (Lun et al., 1984; Ding and Gidaspow, 1990; Syamlal et al., 1993) for solid phases. According to this theory, granular particles are considered as molecular gases, but with energy losses due to collisions between grains. Also, kinetic energy associated with fluctuating motion of particles is defined as granular temperature of particles. The solids pressure and viscosity are considered as a function of granular temperature while defining particles motion in a dense bed. However, Euler- Lagrangian modelling approach considers fluid phase as a continuum, while dispersed phase is considered by tracking a given number of

particles, bubbles or droplets through the continuous phase using Newton's laws of motion. Some constitutive relations are required, such as for accounting energy dissipation by particle collisions using hard-sphere (by empirical coefficient of restitution and friction) (Hoomans et al., 1996) or soft-sphere (empirical spring stiffness and friction coefficient) approach (Tsuji et al., 1993). The Euler-Lagrangian approach of hydrodynamic modelling is better in comparison to Euler- Euler approach for obtaining detailed information about motion of particles in bed. But it has drawback of requirement of large computation capacity to keep macroscopic flow time scale compatible with the very small time scales of particle-particle interactions. Therefore, for industrial scale systems, Euler-Euler is still considered a better option for analysing the hydrodynamics of different phases during heat and mass transfer operations.

CFD models have been studied for examining biomass thermal decomposition in presence of air/steam (Oevermann et al., 2009; Gerber et al., 2010) and inert gas environment (Papadikis et al., 2009b; Bruchmüller et al., 2011; Xue et al., 2011; Bruchmüller et al., 2012). The main focus of these studies has been on fluidized bed reactors because of inherent benefits of excellent heat and mass transfer rates with uniform product distribution. In the model proposed by Lathouwers and Bellan (2001a), kinetic theory of granular flows with CFD approach was applied for analysing the complete process in a FBR. But this model has drawbacks in terms of fulfilment of energy requirement of reactor and achievement of high temperatures of around 225°C for biomass feed. The physical time simulated in this study was also around 5 seconds, which is not sufficient for reaching any considerable results. The tar yield was optimized with variation in operating parameters (Lathouwers and Bellan, 2001b). Papadikis et al. (2009b) studied the pyrolysis of biomass using Euler-Euler-Lagrangian approach of CFD modelling. For this study, momentum transport from fluidizing gas and fluidized sand was considered keeping biomass as a discrete particle in the bubbling fluidized bed (Papadikis et al., 2008; Papadikis et al., 2009a). Based on modelling results, it was concluded that shrinkage does not significantly affect the yield and time in fluidized bed while operating with particle size of order of 0.5 mm. Papadikis et al. (2010b) compared different drag models, namely Gidaspow, Syamlal O'Brien, and Wen-Yu, based on their impact on heat

transfer, degradation rate, product yields and char residence time during biomass pyrolysis. The effect of particle size on heat transfer coefficient had also been studied (Papadikis et al., 2010a). The main drawback of these studies (Papadikis et al., 2009b; Papadikis et al., 2010a; Papadikis et al., 2010b) was that only 1 or 2 reacting particles considered for analysis and the simulation time was limited to 3 to 5 seconds of total real time of process.

Oevermann et al. (2009) presented an Euler- Lagrangian model for wood gasification in bubbling fluidized bed reactor. In this model, the gas phase was modeled using 2-D Navier- Stokes equation, and solid phase by Discrete Element Method (DEM) using soft-sphere approach for particle collision dynamics. Gerber et al. (2010) discussed an Euler- Euler model for wood gasification in bubbling fluidized bed using char as bed material. However, the mechanism chosen for secondary tar reactions in reactor environment did not consider the catalytic effect of char bed on cracking step, and hence, these reactions were considered in gas phase only. Xue et al. (2011) formulated an Euler-Euler model for fast pyrolysis of biomass in fluidized bed. The reactor hydrodynamics was coupled with reaction kinetics and biomass transport based on a simplified single-particle model. It was found that 2-D grid sensitivity had no significant impact on apparent biomass density, vertical velocity, average temperature and product yields (Xue et al., 2012). However, comparison with 3-D domain resulted into some variation in these parameters in bed surface and biomass feed location with no substantial change in the product yields. The effect of change in effective particle diameter, gas temperature and superficial gas velocity on product yields was also analysed (Xue et al., 2012). The simulated product yield of different types of biomass has been calculated and compared for same operating conditions (see Figure 2.15). Bruchmüller et al. (2012) analysed thermo-chemical decomposition of biomass using CFD- DEM approach. The gas phase was modelled as a continuous phase, while both the biomass and the sand phases were treated as discrete phases in the mixture. The modelling results for a 3-D domain were analysed for bed hydrodynamics with different inlet distributor plates as well as for the effect of fluidization velocity, temperature and moisture content on product yield and composition. However, the modelling results were displayed for only 5 seconds of the process after fluidizing the sand bed for initial 5 seconds inside the reactor,

which led to inconsistencies in product yields when compared with steady state experimental data.

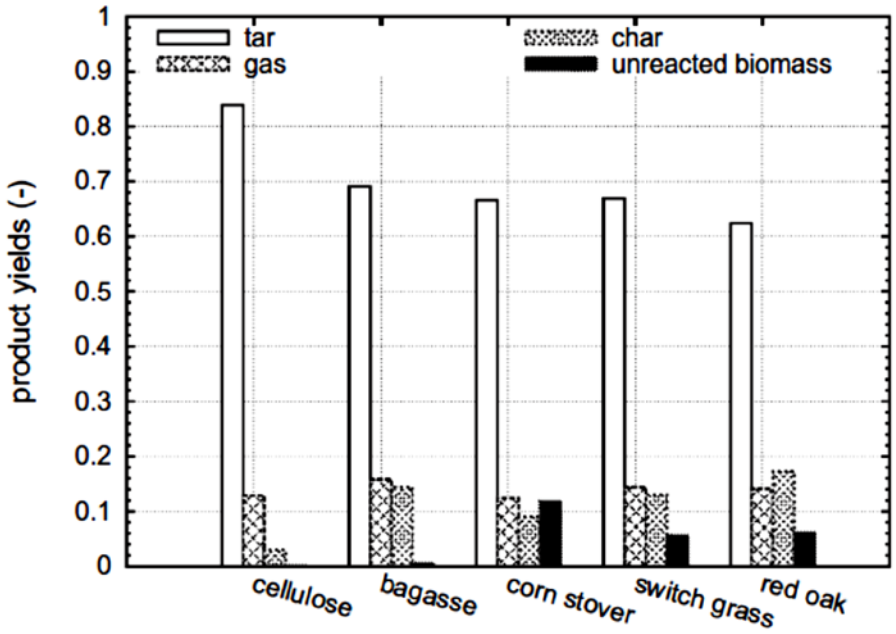


**Figure 2.15:** Simulated product yields for different biomass feedstocks (particle diameter= 0.5 mm, reactor temperature = 500°C, gas velocity = 3x min. fluidization velocity) (Xue et al., 2012).

## 2.3. Pyrolysis process parameters

The thermo-chemical decomposition of biomass in inert atmosphere is dependent on various process parameters such as feedstock type, operating conditions and physico-chemical properties of biomass, which ultimately affect the biomass conversion time or pyrolysis rate with product distribution and quality.

### 2.3.1. Type of feedstock

Biomass is generally composed of three main groups of natural polymeric materials: cellulose, hemicellulose and lignin. Other typical components are grouped as extractives (generally smaller organic molecules or polymers) and minerals (inorganic compounds). These are present in differing proportions in different biomass types and these proportions influence the product distributions on pyrolysis (Alves and Figueiredo, 1989). At pyrolysis temperatures, the main biomass components contribute to product yields broadly as follows: cellulose and hemicellulose components provide the volatile pyrolysis products, while lignin predominantly forms a charred residue (Shafizadeh and Chin Peter P, 1977). But

according to Di Blasi and Branca (2001), the holocellulose (cellulose and hemicellulose) converts mainly to liquids (tars), while the char and gas products are due to lignin decomposition. Extractives contribute to liquid and gas products either through simple volatilisation or decomposition. Minerals, particularly the alkali metals (especially sodium, potassium and calcium), generally remain in the char and can have a catalytic effect on pyrolysis reactions leading to increased char yields depending on other conditions (Nik-Azar et al., 1997), in addition to the effect of ash contribution to char yield (Antal and Grønli, 2003). This elemental contribution in ash also degrades the quality of bio-oil due to some catalytic reactions, and its removal affects the process by causing an increase in bio-oil and decrease in gas products (Luo et al., 2004).

### 2.3.2. Heating rate and Temperature

For fast pyrolysis, a rapid heating rate and a rapid rate for cooling primary vapours are required to minimise the extent of secondary reactions. These reactions not only reduce the liquid yield but also have a negative impact on its quality by giving a more complex mixture with an increased degree of polymerisation and higher viscosity (Shafizadeh and Chin Peter P, 1977). Conversely, in slow pyrolysis, slow heating leads to higher char yields, but the consistency is not confirmed. However, in practical pyrolysis reactors such as fluidized beds, it is quite difficult to maintain controlled heating conditions because neither the heating rate nor the heat flux are independent variables and in fact, are non-stationary and dependent on local conditions (Kersten et al., 2005).

Temperature has a significant impact on char yields and properties. Higher temperatures result into lower char yield in all pyrolysis reactions. The primary reason for this is forcing out of more volatile material from the char at higher temperatures causing reduction in yield. The char yield decreases from 31% to 17% with increase in temperature from 365°C to 606°C (Park et al., 2010). However, there is also an adverse impact of lower temperatures, causing incomplete decomposition of biomass and leading to higher amount of unpyrolyzed solid in char content. Temperature also affects the char composition. Chars produced at higher temperatures have higher carbon contents (Thurner and Mann, 1981; Alves and Figueiredo, 1989). The solid product char contains more than 85 wt% carbon for

temperatures greater than 500°C (Wang et al., 2005). Liquid yields increased with increasing pyrolysis temperatures up to a maximum value, usually at 400-550°C, but yields are also highly dependent on other operating conditions. For a variety of feedstock types, it has been determined that the maximum yield of bio-oil is obtained at temperatures of around 400-550°C with a consistent decrease in char yield and corresponding increase in gas yield (Kersten et al., 2005). Above this temperature range, secondary reactions causing vapour decomposition become more dominant and the condensed liquid yields were reduced (Park et al., 2010). Gas yields are generally low below the optimum temperature (500°C) for liquid yield; above this, gas yields increase strongly with increasing temperatures, as the main products of vapour decomposition are gases (Babu and Chaurasia, 2003). The best bio-oil quality in terms of caloric value and hydrogen over carbon ratio is achieved at the maximum yield temperature i.e. around 500°C (Scott et al., 1988). For temperature ranging between 450-550°C , the water content is about 30-35 wt% of total liquid yield and for higher reaction temperatures, there is considerable increase in water content of liquid fraction of pyrolysis product due to secondary cracking reactions leading to decrease in heating value of bio-oil (Wang et al., 2005). However, the higher heating values of non-condensable gases are obtained at reaction temperatures greater than 500°C in pyrolysis, due to increased production of CO and $CH_4$ as compared to $CO_2$ (Luo et al., 2004).

### 2.3.3. Volatiles residence time and Pressure

Volatiles residence time is dependent on gas flow rate through the reactor which ultimately affects the contact time between primary vapours and hot char and so affects the severity of secondary reactions and also volatile product properties. There is a significant effect of the vapor residence time on product yields in fluidized bed reactor (Liden et al., 1988; Scott et al., 1999). Lower oil yields at prolonged vapor residence time are due to cracking and polymerization reactions of vapours to gases and solids, respectively. However, it was found that the loss of tar yield is limited to around 10% for vapour residence time from 1 to 5 seconds at temperatures around 500°C. Short volatiles residence time of less than 1 second affects the biomass decomposition process by causing incomplete depolymerization of lignin due to

random bond cleavage and inter-reaction of lignin macromolecule, finally resulting in less homogeneous liquid product (Bridgwater et al., 1999) .

Pressure also affects the pyrolysis process. With increase in pressure, volatiles have a smaller specific volume causing higher intra-particle residence time which favours their decomposition while escaping the biomass particle. This also leads to higher concentration (partial pressure) of volatiles, thus increasing the decomposition reaction rate through secondary reactions (Di Blasi, 2008). It was found that high pressure leads to higher char fractions (Bradbury et al., 1979). Alves et al. (1989) showed that chars formed under low flow, high pressure conditions resulted into higher fixed-carbon yields. This effect is useful in maximising the carbon sequestration potential in biochars.

### 2.3.4. Particle size, shape and orientation

Particle size has a significant effect on the heat and mass transfer phenomena during pyrolysis process. Large particles imply large thermal gradients and also the fluid residence times are sufficiently long to result in secondary reactions (Chan et al., 1985). The increasing particle size also causes reductions in liquid yield due to secondary reaction activity leading to increase in gas yield for external temperatures greater than 527°C (Di Blasi, 2002). Bradbury et al. (1979) analysed that small biomass size leads to smaller char fraction. However, experimental studies (Wang et al., 2005) showed that there is no significant influence of the increase in particle size (0.7 - 17 mm) on the product yields and it only affects the heating rate by decreasing it from 1000°C/s to 1.5°C/s; there was a marginal decrease in liquid yield and around 5 % decrease in gas yield with corresponding increase in char yield for increase in particle size from 17 to 20 mm. It was also found that the increasing particle size leads to an increase in water content (40 to 55 wt%) of bio-oil and decrease in carbon content (78.5 to 75 wt%) of solid char product (Wang et al., 2005).

Particle shape also influences the pyrolysis process. A spherical particle has the shortest conversion time due to higher surface/volume ratio. However, at small particle diameters (typically less than 0.2 mm), the rate of reaction becomes dominant and the different particle shapes show nearly equal conversion times (Janse et al., 2000). Park et al. (2010) also stated that spherical particles have less char yield and conversion time as compared to slab-shaped and cylindrical particles. However,

the studies of Lu et al. (2010) showed that spherical particles have the smallest surface to volume ratio, leading to slower rates of heat and mass transfer and higher conversion time as compared to other aspherical particles.

Grain orientation is an important parameter in biomass pyrolysis due to the anisotropic behavior of biomass. Roberts (1971) pointed that permeability for flow along the grains was $10^4$ times that across the grain and thermal conductivity along the grains was twice that across the grains. Chan et al. (1988) determined that decrease in tar yield with corresponding increase in char, water (dehydration reaction) and gas yield due to perpendicular grain heating, is because of low thermal conductivity (almost one-third as compared to parallel or tangential grain direction) and not due to increase in residence time owing to reduction in porosity. Di Blasi (1996a) proposed that secondary reactions occur to a larger extent for perpendicular grain heating as compared to parallel grain heating.

### 2.3.5. Reactor configuration

Different reactor configurations have been studied for the thermal decomposition of biomass in the absence of air. The most important factor which influences reactor selection is the medium of heat transfer to biomass particles inside the reactor during degradation process. In ablative type reactors, heat transfer occurs due to contact of biomass particles with hot surface. This process uses larger particles of biomass and is affected by rate of heat supply to the reactor (Bridgwater et al., 1999). The heat transfer gas or carrier gas is not required, but supplying heat to biomass is problematic because of high heat losses. The major problems with this configuration are achieving long residence times for biomass particles to allow a high degree of conversion, high degree of char attrition and high carry-over of carbon into bio-oil product (Scott et al., 1999). In vacuum pyrolysis, heat transfers by direct contact with hot surface. This process uses short residence time of volatiles and larger biomass particles. But this method has poor heat and mass transfer rates and requires larger scale equipment (Scott et al., 1999). Circulating Fluidized Bed (CFB) uses heat source (fluidizing or carrier gas and solid like sand) for transferring heat to biomass particles by both convection and conduction medium. This process has heat transfer limitations and requires particle size not more than 3 mm for good liquid yields (Bridgwater et al., 1999). CFB configuration has certain disadvantages related

to non-uniformity in biomass particle residence time, requirement of solid recycling of partially reacted feed and of post treatment of bio-oil to reduce char content due to carryover, high char attrition, ash build-up in circulating solids causing cracking of organic molecules in volatile products and loss of bio-oil yield (Scott et al., 1999). Bubbling Fluidized Bed (BFB) uses same mode of heat transfer to biomass particles as that of CFB, but differs in the contribution of convective and conductive heat transfer. In this process, bio-oil quality is desirable with high concentration of desirable chemicals and minimum carryover of char (micro-carbon) into liquid product. There is also rapid elution of char from the reactor, thereby reducing the chances of volatile cracking (Scott et al., 1999).

### 2.3.6. Physico-chemical properties

There are other parameters such as physical and chemical properties of biomass which can influence the pyrolysis process. With increase in thermal conductivity (0.03- 0.4 W $m^{-1}$ $°C^{-1}$) of biomass, there is an increase in final tar yield and decrease in gas yield, keeping char yield constant with some reduction in conversion time. This is due to increase in rate of heat transfer with increasing thermal conductivity, which consequently increases the flow velocity and reduces the intra-particle residence times and secondary reactions activity (Di Blasi, 1997). Babu and Chaurasia (2004b) determined that an increase in emissivity leads to considerable increase in secondary reaction products at the expense of primary reaction products and also a reduction in pyrolysis time due to increase in temperature inside the biomass particle.

With increase in char permeability, there is a decrease in mass flow resistance and increase in flow velocity causing reduction in secondary reaction activity with increase in tar yield and decrease in gas yield. However, the conversion time is not dependent on char permeability (Di Blasi, 1997). With increase in density, there is a decrease in primary tar yield and increase in char and gas yield because of lower temperatures during primary pyrolysis favouring charring reactions. There is also an increase in conversion time due to lower particle heating rate with increase in density. However, if activity of secondary reactions is considered, the tar yield remains constant because of increase in primary degradation rates or volatiles release

rate with increase in density, ultimately balancing the effect of lower primary degradation front temperature (Di Blasi, 1997).

Increase in specific heat capacity of biomass resulted into larger thermal capacity and higher conversion time. There was a reduction in secondary reaction activity and products with increase in specific heat because of increase in flow velocity and reduction in intra- particle residence time (Di Blasi, 1997). However, Babu and Chaurasia (2004a) found that specific heat capacity does not affect the primary and secondary reaction product yields. Conversion time is also not affected with increase in specific heat capacity as the energetics of secondary reactions are not important (Babu and Chaurasia, 2004a). The char forming reactions are considered exothermic in nature, while tar evaporation as endothermic. The extent of these reactions depend on other operating conditions of the process like pressure and flow rate (Mok and Antal, 1983). It was also observed that cellulose decomposition is considered as endothermic process which prevails at lower conversion (below 300°C),while lignin decomposition as exothermic process which prevails at higher conversion (Koufopanos et al., 1991).

Increase in tar content (Di Blasi, 1996a) and decrease in char content (Di Blasi, 2002) with increasing shrinkage level was mainly because of two reasons: higher temperature at primary reaction front (reaction temperature) causing higher reaction rates for tar formation, and reduction in rate of tar degradation and extension of secondary reaction zone due to reduced volatile residence times. The higher heat transfer rates of the shrinking particle also reduce the pyrolysis or conversion time during biomass degradation (Di Blasi, 2002; Babu and Chaurasia, 2004a). Biomass naturally contains some moisture which exists in two basic forms i.e. bound or hygroscopic water, and free or capillary water. Bound water is bonded to the hydroxyl groups of the major constituents of biomass including cellulose, hemicellulose and lignin. After occupation of all available sites, the medium is at its Fiber Saturation Point (FSP), which is around 30 % of dry weight for different types of wood. The free water (above FSP), however, is present in the liquid form in the lumens or voids of the wood and is held by weak capillary forces (Moghtaderi, 2006). When the biomass pyrolysis is conducted at higher temperatures, the water vapour mixes with the volatiles formed from pyrolysis and flows out of the solid

thereby affecting the heat and mass transfer processes during pyrolysis. With increase in moisture content in biomass, the rise in surface temperature slows down because of energy consumption in evaporation reaction, but at the same time, it can cause some changes in biomass structure leading to changes in porosity, permeability and fluid flow. But overall, increase in moisture content causes increase in pyrolysis time with negligible effect on product yield (Bryden et al., 2002). The combined impact of particle shrinkage and moisture content results in overall increase in pyrolysis time with substantial increase in tar yield and decrease in gas yield for large biomass particles (Bryden and Hagge, 2003).

Di Blasi (2002) studied different external heat transfer correlations (like infinite heat transfer condition, Agarwal's model, Ranz-Marshall and whole-bed correlations), and found that both conversion time and char yield increases with decrease in the value of external heat transfer coefficient. Babu and Chaurasia (2004b) stated that the concentration of volatiles increases with increase in convective heat transfer at lower operating temperatures. Kersten et al. (2005) concluded that an increase in external heat transfer coefficient for smaller particles (1-3 mm) caused a reduction in conversion time with no effect on product yield. However, for larger particles, no significant reduction in conversion time is observed because of change in controlling step from external heat transfer to internal heat transfer due to low thermal conductivity of biomass.

## 2.4. Catalytic pyrolysis

The presence of catalyst during pyrolysis process results into cracking reactions and upgradation of biomass pyrolysis products, depending on different operating conditions. Catalyst type and reactor configuration play an important role in affecting the production of primary products during the pyrolysis process. The primary pyrolysis vapours can also be catalytically cracked over different catalysts to give liquid and gaseous fuels. In particular, oxygenates in the pyrolysis liquids or bio-oil, which are reducing the specific energy content of bio-oil can be reduced using zeolite type catalysts (Yaman, 2004). The application of different catalysts in biomass pyrolysis process and upgradation of pyrolysis products has been studied (Bridgwater, 1996). Few kinetic models were also proposed for analysing the

biomass catalytic pyrolysis and also the catalytic reactions of vapour products formed during the thermal conversion process(Adjaye and Bakhshi, 1995; Lv et al., 2004; Lu et al., 2009).

There are a number of important ways in which catalysts modify pyrolysis processes.

1. Decomposition temperature of biomass components strongly decreases.
2. Catalysts affect network of reaction i.e. deoxygenation and allows in situ upgrading of bio-oil by reducing oxygenated organic compounds. The presence of catalysts also reduces polymerization precursors (like multifunctional phenols) for stabilizing bio-oil.
3. Due to decarboxylation, decarbonization and dehydration reactions, there is release of more CO, $CO_2$ and $H_2O$ when catalysts are employed.
4. Catalysts promote the formation of coke due to dehydration reactions (mainly due to high acidity of catalysts).

The effect of different catalysts on biomass pyrolysis products has been given in Table 2.3.

**Table 2.3:** Effect of different catalysts on biomass pyrolysis products.

| Publication | Catalyst | Biomass | Reactor configuration | Products | Findings |
|---|---|---|---|---|---|
| Comparison of the products from the pyrolysis and catalytic pyrolysis of rice husks (Williams and Nugranad, 2000). | ZSM-5 zeolite | Rice husk | Fluidized bed reactor with condensation and off-line gas analysis system. | Oxygenated oil compounds (such as phenols, cresols) and gaseous products | The oxygen containing species in oils convert into $H_2O$, CO and $CO_2$ in presence of catalysts. Increase in aromaticity of the oil compounds due to catalytic activity. Also, the heavy oxygenated compounds in the oil convert into lower molecular weight oxygenated species. |

| | | | | | |
|---|---|---|---|---|---|
| Yields of hydrogen-rich gaseous products via pyrolysis from selected biomass samples(Demirbas, 2001). | $ZnCl_2$, $Na_2CO_3$ and $K_2CO_3$ | Cotton cocoon shell, tea factory waste, olive husk | Stainless steel cylindrical reactor with electrically heated tubular furnace | Gaseous products (CO, $CO_2$, Olefins, $O_2$, $H_2$ , paraffins), liquid and char | Gas yield increases with temperature. $H_2$-rich gaseous products increase with $ZnCl_2$, but pyrolytic gas decreases. $Na_2CO_3$ is better for cotton coccon shell and tea waste than $K_2CO_3$. |
| Catalytic Pyrolysis of Biomass for hydrogen rich fuel gas production (Chen et al., 2003). | $Cr_2O_3$, and some metal oxides (MnO, FeO, $Al_2O_3$, CaO, CuO) | Rice straw, sawdust | Batch pyrolysis assembly- reactor part ( pyrolysis reactor, cracking reactor and heating furnace), condenser and purification part (condenser and dryer) and gas storage part (gas tank or water tank) | Gaseous products ($H_2$ containing gas, $CO_2$, CO), tar, water and char | $Cr_2O_3$ is better than other metal oxides for total as well as $H_2$ containing gas yield. |

| | | | | | |
|---|---|---|---|---|---|
| Kinetic Description of the Catalytic Pyrolysis of Biomass in a conical spouted bed reactor (Atutxa et al., 2005). | HZSM-5 Zeolite | Sawdust | Conical spouted bed reactor with water condensers and filter in downstream | Gas, liquid (light and heavy fraction), and char | With increase in catalyst mass, yield of gas increases, while liquid decreases notably with slight decrease in amount of char. Decarboxylation, decarbonylation and dehydration reactions dominate the process producing $CO_2$, CO, $H_2O$ and coke. Bio-oil is more stable than liquid from thermal pyrolysis and can easily be used for further processing such as steam reforming. |

| | | | | | |
|---|---|---|---|---|---|
| Catalytic Fast Pyrolysis of Biomass in a Fluidized Bed with Fresh and Spent Fluidized Catalytic Cracking (FCC) Catalysts (Zhang et al., 2009b). | Fresh (FC)and Spent (SC) FCC | Corncob | Fluidized bed reactor with condensers, filters, gas collection bag. | Gas, liquid and char | FC and SC remarkably decreases the oil fraction, while increase water, coke and non-condensable gas yield. Catalyst with strong acidity should be avoided for higher oil fraction and less coke. Most of oil fraction is light oil fraction, with reduced multifunctional components of phenols (polymerization precursors). |
| Comparison of non-catalytic and catalytic fast pyrolysis of corncob in a fluidized bed reactor (Zhang et al., 2009a). | HZSM-5 zeolite | Corncob | Fluidized bed reactor with condensers, filters, gas collection bag. | Gas, liquid and char | HZSM-5 catalyst considerably decreases the oil yield, while increase water, coke and non-condensable gas yield. The $O_2$ content in heavy oil fraction converts mainly to CO, $CO_2$ and $H_2O$. And there is an increase in aromatic hydrocarbons in oil content due to presence of catalyst. |

| | | | | | |
|---|---|---|---|---|---|
| Catalytic pyrolysis of biomass for biofuels production (French and Czernik, 2010). | Nickel, Cobalt, Iron, and Gallium-substituted ZSM-5 | Cellulose, lignin and wood | Tubular quartz micro-reactor and a semi-continuous flow reactor | Hydrocarbons, oxygenates such as phenol and cresol, and coke | The substituted catalysts are better than conventional catalysts for higher hydrocarbon yield. The deoxygenation activity reduces with time due to deposition of coke on catalyst, leading to catalyst regeneration after certain period of cracking process. |

### 2.4.1. Biochar catalytic effect

In biomass pyrolysis, the intra-particle secondary reactions can occur both homogeneously in gas phase as well as heterogeneously on solid char matrix, and the extra-particle secondary reactions in reactor environment can include vapour phase cracking as well as heterogeneous conversion on the surface of biomass derived chars (Di Blasi, 2008). There are natural catalysts in biomass which substantially influence the production of products during pyrolysis process (Babu and Chaurasia, 2003). The presence of metallic minerals in biomass contributes to change in outlet composition of pyrolyis products for given operating conditions (Nik-Azar et al., 1997). Boroson et al. (1989a) found that tar formed by primary pyrolysis of wood is very reactive in the presence of wood char causing formation of gaseous components and char (or coke). Di Blasi (1993a) and Grønli and Melaaen (2000) examined the conversion of tar into char molecules due to a repolymerization step during the biomass particle degradation. Bridgwater et al. (1999) also determined that the hot char is catalytically active and favours the cracking of vapours during fast pyrolysis process. The experiments were conducted for studying tar cracking using biomass char as a catalyst in different temperature ranges and it was concluded that both char and thermal cracking are responsible for conversion of tar into gas, secondary tar and char (Abu El-Rub et al., 2008; Gilbert et al., 2009). With these studies (Abu El-Rub et al., 2008; Gilbert et al., 2009), it was also found that pore structure of char particle and mineral content are the important factors for biomass char activity towards tar conversion through gasification and polymerization reactions. Experimental studies were performed to analyse the low temperature catalytic cracking effect of char on biomass pyrolysis (Shen and Zhang, 2005) and oil refinery products (Zhang et al., 2008a). The catalytic activity of biochar was compared with other conventional catalysts for tar reduction, and the *in-situ* cracking of tar compounds during biomass conversion in a biochar bed was also investigated (Abu El-Rub, 2008). Based on this study (Abu El-Rub, 2008), it was found that biochar is a very promising catalyst for solving the tar utilization problems in gasification systems and there is requirement to perform more experimental and modelling studies in this direction.

## 2.5. Summary

Modelling has emerged as a powerful tool for studying the pyrolysis of biomass. A number of mathematical and CFD modelling studies have been conducted for understanding the effect of different operating conditions such as biomass composition, particle size, reactor temperature, and residence time of volatiles. The models have been developed at different scales, i.e., kinetic, particle and reactor, for analysing the parameters such as reaction mechanism, mixing/segregation behaviour of different phases and heat and mass transfer rates required for simulation of the complete process in a large scale reactor. Studies have also been carried out for catalytic cracking of biomass and catalytic upgrading of bio-oil for making its appropriate use as a source of energy in industries using pyrolysis process.

There is, however, uncertainty over the ability of current biomass pyrolysis models for analysing product yields in different reactor configurations. For example, the kinetic parameters of the models of biomass primary degradation and secondary tar cracking reactions are not able to accurately predict the pyrolysis rate for different biomass samples. Furthermore, the effects of biochar activity on secondary tar cracking mechanism inside the particle as well as in reactor environment have not been adequately discussed in these models. Similarly, the particle scale models are not able to account for the overall impact of different operating parameters such as drying and particle shrinkage with change in thermo-physical properties of biomass on the degradation mechanism. This has resulted in inconsistencies in predicting the heat and mass transfer rates inside the biomass particle leading to incorrect analysis of the rate of biomass conversion during thermo-chemical decomposition. Finally, the reactor scale models proposed for studying the biomass degradation in different reactor configurations do not clearly examine the effect of above parameters and biochar *in-situ* catalytic activity for considerable volatiles and solids residence times inside the reactor.

Therefore, considerably more research and development efforts are needed to develop industrial reactor models for accurate analysis of process parameters affecting the product yields. A comprehensive particle scale model needs to be formulated by considering the overall effect of process parameters such as drying, shrinkage and the biochar catalytic activity. A reactor scale model also needs to be

developed for analysing the effect of operating conditions such as particle size and density on the behaviour of different phases in the reactor and on the production rate during the biomass decomposition in presence of volatiles and other inert solids. Multi-scale modelling and experimental studies are required to accurately analyse the tar cracking mechanisms in the presence of different catalysts, and to examine the *in-situ* catalytic effect of biochar on the product yields.

## 2.6. Research direction

In this study, a multi-scale model has been developed for analysing the biomass pyrolysis process. This model has been used to analyse the reactive multi-phase behaviour of biomass with other solid and gaseous phases inside the fluidized bed reactor. The models at different scales have been systematically integrated for application to industrial scale pyrolysis process as shown in Figure 2.16.

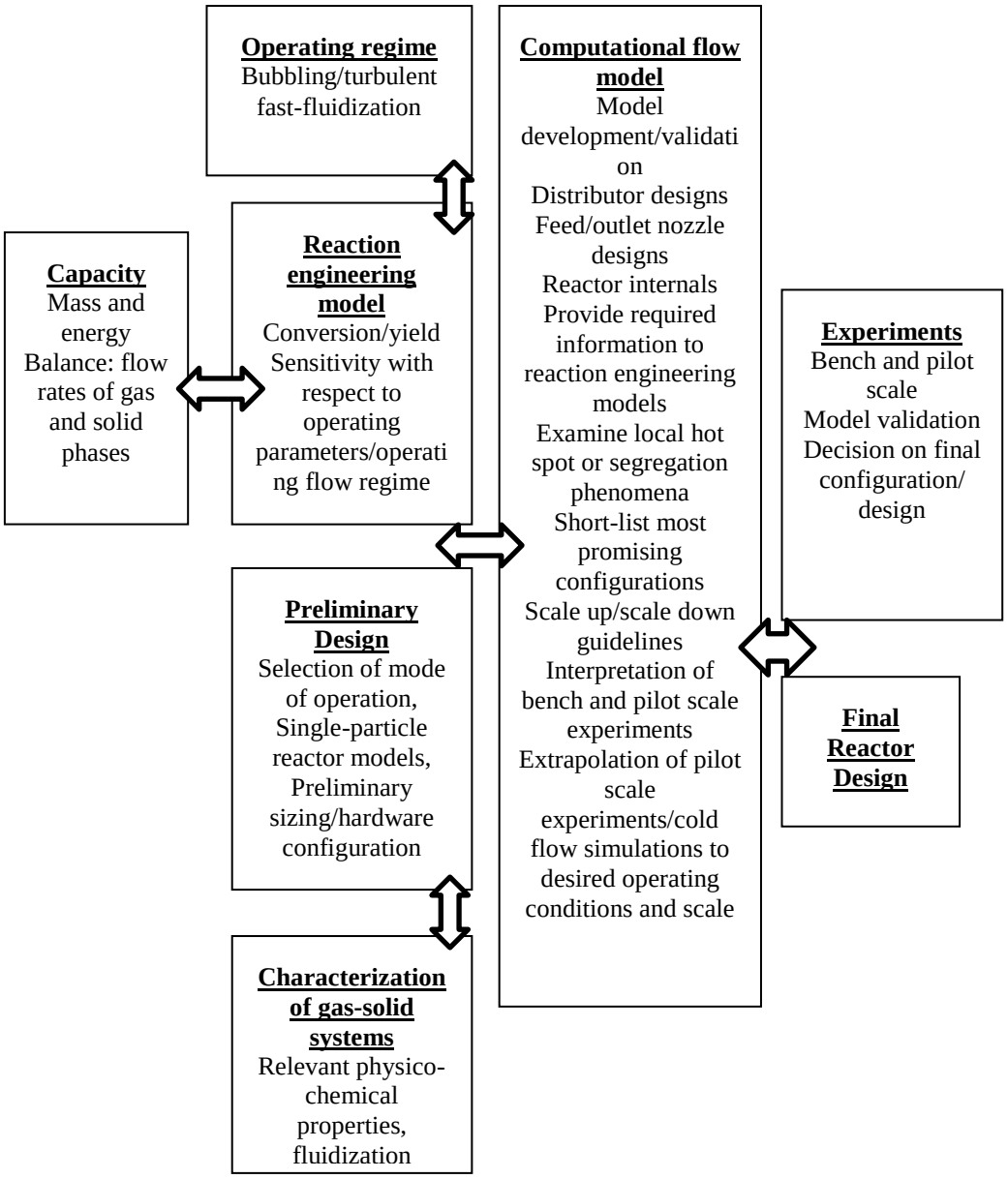


**Figure 2.16:** Modelling mechanisms for fluidized bed reactors (Ranade, 2002).

### 2.6.1. Methodology

For modelling the biomass pyrolysis in a fluidized bed reactor and analysing the effect of operating conditions in the reactor environment, it is required to design a multi-scale model for this process. In this study, the modelling has been conducted at three different scales as shown in Figure 2.17.

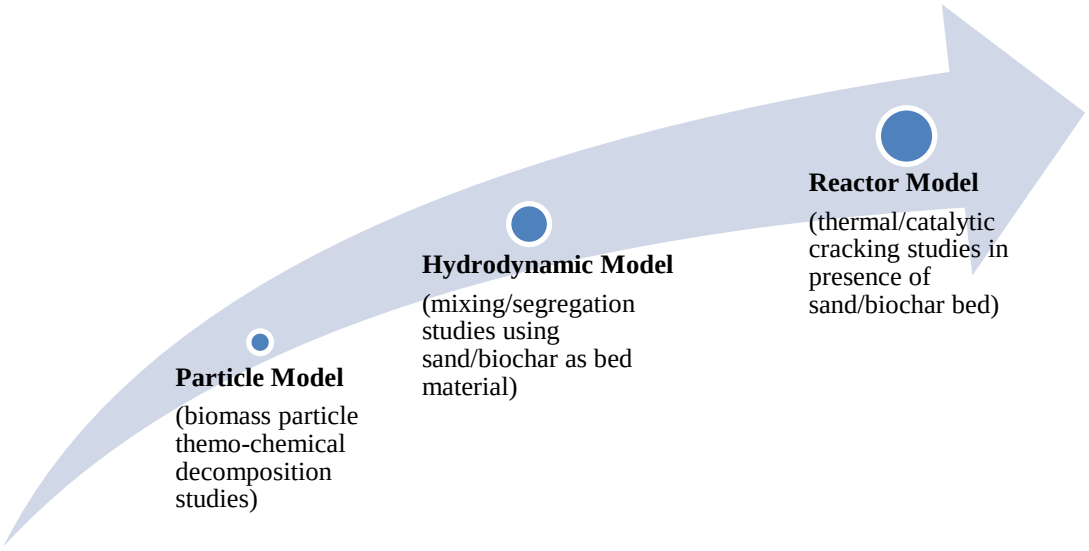


**Figure 2.17:** Models required for the biomass pyrolysis in a bubbling fluidized bed.

### 2.6.2. Approach

In Chapter 3, a phenomenological model has been developed for studying the thermo-chemical decomposition of a biomass particle in inert gas environment. The degradation mechanism was proposed by considering the lumped kinetic model for primary decomposition of biomass as well as the secondary cracking reactions of tar components homogeneously in gas phase and heterogeneously on catalytically active sites of biochar particles produced during the pyrolysis process. The particle model considered the combined effect of different operating parameters, such as particle drying, shrinkage, and change in thermo-physical properties during pyrolysis. The modelling results for different particle sizes and operating temperatures were compared with experimental data for biomass conversion time.

The hydrodynamic behaviour of biomass particles in a bubbling fluidized bed has been studied in Chapter 4. A CFD model for analysing the mixing/ segregation of biomass and biochar particles in the bubbling fluidized bed was developed. Due to lack of experimental data for biomass-biochar mixture, the results were first compared with literature data for biomass-sand mixture. After model validation, the model was extended for analysing the effect of operating parameters such as superficial gas velocity, particle density and diameter on mixing/segregation behaviour. The effect of modelling parameters such as restitution coefficient and drag correlations on bed hydrodynamics was also examined.

The particle and hydrodynamic models were combined for analysing the continuous thermo-chemical degradation of biomass particles in a bubbling fluidized bed reactor in Chapter 5. This CFD model was used to study the combined effect of reaction mechanism, heat and mass transfer and reactor hydrodynamics on product yield and behaviour of biomass decomposition. Due to lack of experimental data for biomass pyrolysis in presence of biochar bed, the model was first compared with the literature data for pyrolysis product yields from an inert sand bed. After model validation, the simulation results in both the sand and biochar bed were analysed to determine the effect of operating parameters such as superficial gas velocity, particle size and reactor temperature on the product yields.

The integration of the particle and hydrodynamic model to formulate the multi-scale biomass pyrolysis model is shown in Figure 2.18.

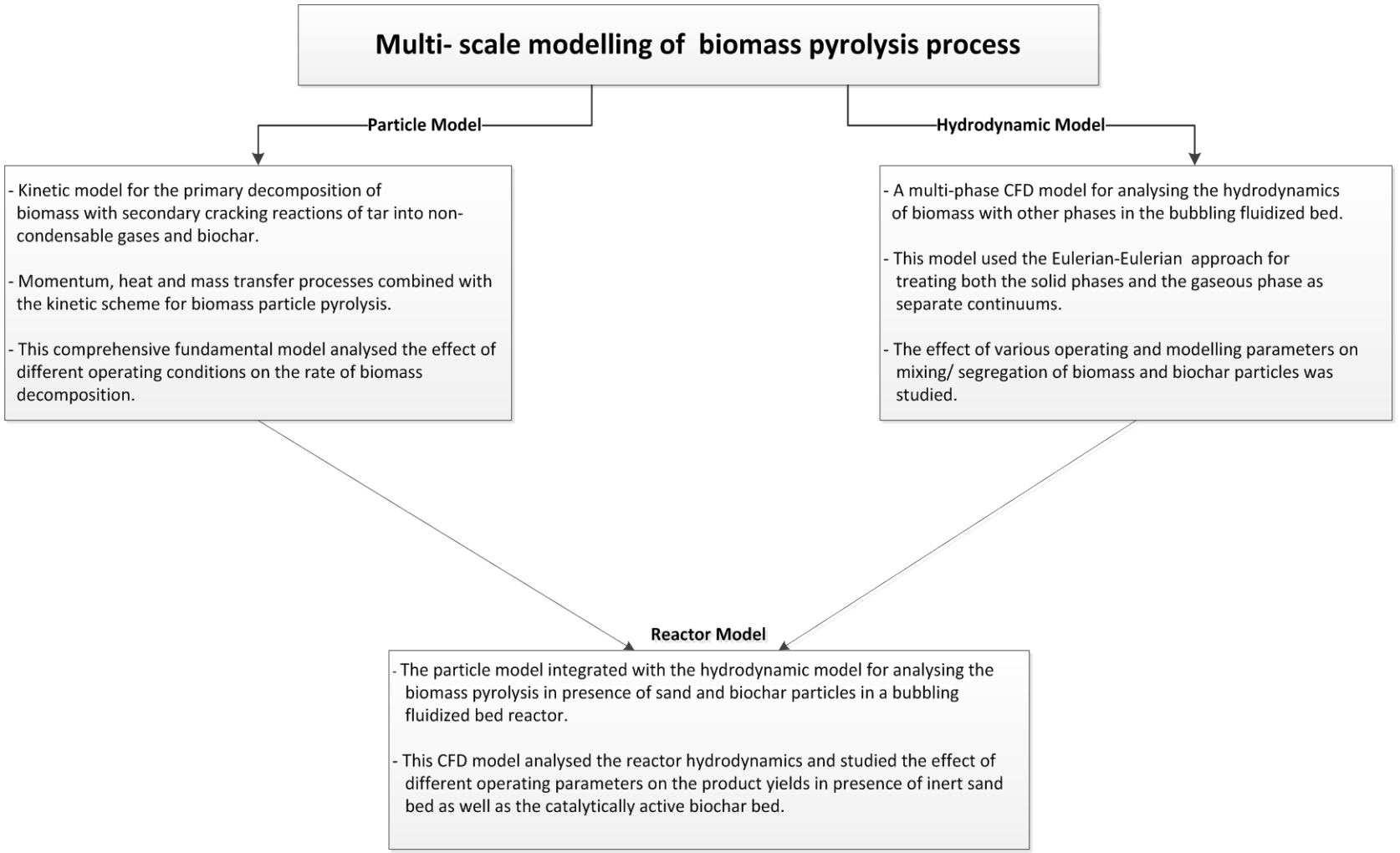


**Figure 2.18:** Scheme for designing the multi-scale biomass pyrolysis model.

# Chapter 3 Phenomenological modelling of biomass pyrolysis processes

Due to the increasing applications of biomass pyrolysis for value added products formation, several modelling studies have been reported in the literature. Thurner and Mann (1981) developed a model for investigating the kinetics of gas, char and tar formation from the pyrolysis of wood. Di Blasi and Branca (2001) found that variation in the product yields and kinetic rates was mainly because of the effect of different heating rates, operating temperatures and experimental setups. In Liden et al. (1988) model, the wood or other biomass decomposes according to two parallel reactions yielding gas with char, and liquid tar which further decomposes by secondary homogeneous reactions into gaseous products. Some more studies had been undertaken for analysing the secondary tar cracking reactions during biomass pyrolysis (Boroson et al., 1989b; Font et al., 1990; Fagbemi et al., 2001; Morf et al., 2002; Baumlin et al., 2005).

For studying the dynamics of pyrolysis process, different models (Kansa et al., 1977; Chan et al., 1985; Koufopanos et al., 1991; Di Blasi, 1993b) have been proposed for understanding transport phenomena with chemical kinetics inside biomass particle. Di Blasi (1996a) proposed a transport model for studying the effect of particle shrinkage on pyrolysis. Some assumptions such as negligible moisture content and no condensation of tar species inside the particle were also taken into account. Bryden and Hagge (2003) analysed the pyrolysis of a moist, shrinking biomass particle in their model. The authors combined the impact of moisture and particle shrinkage on pyrolysis times and product yields were taken into account. Although this model included the effect of shrinkage due to char, it ignored the shrinkage due to the volume occupied by volatiles (Di Blasi, 1996a). Park et al. (2010) studied the degradation mechanism of wood at different temperatures for analysing the endo/exothermicity of the reactions and the effect of pressure generation on particle structure. However, this model did not account for particle shrinkage and diffusive flux for gaseous species. Lu et al. (2010) proposed a model for studying the effect of particle shape and size on the rate of biomass devolatilization. Peters (2011) developed a model for analysing the decomposition rate of different biomass

samples during pyrolysis. However, these models (Lu et al., 2010; Peters, 2011) did not include the effect of particle shrinkage and drying during the pyrolysis.

Although there were currently several models for pyrolysis of biomass particles for predicting the rate of biomass degradation and product yields, most of these models cannot predict the combined effect of all the physical and chemical processes such as moisture content and particle shrinkage. Furthermore, any change in thermo-physical properties of biomass during pyrolysis and catalytic effect of biochar on tar cracking reactions has not been explicitly considered. In this study, a comprehensive model for pyrolysis of biomass particle has been developed, which not only considers the combined impact of process parameters but also includes the catalytic effect of biochar on reaction mechanism.

## 3.1. Model description

In order to develop a comprehensive model for the pyrolysis of biomass particles, kinetic models for both primary decomposition of biomass and secondary tar cracking reactions as well as momentum, mass and energy balances for biomass degradation were included in the model.

### 3.1.1. Kinetic Model

For the kinetics of reactions, a two-stage reaction model has been proposed by considering biomass as a single homogeneous species instead of a mixture of different components like cellulose, hemicellulose and lignin. During this thermo-chemical degradation, biomass actually decomposes into various products by a large number of independent parallel reactions. However, for this study, the reaction products have been lumped into three major classes: gases also known as Non-condensable gas (NCG), high molecular weight organic liquid called as tar (primary and secondary), and a solid residue named as char or biochar (also contains metals/minerals and some amount of ash).

Any increase in temperature favours dehydration and chain cleavage (like decarboxylation, decarbonylation) reactions of solid biomass, which leads to formation of char, light gases and some amount of water. This also causes the

reduction in degree of polymerization of biomass, which further leads to formation of volatiles or primary tar by biomass depolymerization reactions.

The primary tar is mainly comprised of a reactive mixture of oxygenated hydrocarbon compounds, which undergoes reactions such as cracking, partial oxidation and re-polymerization homogeneously (in vapour phase) as well as heterogeneously (adsorption on active sites of biochar matrix/surfaces) at higher temperatures. The major products of these reactions are gaseous components and aromatic secondary tars (Mono-aromatic and Poly-aromatic hydrocarbons) with some amount of water. This step is based on analysis of homogeneous and heterogeneous primary tar cracking reactions, where the secondary cracking of tar inside the particle results into gaseous products and secondary aromatic tar in temperature range of 227 to 827°C (Chan et al., 1985). In a further experimental study, decomposition of sewage sludge at higher temperatures and longer gas residence times in fluidized bed reactor led to increase in non-condensable gases and change in structure of oil compounds due to tar cracking reactions (Shen and Zhang, 2003).

The aromatic secondary tar also reacts heterogeneously and leads to formation of char by re-polymerization reactions at higher temperatures. This step is based on analysis for aromatic tar reactions on catalytic char surfaces. It has been reported in the literature (Wu et al., 2005; Sun et al., 2007; Zhang et al., 2008a; Zhang et al., 2008b) that surfaces of various carbonaceous materials can catalyse the decomposition of hydrocarbons. Based on the experiments performed in temperature range of 400 - 600°C, it was found that tar formed by primary pyrolysis of wood is reactive in the presence of wood char causing formation of gaseous components and char (Boroson et al., 1989a). The kinetic parameters for the conversion of tar into char by re-polymerization step inside the biomass particle was also calculated (Di Blasi, 1993a). Hence, it has been deduced that the biochar in the biomass pyrolysis process can catalyse the further decomposition of the tarry products *in-situ*.

The kinetic reactions for biomass pyrolysis are shown in Figure 3.1. The primary thermal decomposition of biomass (hemicellulose, cellulose and lignin degradation) leads to formation of gases, primary tar and char (reaction 1, 2 and 3 with kinetic constant $K_1$, $K_2$ and $K_3$, respectively). Based on earlier theoretical and experimental

analysis (Chan et al., 1985; Di Blasi, 1993a; Lu et al., 2010) of these decomposition reactions, they have been considered first order in nature with respect to biomass concentration. The homogeneous and heterogeneous cracking of primary tar, inside the particle and in reactor environment, causes formation of gases and aromatic secondary tar (reaction 4 and 5 with kinetic constant $K_4$ and $K_5$, respectively); and further heterogeneous cracking of highly aromatic secondary tar leads to production of char (reaction 6 with kinetic constant $K_6$). Similar to primary biomass decomposition, the secondary tar cracking reactions depend on operating parameters such as temperature. However, there are other parameters such as vapour/gas residence time and available catalytically active sites which affect these reactions. The secondary tar cracking reactions were also considered to be of first order in nature with respect to primary and secondary tar concentration.

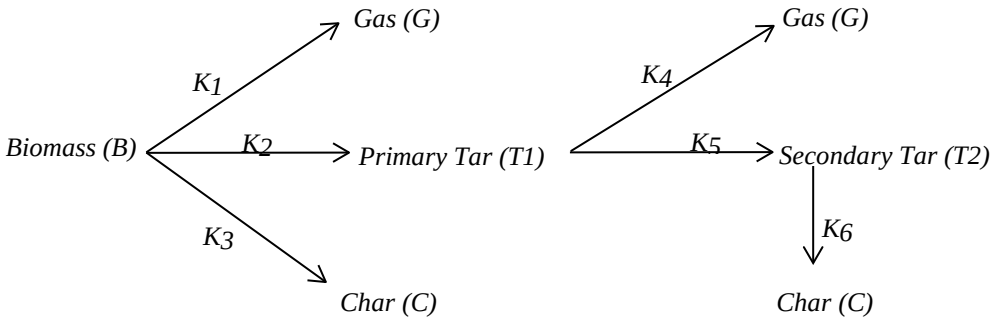


**Figure 3.1:** Proposed kinetic model for biomass degradation mechanism.

During thermal decomposition of biomass, the primary step of gas, tar and char formation requires heat energy for bond breaking reactions, and hence, they are endothermic in nature. The secondary tar cracking liberates some amount of energy due to oxidation reactions, and thus, they are slightly exothermic (Koufopanos et al., 1991). The values of kinetic constants in terms of Arrhenius parameters and heat of reactions required during particle modelling have been given in Table 3.2 and Table 3.3, respectively.

### 3.1.2. Particle Model

A single particle model has been developed for studying transport phenomena with reaction kinetics inside the biomass particle. This model considered the heat and mass transfer effects due to formation of temperature and concentration gradients

inside particle during decomposition. The model also included the effect of particle drying and shrinkage on biomass pyrolysis as a function of thermo-physical properties of biomass during degradation. For deriving the conservation equations, the following assumptions were made:

1. One dimensional time dependent domain.
2. Local thermal equilibrium (no temperature gradient) between vapour and solid phase.
3. Re-condensation of volatiles in cooler regions of the particle was not taken into account because of higher permeability of char as compared to solid biomass.
4. The volatile or gas phases were assumed to follow ideal gas conditions.
5. The kinetic and potential energies of particle were neglected.
6. The heat of reactions for NCG and secondary tar formation by primary tar were considered equal.
7. Particle shape did not change during the degradation process, i.e., cracking or fragmentation was not considered.

The presence of moisture inside particle affects various physical and chemical processes during the decomposition. Moisture content remains mainly as chemically bound water on available absorption sites in biomass or as free water within the pores held by weak capillary forces (Moghtaderi, 2006). Particle drying is an important phenomenon during pyrolysis and governs the rate of mass and heat transfer inside the particle. There are different schemes proposed for considering drying process inside the particle (Bryden et al., 2002). The kinetic scheme proposed by Chan et al. (1985) was utilized in this model for conversion of moisture (*M*) present in particle to water vapour (*W*). According to this scheme, water vapour produced during drying is proportional to amount of moisture present inside the particle. This reaction step includes both water of evaporation as well as water of dehydration. This is quite a simplified and numerically stable scheme, and will lump all the physical processes during drying into a single chemical reaction with kinetic constant $K_{vap}$ (given in Table 3.2).

Particle shrinkage is an important physical phenomenon of degradation mechanism. With decrease in particle size during the process, temperature gradient as well as

residence time of volatiles inside particle is reduced (Babu and Chaurasia, 2004a), which eventually affects the rate of primary decomposition and secondary tar cracking reactions (Di Blasi, 2002). Different schemes such as Shrinking Core Model and Progressive Conversion Model were proposed for considering the particle shrinkage (Kunii and Levenspiel, 1991). In the current model, the shrinkage was assumed to be equal to the fraction of the solid which was devolatilized. This was achieved by treating the total particle volume to be a function of the mass of the biomass, moisture and char, and calculating any change in the "solid" volume of the particle both due to conversion of biomass and vaporization of moisture into pyrolysis products (equation 3.1). However, the particle diameter was treated as constant throughout the process in the model.

$$V = V_0 + \frac{(m_B + m_M) - m_{B,0}}{m_{C,f} - m_{B,0}} (V_f - V_0) \quad (3.1)$$

here the subscript 0 stands for initial state (at start of pyrolysis process) and *f* stands for final state (at end of process). $m_B$ , $m_M$ and $m_C$ are the mass of biomass, moisture and biochar at any time *t* during the process, respectively.

Figure 3.2 shows the mechanism for decomposition of a moist shrinking biomass particle.

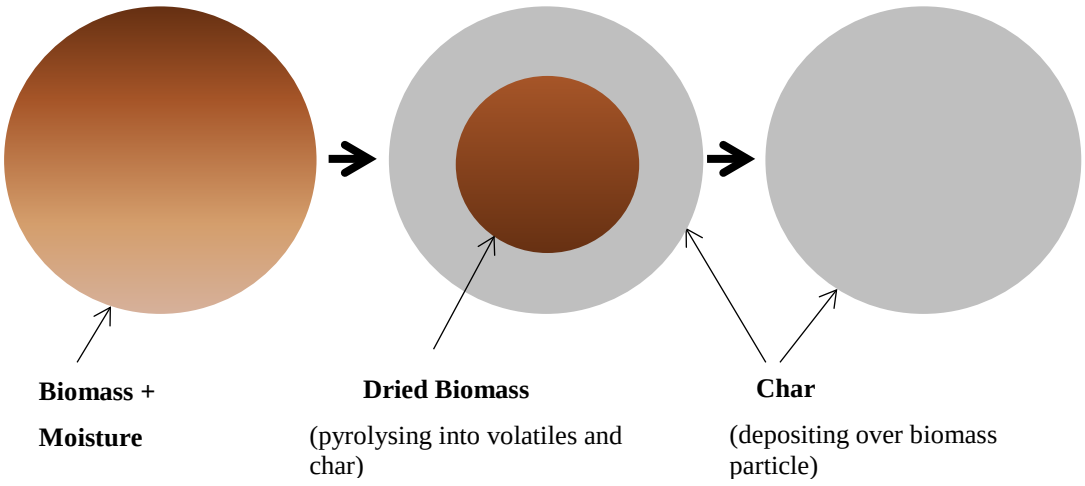


**Figure 3.2:** Schematic for showing decomposition progress in a moist shrinking biomass particle.

Biomass particle acts as a porous medium which allows outflow of vapour products during the pyrolysis process. Conservation of momentum (equation 3.2) in this medium has been given according to modified relationship of Joseph et al. (1982). In

this expression, time derivative of velocity has been neglected because it is barely affecting convection studies due to high kinematic viscosity in comparison to permeability to characteristic time of the process inside porous medium. Also, nonlinear drag due to inertial effects has been considered small and hence, replaced with a quadratic drag term.

$$\nabla P = -\left(\frac{\mu}{\beta} v + C_{fd}\, \beta^{-1/2} \rho_v |v| v\right) \tag{3.2}$$

where $\mu$ is the viscosity of vapour phase, $\beta$ is the permeability of porous solid medium [see Appendix A.1.], $C_{fd}$ is form- drag constant (value taken as 0.55), $v$ is the vapour phase velocity in porous medium and $\nabla P$ is the pressure gradient across the medium. In this model, the vapour conditions were calculated using ideal gas equation of state (equation 3.3).

$$P = \rho_v R_{gc}\, T / M_v \tag{3.3}$$

here $\rho_v$ is the density of the vapour phase, $M_v$ is the molecular weight of the vapour phase, $P$ is pressure inside the particle, $T$ is temperature inside the particle and $R_{gc}$ is universal gas constant.

In this model, a total of eight species have been included for mass balance, these being: biomass, non-condensable gases, primary tar, secondary tar, char, moisture, water vapour and inert gas (such as nitrogen or helium). The mass balance equations are developed for all of these species (equation 3.4-3.6 for solid phases and 3.10-3.14 for vapour phases) including proposed kinetic model and mechanism for evaporation of moisture during the drying of biomass particles.

For solid phase, there are no convective and diffusive transport terms for mass balance. Therefore, the conservation equations for biomass, char and moisture (equation 3.4-3.6) are given in terms of source term or rate of production/consumption only.

$$\frac{\partial(\rho_B V)}{\partial t} = -(K_1 + K_2 + K_3)\, \rho_B V \tag{3.4}$$

$$\frac{\partial(\rho_C V)}{\partial t} = K_3 \rho_B V + K_6 \varepsilon \rho_{T2} V \tag{3.5}$$

and, $$\frac{\partial(\rho_M V)}{\partial t} = -K_{vap} \rho_M V \tag{3.6}$$

where the left side term of equations 3.4-3.6 is accumulation term for solid phases. Here, $\varepsilon$ is porosity or particle voidage [see Appendix A.1.].

For vapour phase, the conservation equations for all species expressed in this generalized form:

$$\left[\frac{\partial\,(\varepsilon\rho_i)}{\partial t} + \nabla.(\varepsilon\rho_i\,\vec{v}) = -\nabla\vec{J}_i + R_i\right] \tag{3.7}$$

where first and second term on left side of equation refers to accumulation and convective transport due to bulk flow, respectively. Whereas first and second term on right side refers to diffusive transport due to concentration gradient and contribution due to chemical reactions (source term), respectively. Here, $\rho_i$ is density, $R_i$ is rate of production/ consumption by chemical reaction and $\vec{J}_i$ is diffusion flux of $i^{th}$ species in vapour phase given as:

$$\vec{J}_i = -\varepsilon D_{eff,i}\nabla\rho_i - D_{T,i}\frac{\nabla T}{T} \tag{3.8}$$

where $D_{eff,i}$ is effective diffusion coefficient [see Appendix A.2.] and $D_{TH,i}$ is thermal (soret) diffusion coefficient of $i^{th}$ species. For one-dimensional particle domain considered for our model, equation 3.7 becomes:

$$\left[\frac{\partial\,(\varepsilon\rho_i)}{\partial t} + \frac{\partial(r^n\varepsilon\rho_i\,v_r)}{r^n\partial r} = \frac{\partial\left(r^n\varepsilon\,D_{eff,i}\frac{\partial\rho_i}{\partial r}\right)}{r^n\partial r} + R_i - \frac{\varepsilon\rho_i}{V}\frac{\partial V}{\partial t}\right] \tag{3.9}$$

The contribution of thermal diffusion is negligible in diffusion flux as compared to molecular diffusion; hence it was neglected (equation 3.9). The last term on right side accounts the effect of volumetric shrinkage of particle on component diffusion. Here *n* is 0 for flat plate or slab shaped particle, 1 for cylindrical particle, and 2 for spherical particle. $v_r$ is the vapour phase velocity in one-dimensional particle domain, which is calculated using equation 3.2.

Hence, for Non-condensable Gases (*G*), the mass conservation equation given as:

$$\frac{\partial\,(\varepsilon\rho_G)}{\partial t} + \frac{\partial(r^n\varepsilon\rho_G\,v_r)}{r^n\partial r} = \frac{\partial\left(r^n\varepsilon D_{eff,G}\frac{\partial\,\rho_G}{\partial r}\right)}{r^n\partial r} + K_1\rho_B + K_4\varepsilon\rho_{T1} - \frac{\varepsilon\rho_G}{V}\frac{\partial V}{\partial t} \tag{3.10}$$

Similarly, for Primary Tar (T1):

$$\frac{\partial\,(\varepsilon\rho_{T1})}{\partial t}+\ \frac{\partial(r^n\varepsilon\rho_{T1}\,v_r)}{r^n\partial r}=\ \frac{\partial\left(r^n\varepsilon D_{eff,T1}\frac{\partial\rho_{T1}}{\partial r}\right)}{r^n\partial r}+\ K_2\rho_B\ -\ (K_4+K_5)\varepsilon\rho_{T1}\ -\ \frac{\varepsilon\rho_{T1}}{V}\frac{\partial V}{\partial t}$$

(3.11)

For Secondary Tar (T2):

$$\frac{\partial\,(\varepsilon\rho_{T2})}{\partial t}+\ \frac{\partial(r^n\varepsilon\rho_{T2}\,v_r)}{r^n\partial r}=\ \frac{\partial\left(r^n\varepsilon D_{eff,T2}\frac{\partial\,\rho_{T2}}{\partial r}\right)}{r^n\partial r}+\ K_5\varepsilon\rho_{T1}\ -\ K_6\varepsilon\rho_{T2}\ -\ \frac{\varepsilon\rho_{T2}}{V}\frac{\partial V}{\partial t}$$

(3.12)

For Water Vapour (W):

$$\frac{\partial\,(\varepsilon\rho_W)}{\partial t}+\ \frac{\partial(r^n\varepsilon\rho_W\,v_r)}{r^n\partial r}=\ \frac{\partial\left(r^n\varepsilon D_{eff,W}\frac{\partial\,\rho_W}{\partial r}\right)}{r^n\partial r}+\ K_{vap}\,\rho_M-\ \frac{\varepsilon\rho_W}{V}\frac{\partial V}{\partial t}\qquad(3.13)$$

and, for Inert Gas (I):

$$\frac{\partial\,(\varepsilon\rho_I)}{\partial t}=\ \frac{\partial\left(r^n\varepsilon D_{eff,I}\frac{\partial\,\rho_I}{\partial r}\right)}{r^n\partial r}-\ \frac{\varepsilon\rho_I}{V}\frac{\partial V}{\partial t}\qquad(3.14)$$

For inert gas (equation 3.14), convective flow inside the particle was considered negligible. There is only diffusive flow which governs mass transfer inside the particle.

Based on mass balance equations of vapour phase components (equation 3.10-3.14), the overall continuity equation for vapour phase given as:

$$\frac{\partial(\varepsilon\rho_v)}{\partial t}+\ \frac{\partial(r^n\varepsilon\rho_v\,v_r)}{r^n\partial r}=K_1\rho_B+K_2\rho_B-\ K_6\varepsilon\rho_{T2}\ +\ K_{vap}\rho_M-\ \frac{\varepsilon\rho_v}{V}\frac{\partial V}{\partial t}\qquad(3.15)$$

For porous biomass particle, the energy balance is given by combining both vapour phase and solid phase in a single conservation equation. The generalized form of this equation is:

$$\left[\frac{\partial}{\partial\mathrm{t}}\left(\varepsilon\rho_vE_v+\ \rho_s\,E_s\right)+\ \nabla.\{\varepsilon\vec{v}(\rho_vE_v+P)\}=\ \nabla.\left(k_{eff}\nabla T-\ \sum_i h_i\,J_i-\ \tau_{eff}.\vec{v}\right)+\ S_R\right]\qquad(3.16)$$

The first and second term on left side of equation 3.16 corresponds to enthalpy accumulation and energy flow due to convective transport, respectively. Whereas, the first term on right side represents the energy contribution due to conduction. Here, $k_{eff}$ is the effective thermal conductivity of the medium, $E_v$ is the total fluid medium energy, $E_s$ is the total solid medium energy due to thermal inertia of solid

medium, and $S_R$ is the heat of chemical reactions or any other volumetric heat source [see Appendix A.3., A.4. and A.5.]. $\sum_i h_i J_i$ is the energy transfer due to species diffusion and $\tau_{eff}.\vec{v}$ is the energy transfer due to viscous dissipation. In our model, the energy transfer due to species diffusion and viscous dissipation were considered negligible.

The overall energy conservation equation in terms of specific enthalpies and species concentration is given as:

$$\frac{\partial[\varepsilon(\rho_G h_{Gv}+\rho_{T1}h_{T1v}+\rho_{T2}h_{T2v}+\rho_W h_{Wv}+\rho_I h_{Iv})+(\rho_B\ h_{Bs}+\rho_C\ h_{Cs}+\rho_M\ h_{Ms})]}{\partial t}+$$

$$\frac{\partial[r^n \varepsilon v_r(\rho_G h_{Gv}+\rho_{T1}h_{T1v}+\rho_{T2}h_{T2v}+\rho_W h_{Wv})]}{r^n \partial r}=\frac{\partial\left(r^n k_{eff}\frac{\partial T}{\partial r}\right)}{r^n \partial r}-\{(K_1\Delta H_1+K_2\Delta H_2+$$

$$K_3\Delta H_3)\rho_B\ +\ (K_4\Delta H_4+K_5\Delta H_5)\varepsilon\rho_{T1}\ +(K_6\Delta H_6)\varepsilon\rho_{T2}\ +\ \left(K_{vap}\Delta H_{vap}\right)\rho_M\ \}-$$

$$\left[\frac{\{\varepsilon(\rho_G h_{Gv}+\rho_{T1}h_{T1v}+\rho_{T2}h_{T2v}+\rho_W h_{Wv}+\rho_I h_{Iv})+(\rho_B\ h_{Bs}+\rho_C\ h_{Cs}+\rho_M\ h_{Ms})\}}{V}\frac{\partial V}{\partial t}\right] \qquad (3.17)$$

Here, $h_{iv}$ and $h_{is}$ are specific enthalpies of $i^{th}$ species in vapour and solid phases, respectively [see Appendix A.4.]. In this equation, the last term on right side represents the effect of particle shrinkage on the total energy (both vapour and solid phase enthalpies) during thermal degradation of biomass. The energy accumulation due to pressure forces inside the particle were considered to be negligible, and therefore, not taken into account.

### 3.2. Numerical Solution

The momentum, mass and heat balance equations were solved using PDE (partial differential equation) solver *pdepe* of MATLAB 7.0, which solves the initial-boundary value problems for systems of parabolic and elliptic PDEs in the one space variable *r* and time *t*. The solver converts the PDEs to ODEs (ordinary differential equation) using a second-order accurate spatial discretization based on a specified grid size. The time integration of ODEs was completed using the differential-algebraic equation solver of MATLAB. The matlab code is provided in Appendix A.8.

### 3.2.1. Initial and Boundary Conditions

At time $t = 0$, the biomass particle was non - reacting. Therefore, the initial conditions were:

$$P\ (t = 0, r) = P_{atm} = 1\ \text{atm} \tag{3.18}$$

$$T\ (t = 0, r) = \ T_0\ = \ 25℃ \tag{3.19}$$

$$v\ (t = 0, r)\ = \ 0 \tag{3.20}$$

$\rho_B\ (t = 0, r)\ = \ \rho_{B,0_b}$ (density of moisture-free solid biomass) (3.21)

$\rho_M\ (t = 0, r) = \ \rho_{M,0}$ (density of available moisture in biomass) (3.22)

$\rho_{B,0}\ = \ \rho_{B,0_b}\ + \rho_{M,0}$ (total biomass density at initial time) (3.23)

$\rho_I\ (t = 0, r)\ = \ 0$ (assuming negligible inert gas inside particle at start of process)

(3.24)

$$\rho_C\ (t = 0, r) = \rho_G\ (t = 0, r) = \rho_{T1}\ (t = 0, r) = \rho_{T2}\ (t = 0, r) = \rho_W\ (t = 0, r) = 0$$

(3.25)

In this case, only half-particle was considered due to symmetrical heating, leading to variation in dependent variables from centre to surface of particle.

At particle centre:

$$\frac{\partial P}{\partial r}(t, r = 0) = \ \ v\ (t, r = 0) = \ 0 \tag{3.26}$$

$$\frac{\partial T}{\partial r}(t, r = 0) = \ 0 \tag{3.27}$$

$$\frac{\partial \rho_G}{\partial r}(t, r = 0) = \frac{\partial \rho_{T_1}}{\partial r}(t, r = 0) = \frac{\partial \rho_{T_2}}{\partial r}(t, r = 0) = \frac{\partial \rho_W}{\partial r}(t, r = 0) = \frac{\partial \rho_I}{\partial r}(t, r = 0) = 0 \tag{3.28}$$

At particle surface: (considering reactor conditions)

$$P\big(t, r = r_p\big) = \ P_{atm} = 1\ \text{atm} \tag{3.29}$$

$$-k_{eff}\frac{\partial T}{\partial r}\ \big(t, r = r_p\big) = h_{heat}(\ T_{su} - T_{bu}) + \ \sigma\omega\big({T_{su}}^4 - T_{wa}^4\ \big) + q_{fu} \tag{3.30}$$

The first component on right side in equation 30 is due to convective heating of particle by inert gas like nitrogen, and the second term corresponds to radiative

component arising due to high temperature conditions inside the reactor. The last term on right side is the heat flux due to heat sources such as furnace or arc lamp, if provided in the pyrolysis setup. Here, $\omega$ is surface emissivity and $h_{heat}$ is heat transfer coefficient [see Appendix A.6. and A.7.]. $T_{su}$ is surface temperature, $T_{bu}$ is bulk gas temperature, $T_{wa}$ is apparatus (reactor) wall temperature and $\sigma$ is Stefan - Boltzmann constant.

$$-D_{eff,i}\,\frac{\partial \rho_i}{\partial r}(t, r = r_p) = h_{mass,i}\left(\rho_{i,su} - \rho_{i,bu}\right) \tag{3.31}$$

where $h_{mass,i}$ is the mass transfer coefficient of $i^{th}$ species [see Appendix A.7.], $\rho_{i,bu}$ is the bulk phase density of i$^{th}$ species and $\rho_{i,su}$ is surface density of $i^{th}$ species. The effect of pressure on the diffusive flow was not considered in equation 3.31. However, the pressure effect in equation 3.2 was due to the outflowing vapours from inside the biomass particle towards the surface. This pressure difference was used for calculating the vapour velocity, which governs the convective flow of volatile components in equations 3.10 to 3.13.

### 3.2.2. Thermo-physical properties and Reaction parameters

For solving the conservation equations, the required values of thermal, physical and chemical properties were taken from the literature (see Table 3.1). Also, the kinetic rate constants (see Table 3.2) and heats of reactions (see Table 3.3) for the proposed reaction model were taken from the available data.

**Table 3.1:** Thermo-physical properties of biomass.

| Property | Value | References |
|---|---|---|
| Biomass Permeability, $\beta_{B,0}$ (m$^2$) | $\beta_{B,0\ (across)}$: $10^{-14}$, $\beta_{B,0\ (along)}$ : $10^{-11}$ | Di Blasi (1998) |
| Char Permeability, $\beta_{C,f}$ (m$^2$) | $\beta_{C,f\ (across)}$ : 5x$10^{-12}$, $\beta_{C,f\ (along)}$ : 5x$10^{-11}$ | Di Blasi (1998) |
| Biomass Thermal Conductivity, $k_{B,0}$ | $k_{B,0\ (across)}$: 10.46x$10^{-2}$, $k_{B,0\ (along)}$: 25.5x$10^{-2}$ | Di Blasi (1998) |

| | | |
|---|---|---|
| (W/m-°C) | | |
| Char Thermal Conductivity, $k_{C,f}$ (W/m-°C) | $k_{C,f\ (across)}$:7.1x10$^{-2}$, $k_{C,f\ (along)}$:10.5x10$^{-2}$ | Di Blasi (1998) |
| Vapour Phase Thermal Conductivity, $k_v$ (W/m-°C) | 25.77x10$^{-3}$ | Di Blasi (1998) |
| Initial Porosity, $\varepsilon_{B,0}$ | 0.4 | Galgano and Di Blasi (2003) |
| Final Porosity, $\varepsilon_{C,f}$ | 0.91 | Assumed |
| Molecular Diffusivity, $D_i$ (m$^2$/s) (considering equal for all vapour phase species) | 10$^{-6}$ | Chan et al. (1985) |
| Vapour Phase Molecular Weight (kg/kmol) | Tar : 145, NCG : 31, Inert : 28, Water Vapour: 18 | Janse et al. (2000) |
| Heat Capacity# (J/kg-°C) | Wood : 2300, Char : 1100 , Tar : 1100, NCG: 1100 , Inert : 1040; Water Vapour : 1996, Moisture : 4180 | Janse et al. (2000) |
| Initial Emissivity, $\omega_{B,0}$ | 0.6 | Branca and Di Blasi (2003) |
| Final Emissivity, $\omega_{C,f}$ | 1 | Branca and Di Blasi (2003) |
| Initial Pore Diameter, $d_{poreB,0}$ (m) | 5x10$^{-5}$ | Grønli and Melaaen (2000) |

| | | |
|---|---|---|
| Final Pore Diameter, $d_{poreC,f}$ (m) | $10^{-4}$ | Grønli and Melaaen (2000) |
| Vapour Phase Viscosity, (kg/m-s) | Tar : $3x10^{-5}$ , NCG : $3x10^{-5}$, Inert : $3x10^{-5}$<br>Water Vapour : $1.3\ x10^{-5}$ | Janse et al. (2000) |

# Constant values of heat capacities were taken from literature as a valid assumption for considering thermal effects during biomass particle pyrolysis.

**Table 3.2:** Kinetic rate parameters.

| **Kinetic Constant, $K_i$** | **Pre-exponential Factor, $A$ ($s^{-1}$)** | **Activation Energy, $E$ (J/kmol)** | **References** |
|---|---|---|---|
| $K_1$ | $4.38x\ 10^9$ | $1.527x10^8$ | Di Blasi and Branca (2001) |
| $K_2$ | $1.08x\ 10^{10}$ | $1.48x10^8$ | Di Blasi and Branca (2001) |
| $K_3$ | $3.27x\ 10^6$ | $1.117x10^8$ | Di Blasi and Branca (2001) |
| $K_4$ | $1.48x\ 10^6$ | $1.44\ x10^8$ | Chan et al. (1985)* |
| $K_5$ | $1.48x\ 10^6$ | $1.44\ x10^8$ | Chan et al. (1985)* |
| $K_6$ | $1x\ 10^5$ | $1.08x10^8$ | Di Blasi (1993a) |
| $K_{vap}$ | $5.13x\ 10^{10}$ | $8.8x10^7$ | Bryden and Hagge (2003) |

* Gas to secondary tar equals to 0.78 to 0.22, by primary tar decomposition reaction.

**Table 3.3:** Heat of reactions.

| Reaction | Heat of Reaction (J/kg) | References |
|---|---|---|
| $\Delta H_1$ | 64000 | Park et al. (2010) |
| $\Delta H_2$ | 64000 | Park et al. (2010) |
| $\Delta H_3$ | 64000 | Park et al. (2010) |
| $\Delta H_4$ | -42000 | Di Blasi (1993a) |
| $\Delta H_5$ | -42000 | Assumed^ |
| $\Delta H_6$ | -42000 | Di Blasi (1993a) |
| $\Delta H_{vap}$ | 2440000 | Bryden and Hagge (2003) |

^Heat of reactions for secondary tar and NCG formation from primary tar was kept same.

## 3.3. Results and Discussion

The model results were validated using experimental data available in the literature. The effect of temperature, particle size, moisture content and shrinkage on biomass conversion in different operating conditions has been analysed.

Validation of model results has been performed using experimental studies of Sreekanth and Kolar (2009) as shown in Figure 3.3. The conversion time of a 10 mm diameter and 10 mm long wood particle (*Casuarina equisetifolia*) with about 10% moisture content was analysed in a lab-scale fluidized bed combustor. The density of dry wood particles was 500 kg/m$^3$. The bed consists of sand particles (550 µm size) at a temperature of around 834°C. According to their analysis (Sreekanth and Kolar, 2009), the conversion time is inferred as the time at which the dry wood density reduces to 1% of initial value. This density is considered as the density at particle centre for model analysis. The heat transfer coefficient calculated using correlations given in Appendix A.7 underestimates the rate of heat transfer in fluidized bed conditions. Therefore, for model comparison with existing studies from fluidized systems, heat transfer coefficient values as applicable under respective conditions

were used. In this case, the heat transfer coefficient of 285 W/m$^2$-°C (Sreekanth and Kolar, 2009) has been used. However, the mass transfer rate is not significantly affecting the process, and hence, mass transfer coefficient values were kept same as calculated using given correlations in Appendix A.7 for fluidized bed studies.

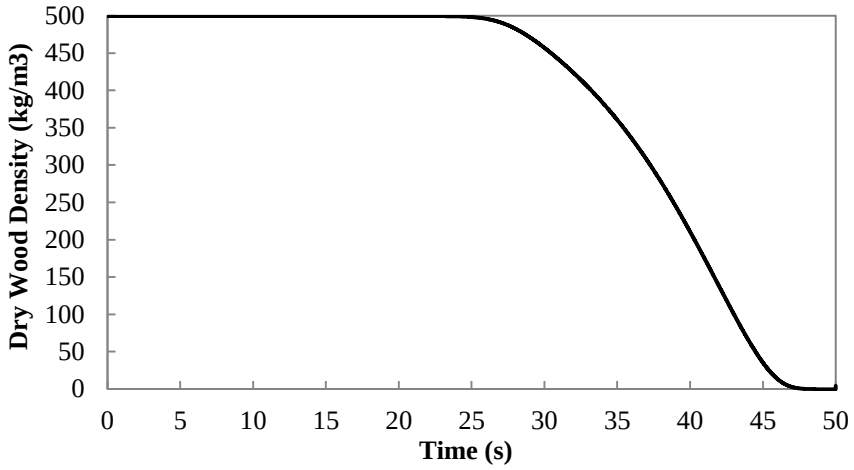


**Figure 3.3:** Estimation of conversion time for a moist wood particle in a fluidized bed reactor (particle diameter = 10mm, reactor temperature = 834°C).

It has been clear from Figure 3.3 that the density at the centre starts decreasing after about 26 seconds. The pyrolysis reactions at the centre started after that time, and led to conversion of wood to char and other volatile products. The density at the centre reduces to 1% of its initial value after about 46.7 seconds which compared well with the experimental value of 46 seconds (Sreekanth and Kolar, 2009).

### 3.3.1. Effect of reactor temperature

The simulation results were also compared with experiments of Park et al. (2010) for a spherical biomass particle (moisture free) of 25.4 mm diameter in the temperature range of 415 to 606°C in a vertical tube furnace. The results are shown in Figure 3.4 for three different values of temperature. It was found that the results were quite satisfactory in that range, but there were some deviations in mass loss profile at lower temperatures. Also, there was negligible decrease in the mass of solid at the start of the process, but thereafter, there was constant rate of mass loss, finally reaching to a fixed (around 20 % here) value of remaining solid product yield. The deviation at the lower temperatures was because of the incapability of model to predict the devolatilization kinetics, which was mainly due to uncertainties in values

of parameters such as activation energies, and heat of reactions values from the literature for a variety of biomass samples. For large size particles, conductive heat transfer determines the global devolatilization rate at higher temperatures, while the rate is controlled by reaction kinetics at lower temperatures (Chan et al., 1985). Therefore, for analysing the mass loss profile of larger scale particles at lower temperatures, it is highly desired to accurately estimate the reaction kinetic constants of particular biomass samples.

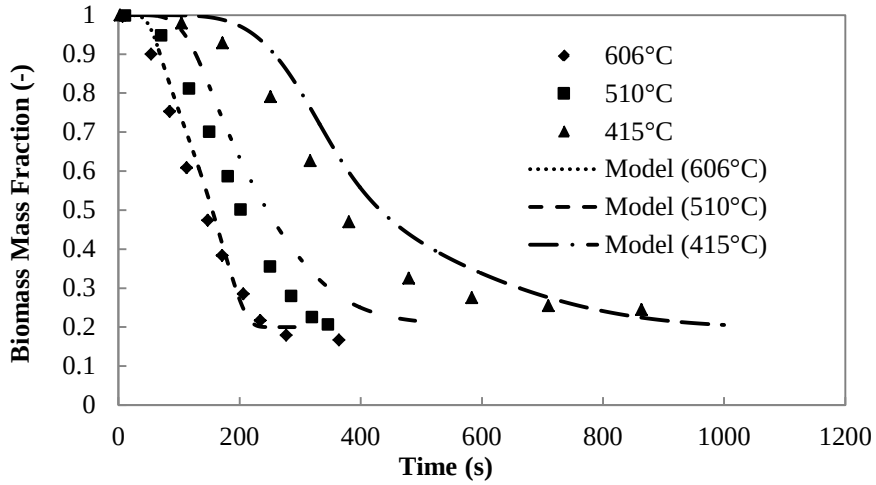


**Figure 3.4:** Biomass fraction comparison between proposed model and experiments (Park et al., 2010) for different temperatures (particle diameter = 25.4 mm).

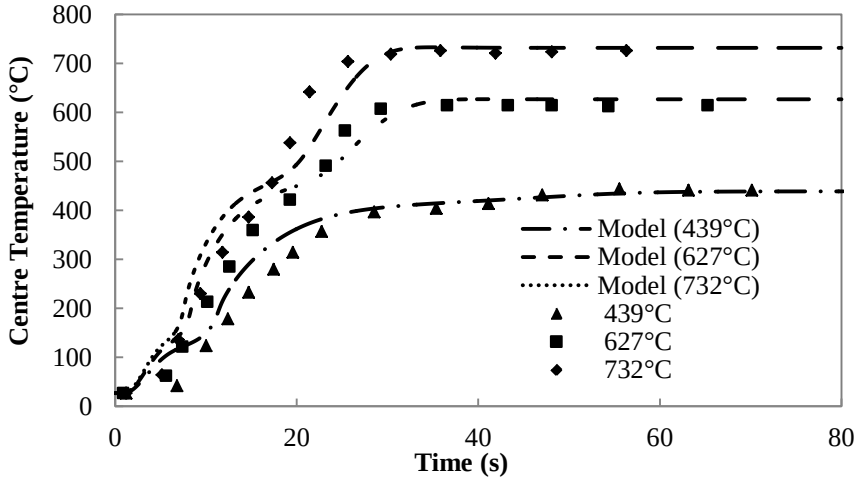


**Figure 3.5:** Comparison of particle centre temperature with experiments (Di Blasi & Branca, 2002) at different temperatures for 4 mm diameter particle.

The simulation results for studying the effect of operating temperature in fluidized bed conditions were compared with experimental analysis of Di Blasi and Branca (2002) using cylindrical beech wood particles of 4 mm diameter and 20 mm length (see Figure 3.5). The thermal conductivity for beech wood particles considered here was 0.209 W/m-°C across the fibres and 0.349 W/m-°C along the fibres (Di Blasi and Branca, 2002). For this study, the heat transfer coefficient of 285 W/m$^2$-°C (Sreekanth and Kolar, 2009) has been used. From the figure, it can be seen that modelling results have shown good agreement with experimental values. The characteristic process time (or conversion time) is directly dependent on duration of plateau of particle centre temperature (Di Blasi et al., 2001; Di Blasi and Branca, 2002). Based on the results, it has been analysed that with increase in outlet temperature, the duration of plateau decreases leading to shorter conversion time of particle. With increase in operating temperature in a reactor configuration for a fixed size particle, the rate of heat transfer inside the particle and rate of chemical reactions increases, leading to a reduction in overall time for completion of pyrolysis process. However, temperature has to be chosen with other operating parameters such as particle size and vapour residence time for getting desired product yield, as these parameters also affect the rate of secondary tar cracking reactions in reactor environment which lead to variation in product compositions.

### 3.3.2. Effect of particle size

For analysing the impact of particle size on the degradation process, model results were compared with experiments of Di Blasi and Branca (2002) for 3 different diameters of cylindrical beech wood particles (having constant length of 20 mm) pyrolyzing at temperature of around 534°C in a fluidized sand bed reactor, operating at about 8 times of the minimum fluidization conditions. The thermal conductivity for beech wood particles was assumed to be 0.209 W/m K across the fibres and 0.349 W/m K along the fibres (Di Blasi and Branca, 2002), and heat transfer coefficient value of 285 W/m$^2$-°C (Sreekanth and Kolar, 2009) has been used. Based on results (shown in Figure 3.6) for rise in particle centre temperature with time, it was found that with increase in particle diameter, there has been decrease in internal heat transfer rate by conduction. This leads to delay in heating of particle core and increase the overall conversion time of biomass.

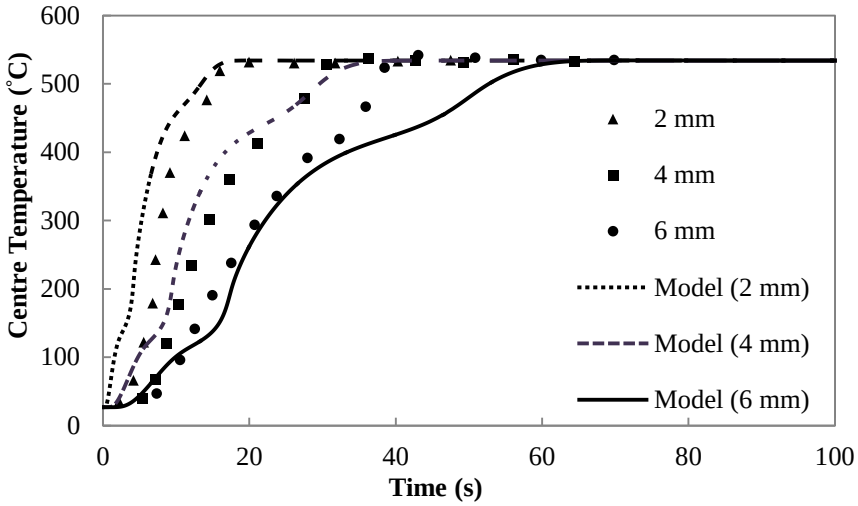


**Figure 3.6:** Comparison of particle centre temperature for different sized biomass particles with experiments (Di Blasi & Branca, 2002) (reactor temperature = 534°C).

Based on modelling comparison between surface and centre temperature for different sized cylindrical particles (shown in Figure 3.7), it was found that with increase in particle diameter, the heat transfer resistances increased. For 1 mm particle diameter, temperature gradient between surface and centre was very small, while it increased for 2 mm and 4 mm diameter particles. Therefore, smaller size biomass particles converted to volatiles and solid products at a faster rate for given operating conditions. From the results, it has been also predicted that for particle sizing <= 1 mm, the heat transfer resistances inside the particle can be neglected and a uniform temperature can be assumed throughout the biomass particle during the pyrolysis.

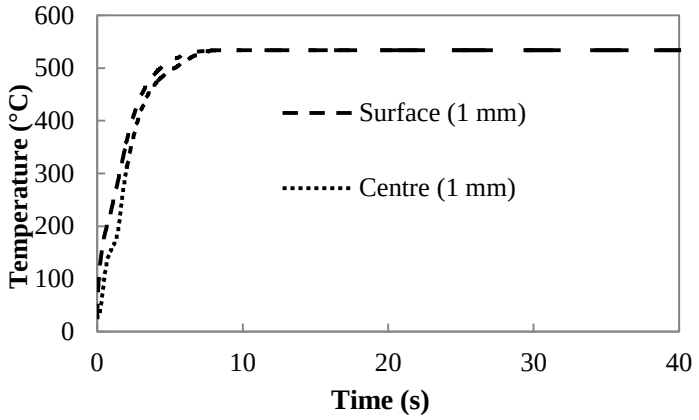


**(a)**

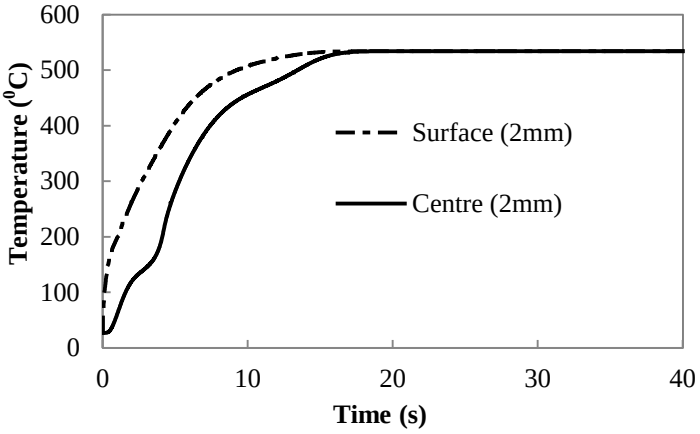


**(b)**

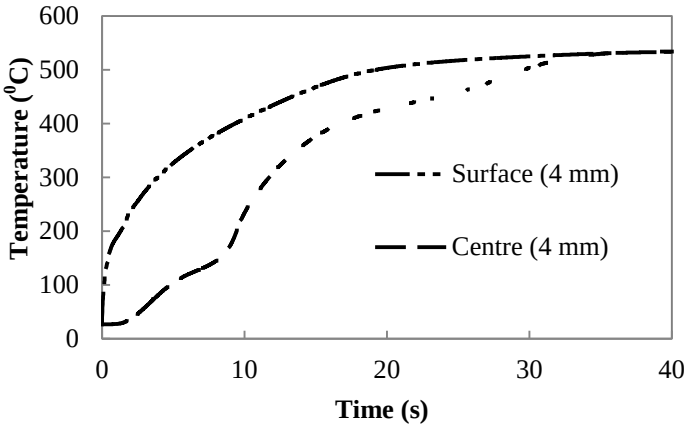


**(c)**

**Figure 3.7:** Surface and centre temperature comparison for different sized particles in fluidized bed conditions (reactor temperature = 534°C). **(a).** particle diameter: 1mm; **(b).** particle diameter: 2mm; **(c).** particle diameter: 4mm.

Also with increase in particle size, the biomass conversion rate decreased. However, small size particles favour entrainment and cause incomplete conversion of biomass inside the reactor. This leads to choosing an optimum particle size with other operating conditions, such as gas velocity and temperature, for allowing complete conversion of biomass inside the reactor.

### 3.3.3. Effect of moisture content

Figure 3.8 shows the effect of moisture content on the biomass conversion. The operating conditions such as reactor temperature (834°C) and particle size (diameter=10 mm, length = 10 mm) were kept same as given by Sreekanth and Kolar (2009). It was found that the total time required for completion of the process (dry biomass density at centre = 0) is around 43.6 seconds for 0%, 48.1 seconds for 10% and 52.8 seconds for 20% moisture content. With an increase in the moisture content, the time required for evaporation of available water inside the particle increased. This led to the delay in onset of biomass conversion (around 22 seconds for 0%, 26 seconds for 10% and 30 seconds for 20%) and hence, increased the overall pyrolysis time for the process.

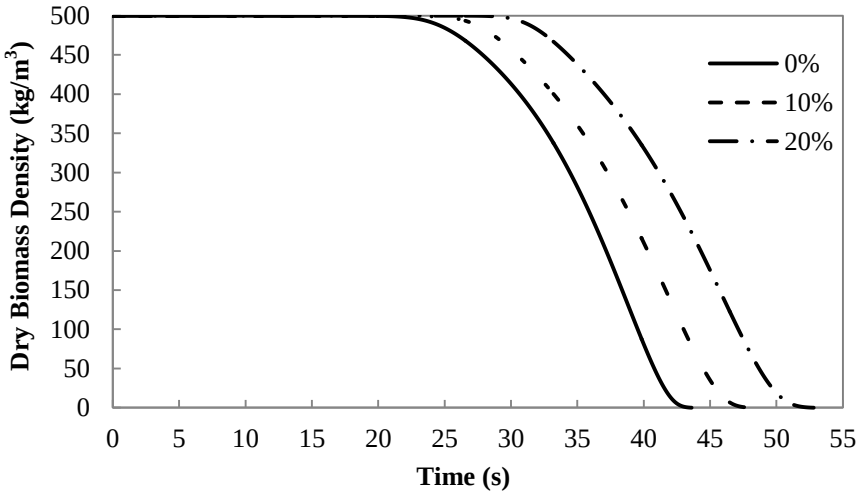


**Figure 3.8:** Effect of moisture content on the biomass conversion (reactor temperature = 834°C, particle diameter=10 mm).

### 3.3.4. Effect of particle shrinkage

Figure 3.9 shows the effect of particle shrinkage on the biomass conversion rate. The operating temperature and diameter of spherical particle was kept at 550°C and 25.4 mm, respectively. The heat and mass transfer conditions were considered the same as

used by Park et al. (2010). It was found that due to particle shrinkage, the rate of conversion of biomass to solid and volatile products increases. This is due to the fact that volumetric shrinkage favours the higher rate of heat transfer which leads to faster decomposition of biomass particle. Therefore, the biomass converted to final products in a lesser time for a shrinking particle (about 260 seconds) as compared to particle with a constant diameter (about 390 seconds).

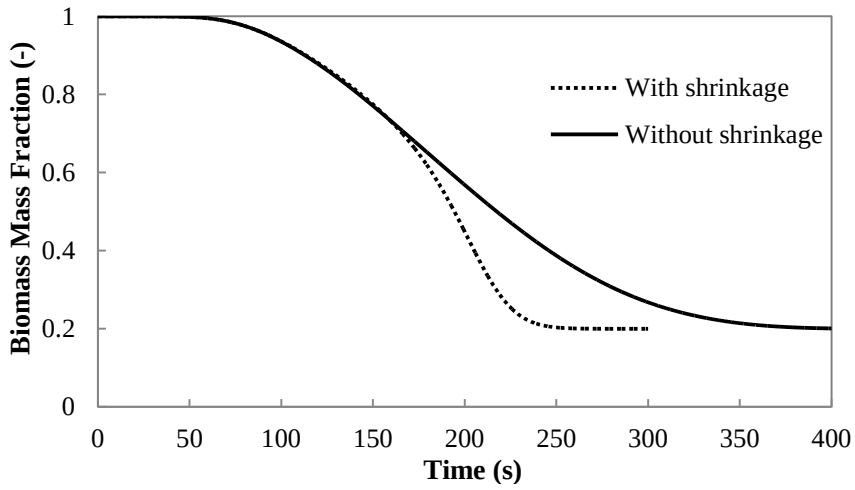


**Figure 3.9:** Effect of particle shrinkage on the biomass conversion (operating temperature = 550 °C, particle diameter = 25.4 mm).

## 3.4. Conclusions

A detailed phenomenological model of thermo-chemical decomposition of biomass has been developed. The model includes the kinetics of both primary solid phase and secondary gaseous phase (tar) reactions on a lumped basis. The model predictions compared well with the available experimental results for the effect of operating temperature and particle size on the biomass conversion. The effect of the moisture content and particle shrinkage was further analysed, and it was found that both parameters significantly affect the rate of biomass decomposition. However, there is the requirement for extending the modelling results for studying the effect of reactor hydrodynamics with operating conditions on product yields in a large-scale reactor.

# Chapter 4 Hydrodynamic modelling of biomass in a bubbling fluidized bed

Due to their high rates of heat and mass transfer, fluidized bed reactors are widely used as pyrolysis reactors. These reactors also provide the opportunity to separate the solid products from the volatile components. Since the biomass particles themselves cannot be uniformly mixed in a fluidized bed due to their peculiar shapes, sizes and densities, and hence, a fluidizing medium such as silica sand is utilized for enhancing the mixing, and heat and mass transfer rates. For biomass pyrolysis, the behaviour of the biomass particles in a reactor has to be analysed in conjunction with the fluidizing media.

As discussed in Chapter 2, the hydrodynamics of the fluidized beds are best studied using the Euler-Euler approach because of its ability to handle larger-scale systems. In this approach, both continuous and discrete phases are treated as inter-penetrating continua, and the interaction between them is accounted for using a drag force concept (Boemer et al., 1998; Hulme et al., 2005; Patil et al., 2005). In most of the previous studies, the main focus has been to understand the hydrodynamics of a single solid phase in the presence of a carrier gas. There have also been studies on the hydrodynamics of fluidized bed reactors with more than one discrete phases, i.e, in multi-phase systems. The major focus of these studies has been on analysing the segregation and mixing mechanisms of solid particles in dense gas fluidized beds. Similar to the “two-fluids” model, these studies have been based on the kinetic theory of granular fluids coupled with other constitutive models. For multi-phase systems, the component which tends to sink in the bed is known as the jetsam, while the component which tends to float is known as the flotsam. Fan and Fox (2008) accounted for the particle-particle interactions using the correlation of Syamlal (1987) which also includes the contribution of hindrance effect of particles. They (Fan and Fox, 2008) analyzed relative segregation rates as a function of superficial gas velocity and mass fractions of different size particles. The segregation rates of binary mixtures in dense gas-solid fluidized beds using both the Eulerian (Multi-Fluid Model) and Lagrangian approaches (Discrete Particle Model) were studied

(van Sint Annaland et al., 2009a; van Sint Annaland et al., 2009b). The authors concluded that the deviation in the segregation rate and granular temperature in segregating systems is mainly because of neglecting the frictional stresses in their model, which then overestimated the emulsion phase mobility. They also compared their simulation results of segregation rates with the experimental data (Goldschmidt et al., 2003) using a digital image analysis technique for colored glass beads of size ranging between 1.5 and 2.5 mm to calculate the particle-particle and particle-wall collision parameters in a pseudo two- dimensional lab -scale fluidized bed. Goldschmidt et al. (2000) investigated the effect of coefficient of restitution on the bubble dynamics in two-fluid systems, and on the mixing and segregation in multi-fluid systems. Huilin et al. (2003a) proposed a multi-fluid Eulerian model for binary mixtures using the kinetic theory of granular flow with gas-particle and particle-particle interactions in gas bubbling fluidized bed. They analyzed the bed hydrodynamics by evaluating the particle size distribution and energy dissipation due to particle-particle collisions. Huilin et al. (2007) further utilized both multi-fluid model (Huilin et al., 2003a) and discrete hard sphere model for studying the particle segregation phenomena in fluidized beds using particles of different sizes and densities. The authors compared results of a multi-fluid approach for binary mixtures with the experimental studies of Formisani et al. (2001) and Huilin et al. (2003b), and concluded that better particle mixing is obtained by increasing the fluidization velocity to well above the minimum fluidization velocities of both heavier and lighter particles. Their models did not consider the effect of frictional stresses in the dense bed on the granular temperature and other particle closure relations.

The aforementioned models mainly focus on the segregation rate of binary mixtures of different size particles. However, there have been very few studies (Chiba et al., 1980; Leaper et al., 2004) on the behavior of bi-dispersed phases having variable particle sizes and densities in bubbling fluidized beds. According to these studies (Chiba et al., 1980; Leaper et al., 2004), the particle density has a higher impact on the segregation rate as compared to the particle size. Some experimental studies (Rao and Bheemarasetti, 2001; Abdullah et al., 2003; Clarke et al., 2005; Zhong et al., 2008) have been performed for the analysis of certain fluidization characteristics of biomass such as the minimum fluidization velocities for different mixtures in the

reactor. A review of experimental analysis of biomass hydrodynamics in a fluidized bed reactor has been given by Cui and Grace (2007). Qiaoqun et al. (2005) carried out an experimental as well as a modelling study of a mixture of biomass and sand particles, and examined the pressure drop profile of the mixture with respect to the minimum fluidization velocity. They also studied the segregation of sand and rice husk particles with time, and the effect of superficial gas velocity, bed particle diameter and restitution coefficient on the mixing behavior. Zhang et al. (2009c) experimentally examined the mixing/segregation pattern by varying mass ratio of biomass (cotton stalk) to sand and superficial gas velocity in the bed. Zhong et al. (2012) had studied the effect of particle-wall interaction parameters such as specularity coefficient and restitution coefficient on mixing/segregation of different size and density particles in a low velocity bubbling fluidized bed.

However, the modelling and experimental studies so far are not sufficient for evaluating optimal conditions for uniform mixing of biomass particles with the bed material. In addition, when a catalyst is used as the bed material, it is very important to have uniform mixing of biomass with the catalyst particles because any segregation between the biomass and catalyst particles will adversely impact the catalytic cracking of the volatiles fractions. Hence, to achieve improved conditions for heat and mass transfer in the pyrolysis process, there is need to conduct detailed CFD simulations for studying the hydrodynamics of the fluidized bed. There is further requirement to study the effect of various operating and modelling parameters such as superficial gas velocity, bed material density and particle size, biomass density and particle size, drag correlations and wall boundary conditions on the simulation results. In this study, a dynamic multi-phase CFD model has been developed for examining the fluidization of biomass particles with other solid phases such as sand or biochar particles.

## 4.1. Model description

The CFD model was developed using the Euler-Euler (EE) approach, which treats the gas phase, biomass and sand/biochar particles as inter-penetrating continuums. The general conservation equations were formulated for mass, momentum and fluctuating kinetic energy of solid phases by incorporating the concept of phasic

volume fraction (the volume fraction representing the space occupied by each phase). The additional closure laws such as gas-solid and solid-solid drag coefficients, and solid shear and bulk viscosity were also included in the model (ANSYS FLUENT).

### 4.1.1. Conservation Equations

The overall continuity for the continuous primary and dispersed secondary phases was defined using the mass conservation equation:

$$\left[\frac{\partial\left(\alpha_q\rho_q\right)}{\partial t}+\ \nabla.\left(\alpha_q\rho_q\ \vec{v}_q\right)=\ 0\right] \tag{4.1}$$

where $\alpha_q$ is the phasic volume fraction of phase $q$ (gas phase and different solid phases), $\rho_q$ is the physical density of phase $q$ and $\vec{v}_q$ is the velocity of phase $q$. For continuity equations of each phase, mass transfer between the phases, and the source term for mass generation or consumption have not been considered.

For the gas phase ($g$), the momentum balance has been specified using the Navier-Stokes equation:

$$\left[\frac{\partial\left(\alpha_g\rho_g\vec{v}_g\right)}{\partial t}+\ \nabla.\left(\alpha_g\rho_g\ \vec{v}_g\vec{v}_g\right)=\ -\alpha_g\ \nabla p+\ \nabla.\bar{\tau}_g+\ \alpha_g\rho_g\vec{g}\ +\sum_{s=1}^{n}\vec{R}_{gs}\right] \tag{4.2}$$

where $\vec{R}_{gs}$ is the interaction force between gas phase and $n$ solid phases ($s$ =1, 2,_ _ _, $n$), $\bar{\tau}_g$ is the stress-strain tensor for gas phase, $\vec{g}$ is the acceleration due to gravity and, $p$ is the pressure shared by all phases.

$$\vec{R}_{gs}\ =\ K_{gs}\ \left(\vec{v}_g-\ \vec{v}_s\right) \tag{4.3}$$

where $K_{gs}$ is the gas-solid momentum exchange coefficient.

For the $s^{th}$ solid phase, the momentum balance has been defined similarly as that for the gas phase:

$$\left[\frac{\partial\left(\alpha_s\rho_s\vec{v}_s\right)}{\partial t}+\ \nabla.\left(\alpha_s\rho_s\ \vec{v}_s\vec{v}_s\right)=\ -\alpha_s\ \nabla p-\nabla p_s\ +\ \nabla.\bar{\tau}_s+\ \alpha_s\rho_s\vec{g}\ +\sum_{l=1}^{N}\vec{R}_{ls}\right] \tag{4.4}$$

where $p_s$ is the pressure of $s^{th}$ solid phase, and $\bar{\tau}_s$ is the stress-strain tensor for $s^{th}$ solid phase.

$$\vec{R}_{ls} = K_{ls} (\vec{v}_l - \vec{v}_s) \quad (4.5)$$

where $K_{ls}$ is the momentum exchange coefficient between $l^{th}$ fluid (gas) or solid phase and $s^{th}$ solid phase and *N* is the total number of phases. In these equations, the contribution due to any other external force was not considered. Also, the contribution of the lift force (insignificant as compared to interaction force) and virtual mass force (only significant when secondary phase density is much smaller than primary phase density) were neglected due to negligible impact on the momentum equation.

The kinetic energy of fluctuating particle motion was represented using a granular temperature of the solid phase ($\theta_s$), which is proportional to the mean square of fluctuating velocity of solid particles:

$$\frac{3}{2}\left[\frac{\partial (\alpha_s \rho_s \theta_s)}{\partial t} + \nabla.(\alpha_s \rho_s \vec{v}_s \theta_s)\right] = -(p_s \bar{I} + \bar{\tau}_s): \nabla \vec{v}_s + \nabla.(k_{\theta_s} \nabla \theta_s) - \gamma_{\theta_s} + \Phi_{ls} \quad (4.6)$$

Here, the second term on the left hand side of equation is a contribution due to convective granular energy. Whereas, $(p_s \bar{I} + \bar{\tau}_s): \nabla \vec{v}_s$ is the generation of energy due to solid stress tensor, $k_{\theta_s} \nabla \theta_s$ is the contribution due to diffusive granular energy (here, $k_{\theta_s}$ is diffusion coefficient), and $\gamma_{\theta_s}$ is the collision dissipation of energy. $\Phi_{ls}$ is energy exchange between the $l^{th}$ fluid or solid phase and $s^{th}$ solid phase:

$$\Phi_{ls} = -3K_{ls}\theta_s \quad (4.7)$$

### 4.1.2. Additional closure equations for multi-phase flow

Similar to thermal motion of gas molecules, the intensity of random motion of particles arising from particle-particle collisions determines the stresses, viscosity and pressure of the solid phase (Ding and Gidaspow, 1990). Therefore, for the solid phases, a set of constitutive relations for transport properties such as the granular temperature, pressure and viscosity were defined using the kinetic theory of granular

fluids. These closure equations with the drag coefficient correlations are given in Appendix B.

### 4.1.3. Simulation scheme

The coupled equations of phasic momentum, shared pressure and phasic volume fraction for a given multi-phase flow were solved using ANSYS FLUENT version 14.0. The phase coupled SIMPLE algorithm was utilized for solving these equations. With this, a pressure correction equation was formulated based on continuity equation. In this scheme, the coupled per phase velocities were solved in a segregated manner. The coefficients for the pressure correction equation were derived from the coupled per phase momentum equations. This algorithm was integrated with an iterative time advancement scheme, where all the equations were solved iteratively for a given time step until the convergence criteria were met as per Figure 4.1(ANSYS FLUENT).

### 4.1.4. Solution procedure, initial and boundary conditions

The simulations were carried out in a 2-dimensional (2-D) fluidized bed reactor domain as shown in Figure 4.2. The 2-D configuration is a slice of the actual reactor, which has height and width as the height and diameter of the reactor, respectively. The simulation domain was divided into a fixed number of control volumes by defining grid cells in both horizontal and vertical directions. The equations were solved using a second order upwind differencing scheme for spatial discretization and second order implicit scheme for transient formulation with a time step size of $10^{-4}$ seconds. An initial bed height of given volume fractions of biomass and fluidizing bed material was specified at the start of each simulation. The coefficient of restitution for the biomass and the bed material (sand or biochar) particles were taken as 0.6 and 0.9 for the initial simulations, respectively. The simulations were conducted for a period of 30 seconds of real simulation time. The time-averaged parametric values were taken from 10 seconds (by which a dynamic steady state was achieved) to 30 seconds of simulation results. The specifications of the computational domain are given in Table 4.1.

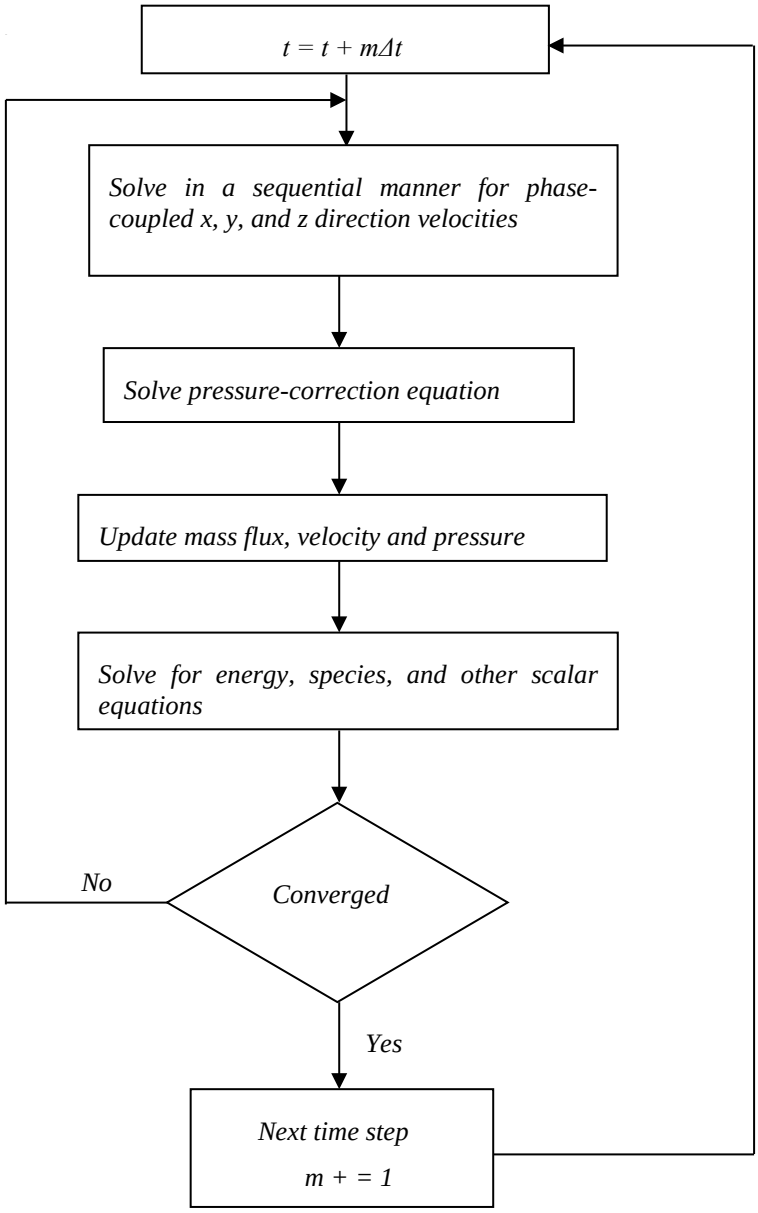


**Figure 4.1:** Flowchart showing scheme used for solving equations for multi-phase CFD model (Δt is the time step size chosen for the simulation).

**Table 4.1:** Specifications of the computational domain employed in the multi-phase simulation.

| | | | |
|---|---|---|---|
| Reactor height, L<br>mm | 2000 | Reactor width, W<br>mm | 450 |
| Grid cells in vertical direction | 163 | Grid cells in horizontal direction | 75 |
| Initial bed height, h<br>mm | 380 | | |

For the gas phase, the initial velocity was specified at the bottom of the bed. For the granular phases, the inlet velocities were assigned as zero. The pressure boundary conditions were applied at the top of the bed, which was fixed to a reference value of 1 atm. For the gas phase, a no-slip boundary condition was used on the walls. For the granular phase, the shear force at the walls was defined by the equation given by Sinclair and Jackson (1989):

$$\bar{\tau}_s = \frac{-\sqrt{3}\pi\,\alpha_s}{6\alpha_{s,max}}\phi\rho_s g_0\sqrt{\theta_s}\,\vec{u}_s \tag{4.8}$$

where $\vec{u}_s$ is the particle slip velocity parallel to the wall, $\phi$ is the specularity coefficient between particle and wall (assumed value of 0.5, for partial slip conditions) and $g_0$ is radial distribution function (see Appendix B).

The granular temperature for the solid phase at the wall (Johnson and Jackson, 1987):

$$q_s = \frac{\sqrt{3}\pi\,\alpha_s}{6\alpha_{s,max}}\phi\rho_s g_0\sqrt{\theta_s}\,\vec{u}_s.\vec{u}_s - \frac{\sqrt{3}\pi\,\alpha_s}{4\alpha_{s,max}}(1-{e_{sw}}^2)\rho_s g_0{\theta_s}^{3/2} \tag{4.9}$$

where $e_{sw}$ is the coefficient of restitution at wall ( assumed equal to particle's restitution coefficient).

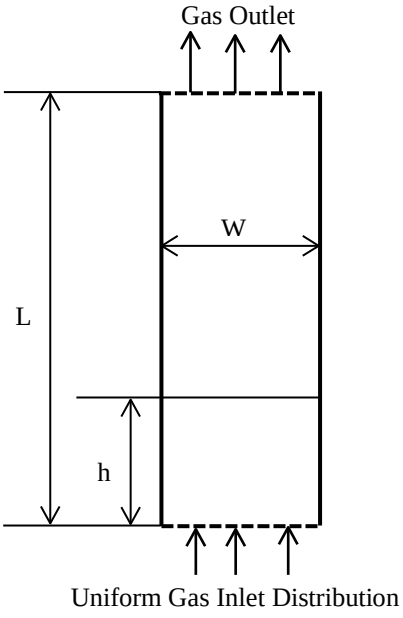


**Figure 4.2:** 2-D domain of fluidized bed systems.

## 4.2. Results and discussion

Since currently there are no experimental data available for "biomass-biochar" system, initial simulations were carried out with biomass and "sand", and the results were compared with existing literature data (Qiaoqun et al., 2005). After the model was validated, simulations were conducted for the mixtures of biomass and biochar (as bed material) particles. The biomass, sand and biochar particles were considered mono-sized and spherical in shape for the present modeling purposes.

A mixture of rice-husk (5.82 wt%) and sand particles (94.18 wt%) were used for the initial simulations. The initial volume fractions for the rice husk and sand particles in the bed were kept as 0.0867 and 0.5133, respectively. The average diameter and the density of the rice husk were 1.54 mm and 950.6 kg/m$^3$, respectively; and that of sand were 0.44 mm and 2600 kg/m$^3$, respectively (Qiaoqun et al., 2005). The minimum fluidization velocity of the mixture was calculated by the Chitester et al. (1984) correlation. For current data, the $u_{mf}$ of the binary mixture of rice husk and sand was calculated to be 0.22 m/s. This is in agreement with the experimental values calculated by Rao and Bheemarasetti (2001). Because of relative size and density of sand and rice husk particles, and depending on the gas phase velocity, they behaved as jetsam and flotsam in the bed, respectively.

According to Figure 4.3, it is clear that the time averaged rice husk mass distribution at a superficial gas velocity of 0.79 m/s was in agreement between the simulation results and the experimental (Qiaoqun et al., 2005) data along the dimensionless bed height (y/H). Some discrepancy between the simulation and experimental results occurred in the top section of the bed because of possible experimental error, which becomes apparent on calculating the weighted average of rice husk mass fraction by considering the area under the experimental data points in Figure 4.3. The calculated value of average rice husk from experimental data was approximately 6.3% compared to actual initial value of 5.82%.

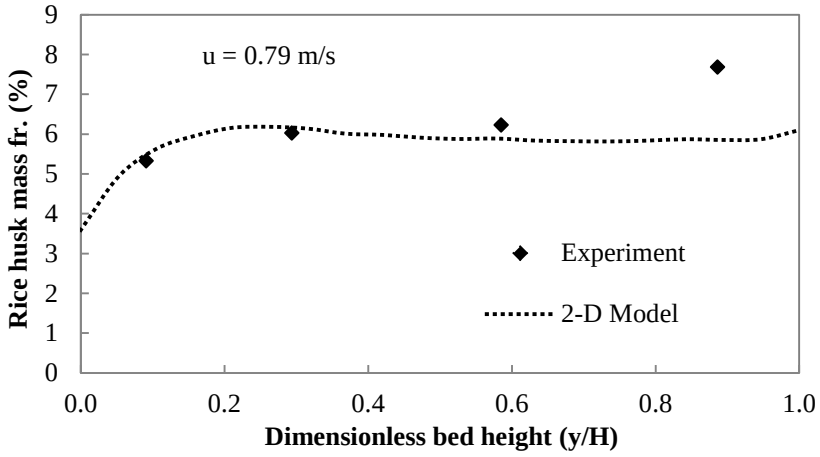


**Figure 4.3:** Time averaged rice husk mass distribution comparison with experimental results (Qiaoqun et al., 2005).

### 4.2.1. Effect of superficial gas velocity and sand/biochar density

Figure 4.4 qualitatively shows fluidization behaviour of rice husk particles in the rice husk-sand bed, which was initially patched to have a uniform volume fraction of both solid phases (rice husk and sand). The results are shown for 2, 4, 6, 8 and 10 seconds of real time for 5 different gas velocities. It is clear from Figure 4.4 (a) that for gas velocities (e.g., u = 0.20 m/s) lower than the minimum fluidization velocity, there was negligible bubbles formation and the accumulation of lighter and larger rice husk particles in the top section of the bed was mainly due to percolation of heavier and smaller sand particles towards the bottom section of the bed. Increasing the gas velocity beyond the minimum fluidization velocity, as shown in Figure 4.4 (b), led to formation of small bubbles favoring weak distribution of rice husk particles along the bed height with time. This actually contributed to higher concentration of rice husk particles in the top section of the bed as compared to the bottom section of the bed. With further increases in the gas velocity (Figure 4.4 (c-e)), the size of gas bubbles increased, which then caused vigorous movement and better distribution of the rice husk particles along the bed height.

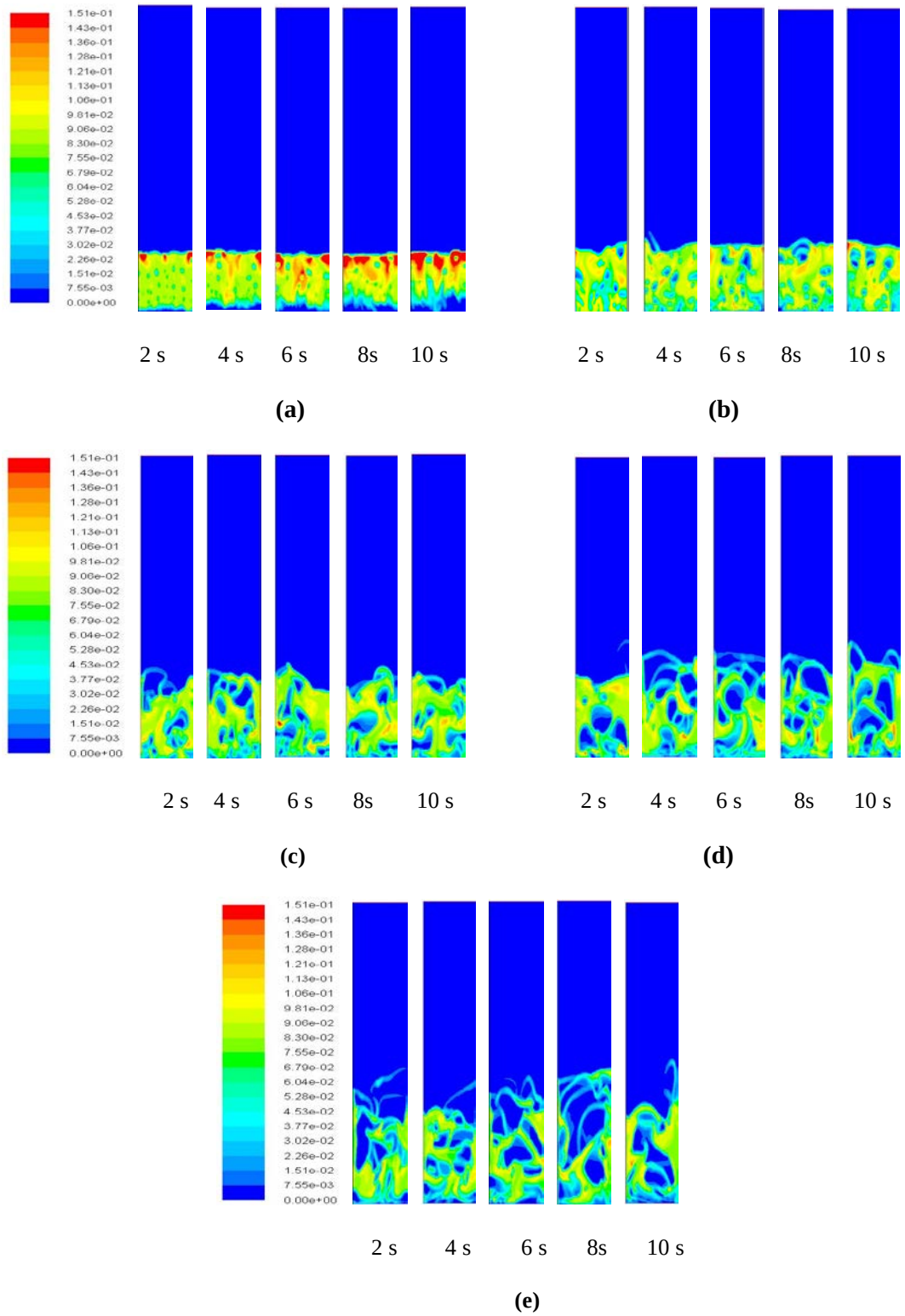


**Figure 4.4:** Volume fraction profile of rice husk at different superficial gas velocities in rice husk-sand mixture. **(a).** u = 0.20 m/s ($u/u_{mf}$ = 0.9); **(b).** u = 0.3 m/s ($u/u_{mf}$ = 1.4); **(c).** u = 0.58 m/s ($u/u_{mf}$ = 2.6); **(d).** u = 0.79 m/s ($u/u_{mf}$ = 3.6); **(e).** u = 1.1 m/s ($u/u_{mf}$ =5).

Figure 4.5 shows the time- averaged rice husk mass distribution along the bed height at different superficial gas velocities in rice husk-sand mixture. The rice husk mass fraction was based on the total solids in the bed without considering the gas phase. It is clear that for the velocities just above the minimum fluidization velocity (at u= 0.3 m/s), there was considerable segregation between the rice husk and sand particles. According to this segregation, the rice husk particles behaved as flotsam with higher concentrations in the top section of the bed, while sand particles behaved as jetsam with higher concentrations in the bottom section of the bed. For velocities around 2.5 times of the minimum fluidization velocity (at u = 0.58 m/s), there was weak mixing in the bed with an increase in bubble size and velocity. This mixing was due to movement of bubbles across the bed leading to transportation of rice husk particles from the top to the bottom of the bed, and of sand particles from the bottom to the top of the bed. However, the segregation between the rice husk and sand particles was noticeable at these velocities. For velocities around 5 times of the minimum fluidization velocity (at u = 1.1 m/s), formation of larger bubbles led to more uniform circulation of both the solid phases across the bed height. Therefore, at these velocities, the better mixing of rice husk and sand particles in the bed was observed.

The grid sensitivity analysis for the fluidized bed configuration given in Table 4.1 is shown in Figure 4.6. It was seen that there is no considerable effect of grid size on the segregation behaviour of rice husk and sand particles for given fluidizing conditions.

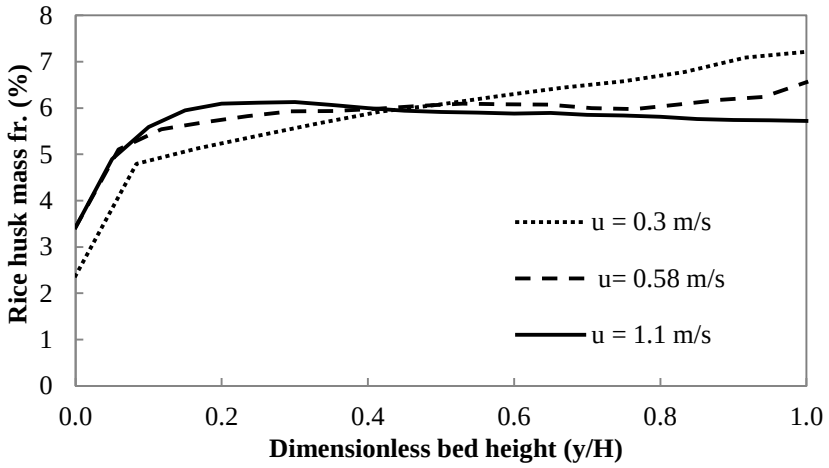


**Figure 4.5:** Time averaged rice husk mass distribution at different gas velocities in sand bed.

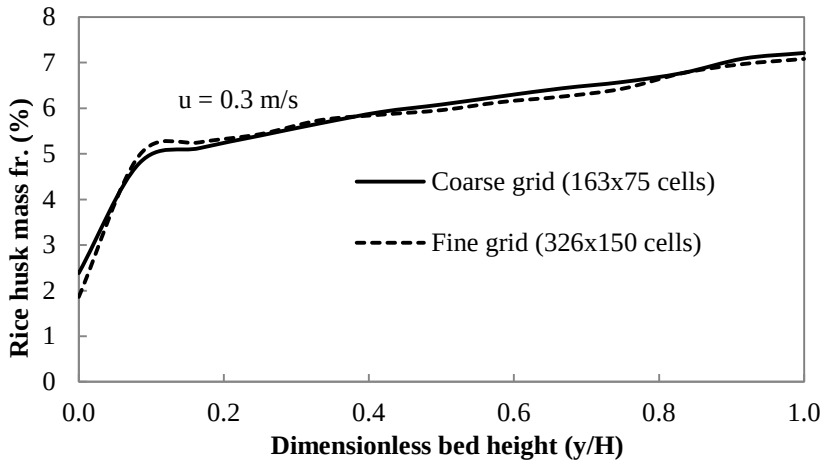


**Figure 4.6:** Effect of 2-D grid size on segregation behaviour of rice husk- sand mixture.

For this work, biochar produced from pyrolysis of biomass was utilized as a source of bed material for examining biomass fluidization patterns. Consequently, a pine char was used as the bed material for analyzing fluidization of the rice husk as the biomass. The density of the char particles was 1470 kg/m$^3$ (Brown et al., 2006). The averaged mass fraction of rice husk (1.54 mm average diameter) was again kept at 5.82 wt% in the rice husk-biochar mixture. The initial volume fraction for the rice husk and biochar particles in the bed was kept as 0.0523 and 0.5477 respectively. The $u_{mf}$ of the rice husk-biochar mixture was calculated to be 0.45 m/s using Chitester et al. (1984) correlation for biochar particles of 1 mm average diameter.

Figure 4.7 shows volume fraction profile of rice husk in the rice husk-biochar bed, which was initially patched to have a uniform volume fraction of both solid phases (rice husk and biochar). As per Figure 4.7 (a), the bubbles started to form at the minimum fluidization velocity allowing some movement of the rice husk particles in the bed. With an increase in the gas velocity above the minimum fluidization velocity (as shown in Figure 4.7 (b-d)), there was an improved distribution of the rice husk particles along the bed height. This phenomenon of the bubble formation was similar to that observed for rice husk-sand mixture with respect to the superficial gas velocity. However, the bubble formation in case of rice husk-biochar mixture was enhanced in terms of bubble size when compared with those for the rice husk-sand mixture (Figure 4.4 (b-d)) in the given $u/u_{mf}$ range. This shows that there was a better circulation of rice husk in the biochar bed as compared to that in the sand bed.

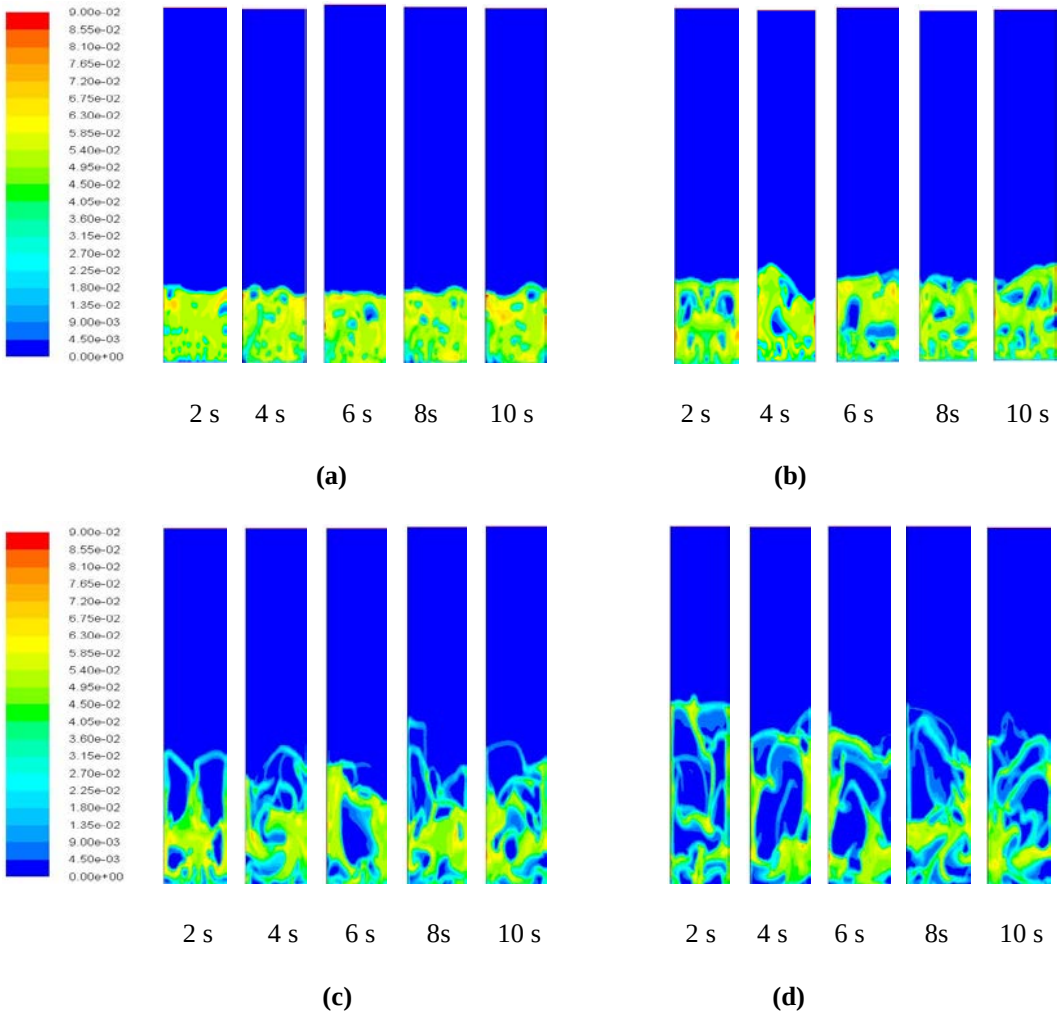


**Figure 4.7:** Volume fraction profile of rice husk at different superficial gas velocities in rice husk-biochar mixture. **(a).** u = 0.45 m/s ($u/u_{mf}$ = 1); **(b).** u = 0.68 m/s ($u/u_{mf}$ = 1.5); **(c).** u = 1.14 m/s ($u/u_{mf}$ = 2.5); **(d).** u = 1.59 m/s ($u/u_{mf}$ = 3.5).

A time- averaged distribution of rice husk particles with respect to the dimensionless bed height at different gas velocities in rice husk-biochar mixture is shown in Figure 4.8. In this case, the rice husk particles were lighter and behaved as flotsam, while the biochar particles were heavier and behaved as jetsam in the bed. There was a uniform segregation between the rice husk and biochar particles across the bed height at the minimum fluidization velocity. With an increase in velocity just above $u_{mf}$ (u = 0.54 m/s), there was weak mixing between the two phases due to movement of bubbles across the bed, which led to re-distribution of both rice husk and biochar particles in the bed. The mixing between the two solid phases improved at velocities close to 2.5 times of the minimum fluidization velocity (u = 1.14 m/s). At velocities close to this value, there was a uniform mixing between the rice husk and biochar

particles along the bed height. According to Figure 4.8, the uniform mixing between the rice husk and biochar particles occurred at a lower $u/u_{mf}$ (~ 2.5 $u_{mf}$) as compared to that for the rice husk-sand mixture (~ 5$u_{mf}$ as shown in Figure 4.5). This is because of the lesser density difference between the rice husk and biochar particles which favors the mixing between them. However, the velocity at the onset of the uniform mixing was in the same range for both mixtures, i.e., around 1.1 m/s.

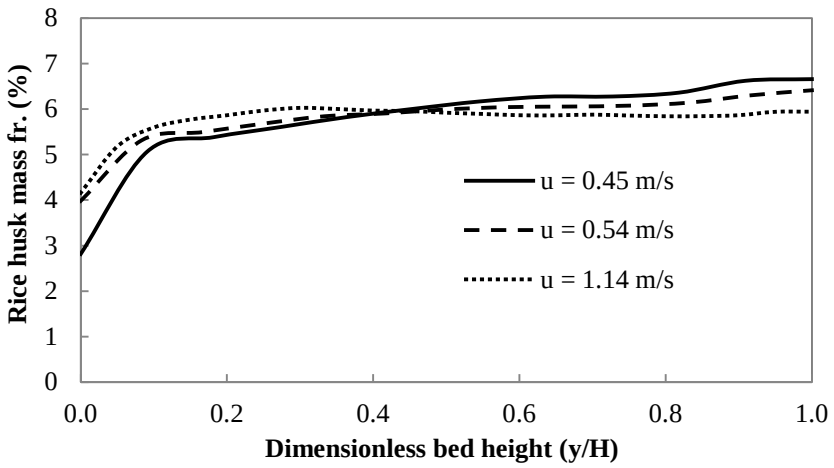


**Figure 4.8:** Time averaged rice husk mass distribution at different gas velocities in biochar bed.

### 4.2.2. Effect of biochar particle diameter

It is clear from Figure 4.9 that the size of biochar particles in the bed had a considerable effect on the rice husk distribution across the bed height. With an increase in the biochar particle diameter from 1 mm to 1.25 m or 1.5 mm, the segregation of the rice husk and biochar particles was also increased across the bed height. It is clear that larger biochar particles moved towards the bottom of the bed leading to a lower concentration of the rice husk particles in that region as compared to that in smaller biochar particles bed. It also caused the movement of rice husk particles towards the top of the bed favouring a higher concentration in that region. As the minimum fluidization velocity of larger char particles was higher, the frequency of bubbles formation reduces at a given gas velocity contributing to the weak mixing between rice husk and biochar particles in the bed.

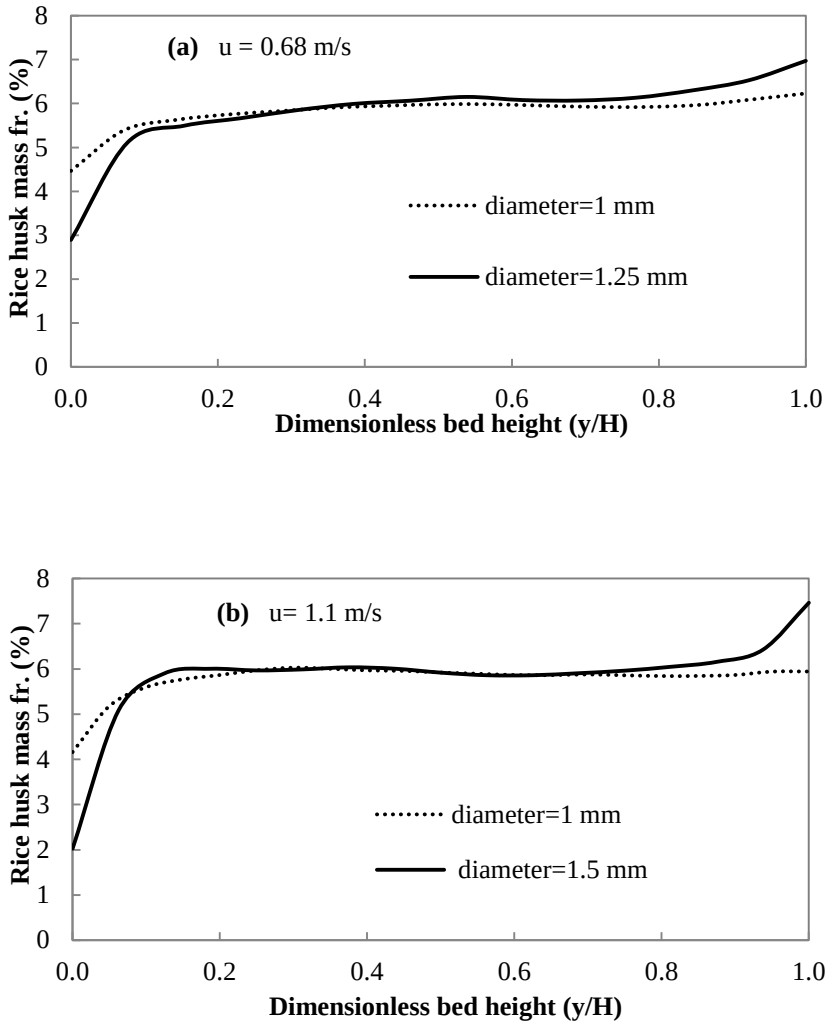


**Figure 4.9:** Time averaged rice husk mass distribution for different biochar average particle diameters.

### 4.2.3. Effect of biomass density

It is clear from Figure 4.10 that for a fixed superficial gas velocity, on changing the density of biomass particles in the bed, there was a considerable change in the biomass distribution across the bed height. For example, for gas superficial velocity of 0.68 m/s, on increasing the biomass density from 584 kg/m$^3$ (pinewood) (http://www.csudh.edu) to 950.6 kg/m$^3$ (rice husk) (the average particle diameter is 1.54 mm for both types of biomass), the segregation of biomass particles in the biochar bed decreased. This led to a better distribution of rice husk particles in the bed compared to pinewood particles which had significantly lower concentration in the bottom part of the bed and higher in top section of the bed due to segregation. This was mainly because the density difference between rice husk and biochar

particles was relatively small compared with the difference between pinewood and biochar particles. The simulation results for the fluidization behavior of pinewood particles and the effect of superficial gas velocities on mixing/segregation of pinewood-biochar mixture are shown in Figure 4.11 and Figure 4.12, respectively. The initial volume fraction for the pinewood and biochar particles in the bed was kept the same as 0.081 and 0.519 respectively.

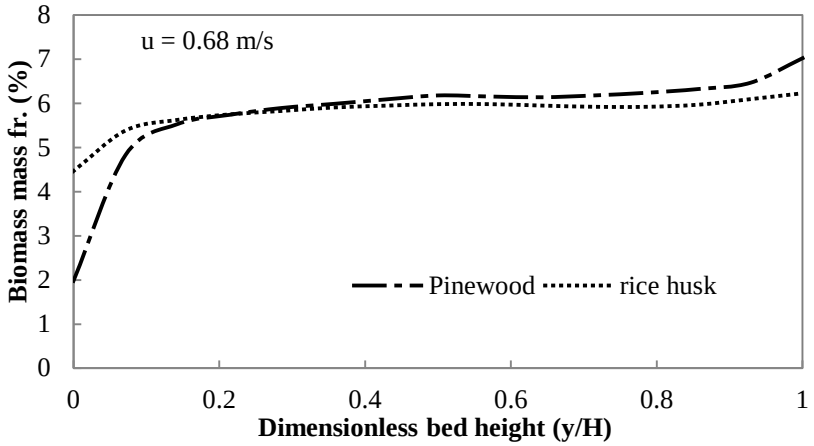


**Figure 4.10:** Time averaged mass distribution of pinewood and rice husk in biochar bed.

### 4.2.4. Effect of biomass particle diameter

Figure 4.13 shows the mass distribution of pinewood for different biomass (pinewood) particle sizes with respect to dimensionless bed height. There was a minor difference in the distribution of biomass particles in the biochar bed on increasing the average particle diameter. As the mass fraction of biomass was considerably less than the biochar in the bed, the effect of change of biomass particle diameter was negligible on mixing/segregation behaviour of both solid phases.

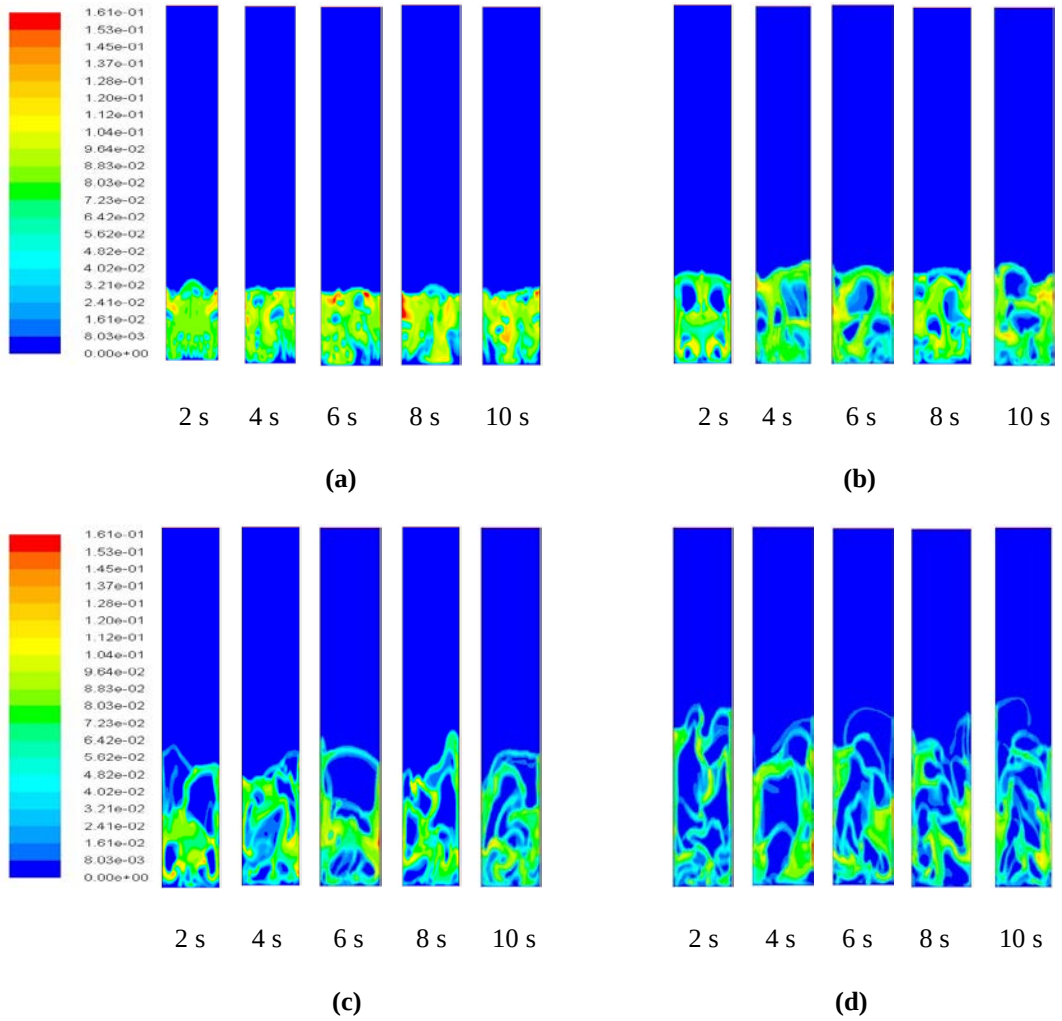


**Figure 4.11:** Volume fraction profile of pinewood at different superficial gas velocities in pinewood-biochar mixture. **(a).** u = 0.45 m/s ($u/u_{mf}$ = 1); **(b).** u = 0.68 m/s ($u/u_{mf}$ = 1.5); **(c).** u = 1.14 m/s ($u/u_{mf}$ = 2.5); **(d).** u = 1.59 m/s ($u/u_{mf}$ = 3.5).

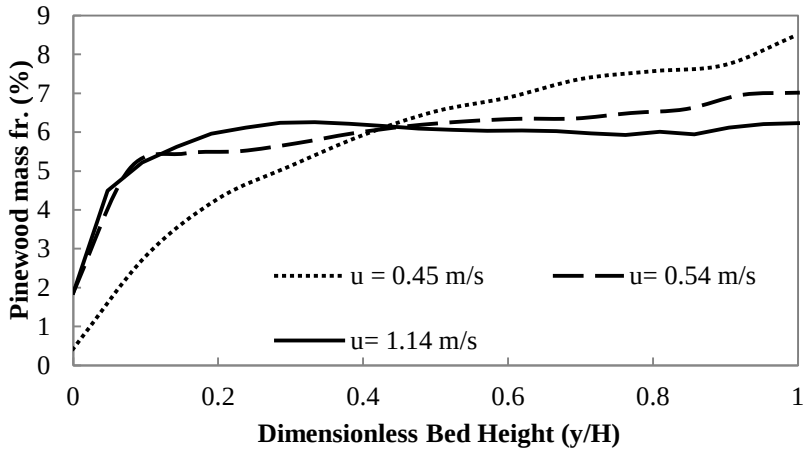


**Figure 4.12:** Time averaged pinewood mass distribution at different gas velocities in biochar bed.

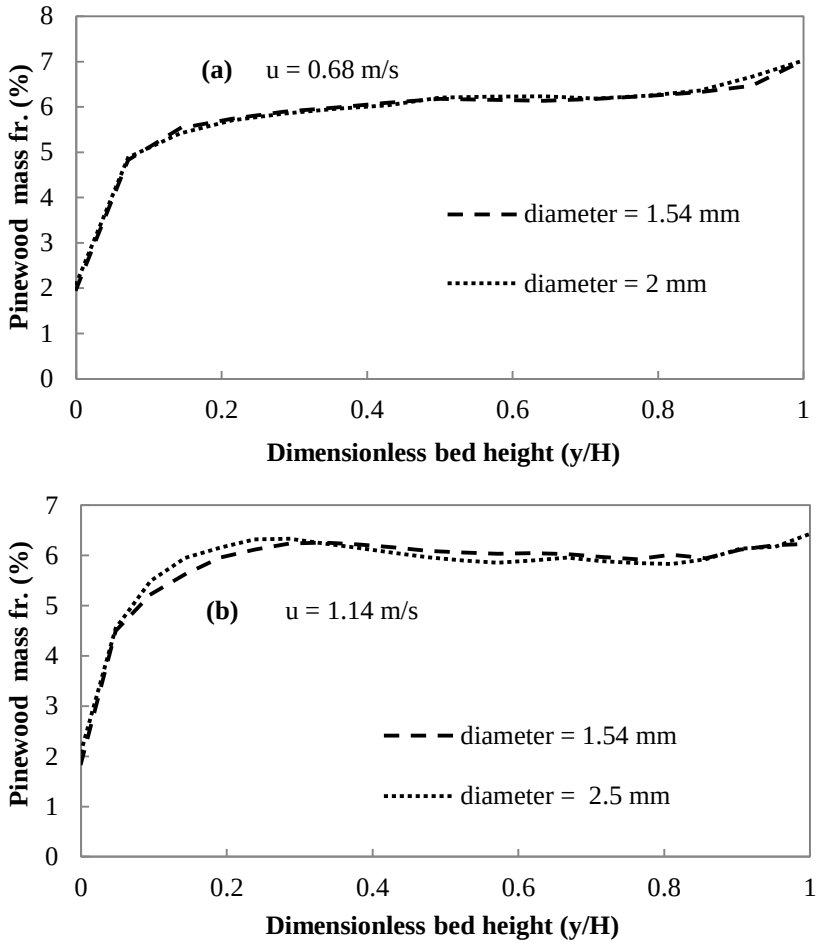


**Figure 4.13:** Time averaged pinewood mass distribution for different pinewood average particle diameters.

The granular temperature represents the motion of particles in the bed. The higher the motion of the particles of any solid phase, the higher will be the granular temperature. The area-weighted bed average granular temperature of both rice husk (5.82 wt.%) and biochar particles with respect to time is shown in Figure 4.14. Clearly, the granular temperature was unequal for both types of particles. It is higher for the rice husk particles than that of the biochar particles in the bed. This result suggests that the kinetic energy of fluctuations is higher for rice husk particles, relative to that for biochar particles.

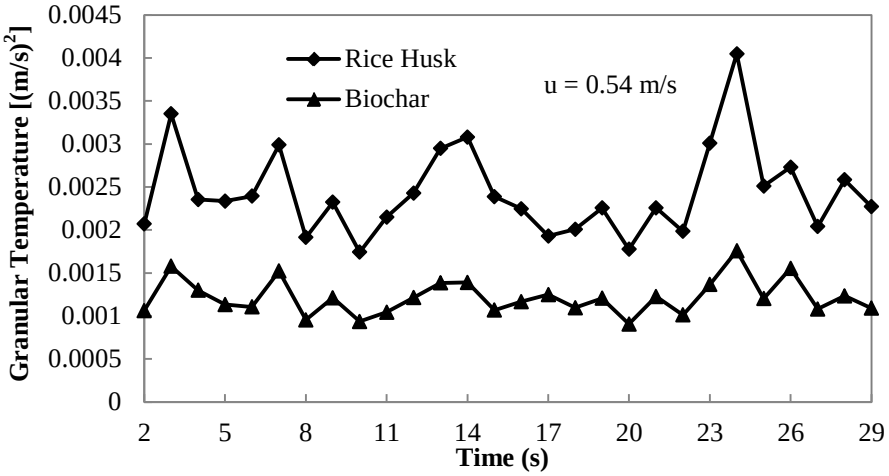


**Figure 4.14:** Area-weighted averaged granular temperature of rice husk and biochar particles.

The time-averaged distribution of vertical velocities of pinewood (5.82 wt%) and biochar particles at superficial gas velocity of 0.54 m/s is shown in Figure 4.12. It is clear that at the centre of the bed, both pinewood and biochar particles flow upward with positive velocities, while near the walls, they flow downward with negative velocities. The velocity of pinewood particles was marginally higher than biochar particles in the centre region of the bed. However, there is not much difference in their velocities in the wall region.

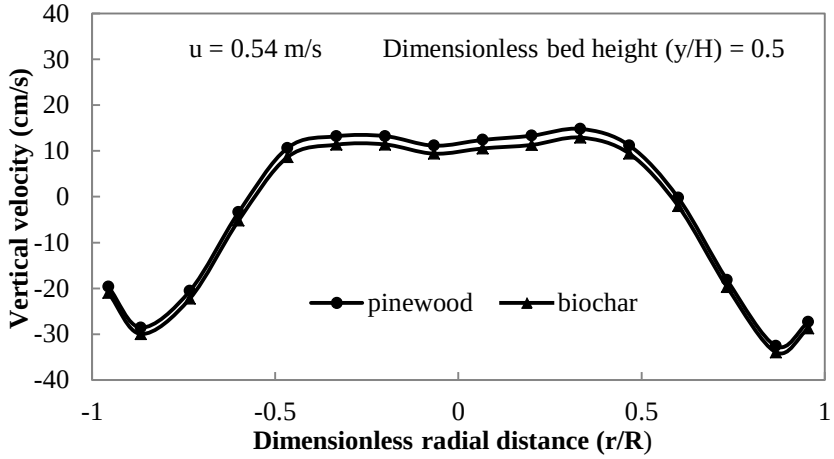


**Figure 4.15:** Distribution of vertical velocity of pinewood and biochar particles.

### 4.2.5. 2-D vs 3-D configuration

Simulations were also conducted using a 3-dimensional (3-D) fluidized bed domain (shown in Figure 4.16) , the height (L), width (W) and length (T) of which were kept as 2000 mm, 450 mm and 245 mm, respectively. The number of grid cells along the

height, width and length direction was 160, 36 and 20, respectively. The experimental result of Qiaoqun et al. (2005) for a mixture of rice husk (5.82 wt %) and sand (94.18 wt%) were used for validating 3-D results. The initial bed height (h) for the mixture was kept as 380 mm. The average diameter and density of rice husk particles were 1.54 mm and 950.6 kg/m$^3$, respectively; and the average diameter and density of sand particles were 0.44 mm and 2600 kg/m$^3$, respectively. The superficial gas velocity (u) in the bed was maintained at 0.79 m/s. The initial volume fraction for the rice husk and sand particles in the bed were kept as 0.0867 and 0.5133, respectively. The conservation equations were solved with additional closure laws and initial-boundary conditions as for 2-D simulations. However, for the transient formulation, the time step size of $10^{-5}$ seconds was used. As per Figure 4.17, it was found that the 3-D configuration results were in good agreement with the experimental data for time averaged rice husk mass distribution in the mixture along the dimensionless bed height. However, there was noticeable difference in the rice husk mass fr. (%) in top section of the bed between both the results. This was possibly due to the experimental error that led to the weighted average rice husk mass fraction in the bed around 6.3% compared to actual initial value of 5.82%.

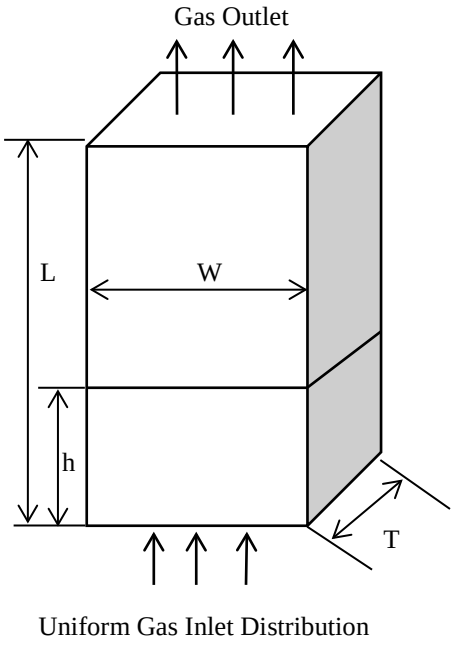


**Figure 4.16:** 3-D domain for fluidized bed systems.

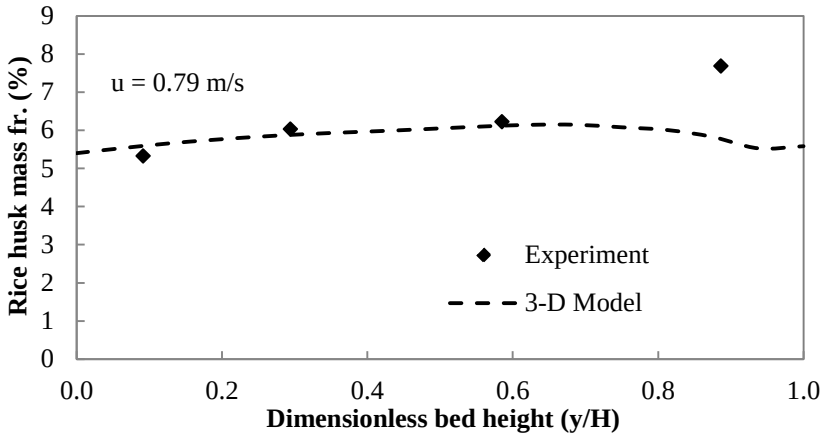


**Figure 4.17:** Time averaged rice husk mass distribution (3-D model) comparison with experimental data (Qiaoqun et al., 2005).

After 3-D model validation, the simulation results for mixing/segregation behaviour in 2-D and 3-D configuration were compared. A 2-D configuration with height and width of 342.9 mm and 38.1 mm; and a 3-D configuration with height, width and length of 342.9 mm, 38.1 mm and 20.7 mm were used, respectively. The simulation domain consisted of 10 grid cells in the horizontal direction and 90 grid cells in the vertical direction for the 2-D domain. The number of grid cells along the height, width and length direction for the 3-D domain was 90, 10 and 5, respectively. The initial bed height was kept as 38.1 mm for both cases. The bed contained averaged mass fraction of 5.82 wt % of pinewood in the pinewood-biochar mixture. This gave initial volume fraction for the pinewood and biochar particles in the bed to be as 0.081 and 0.519 respectively. The superficial gas velocity was maintained at 1.35 m/s. The coefficient of restitution for both pinewood and biochar particles was assigned as 0.9. A no slip boundary condition was used for the gas phase, while a free slip boundary condition was used for both solid phases. The time averaged volume fractions of pinewood and biochar particles for 2-D and 3-D configuration along the reactor length were shown in Figure 4.18. From the figure, it can be seen that the average height of pinewood and biochar particles in the bed was slightly higher in the 2-D model as compared to 3-D model. It is mainly due to the difference in the frequency of bubbles formation and bubbles size leading to variation in axial and lateral movement of solid phases. From the figure, it was also found that the bottom section of the bed contained mainly the biochar particles with only small amount of pinewood particles. This is due to the fact that the formation of bubbles

was weak leading to the segregation of particles based on difference in their densities in the bottom section of the bed. However, the uniform bubbles distribution at higher sections of the bed favours the movement of both the solid phases along the bed height. The pinewood mass fraction (%) in the mixture along the dimensionless bed height for 2-D and 3-D model is shown in Figure 4.19, where it was clear that the pinewood distribution was in close agreement between 2-D and 3-D model. It was also found that the mass fraction of pinewood particles was lower in the bottom section as compared to top section of the bed due to considerable segregation between both solid phases.

The grid sensitivity analysis for the above mentioned 2-D configuration is shown in Figure 4.20. According to the figure, it was seen that there is no significant effect of grid size on the segregation behaviour of pinewood and biochar particles for given fluidizing conditions.

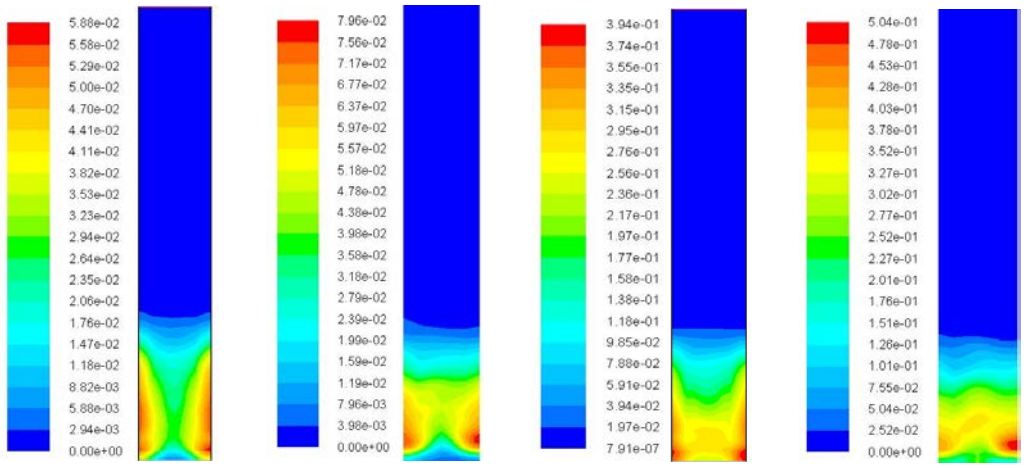


**Figure 4.18:** Time-averaged volume fraction of pinewood and biochar particles for 2-D and 3-D model (u = 1.35 m/s). **(a).** pinewood (2-D); **(b).** pinewood (3-D); **(c).** biochar (2-D); **(d).** biochar (3-D).

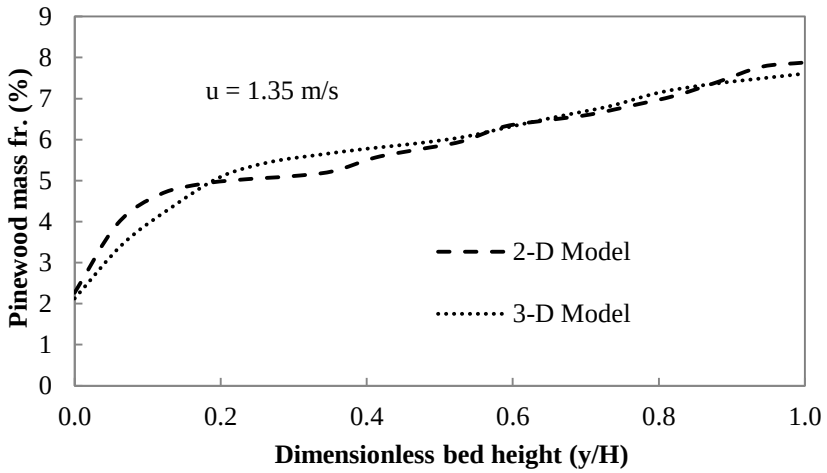


**Figure 4.19:** Comparison of 2-D and 3-D model for time averaged pinewood mass distribution.

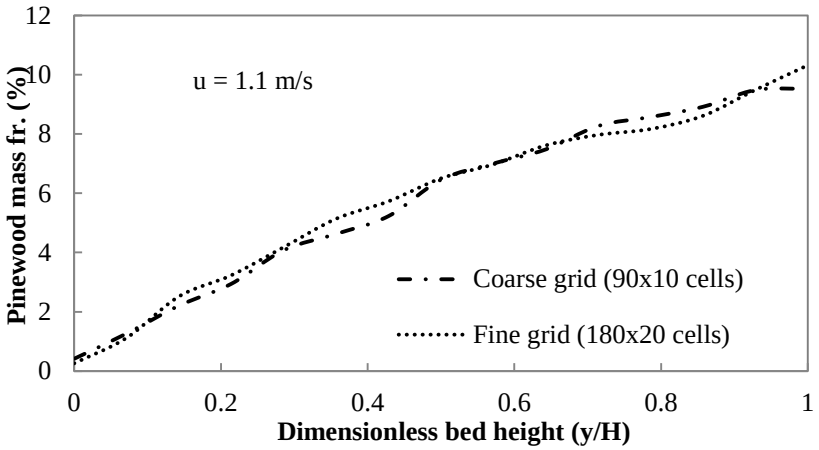


**Figure 4.20:** Effect of 2-D grid size on segregation behavior of pinewood- biochar mixture.

### 4.2.6. Effect of drag correlations

Figure 4.21 shows a plot of time- averaged velocity magnitude of pinewood particles along the bed height for different drag correlations in a 2-D configuration (342.9 mm x 38.1 mm). It is clear from the figure for all drag models, the pinewood particles exhibited recirculation in the bed due to the movement of gas bubbles along the bed height. However, in the top section of the bed for all models except Syamlal- Obrien model, the particles had the tendency to move downwards due to collapsing of bubbles. Figure 4.22 shows the distribution of pinewood particles in the mixture along the dimensionless bed height for different drag correlations, where it become clear that the time- averaged distribution of pinewood particles in the bed was almost identical for the Syamlal-Obrien and Gidaspow models. However, the Huilin-

Gidaspow model predicted slightly lesser segregation between the pinewood and biochar particles when compared with the Syamlal-Obrien and Gidaspow models.

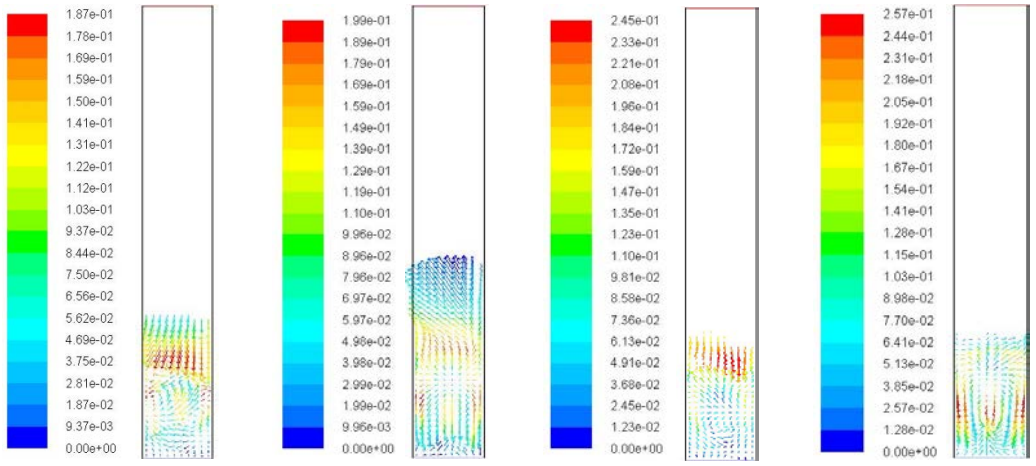


**Figure 4.21:** Time averaged velocity magnitude (m/s) of pinewood particles for different drag correlations. **(a).** Gidaspow; **(b).** Syamlal-Obrien; **(c).** Gibilaro; **(d).** Huilin-Gidapow.

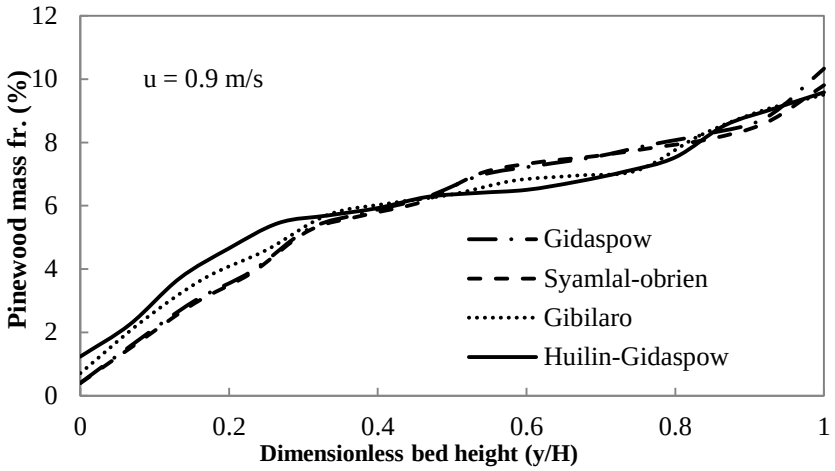


**Figure 4.22:** Time averaged pinewood mass distribution for different drag correlations.

### 4.2.7. Effect of wall boundary conditions

The interaction between wall and solid phase is accounted for using a specularity coefficient. Its value ranges between 0 and 1. When the value is 0, the granular particles have no shear stress at the walls and they follow free slip condition. With increase in the value, the lateral momentum transfer increases at the walls. For no

slip condition, the value of specularity coefficient would be 1 and the wall shear stress would be maximum at this value.

Figure 4.23 shows the time averaged distribution of velocity of pinewood particles in the bed for different values of specularity coefficient in a 2-D configuration (342.9 mm x 38.1 mm). It is clear that for zero shear stress condition, there is no friction between the particles and wall, thus resulting into higher particle velocity along the wall region. With increase in the specularity coefficient to 0.5, it was found that the friction increases which lowers the movement of particles in the bed. However, for no slip condition, the particle velocity was higher when compared to those using the specularity coefficient of 0.5 throughout the bed. As seen from Figure 4.24, higher amount of pinewood particles were retained along the walls for the free slip and no slip conditions when compared to those using the specularity coefficient of 0.5. However, for the no slip condition, the distribution of pinewood particles near the wall region was more uniform than those with the free slip condition and the specularity coefficient of 0.5.

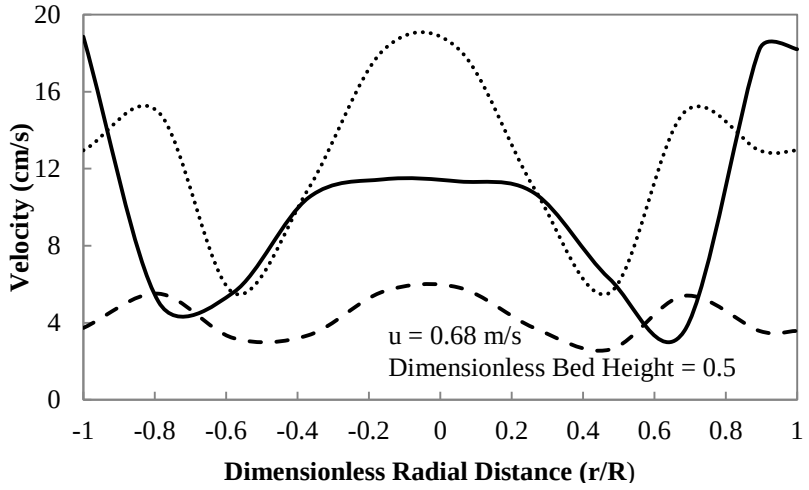


**Figure 4.23:** Distribution of time averaged velocity of pinewood particles for different wall boundary conditions. (——specularity coefficient = 0); ( – – specularity coefficient = 0.5); (····· specularity coefficient = 1).

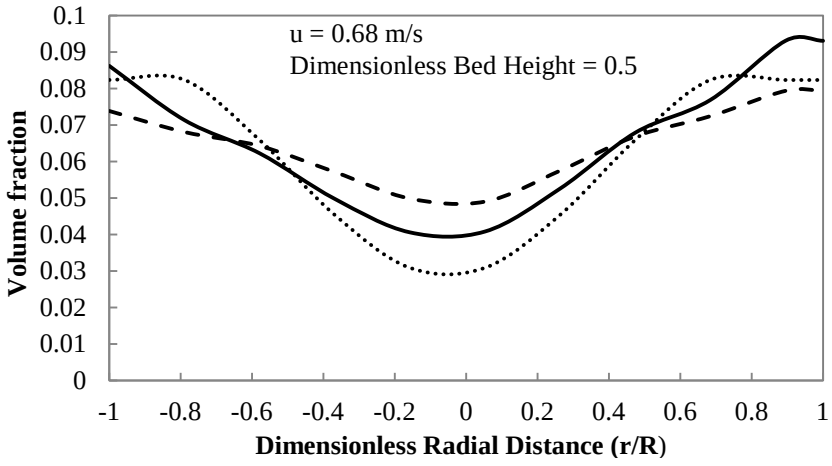


**Figure 4.24:** Distribution of time averaged volume fraction of pinewood particles for different wall boundary conditions. ( —— specularity coefficient = 0); ( – – specularity coefficient 0.5); (····· specularity coefficient = 1).

Figure 4.25 shows time-averaged mass distribution of pinewood in the pinewood-biochar mixture along the bed height for different specularity coefficients. It was found that due to higher particle velocity for free slip condition, the pinewood and biochar particles had a uniform movement along the bed height, which led to better mixing of both the phases. With increase in the specularity coefficient to 0.5, the mixing between the solid phases was reduced and a uniform segregation was observed. With further increase in the specularity coefficient to 1, there was an increase in shear force along the walls leading towards no slip condition between the particles and wall. This resulted into better distribution of pinewood particles in the mixture along the bed height as compared to the specularity coefficient value of 0.5 at such lower superficial gas velocities. However, it is required to further study the effect of specularity coefficient on mixing behavior of different solid phases at higher gas velocities and validate the simulation results with experimental data.

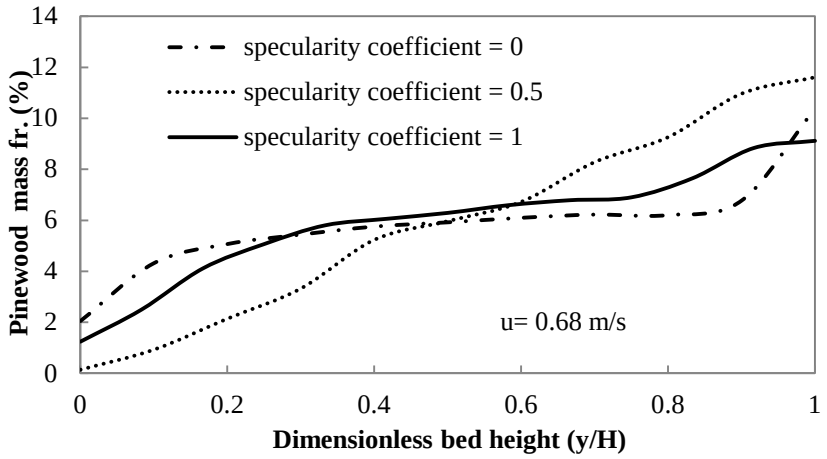


**Figure 4.25:** Time averaged pinewood mass distribution for different wall boundary conditions.

### 4.2.8. Effect of restitution coefficient

The coefficient of restitution of solid phases accounts for the elasticity of particle-particle collisions in the bed. This factor also affects the formation of bubbles in the gas phase by influencing the momentum and fluctuating energy of solid phases during interactions (ANSYS FLUENT). Figure 4.26 shows the effect of restitution coefficient of both pinewood and biochar particles in a 2-D configuration (342.9 mm x 38.1 mm). The partial slip boundary condition was used for both pinewood and biochar particles. It is clear that in the lower region of the bed, there was a decrease in the mass fraction of pinewood on increasing the restitution coefficient, and a considerably opposite trend was seen in the upper region of the bed.

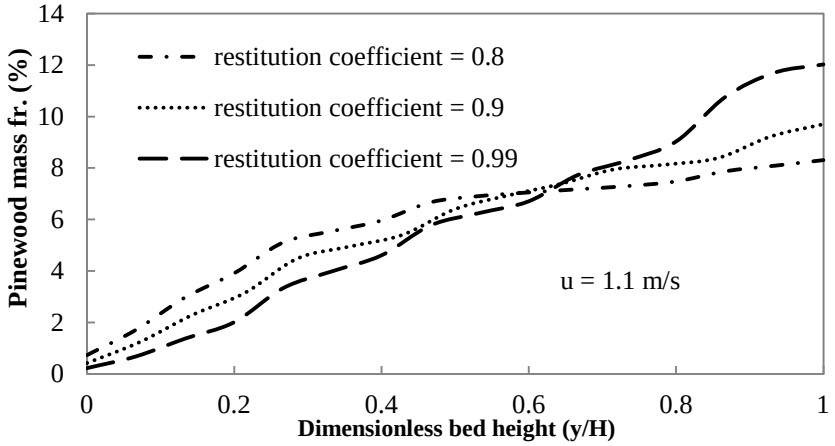


**Figure 4.26:** Time averaged pinewood mass distribution at different values of the restitution coefficient of pinewood and biochar particles.

The effect of the restitution coefficient of biomass (rice husk/pinewood) and biochar particles on mixing/segregation behaviour for the 2-D configuration (given in Table 4.1) is shown in Figure 4.27 and Figure 4.28 respectively. As seen from the Figure 4.27, with an increase in the restitution coefficient of rice husk (restitution coefficient for biochar kept as 0.9), there was a slight increase in the number of rice husk particles in the bottom section of the bed, while there was a marginal decrease in the rice husk mass fraction in the top section of the bed. Figure 4.28 shows the effect of the restitution coefficient of biochar particles (the restitution coefficient for pinewood particles was kept as 0.8). Based on the results, it was found that on increasing the restitution coefficient of biochar, the pinewood mass fr. (%) showed a small decrease in the bottom section of the bed, while it marginally increased in the top section of the bed. However, the effect of restitution coefficient on distribution of biomass particles in the bed was not significant for the conditions studied here. Therefore, there is a requirement to further study the effect of these modelling parameters using experimental data for gaining confidence in the model results.

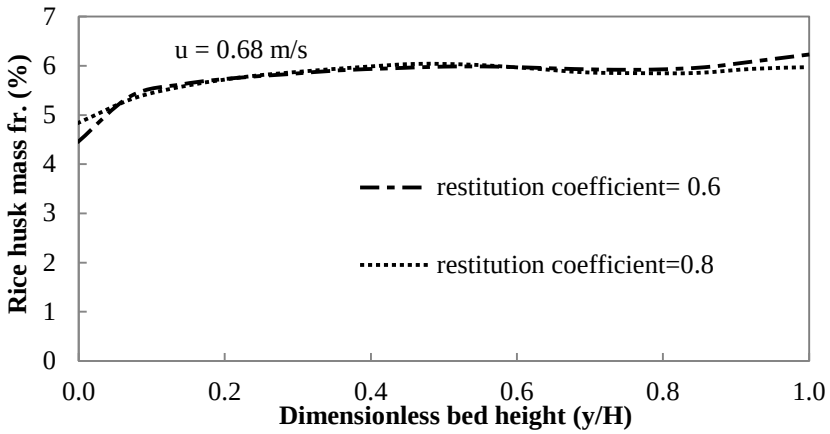


**Figure 4.27:** Time averaged rice husk mass distribution at different values of the restitution coefficient of rice husk particles (restitution coefficient for biochar =0.9).

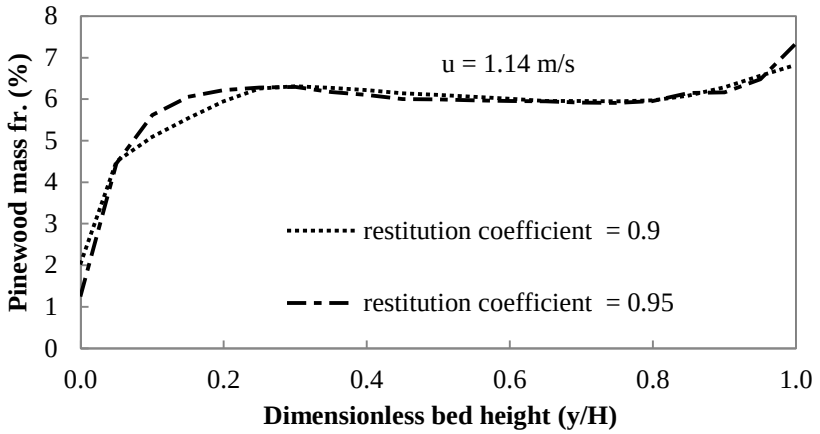


**Figure 4.28:** Time averaged pinewood mass distribution at different values of the restitution coefficient of biochar particles (restitution coefficient for pinewood =0.8).

### 4.2.9. Euler-Euler (EE) vs Euler-Lagrangian (EL) Model

In this study, the hydrodynamic behaviour of biomass and biochar particles was examined in a bubbling fluidized bed using the EL model. The interaction between particulate and continuous phases was accounted using the Dense Discrete Phase Model (DDPM) and the particles were tracked using the Discrete Element Method (DEM) in this EL approach. The DDPM model is useful for efficiently simulating the systems with large number of particles such as bubbling fluidized beds by preventing the unlimited accumulation of particles for flows operating close to the packing limit. The mass and momentum conservation for the discrete phase was defined similarly as given for the solid phase by equation 4.1 and 4.4 respectively. On the other hand, the DEM implementation accounts for the forces in the momentum conservation equation due to particle collisions using a spring-dashpot (soft sphere) approach. The spring-dashpot collision law calculates the force normal to the particle surface using parameters such as the spring constant and the coefficient of restitution. The value of spring constant was kept as 100 and the coefficient of restitution as 0.9 for this study. The friction collision law in the DEM approach is based on the Coulomb friction and is equal to the friction coefficient times the force normal to the particle surface. The friction coefficient is calculated using the default values of the governing parameters. The details of the DDPM and DEM models may be found elsewhere (ANSYS FLUENT). The granular temperature with other granular properties was not considered for the discrete phase

in this model. For the EE model, both solid phases were treated similarly as discussed earlier in section 4.1. For the EL model, only the biomass particles were treated as the discrete phase (the biomass particles were patched in the bed using an injection file given in Appendix C), while the biochar particles were treated as the secondary continuous phase. For the EE model, both the 2-D (342.9 mm x 38.1 mm) and 3-D configurations (342.9 mm x 38.1 mm x 20.7 mm) were used; while for the EL model, only the 3-D configuration (342.9 mm x 38.1 mm x 20.7 mm) was used. For unsteady particle tracking, a time step of $10^{-6}$ seconds was used with the fluid flow time step of $10^{-4}$ seconds. Figure 4.29 shows the unsteady tracking of pinewood particles in the bubbling fluidized bed at superficial gas velocity of 1.1 m/s. Figure 4.30 shows the time averaged volume fraction of pinewood and biochar particles using the EE (2-D) and EL (3-D) models. In this case, the Syamlal-Obrien drag correlation (ANSYS FLUENT) was used for calculating the averaged discrete phase drag force on the biomass phase due to both gas and biochar phases. The no-slip boundary condition was used for the gas and discrete phase, while the partial slip boundary condition was used for the biochar phase. Based on the results, it was found that the segregation of pinewood and biochar particles has been clearly visible using both EE and EL models. However, the final bed height was lower for pinewood and biochar particles using the EL model as compared to the EE model. From Figure 4.31, it was clear that there was a discrepancy in the distribution of pinewood particles along the bed height between EE and EL model.

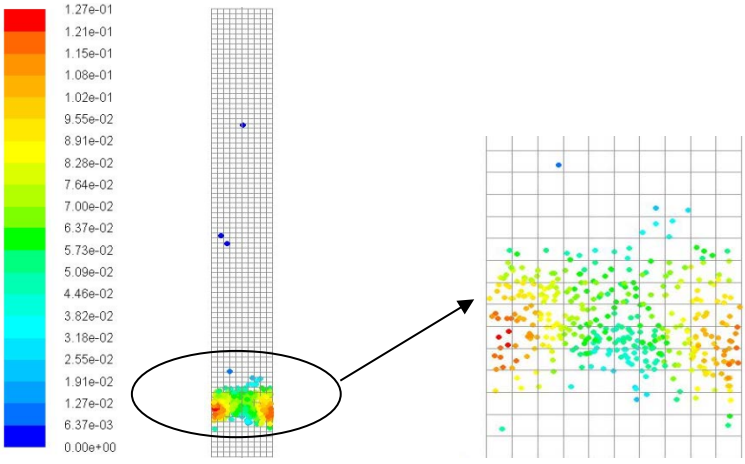


**Figure 4.29:** Unsteady tracking of pinewood particles in the bubbling fluidized biochar bed (colored by time averaged volume fraction of discrete phase).

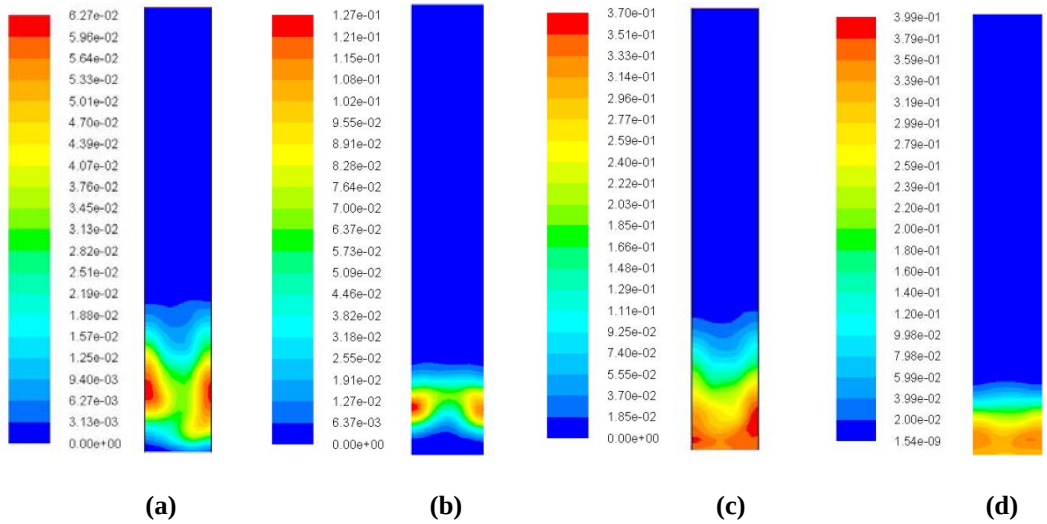


**Figure 4.30:** Time averaged volume fraction of pinewood and char using EE and EL model (u = 1.1 m/s). **(a).** pinewood (EE 2-D); **(b).** pinewood ( EL 3-D); **(c).** biochar (EE 2-D); **(d).** biochar (EL 3-D).

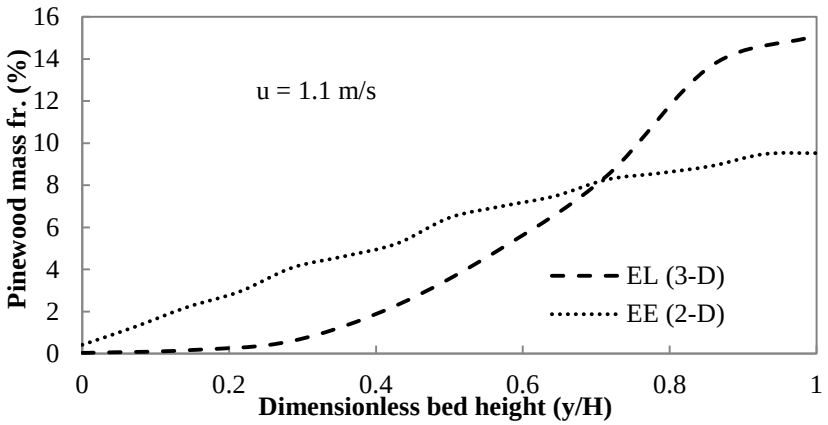


**Figure 4.31:** Comparison of EE (2-D) and EL (3-D) model for time averaged pinewood mass distribution.

Figure 4.32 shows the time averaged volume fraction of pinewood particles using EE (3-D) and EL (3-D) models at superficial gas velocity of 0.68 m/s. In this case, the Gidaspow drag correlation (ANSYS FLUENT) was used for calculating the averaged discrete phase drag force on the biomass phase due to both gas and biochar phases. The no slip boundary condition was used for the gas phase, the partial slip condition was used for the biochar phase and the free slip condition was used for the biomass phase. It is clear that the final bed height predicted lower using the EL approach for both pinewood and biochar particles when compared to the EE approach. The accumulation of pinewood particles at a certain height in the bed was also higher for EL model as compared to EE model. From Figure 4.33, it was clear

that there is considerable difference in the distribution of pinewood particles along the dimensionless bed height between EE (2-D and 3-D) and EL (3-D) model. This shows that the impact of different modelling parameters on the hydrodynamic behaviour of the mixture has to be examined properly for EL model. Therefore, there is the requirement to analyse the effect of the granular properties such as granular temperature in DDPM model on the motion of discrete phase; and to study the sensitivity of collision parameters in DEM model on the mixing/segregation of solid phases.

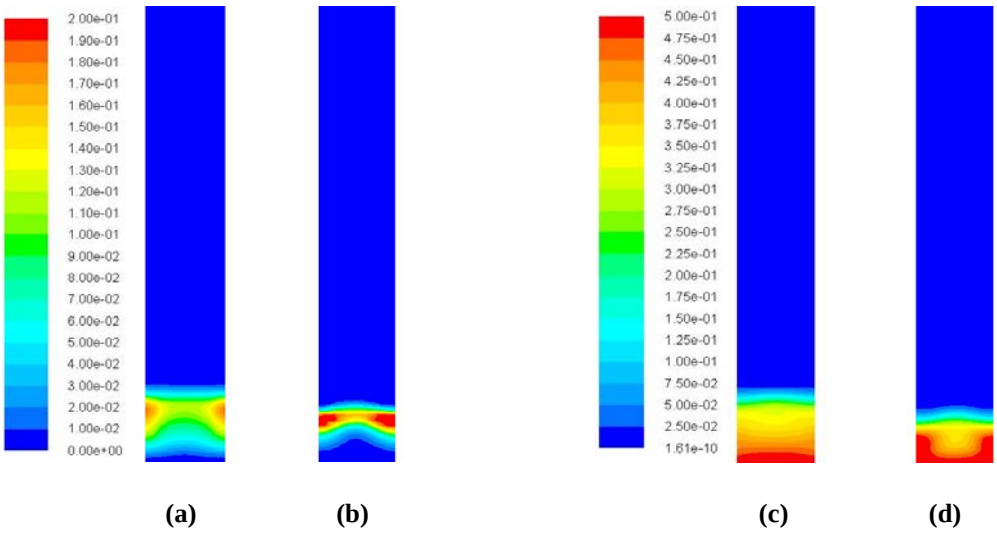


**Figure 4.32:** Time averaged volume fraction of pinewood and char using EE and EL model (u= 0 .68 m/s). **(a).** pinewood (EE 3-D); **(b).** pinewood (EL 3-D); **(c).** biochar (EE 3-D); **(d).** biochar (EL 3-D).

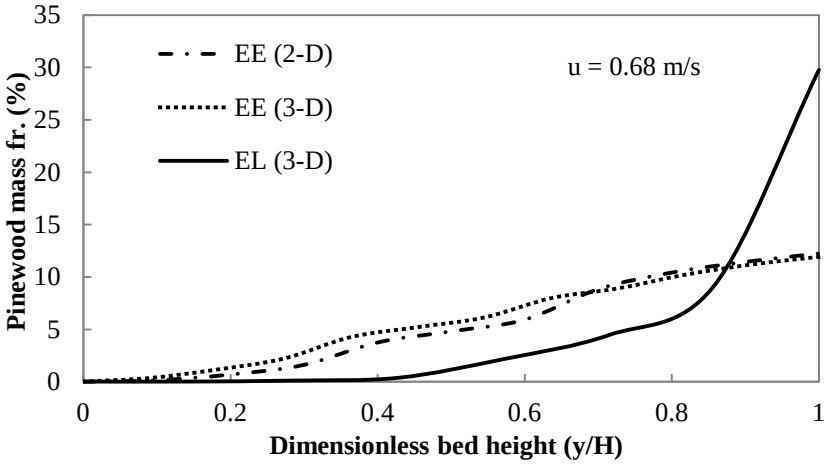


**Figure 4.33:** Comparison of EE (2-D and 3-D) and EL (3-D) model for time averaged pinewood mass distribution.

## 4.3. Conclusions

A multi-phase hydrodynamic model for studying the behavior of biomass in bubbling fluidized bed was developed. The model was validated using the published experimental data for a rice husk-sand mixture in a fluidized bed reactor. Simulations were performed to study the effect of superficial gas velocity on fluidization characteristics of the rice husk-sand mixture. It was found that an increase in the gas velocity to above the minimum fluidization velocity of the mixture favours better mixing of the solid phases with bubbles movement in the bed. Further simulations were conducted to examine the behaviour of the rice husk in a bed of biochar particles. The rice husk-biochar mixture attained uniform mixing at a lower $u/u_{mf}$ value as compared to the rice husk-sand mixture, due to the lesser density difference between the biomass and biochar particles. In addition to the superficial gas velocity, the biochar particle diameter and biomass density had a significant impact on the mixing/segregation patterns of the biomass, whilst the biomass particle diameter had only a mild impact on the behavior. Furthermore, the variation in the granular temperature (which describes the random kinetic energy of particles) with time was also examined for both rice husk and biochar particles. This led to the conclusion that the kinetic energy of fluctuations is higher for rice husk particles, while it is lower for biochar particles. The vertical velocity of pinewood particles calculated along the dimensionless radial distance was higher than biochar particles in the center of the bed, while there was marginal difference near the wall region. It was seen that the hydrodynamics of the bed being affected due to bubbles formation in a 2-D model as compared to a 3-D model. However, the biomass distribution in the mixture was almost the same for the 2-D and 3-D models along the bed height. It was found that the effect of different drag correlations on biomass-biochar mixing/segregation behaviour is considerable for the fluidization conditions considered in this study. It was further analyzed that the value of specularity coefficient affects the segregation rate of different size and density particles at lower superficial gas velocities and there is a need to study the effect of this parameter on mixing behavior at higher gas velocities. The restitution coefficient of biomass and biochar particles also affects the mixing/segregation behavior of the solid phases in the bubbling fluidized bed. However, there is the need to further analyze the effect of

these modeling parameters on mixing/segregation behavior with experimental verification. For EL modelling, there is the need to examine the effect of modeling parameters such as granular properties of the discrete phase on mixing/segregation behavior of biomass-biochar mixture for better analysis of bed hydrodynamics.

# Chapter 5 Modelling of biomass pyrolysis in a bubbling fluidized bed

CFD modelling is used extensively for studying the thermo-chemical reactions with heat and mass transfer in various reactor configurations. Different thermo-chemical processes such as combustion and gasification (Fletcher et al., 1998; Fletcher et al., 2000; Jones et al., 2000; Yan and Lai, 2006; Jin, 2013; Wu et al., 2013) have been simulated using CFD techniques. CFD models for studying biomass pyrolysis have also been developed. Papadikis et al. (2009b) studied the pyrolysis of biomass inside a fluidized bed reactor with Euler-Euler-Lagrangian approach of CFD modeling. Oevermann et al. (2009) developed an Euler- Lagrangian model for wood gasification in a bubbling fluidized bed reactor. Gerber et al. (2010) proposed an Euler- Euler model for wood gasification in bubbling fluidized bed using char as bed material. However, due to the consideration that pyrolysis reactions are orders of magnitude higher than gasification reactions, the char produced from wood was taken separately with fixed diameter, instead of within wood solid phase. An Euler-Euler model for fast pyrolysis of biomass in fluidized bed was proposed by Xue et al. (2011). The results for apparent biomass density, vertical velocity, average temperature and product yields were also compared for different 2-D grid sizes and between 2-D and 3-D domain (Xue et al., 2012). Bruchmüller et al. (2012) studied the thermo-chemical decomposition of biomass using Computational Fluid Dynamics- Discrete Element Model (CFD- DEM) approach. The effect of fluidization velocity, temperature and moisture content on product yield and composition was analyzed and compared with experimental results.

In the previous studies, the focus has been mainly on biomass thermal decomposition in presence of inert sand bed. The objective of this study was to analyze both primary and secondary pyrolysis reactions in dense bed and in freeboard regions in presence of an inert bed as well as a catalyst bed. For examining the rates of heat, mass and momentum transfer during pyrolysis process, bubbling fluidized bed has been chosen which allows better mixing of different phases during biomass degradation and also favours the separation of biomass and biochar particles from

other volatile products. In several studies, biochar, a by-product of biomass pyrolysis, has been used as a bed material. Biochar acts as a catalyst and favors the decomposition of biomass at lower temperatures and also leads to cracking of high molecular weight tarry components (oxygenated compounds mainly) into lighter gaseous components (Morf, 2001; El-Rub, 2008). This increases the gaseous products yield with reduction of liquid compounds that causes polymerization problems during storage of bio-oil. The presence of biochar in the reactor also favors the conversion of tar compounds into poly-aromatic hydrocarbons (PAH), which further re-polymerize and convert into biochar product (Morf, 2001). Hence, a biochar bed reduces the production of tar with simultaneous increase in gas and biochar yields.

In this study, a CFD model was developed for biomass pyrolysis in the presence of inert sand and catalytic biochar particles for analyzing the effect of several parameters such as reactor temperature and particle size on the product yield under bubbling fluidized bed conditions. Although the model did not consider the intra-particle heat and mass transfer effects for the particle range ($\leq$1 mm) analyzed in this study, it did consider the inter-particle heat transfer in the bed and in the freeboard region with particle degradation, tar cracking reactions and variation in the thermo-physical properties with the change in biomass composition. The mass transfer mechanisms inside the reactor were treated using kinetic reactions given for the process in section 3.1.1. Furthermore, the product distribution was analyzed quantitatively by lumping them as gas, tar and biochar.

## 5.1. Model description

The kinetic mechanism with particle scale degradation of biomass and the hydrodynamic model of the previous chapters were utilized for developing a reactive multi-phase CFD model. The model considered the bed hydrodynamics and mixing/segregation of the solid phases, as well as heat and mass transfer effects during biomass thermo-chemical decomposition in a fluidized bed reactor.

### 5.1.1. Kinetic Model

The reaction mechanism proposed for the biomass pyrolysis is same as discussed in phenomenological model developed in chapter 3 (Figure 3.1). During pyrolysis process in the bubbling fluidized bed, the gas mixture (*g*), bio- mixture (*s1*) and bed particles (*s2*) such as sand or a catalyst are present in the reactor. The gas mixture contains primary tar (*T1*), secondary tar (*T2*), non-condensable gases (*G*), water vapor (*W*) and inert gas (*I*) such as nitrogen. The bio-mixture contains biomass (*B*), biochar or char (*C*) and moisture (*M*) content. As per this lumped model, the biomass decomposes to give non-condensable gases (such as CO, $CO_2$ and $H_2$), primary tar (bio-oil) and char (solid carbon product containing mineral matter). The primary tar (containing oxygenated compounds such as acetols) further reacts homogeneously in the gas phase as well as heterogeneously on the surface of catalytically active sites (such as on char surfaces) to convert into NCG and higher molecular weight secondary tar (such as PAHs). The secondary tar also re-polymerizes heterogeneously into char particles in the presence of catalytic reactor environment. The bio-mixture is assumed to be filled with gas in the pores available inside the char particles. This leads to lower density of char particles produced after removal of volatiles from the biomass. The moisture converts into water vapor during drying of biomass particles in the reactor. This mechanism has been considered using a separate reaction scheme and discussed in section 3.1.2 . The bed particles do not react, and hence, no kinetic scheme given in the model. All the reactions in the solid and gas phase are first order in nature with rate constants given using Arrhenius kinetic expressions.

Based on the model details, the rate of generation or consumption for all the solid and gas phase species given as:

For Biomass, $S_{s1,B}$ = $-(K_1 + K_2 + K_3)\,\alpha_{s1}\rho_{s1}X_{s1,B}$ (5.1)

For Char, $S_{s1,C}$ = $K_3\alpha_{s1}\rho_{s1}X_{s1,B} + K_6\,\alpha_g\rho_g X_{g,T2}$ (5.2)

For Moisture, $S_{s1,M}$ = $-K_{vap}\alpha_{s1}\rho_{s1}X_{s1,M}$ (5.3)

For Non-Condensable Gas, $S_{g,G}$ = $K_1\alpha_{s1}\rho_{s1}X_{s1,B} + K_4\,\alpha_g\rho_g X_{g,T1}$ (5.4)

For Primary Tar, $S_{g,T1}$ = $K_2\alpha_{s1}\rho_{s1}X_{s1,B} - (K_4 + K_5)\alpha_g\rho_g X_{g,T1}$ 5.5)

For Secondary Tar, $S_{g,T2} = K_5 \alpha_g \rho_g X_{g,T1} - K_6\, \alpha_g \rho_g X_{g,T2}$ (5.6)

For Water Vapor, $S_{g,W} = K_{vap} \alpha_{s1} \rho_{s1} X_{s1,M}$ (5.7)

Here $K_1$, $K_2$, $K_3$, $K_4$, $K_5$, $K_6$ and $K_{vap}$ are the kinetic constants given for the kinetic reactions (Figure 3.1 ) for biomass particle pyrolysis in chapter 3.

### 5.1.2. Multi-phase reactor model

The Eulerian-Eulerian (EE) approach was applied for this multi-phase reactor model. The continuity, momentum and energy equations were solved for each phase, and a single pressure was shared by all phases. In this model, the turbulence was not resolved both in the dense bed and in the freeboard region due to consideration of Reynolds number in the range of laminar flow (van Wachem et al., 2001).

For the gas phase, a set of mass, momentum and energy conservation equations are formulated. The continuity equation for the gas mixture phase given as:

$$\left[\frac{\partial \left(\alpha_g \rho_g\right)}{\partial t} + \nabla . \left(\alpha_g \rho_g \vec{v}_g\right) = S_g\right] \quad (5.8)$$

where $\rho_g, \overrightarrow{v_g}$ and $\alpha_g$ are the bulk density, velocity and volume fraction of the gas mixture phase, respectively. The sum of volume fractions of gas phase and the solid phases equals to unity. $S_g$ is the source term due to generation/consumption of gas phase species in the reactor. This source term accounts for the inter-phase mass transfer due to chemical reactions. The source term $S_g$ is the sum of the reaction rate terms $S_{g,G}$, $S_{g,T1}$, $S_{g,T2}$ *and* $S_{g,W}$ for non-condensable gases, primary tar, secondary tar and water vapor in the gas phase, respectively. For $i^{th}$ species in the gas phase, the conservation equation given as:

$$\frac{\partial \left(\alpha_g \rho_g X_{g,i}\right)}{\partial t} + \nabla . \left(\alpha_g \rho_g X_{g,i} \vec{v}_g\right) = -\nabla . \left(\alpha_g \rho_g D_{g,i} \nabla X_{g,i}\right) + S_{g,i} \quad (5.9)$$

where $S_{g,i}$ is the reaction rate term. $X_{g,i}$ and $D_{g,i}$ are the mass fraction and diffusion coefficient of $i^{th}$ species in the gas phase mixture, respectively.

The momentum balance for the gas mixture phase given as:

$$\left[\frac{\partial\left(\alpha_g\rho_g\vec{v}_g\right)}{\partial t}+\ \nabla.\left(\alpha_g\rho_g\ \vec{v}_g\vec{v}_g\right)=\ -\alpha_g\ \nabla p+\ \nabla.\bar{\tau}_g+\ \alpha_g\rho_g\vec{g}\ +\sum_{s=1}^{n}(\vec{R}_{gs}+\ \vec{v}_{sg}\dot{m}_{sg}-\ \vec{v}_{gs}\dot{m}_{gs})\right] \quad (5.10)$$

where $\vec{R}_{gs}$ is the interaction force between the gas ($g$) phase and $n$ solid ($s$) phases, $\bar{\tau}_g$ is the stress-strain tensor for gas phase, $\vec{g}$ is the acceleration due to gravity and, $p$ is the pressure shared by all the phases. The interaction force includes the momentum transfer due to the drag force between the gas and the solid phases (as discussed in section 4.1.1). The last two terms are due to the mass transfer between the gas and the solid phases caused by thermal degradation of biomass particles and secondary tar cracking reactions. $\vec{v}_{sg}$ is the interphase velocity defined as follows: if $\dot{m}_{sg} > 0$ (i.e., phase $s$ mass is being transferred to phase $g$), then $\vec{v}_{sg} = \vec{v}_s$; if $\dot{m}_{sg} < 0$ (i.e., phase $g$ mass is being transferred to phase $s$), then $\vec{v}_{sg} = \vec{v}_g$. Similarly, if $\dot{m}_{gs} > 0$, then $\vec{v}_{gs} = \vec{v}_g$; if $\dot{m}_{gs} < 0$, then $\vec{v}_{gs} = \vec{v}_s$.

The energy conservation equation for the gas phase given as

$$\left[\frac{\partial\left(\alpha_g\rho_g H_g\right)}{\partial t}+\ \nabla.\left(\alpha_g\rho_g\ \vec{v}_g H_g\right)=\ -\nabla\vec{q}_g+\Delta H_{rg}\ +\sum_{s=1}^{n}H_{sg}\right] \quad (5.11)$$

where $H_g$ and $\vec{q}_g$are the specific enthalpy and the conductive heat flux of the gas phase, respectively. $\Delta H_{rg}$ is the source term that includes enthalpy change due to gas phase chemical reactions. $H_{sg}$ is the contribution due to inter-phase heat transfer between gas ($g$) and solid ($s$) phases.

$$H_g=\ \int C_{p,g}dT_g \quad (5.12)$$

where $C_{p,g}$is the specific heat at constant pressure of gas phase.

$$H_{sg}=h_{sg}(T_{sn}-\ T_g) \quad (5.13)$$

where $h_{sg}$ is the convective heat transfer coefficient between the $n^{th}$ solid phase and the gas phase. $T_{sn}$ and $T_g$ are the temperature of the $n^{th}$ solid and the gas phase, respectively.

For the solid phases, a set of mass, momentum and energy conservation equations are formulated. The continuity equation for the solid phases given as:

$$\left[\frac{\partial\left(\alpha_{sn}\rho_{sn}\right)}{\partial t}+\ \nabla.\left(\alpha_{sn}\rho_{sn}\,\vec{v}_{sn}\right)=\ S_{sn}\right] \tag{5.14}$$

where $\rho_{sn}$, $\vec{v}_{sn}$ and $\alpha_{sn}$ are the bulk density, velocity and volume fraction of the $n^{\text{th}}$ solid phase, respectively. The source term $S_{sn}$ is the sum of the reaction rate terms $S_{s1,B}$, $S_{s1,C}$ *and* $S_{s1,M}$ for biomass, char and moisture in the bio-mixture phase, respectively. For sand phase, all the reactions rates are considered zero. For $i^{th}$ species in the $n^{th}$ solid phase, the conservation equation given as:

$$\frac{\partial\left(\alpha_{sn}\rho_{sn}\,X_{sn,i}\right)}{\partial t}+\ \nabla.\left(\alpha_{sn}\rho_{sn}X_{sn,i}\,\vec{v}_{sn}\right)=-\nabla.\left(\alpha_{sn}\rho_{sn}D_{sn,i}\,\nabla X_{sn,i}\right)+\ S_{sn,i} \tag{5.15}$$

where $S_{sn,i}$ is the reaction rate term. $X_{sn,i}$ and $D_{sn,i}$ are the mass fraction and diffusion coefficient of $i^{th}$ species in the solid phase mixture, respectively.

The momentum balance for the solid phases given as:

$$\left[\frac{\partial\left(\alpha_{sn}\rho_{sn}\vec{v}_{sn}\right)}{\partial t}+\ \nabla.\left(\alpha_{sn}\rho_{sn}\,\vec{v}_{sn}\vec{v}_{sn}\right)=\ -\alpha_{sn}\,\nabla p\ -\nabla p_{sn}+\ \nabla.\bar{\tau}_{sn}+\ \alpha_{sn}\rho_{sn}\vec{g}\ +\ \sum_{l=1}^{N}(\vec{R}_{ln}+\vec{v}_{sg}\dot{m}_{sg}-\ \vec{v}_{gs}\dot{m}_{gs})\right] \tag{5.16}$$

where $\vec{R}_{ln}$ is the interaction force between the $l^{th}$ gas or the solid phase and $n^{th}$ solid phase (total number of phases are $N$), $\bar{\tau}_{sn}$ is the stress-strain tensor for $n^{th}$ solid phase, and $p_{sn}$ is the pressure of the $n^{th}$ solid phase. The interaction force includes the momentum transfer due to the drag force between the gas and the solid phases (as discussed in section 4.1.1). The last two terms are due to the mass transfer between the gas and the solid phases as described for equation 5.10.

The energy conservation equation for the $n^{th}$ solid phase given as:

$$\left[\frac{\partial\left(\alpha_{sn}\rho_{sn}H_{sn}\right)}{\partial t}+\ \nabla.\left(\alpha_{sn}\rho_{sn}\,\vec{v}_{sn}H_{sn}\right)=\ -\nabla\vec{q}_{sn}+\Delta H_{rsn}\ +\sum_{s=1}^{n}H_{gs}\right] \tag{5.17}$$

where $H_{sn}$ and $\vec{q}_{sn}$ are the specific enthalpy and the conductive heat flux of the $n^{th}$ solid phase, respectively. $\Delta H_{rsn}$ is the source term that includes enthalpy change due to solid phase chemical reactions. $H_{gs}$ is the contribution due to inter-phase heat

transfer between gas ($g$) and solid ($s$) phases. The radiative heat transfer is not taken into account for this model.

$$H_{sn} = \int C_{p,sn} dT_s \tag{5.18}$$

where $C_{p,sn}$ is the specific heat at constant pressure of $n^{th}$ solid phase.

$$H_{gs} = h_{gs}(T_g - T_{sn}) \tag{5.19}$$

where $h_{gs}$ (=$h_{sg}$) is the convective heat transfer coefficient between the gas phase and the $n^{th}$ solid phase.

The kinetic energy of fluctuating particle motion has been represented using granular temperature of $n^{th}$ solid phase ($\theta_{sn}$), which is proportional to mean square of fluctuating velocity of solid particles. The conservation of fluctuating kinetic energy of solid phases given using an algebraic formulation as:

$$\frac{3}{2}\frac{\partial(\alpha_{sn}\rho_{sn}\theta_{sn})}{\partial t} = -(p_{sn}\bar{I} + \bar{\tau}_{sn}) : \nabla \vec{v}_{sn} - \gamma_{\theta_{sn}} + \Phi_{ln} \tag{5.20}$$

where $(p_{sn}\bar{I} + \bar{\tau}_{sn}) : \nabla \vec{v}_{sn}$ is generation of energy due to stress tensor for $n^{th}$ solid phase, $\gamma_{\theta_{sn}}$ is collision dissipation of energy for $n^{th}$ solid phase and $\Phi_{ln}$ is energy exchange between the $l^{th}$ gas or solid phase and $n^{th}$ solid phase.

The constitutive relations for gas-solid multi-phase flow such as gas and solid stress-strain tensor, solids pressure and drag coefficients were taken from Appendix B. The conductive heat flux for the gas and the solid phases has been calculated using Fourier law as discussed in section 3.1.2. The convective heat transfer coefficient ($h_{sg}$) for gas-solid heat transfer is calculated using a Nusselt number correlation given by Gunn (1978). This correlation is valid for granular flows and applicable for gas phase volume fraction in the range of 0.35-1.

### 5.1.3. Thermo-physical properties and kinetic parameters

Some of the thermal and physical properties are given in Table 5.1. However, these properties vary during the pyrolysis process. For the gas phase mixture, the density being calculated using the expression:

$$\rho_g = \frac{p+p_{op}}{R_{gc}T_g \sum_i \frac{X_{g,i}}{M_{wg,i}}} \tag{5.21}$$

where $p_{op}$ is the operating pressure and $M_{wg,i}$ is the molecular weight of the $i^{th}$ species in the gas phase mixture. For the solid phase mixture, the density being calculated using the expression:

$$\rho_{sn} = \frac{1}{\sum_i \frac{X_{sn,i}}{\rho_{sn,i}}} \tag{5.22}$$

where, $\rho_{sn,i}$ is the density of the $i^{th}$ species in the mixture of $n^{th}$ solid phase. The properties such as specific heat and thermal conductivity for a mixture given as

$$\emptyset = \sum_i X_i \emptyset_i \tag{5.23}$$

where $\emptyset$, $X_i$, $\emptyset_i$ are the property of the mixture, mass fraction of $i^{th}$ species and the property of $i^{th}$ species in the mixture, respectively. The effect of particle shrinkage was not considered due to small biomass size and the biomass particle diameter was kept constant during the simulations. The kinetic parameters and the heat of reactions required for this model were taken from Table 3.2 and Table 3.3, respectively.

**Table 5.1:** Thermo-physical properties required during simulation.

| **Property** | **Value** | **Reference** |
|---|---|---|
| Biomass density (kg/m$^3$) | 660 | (Bruchmüller et al., 2012) |
| Char density (kg/m$^3$) | 350 | (Bruchmüller et al., 2012) |
| Sand density (kg/m$^3$) | 2649 | (Xue et al., 2011) |
| Biomass specific heat (J/kg- °C) | 1112 + 4.85$T_{s1}$ | (Bruchmüller et al., 2012) |
| Char specific heat (J/kg- °C) | 1003.2 + 2.09$T_{s1}$ | (Bruchmüller et al., 2012) |

| | | |
|---|---|---|
| Sand specific heat (J/kg- °C) | 860 | (Bruchmüller et al., 2012) |
| Biomass thermal conductivity (W/m-°C) | 0.1798 | (Di Blasi, 1998) |
| Char thermal conductivity (W/m-°C) | 0.088 | (Di Blasi, 1998) |
| Sand thermal conductivity (W/m-°C) | 0.2 | |

### 5.1.4. CFD simulation scheme

The simulation scheme used was similar to the one developed for studying the hydrodynamics of biomass and sand/biochar particles in chapter 4. The details of that scheme were given in section 4.1.3.

### 5.1.5. Solution procedure and initial-boundary conditions

All the simulations were carried out in a 2-dimensional (2-D) fluidized bed reactor domain as shown in Figure 5.1. The simulation domain was divided into fixed number of control volumes by defining grid cells in both horizontal and vertical directions (Table 5.2). The equations were solved using a second order upwind differencing scheme for spatial discretization and second order implicit scheme for transient formulation with a time step size of $10^{-4}$ seconds. An initial bed height of a fixed volume fraction of bed material (sand or biochar) was specified at the start of each simulation. The simulations were conducted for a period of around 60-65 seconds of real simulation time. The time-averaged parametric values were taken from the final 40-50 seconds of the simulation results.

For the gas phase, the initial velocity was specified at the gas inlet of the bed. For the bed material phase, the inlet velocity was assigned as zero. The initial temperature of the gas and the bed material phase kept at 500°C.The biomass entered the reactor at temperature of 27°C. The flow rate at the biomass inlet kept at 100 g/h. The pressure boundary conditions were applied at the outlet of the bed, which was fixed to a reference value of 1 atm. For the gas and the solid phases, a no-slip boundary

condition was used on the walls. The temperature of 500°C was defined as thermal boundary conditions for the isothermal walls. The value of coefficient of restitution for solid phases was taken as 0.97 and the angle of internal friction was used as 55.0. The specifications of the 2-D computational domain are shown in Table 2. The conditions required for initiating the simulations for biomass pyrolysis in sand bed or in biochar bed are listed in Table 5.3.

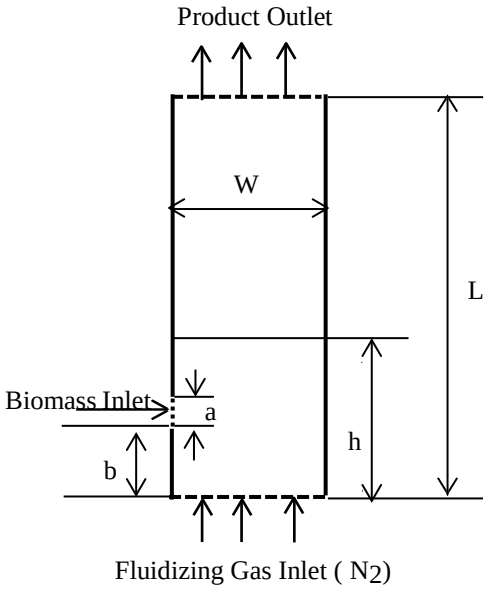


**Figure 5.1:** 2-D fluidized bed reactor domain for biomass pyrolysis.

**Table 5.2:** Specifications of the computational domain employed in the biomass pyrolysis simulations.

| | | | |
|---|---|---|---|
| Reactor height, L mm | 342.9 | Reactor width, W mm | 38.1 |
| Biomass inlet area, a mm | 7.3 | Biomass inlet height, b mm | 13.3 |
| Grid cells in vertical direction | 91 | Grid cells in horizontal direction | 10 |

**Table 5.3:** Initial conditions required for the pyrolysis process in the fluidized bed reactor.

| Phase | Species | Mass fraction | Volume fraction (bed, freeboard) | Temperature (°C) |
|---|---|---|---|---|
| Gas Mixture (*g*) | $N_2$ | 1 | 0.41,1 | 500 |
| | Non-condensable gases | 0 | | |
| | Primary Tar | 0 | | |
| | Secondary Tar | 0 | | |
| | Water vapor | 0 | | |
| Bio-mixture (*s1*) | Biomass | 1 | 0,0 | 27 |
| | Biochar | 0 | | |
| | Moisture | 0 | | |
| Bed material (*s2*) | Sand or Biochar | 1 | 0.59,0 | 500 |

## 5.2. Results and discussion

There is a lack of adequate experimental data for the pyrolysis of biomass in presence of biochar bed, initial simulations were carried out with biomass pyrolysis in the sand bed, and the results were compared with existing literature data (Xue et al., 2012). After the model was validated, simulations were conducted for biomass thermo-chemical degradation with cracking reactions in the presence of biochar (as bed material) particles. The kinetic model used here for analyzing the thermal decomposition of biomass, and its products in the presence of biochar catalytic activity was validated earlier in Chapter 3. The biomass, sand and biochar particles were considered mono-sized and spherical in shape. The effects of operating parameters such as superficial gas velocity, reactor temperature, and biomass particle size on the product distribution have also been analyzed for both the inert sand bed and biochar bed.

### 5.2.1. Biomass pyrolysis in sand bed

For this study, the experimental data (Xue et al., 2012) using red oak as a biomass source have been utilized. The particle diameter of red oak was 0.4 mm, while that of sand particles was 0.52 mm. The initial bed height (h) for the sand bed was kept as 55 mm. The decomposition of red oak in sand bed led to formation of non-condensable gases, primary tar and char. The author did not use a catalyst and the char produced during the pyrolysis also contains very small amounts of alkali and alkaline earth metals that favour the cracking of tar into non-condensable gases and char (Xue et al., 2012). The authors also did not consider the presence of moisture in the biomass. The minimum fluidization velocity ($u_{mf}$) for the sand bed was calculated around 0.28 m/s (Daizo and Levenspiel, 1991).

The superficial gas velocity plays an important role in thermal cracking of tar in fluidized bed system. According to Lathouwers and Bellan (2001b), the ratio of mean gas residence time to tar conversion time ($\tau$) should be greater than 0.1 for conducting these reactions in a given fluidized bed reactor configuration. When the operational data ($u= 2.6u_{mf}$, T= 500°C) of Xue et al. (2012) are used with the kinetic data of Liden et al. (1988), it gives $\tau$ to be only 0.099, which does not favour the thermal cracking of tar. Therefore, only thermal decomposition of biomass was considered for this case. The kinetic parameters for the biomass degradation into non-condensable gases, primary tar (considered as tar) and biochar are shown in Table 3.2.

Figure 5.2 shows the instantaneous volume fraction profile of gas (gas mixture) phase in the bubbling fluidized sand bed. It is clear that there is formation of bubbles in the bed due to the volatiles produced during biomass pyrolysis (small bubble growth has been seen around biomass inlet). These small bubbles coalesce with the bubbles formed due to the fluidized gas ($N_2$) from the bottom of the reactor, and lead to formation of larger bubbles that leave from the bed into the freeboard (visible in top section of the bed). The movement of bubbles from the bottom to top of the reactor favours the mixing of biomass particles in the bed.

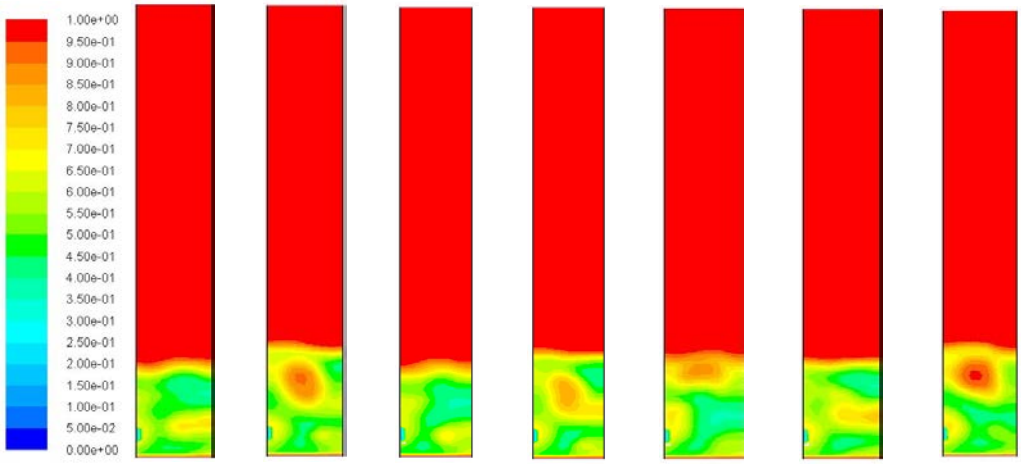


**Figure 5.2:** Instantaneous volume fraction of gas phase during biomass pyrolysis in the bubbling fluidized bed reactor (Time interval is 0.1 s between each profile, Reactor temperature = 500°C, u = 2.6$u_{mf}$).

Figure 5.3 shows the time-averaged volume fractions of gas (gas mixture), sand and biomass (bio-mixture) phase in the reactor. It is clear that the bubbles formation due to fluidized gas and biomass pyrolysis allows the mixing of sand and biomass particles in the bed. However, at this superficial gas velocity (u = 2.6$u_{mf}$), there is still some segregation between biomass and sand particles which reduces the rate of biomass decomposition due to a decrease in the heat and mass transfer rates. Therefore, it is favourable to further increase the superficial gas velocity to around 3-3.5 times of the minimum fluidization velocity for uniform mixing of biomass and bed particles that leads to higher rate of biomass pyrolysis.

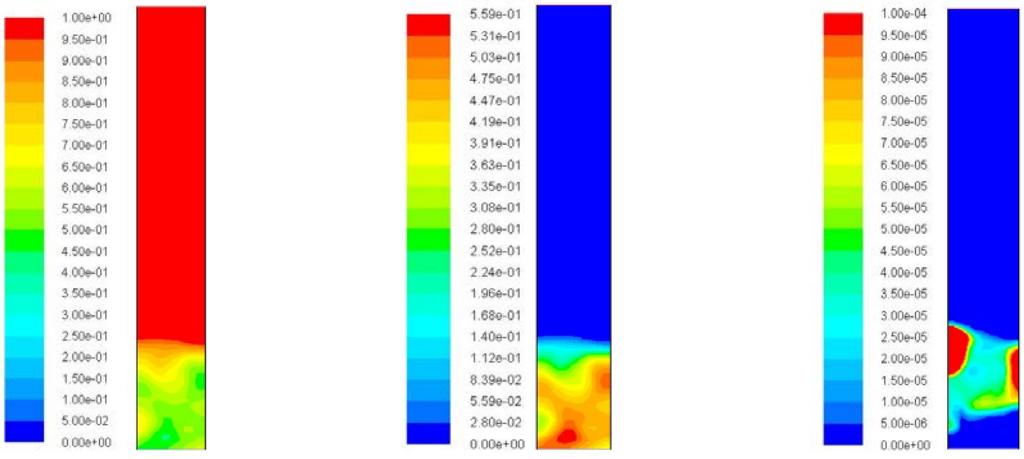


**Gas Phase** **Sand Phase** **Biomass Phase**

**Figure 5.3:** Time-averaged volume fractions of gas, sand and biomass phase in the bubbling fluidized bed reactor (Reactor temperature = 500°C, u = 2.6$u_{mf}$).

Figure 5.4 shows the instantaneous temperature profiles of gas (gas mixture), sand and biomass (bio-mixutre) phases in the reactor, which shows that there was only a negligible change in the temperature of gas and sand phase throughout the reactor. However, there was significant change in the temperature of biomass phase in the fluidized bed. The temperature in the bed increased from 27°C to 500°C. This increase in temperature was due to a convective heat transfer from the gas phase and conductive heat transfer from both the gas and sand phase to biomass particles. In the freeboard region, the temperature for biomass particles stayed in the range of reactor temperature, i.e., around 500°C.

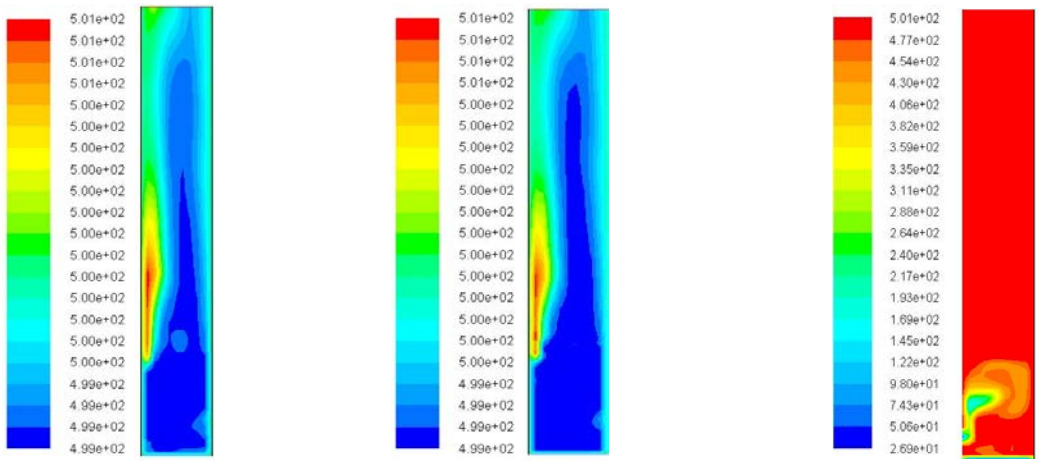


**Figure 5.4:** Instantaneous temperature profiles of gas, sand and biomass phase in the bubbling fluidized bed reactor (Reactor temperature = 500°C, u = $2.6u_{mf}$).

Figure 5.5 shows the time-averaged partial density distribution ($\rho\alpha X$) of gaseous and solid phase components in the reactor. As can be seen from the figure that the gas phase components, i.e., tar and non-condensable gas (NCG) densities increased in both the bed and freeboard region because of the decomposition of biomass. However, there is a difference in the densities of tar and NCG in the reactor due to different rates of formation of these components during biomass pyrolysis. For solid phase components, the biochar remains with the unreacted biomass fraction in the reactor and gets accumulated in top section of the bed. After the removal of tar and NCG, there was an increase in the mass fraction of biochar from 0 to 1 in the biomass phase. The terminal velocity of biochar particles was calculated to be around 0.91 m/s, which is higher than the superficial gas velocity. However, at this

superficial gas velocity, there was no entrainment of biochar particles from the bed, and therefore, the gas velocity should be increased for operating the reactor in continuous manner.

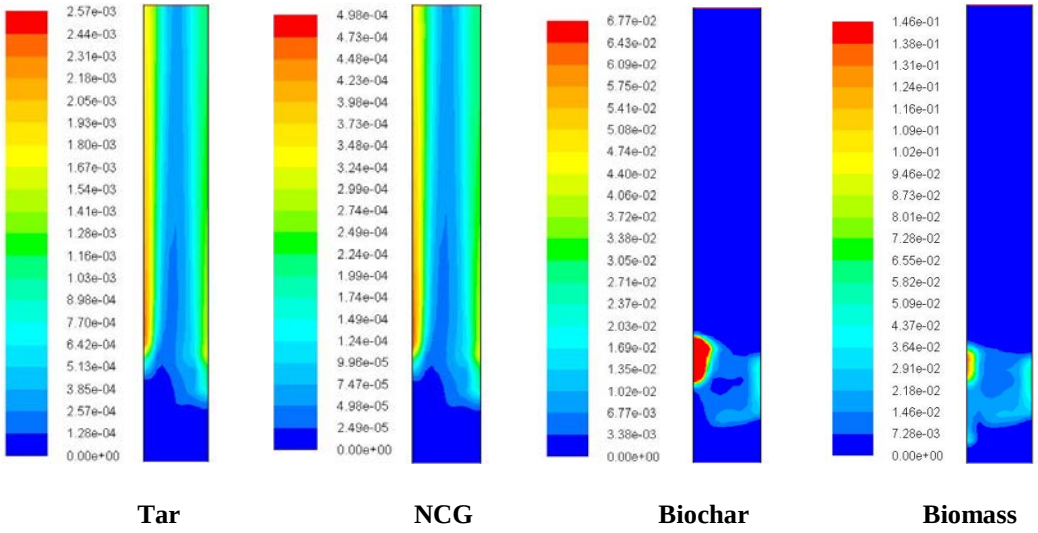


**Figure 5.5:** Time-averaged partial density distribution of gaseous and solid phase components in the bubbling fluidized bed reactor (Reactor temperature = 500°C, u = 2.6$u_{mf}$).

Figure 5.6 shows the time-averaged vertical velocity of gas (gas mixture), sand and biomass (bio-mixture) phase in the reactor. It is clear that at u= 2.6$u_{mf}$, both sand and biomass phases fluidized noticeably with significant motion, neither of the solid phases would leave the reactor at this gas velocity because of the downward movement of both solid phases in top section of the bed. It is also clear that the gas velocity was higher than the superficial gas velocity (u = 0.73 m/s) in the freeboard due to increase in mass flow rate of gas phase by addition of pyrolysis products, i.e. tar and NCG in that region.

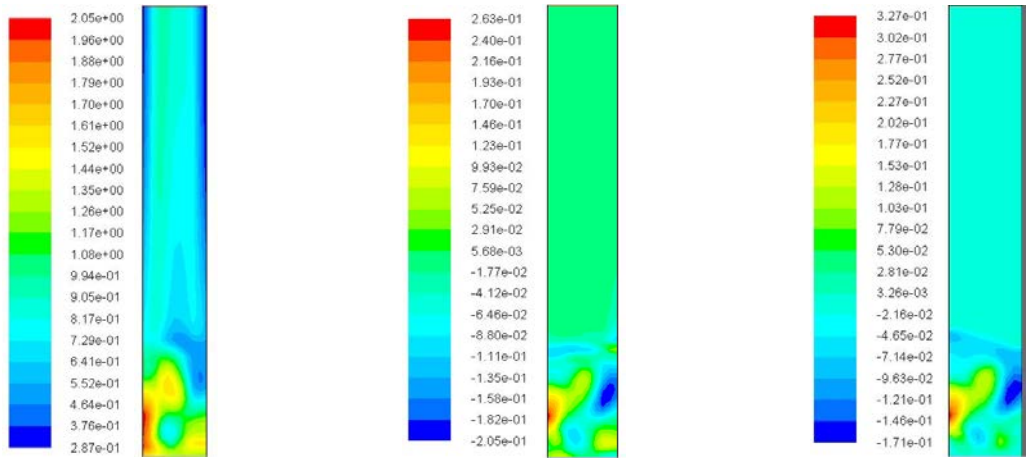


**Gas Phase** **Sand Phase** **Biomass Phase**

**Figure 5.6:** Time-averaged vertical velocity (m/s) of gas, sand and biomass phase in the bubbling fluidized bed reactor (Reactor temperature = 500°C, u = 2.6$u_{mf}$).

The yield (λ) of products from the simulations was calculated using equation 5.24.

$$\lambda = \frac{\int_0^t \int_{outlet} (\rho \alpha v X)\, dA\, dt + \int_{reactor} (\rho \alpha X)\, dV}{MB} \quad (5.24)$$

where *A* is the outlet area of reactor, *V* is the reactor volume and *MB* is the total biomass fed inside the reactor. The total yield of tar, non-condensable gases and char was calculated by adding the amount of these products exiting the reactor as well as the amount still residing inside the reactor. In addition to product species, some amount of the partially converted biomass also remains inside the reactor. It was assumed that the produced char as well as the partially converted biomass constitute as the overall char output from the reactor. The product yield calculated using this equation was compared with the experimental data as shown in Table 5.4.

**Table 5.4:** Comparison of product yield (wt. %) between model and experiments (Temperature = 500°C, u = 2.6$u_{mf}$)

| **Method** | **Tar** | **Non-condensable gases** | **Char** |
|---|---|---|---|
| Experiments (Xue et al., 2012) | 71.7 ± 1.4 | 20.5 ± 1.3 | 13.0 ± 1.5 |
| Model | 77.7 | 15.1 | 7.2 |

The apparent error in experimental data in Table 5.4, where the overall mass balance of species adds up to 105.2 wt.% could be attributed to experimental uncertainties due to the presence of non-condensable carrier phase $N_2$ (Xue et al., 2012). After

accounting for this error, the yield of non-condensable gases from experiments was 15.3 wt. %, which compared well with the simulation value of 15.1 wt.%. The tar and char content from the modelling results were also in range of the experimental values.

Figure 5.7 shows the effect of reactor temperature on the yield of pyrolysis products at superficial gas velocity of 0.73 m/s. It is clear that that the maximum yield of tar occurred at around 500°C. On increasing the temperature above 500°C, the conditions were more favourable for thermal cracking of primary tar into non-condensable gases (gas residence time to tar conversion time is greater than 0.1) which increased the yield of NCG at the expense of tar. However, the conversion of primary tar into secondary tar and secondary tar polymerizarion into biochar mainly occurs at temperatures higher than 800°C due to thermal cracking (Morf, 2001); and therefore, these reactions were not considered in this study. At temperature lower than 500°C, the conditions were more favourable for conversion of biomass into biochar leading to higher yields of biochar with lower yields of both tar and NCG. Figure 5.8 shows instantaneous partial density distribution of volatile products at temperatures higher than 500°C. From the figure, it is clear that at 600°C in the freeboard region, due to conversion of tar into NCG, the partial density of NCG increased (due to both primary and secondary reactions), while the partial density of tar decreased. At temperature around 700°C, the reaction rate increased for tar to NCG conversion leading to negligible tar at the reactor outlet with higher concentration of NCG in the freeboard region.

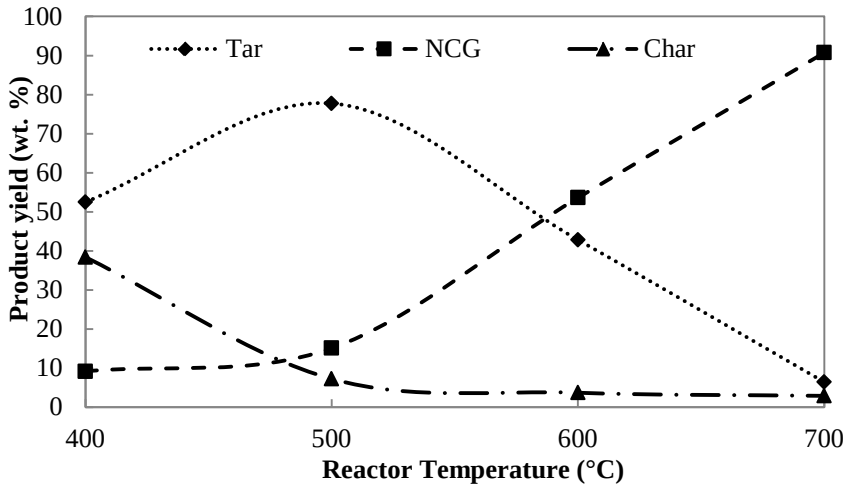


**Figure 5.7:** Product yield at different reactor temperatures in sand bed (u = 0.73 m/s, particle

diameter= 0.4 mm).

Figure 5.9 shows the yield of pyrolysis products at different gas velocities. For lower superficial gas velocities (less than $2.6u_{mf}$), the ratio of mean gas residence time to tar conversion time would be higher than 0.1, thus leading to thermal cracking of primary tar. However, as the thermal cracking of tar into NCG is highly dependent on the gas residence time, it was seen that with a decrease in the gas velocity from $2.1u_{mf}$ to $1.5u_{mf}$, there was a considerable increase in the amount of NCG with a simultaneous decrease in the tar content in the reactor. Finally, there was no significant effect of superficial gas velocity on the biochar yields.

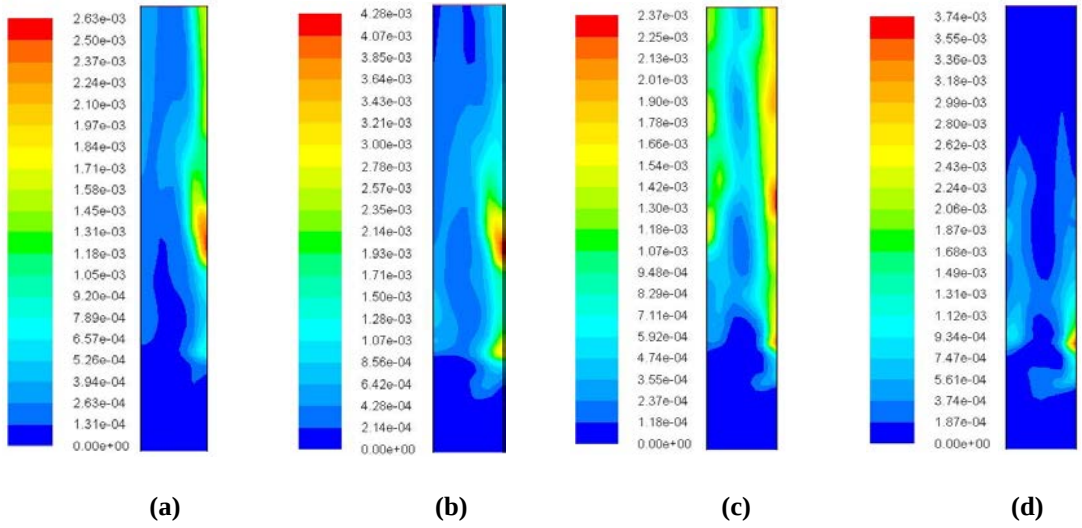


**Figure 5.8:** Instantaneous partial density distribution of tar and NCG at different temperatures in sand bed; **(a).** NCG (T = 600°C); **(b).** Tar (T = 600°C); **(c).** NCG (T = 700°C); **(d).** Tar (T = 700°C).

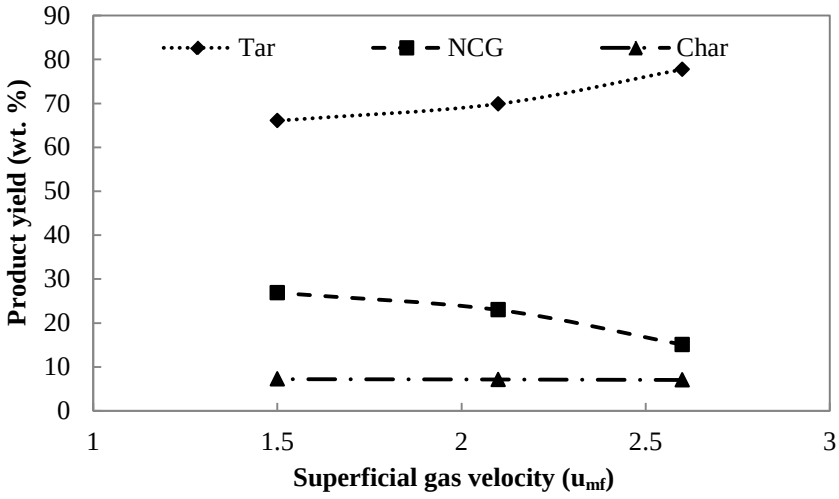


**Figure 5.9:** Product yield at different superficial gas velocities in sand bed (Temperature= 500°C, particle diameter= 0.4 mm).

Table 5.5 shows the product yields at different superficial gas velocities and reactor temperatures. It was found that the both gas velocity and reactor temperature have a significant impact on the thermal cracking of tar into non-condensable gases. Therefore, at a given temperature, an increase in the gas velocity reduces the gas residence time inside the reactor, thus leading to lower conversion of tar into NCG. Also, with an increase in the temperature at a given velocity, the rate of thermal cracking increases, that leads to a considerable increase in the yield of NCG with simultaneous decrease in the tar content. However, any increase in the temperature above 600°C causes slight reduction in biochar yields due to higher conversion of biomass to volatile products.

**Table 5.5:** Product yield comparison at different superficial gas velocities and reactor temperatures in sand bed (particle diameter = 0.4 mm).

| **Yield (wt. %)** | **u = 0.42 m/s** | | **u = 0.73 m/s** | |
|---|---|---|---|---|
| | **T = 600°C** | **T = 700°C** | **T = 600°C** | **T=700°C** |
| Tar | 28.9 | 1.4 | 42.8 | 6.4 |
| NCG | 67.2 | 95.5 | 53.5 | 90.7 |
| Char | 3.9 | 3.1 | 3.7 | 2.9 |

Figure 5.10 shows the time averaged volume fraction of biomass (bio-mixture) phase in the bubbling fluidized sand bed for different biomass particle sizes at superficial gas velocity of 0.63 m/s and reactor temperature of 500°C. From the figure, it is clear that with an increase in the particle size, there was a better distribution of biomass particles throughout the bed. This was due to the fact that smaller biomass particles have a tendency to move upwards with the gas phase, where they segregate from the sand particles. However, the larger particles tend to remain in the bed due to lower drag force, and favour the mixing between different size and density particles in the bed.

Figure 5.11 shows the effect of biomass particle size on product yields. It was found on increasing the biomass particle diameter, the yield of volatile products (both tar and NCG) decreases slightly with a corresponding increase in the yield of char product. This was due to the fact that the lower rate of convective heat transfer

(Nusselt's correlation) to the larger biomass particles leads to higher amount of char in the bio-mixture phase. Therefore, it is important to choose an optimum particle size along with other operating conditions such as reactor temperature and gas velocity for the desired product yield from biomass pyrolysis in a bubbling fluidized bed.

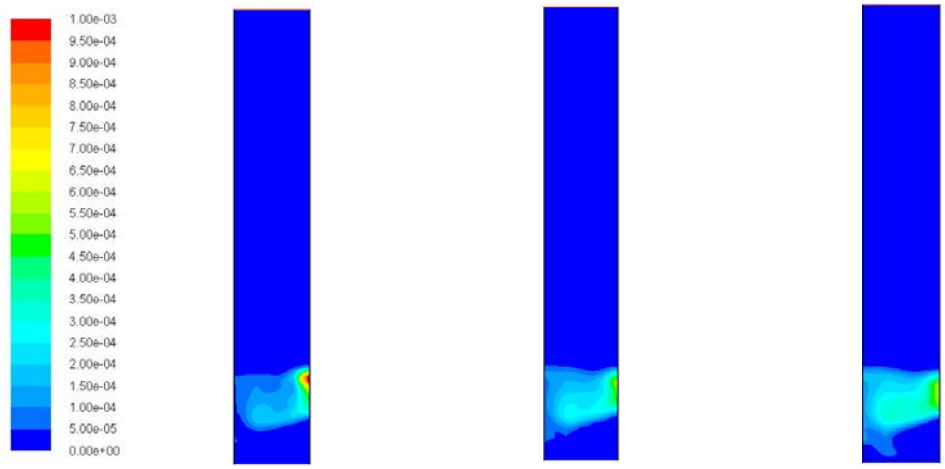


**Figure 5.10**: Time averaged volume fraction of biomass phase in sand bed for different biomass particle sizes (u = 0.63 m/s, Reactor temperature = 500°C); **(a).** particle diameter = 0.4 mm; **(b).** particle diameter =0.6 mm; **(c).** particle diameter = 0.8 mm.

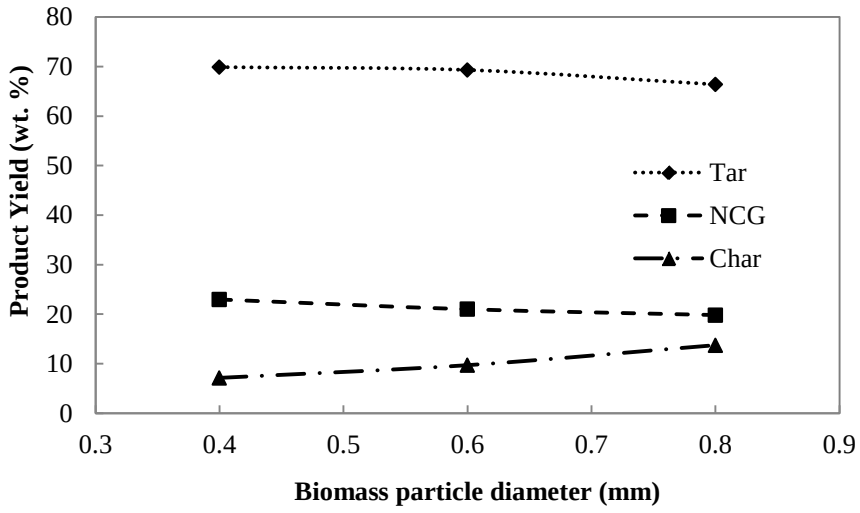


**Figure 5.11:** Product yields for different biomass particle sizes in sand bed (u= 0.63 m/s, Reactor temperature = 500°C).

### 5.2.2. Biomass pyrolysis in biochar bed

In this study, instead of the inert sand bed, a bed of biochar particles containing the active mineral content was used for biomass fluidization. As in the inert sand bed

studies, red oak particles were used as the biomass (properties given in Table 5.1). The density of biochar particles was assumed to be 1470 kg/m$^3$ (Brown et al., 2006). The specific heat of biochar bed was taken from Table 5.1. The initial bed height (h) for the biochar bed was kept as 80 mm. The minimum fluidization velocity ($u_{mf}$) for the biochar bed was calculated as 0.45 m/s (Daizo and Levenspiel, 1991). Due to presence of biochar, the secondary reactions of tar would also take place in the reactor from the outset. The real effect of the catalytic activity of biochar on pyrolysis products is not known, and therefore, it was considered that biochar lowers the temperature required for secondary reactions, and thus favors the cracking and polymerization reactions. This leads to the cracking of primary tar into non-condensable gases and secondary tar, both in the dense bed and in the freeboard region; and the secondary tar re-polymerization into char in the dense bed. The kinetic parameters for the cracking reactions of primary tar and secondary tar conversion to char were taken from literature as given in Table 3.2. The superficial gas velocities and reactor temperatures investigated in this study do not favor thermal cracking of tar compounds (mean gas residence time to tar conversion time is less than 0.1). Furthermore, in the current model, the char produced by biomass degradation was considered to be in the bio-mixture phase, whereas the char produced by secondary tar polymerization was considered to be in the biochar bed. The thermo-physical properties of produced char were used from Table 5.1. The non-condensable gases produced by both biomass and primary tar reaction were considered to be in the gas phase.

Figure 5.12 shows the time averaged volume fraction of gas (gas mixture), biochar (bed) and biomass (bio-mixture) phase in the reactor. It was found that at such low superficial gas velocities ($u = 1.5u_{mf}$), there was a channelling of the feed gas with the volatiles formed due to biomass pyrolysis. This also leads to segregation between biomass and biochar particles in the bed. Hence, to improve the heat and mass transfer rates, the gas velocity should be increased for adequate mixing between different solid phases.

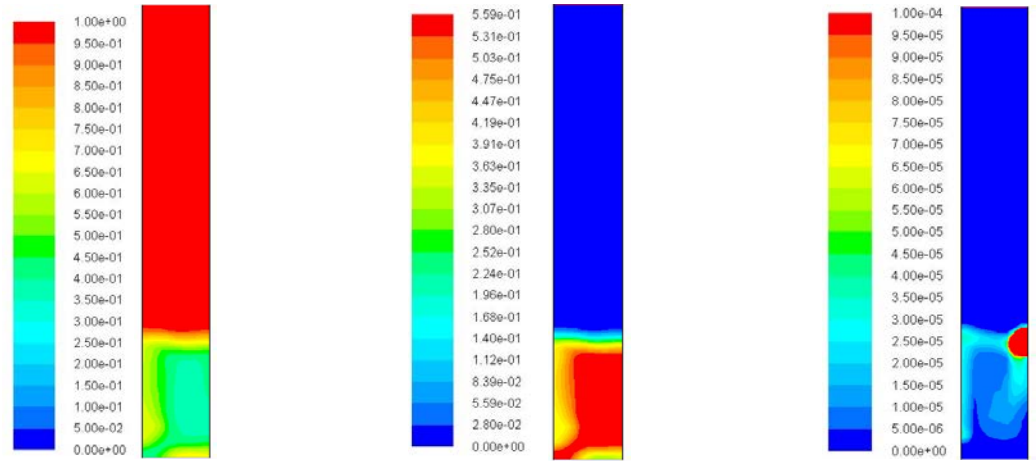


**Figure 5.12:** Time-averaged volume fractions of gas, biochar and biomass phase in the bubbling fluidized bed reactor (Reactor temperature = 500°C, u = 1.5$u_{mf}$).

Figure 5.13 shows the time averaged partial density distribution ($\rho\alpha X$) of gaseous and solid components produced by secondary cracking reactions. From the figure, it is clear that there was considerable formation of volatile products by primary tar cracking in the freeboard region. There was also formation of biochar by secondary tar polymerization reaction which remains in the bed under the prevailing fluidization condition.

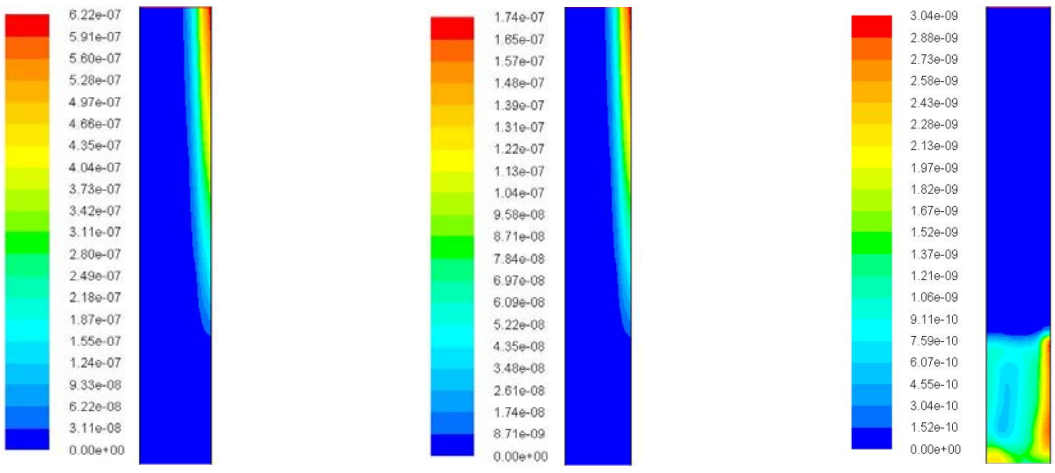


**Figure 5.13:** Time averaged partial density distribution of gaseous and solid products by catalytic cracking reactions (Reactor temperature = 500°C, u = 1.5$u_{mf}$). **(a).** NCG (from primary tar); **(b).** Secondary tar (from primary tar); **(c).** Biochar (from secondary tar).

At higher temperatures (with same superficial gas velocities), the catalytic conversion of primary tar into NCG and secondary tar increased significantly

(see Figure 5.14). This leads to higher partial density of NCG and secondary tar near the reactor outlet at 800°C when compared with that at 500°C (see Figure 5.13). The secondary tar polymerization to biochar also increased at 800°C causing higher concentration of biochar inside the bed as compared to that in Figure 5.13.

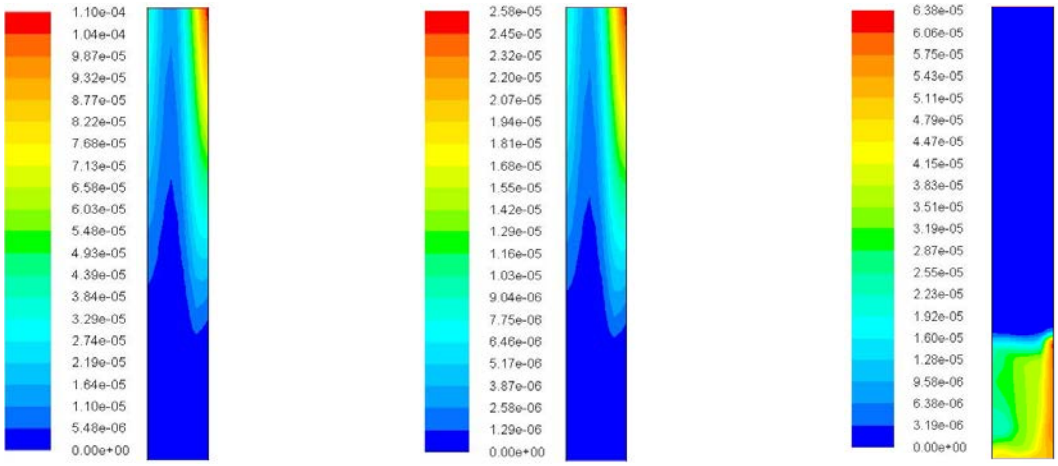


**(a)** **(b)** **(c)**

**Figure 5.14:** Time averaged partial density distribution of gaseous and solid products by catalytic cracking reactions (Reactor temperature = 800°C, u = $1.5u_{mf}$). **(a).** NCG (from primary tar); **(b).** Secondary tar (from primary tar); **(c).** Biochar (from secondary tar).

Table 5.6 shows the effect of reactor temperature on the product yield during biomass pyrolysis in presence of biochar bed. It was found that with any increase in the temperature above 500°C, there was an increase in the yield of tar and NCG due to higher rate of biomass decomposition into volatile products as compared to solid biochar product. However, upon increasing the temperature beyond 600°C, there was a slight decrease in the tar yield with a corresponding increase in the NCG yield. This is mainly due to the cracking of primary tar into NCG at this operating temperature. Finally, increasing the temperature to about 800°C caused a further reduction in the tar content. However, both secondary tar (around 1 wt. %) and NCG (around 3.3 wt. %) were formed by primary tar cracking reactions after 800°C. The production of biochar (wt. %) by secondary tar polymerization reaction was negligible under the operating conditions investigated in this study.

**Table 5.6:** Product yield comparison at different reactor temperatures in biochar bed (u= $1.5u_{mf}$, particle diameter = 0.4 mm).

| **Yield (wt.%)** | **T =500°C** | **T =600°C** | **T =700°C** | **T =800°C** |
|---|---|---|---|---|
| Tar | 77.7 | 79 | 78.3 | 76.2 |
| NCG | 15.4 | 16.4 | 17.4 | 20.2 |
| Char | 6.9 | 4.6 | 4.3 | 3.6 |

Figure 5.15 shows the time averaged vertical velocity of gas (gas mixture), biochar (bed) and biomass (bio-mixture) phase in the bubbling fluidized bed. From the figure, it is clear that due to formation of bubbles of inlet gas and volatile products, the vertical velocity of gas phase is highest near the biomass inlet. The gas bubbles then provide the upward movement to biomass and biochar particles from bottom to top section of the bed, leading to higher velocities for the both solid phases. Furthermore, at such high gas velocities, there would be entrainment of both biomass and biochar particles from the reactor (vertical velocities are positive for both the solid phases near reactor outlet).

Table 5.7 shows the effect of superficial gas velocity on the product distribution in the presence of biochar bed. It was seen that with an increase in the gas velocity, there was an increase in the tar yield with a simultaneous decrease in the NCG content. This was due to the fact that at higher gas velocities, the residence time for volatiles reduces leading to lower conversion of primary tar into NCG under the operating conditions considered in this study. However, the reduction in the biochar yield on increasing the gas velocity was due to the increased rate of biomass conversion to volatile products as compared to solid biochar.

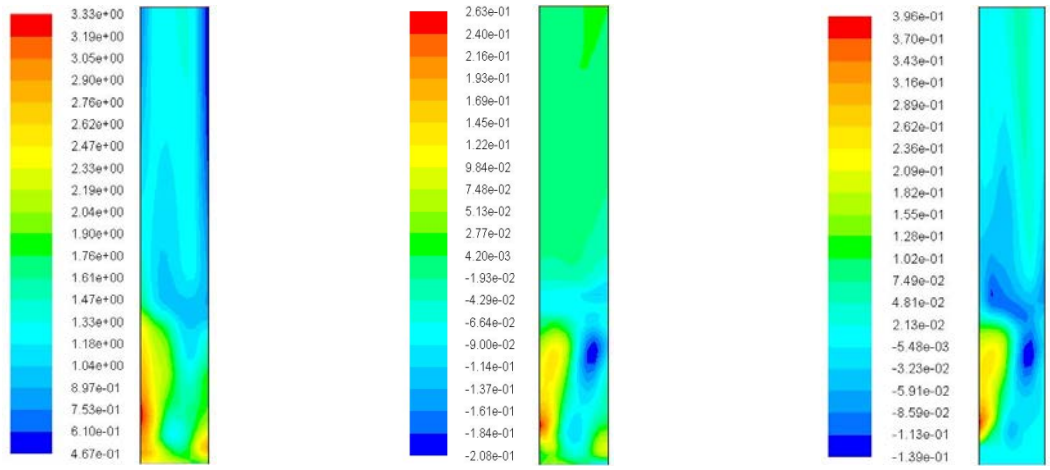


**Figure 5.15:** Time-averaged vertical velocity (m/s) of gas, biochar and biomass phase in the bubbling fluidized bed reactor (Reactor temperature=800°C, u=2.5$u_{mf}$).

**Table 5.7:** Product yield comparison at different superficial gas velocities in biochar bed (Reactor temperature = 800°C, particle diameter = 0.4 mm).

| **Yield (wt.%)** | **u =1.5$u_{mf}$** | **u =2$u_{mf}$** | **u =2.5$u_{mf}$** |
|---|---|---|---|
| Tar | 76.2 | 77.1 | 78.4 |
| NCG | 20.2 | 19.3 | 19.2 |
| Char | 3.6 | 3.6 | 2.4 |

Figure 5.16 shows the time averaged volume fraction of biomass (bio-mixture) phase in the bubbling fluidized biochar bed. It was found that with an increase in biomass particle diameter, there is a better distribution of biomass particles throughout the bed. This leads to improved mixing of biomass and biochar particles along the reactor height which favors the biomass degradation during pyrolysis in bubbling fluidized bed.

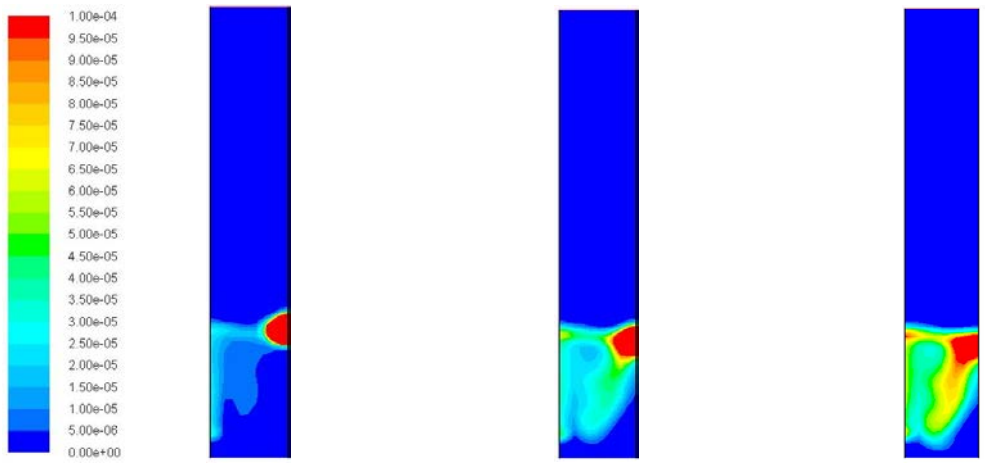


**Figure 5.16:** Time averaged volume fraction of biomass phase in biochar bed for different biomass particle sizes (u = 0.9 m/s, Reactor temperature = 800°C); (a) particle diameter = 0.4 mm; (b) particle diameter =0.7 mm; (c) particle diameter = 1 mm.

Table 5.8 shows the effect of biomass particle size on pyrolysis product yield in the presence of biochar bed. It is clear that on increasing the particle diameter, there was a slight reduction in the volatile product yield with a corresponding increase in the biochar content. This was due to the fact that with higher particle size, the rate of convective heat transfer to the biomass particles is reduced leading to higher amount of solid biochar product. However, there was no significant effect of biomass particle size on tar cracking reactions under the operating conditions considered in this study.

**Table 5.8:** Product yield comparison at different biomass particle sizes in biochar bed (u= $2u_{mf}$, Reactor temperature = 800°C).

| **Yield (wt.%)** | **D = 0.4 mm** | **D = 0.7 mm** | **D = 1 mm** |
|---|---|---|---|
| Tar | 77.1 | 77 | 76.2 |
| NCG | 19.3 | 19.2 | 19.1 |
| Char | 3.6 | 3.8 | 4.7 |

## 5.3. Conclusions

A multi-phase CFD model for studying biomass pyrolysis in a bubbling fluidized bed was developed. The model was validated using the experimental data for biomass pyrolysis in the presence of a sand bed. The simulation results were examined to analyze the effect of reactor temperature, superficial gas velocity and biomass particle size on the bed hydrodynamics and product yield in the inert sand bed. It was found that at temperatures higher that 500°C, there was a significant conversion of primary tar into NCG due to thermal cracking inside the reactor. Any increase in the superficial gas velocity favoured production of tar due to lower residence time available for the tar cracking reactions. An increase in the biomass particle size led to reduction in volatile product yields with simultaneous increase in the biochar yield due to a decrease in the rate of heat transfer inside the particle. The model was further used for analyzing the biomass pyrolysis in the biochar bed inside the bubbling fluidized reactor. The effects of temperature, superficial gas velocity and biomass particle diameter on the bed hydrodynamics and product yield were also studied. Based on simulation results, it was found that higher reactor temperature (around 800°C) favors the catalytic cracking of primary tar into NCG and secondary tar. However, the effect of superficial gas velocity and particle size was not significant on catalytic cracking reactions. Furthermore, there is a need to accurately estimate the kinetic constants of tar cracking reactions in the presence of biochar particles for considering the real effect of biochar catalytic activity; and to study the combined effect of catalytic cracking in the presence of biochar particles and thermal cracking of tar compounds for estimating the accurate yield of biomass pyrolysis products in a bubbling fluidized bed reactor.

# Chapter 6 Concluding Remarks and Recommendations

## 6.1. Concluding Remarks

For analysing the biomass pyrolysis process, a multi-scale modelling scheme has been proposed. This scheme includes particle as well as reactor scale studies of the process. A phenomenological model has been developed for examining the biomass thermo-chemical decomposition at particle level with an emphasis on the effect of catalytic activity of biochar. The hydrodynamic model has been developed for studying the mixing/segregation behaviour of biomass and sand/biochar particles in a bubbling fluidized bed. The model was then integrated for analysing the biomass pyrolysis in a bubbling fluidized reactor in presence of inert sand and catalytically active biochar particles.

### 6.1.1. Phenomenological modelling of biomass pyrolysis processes

The particle model has been developed for predicting the combined effect of physical and chemical processes such as particle shrinkage and drying during biomass pyrolysis. This detailed phenomenological model includes the kinetics of both primary and secondary decomposition of biomass products on a lumped basis. The model also considers the catalytic effect of biochar on the reaction mechanism. The modelling results were validated using experimental data and the effect of different operating parameters on rate of biomass decomposition was analysed. Based on the results, following important conclusions may be made from this study:

1. The biomass particle size and reactor temperature strongly influences the rate of biomass conversion to pyrolysis products.
2. On increasing the reactor temperature, the rate of heat transfer and chemical reaction increases, leading to a reduction in overall time for biomass pyrolysis.
3. An increase in the particle size leads to a decrease in both conductive and convective heat transfer which causes delay in heating of particle core, and increase biomass conversion time. However, for particle sizes less than 1 mm, a uniform temperature throughout the particle exists due to negligible heat transfer resistance inside the particle.

4. On increasing the moisture content, the time required for evaporation of available water inside the particle increases which leads to delays in the onset of biomass conversion, and increase the overall pyrolysis time.
5. The particle shrinkage causes reduction in particle size which favours higher rate of heat transfer, and faster decomposition of biomass particles.

### 6.1.2. Hydrodynamic modelling of biomass in a bubbling fluidized bed

A multi-fluid CFD model for studying fluidization of biomass with other solid particles such as sand or biochar in a bubbling fluidized bed has been developed. The Euler-Euler (EE) modelling approach was applied for the gas and different solid phases, and the model was validated using the available experimental data. The effect of different process and modelling parameters was examined on the mixing/segregation behaviour of mixture of biomass and sand/biochar particles using simulation results. Following specific conclusions may be drawn from this study:

1. The increase in gas velocity to above minimum fluidization velocity favours the mixing of solid phases with bubbles movement in the bed.
2. The density of both biomass and biochar particles affects the rate of mixing/segregation in the bubbling bed. The particle size of biochar particles has a significant impact, whilst the biomass particle size has a negligible impact on fluidization behaviour of solid phases for given operating conditions.
3. The granular temperature (kinetic energy of fluctuation of particles) is higher for biomass as compared to biochar particles. The vertical velocity is higher for biomass as compared to biochar particles in centre of the bed with marginal difference along the wall region.
4. Although the distribution of bubbles was different in the 2-D and 3-D bed, the biomass distribution in the mixture was same for both the configurations.
5. The modelling parameters for particle-particle and particle-wall interactions such as restitution coefficient and specularity coefficient significantly affect the rate of mixing/segregation of biomass-biochar mixture. However, the drag coefficient had a relatively negligible impact on the simulation results.

6. For Euler-Lagrangian (EL) modelling, there is the requirement to analyse the impact of granular properties in DDPM model on the motion of discrete phase for better estimation of mixing/segregation of biomass and biochar particles in the bubbling fluidized bed.

### 6.1.3. Modelling of biomass pyrolysis in a bubbling fluidized bed

A multi-scale CFD model using both phenomenological and hydrodynamic model has been developed for studying biomass pyrolysis in a bubbling fluidized bed reactor. The kinetic mechanism was combined with the reactor hydrodynamics using Euler-Euler framework and the modelling results were validated using the available experimental data. The effect of different operating parameters were analysed on product yield in the inert sand and catalytically active biochar bed. Following are significant conclusions of this study:

1. At temperatures higher than 500°C, there was significant conversion of primary tar into NCG due to thermal cracking inside the bubbling fluidized bed reactor. However, for temperatures lower than 500°C, the formation of biochar was favoured as compared to volatile products.
2. The increase in superficial gas velocity leads to higher concentration of tar due to lower residence time for tar cracking into gaseous products.
3. The increase in biomass particle size causes reduction in the rate of heat transfer inside the particle which leads to higher yields of biochar as compared to tar and NCG.
4. The higher reactor temperature favours cracking of primary tar into NCG and secondary tar in the presence of biochar particles. However, the effect of superficial gas velocity and biomass particle size was not significant on catalytic cracking reactions.
5. There is requirement to calculate the real effect of biochar catalytic activity on primary tar cracking and secondary tar polymerization reactions.
6. There is a need of further study to investigate the combined effect of thermal and catalytic cracking on biomass pyrolysis.

## 6.2. Recommendations

Based on the conclusions from the previous section, the following are important recommendations for future research work:

1. The accurate estimation of the kinetic parameters for tar, NCG and biochar formation during the biomass pyrolysis and tar cracking in the presence of biochar is required.
2. The experimental studies for examining the mixing/segregation behaviour of biomass-biochar particles in the bubbling fluidized bed should be conducted. Furthermore, the experimental data needs to be compared with the CFD simulation results for predicting the sensitivity of different operating and modelling parameters on the bed hydrodynamics.
3. The effect of other operating parameters such as bed height and biochar particle size on biomass catalytic pyrolysis needs to be studied.
4. The biomass pyrolysis using DDPM-DEM model for considering the degradation of individual particles in the bubbling fluidized bed reactor is required. This would provide a better understanding of the thermo-chemical phenomena and leads to improvement in the reactor design and process efficiency. Furthermore, there is the need to calculate the reaction rates with distributed kinetic models such as CPD for analysing the distribution of pyrolysis products at different reactor conditions. This can be achieved by integrating the CPD model for biomass pyrolysis with the DDPM-DEM model in the CFD framework.

# Appendix

## Appendix A

### A.1. Porosity and Permeability

There is variation in physical and chemical properties of particle during thermo-chemical conversion of solid biomass into char. Both these properties of biomass also vary with time during conversion and are dependent on apparent densities of biomass, moisture and char:

$$\varepsilon = \varepsilon_{B,0} + \frac{(\rho_B+\rho_M)-\rho_{B,0}}{\rho_{C,f}-\rho_{B,0}} (\varepsilon_{C,f} - \varepsilon_{B,0})$$

$$\beta = \beta_{B,0} + \frac{(\rho_B+\rho_M)-\rho_{B,0}}{\rho_{C,f}-\rho_{B,0}} (\beta_{C,f} - \beta_{B,0})$$

Here, 0 stands for initial state (at the start of process) and *f* stands for final state (at the end of process).

For considering particle anisotropy, i.e., large variation in some properties of solid biomass and char along and across the grain direction, the permeability for both biomass and char are taken by averaging out their permeability in these directions.

$\beta_{B,0} = ( \beta_{B,0\,(across)} + \beta_{B,0\,(along)} ) / 2$

and, $\beta_{C,f} = ( \beta_{C,f\ (across)} + \beta_{C,f\,(along)} ) / 2$

### A.2. Effective Diffusivity

According to the porous media theory, effective diffusivity, $D_{eff,i} = \varepsilon * D_i/\tau$

where, $D_i$ is molecular diffusivity of $i^{th}$ species ( neglecting the contribution due to Knudsen diffusion) and $\tau$ is tortuosity (taken as 1 in this case)

### A.3. Effective Thermal Conductivity

The effective thermal conductivity of biomass particle is due to contribution of both molecular conductivity and radiative conductivity.

$k_{eff} = k_{cond} + k_{rad}$

where, $k_{cond}$ is conductive contribution to thermal conductivity = $\varepsilon\, k_v + k_s$

$k_v$ is vapour phase thermal conductivity.

$k_s$ is solid medium thermal conductivity, which is also a function of apparent biomass, moisture and char densities.

$$k_s = k_{B,0} + \frac{(\rho_B+\rho_M)\,\rho_{B,0}}{\rho_{C,f}-\rho_{B,0}}\,(k_{C,f} - k_{B,0})$$

For considering particle anisotropy, the thermal conductivity for both biomass and char are also taken by averaging out their thermal conductivity across and along the grain direction.

$$k_{B,0} = (k_{B,0\,(across)} + k_{B,0\,(along)})/2$$

and, $$k_{C,f} = (k_{C,f\ (across)} + k_{C,f\,(along)})/2$$

and, $k_{rad}$ is radiative contribution to thermal conductivity (given as a function of 3rd power of particle temperature)

$$k_{rad} = \frac{4}{1}(\sigma e d_{pore} T^3)$$

where, $d_{pore}$ is pore diameter (given as a function of apparent densities of biomass, moisture and char)

$$d_{pore} = d_{poreB,0} + \frac{(\rho_B+\rho_M)\,\rho_{B,0}}{\rho_{C,f}-\rho_{B,0}}\,(d_{poreC,f} - d_{poreB,0})$$

and, $e$ is emissivity (value taken as 1).

**A.4. Vapour and Solid Phase Enthalpy**

$E_v = h_v - P/\rho_v$

where, $h_v = \sum_i Y_{iv}\, h_{iv}$

Here, $Y_{iv}$ is mass fraction of i$^{th}$ species in vapour phase (also includes water vapour due to particle drying),

$h_{iv} = \int_{T_o}^{T} C_{p,iv}\, dT$ ($C_{p,iv}$ is specific heat of $i^{th}$ species in vapour phase)

and, $P$ is pressure inside the particle due to volatile phase

Similarly, $E_s = h_s = \sum_i Y_{is}\, h_{is}$

where, $Y_{is}$ is mass fraction of $i^{th}$ species in solid phase

and, $h_{is} = \int_{T_o}^{T} C_{p,is}\, dT$ ($C_{p,is}$ is specific heat of $i^{th}$ species in solid phase)

**A.5. Heat of Reaction**

$$S_R = -\{(K_1\Delta H_1 + K_2\Delta H_2 + K_3\Delta H_3)\rho_B + (K_4\Delta H_4 + K\Delta H_5)\varepsilon\rho_{T1} + (K_6\Delta H_6)\varepsilon\rho_{T2} + (K_{vap}\Delta H_{vap})\rho_M\}$$

Here, $\Delta H_1$, $\Delta H_2$ and $\Delta H_3$ are heats of reactions for gas, tar and char formation by primary biomass decomposition, whereas $\Delta H_4$, $\Delta H_5$ and $\Delta H_6$ are heat of reactions for secondary tar cracking reactions. In this model, the heat energy required for moisture evaporation is also considered, and given as heat of reaction, $\Delta H_{vap}$ for particle drying during pyrolysis.

**A.6. Surface Emissivity**

It is also given as a function of apparent densities of biomass, moisture and char:

$$\omega = \omega_{B,0} + \frac{(\rho_B+\rho_M)-\rho_{B,0}}{\rho_{C,f}-\rho_{B,0}}(\omega_{C,f} - \omega_{B,0})$$

**A.7. Heat and Mass Transfer Coefficients**

The heat transfer coefficient can be calculated using correlations available in Bird et al. (2007) for forced convection around submerged objects (flat, cylindrical and spherical shaped) :

For spherical particle,

$Nu = 2 + 0.6\,(Re)^{1/2}\,(Pr)^{1/3}$

For cylindrical particle,

$Nu = (0.376(Re)^{1/2} + 0.057\,(Re)^{2/3})(Pr)^{1/3} + 0.92\,[\,ln(7.4055/Re) + 4.18Re]^{-1/3}\,(Re)^{1/3}\,(Pr)^{1/3}$

For flat or slab shaped particle,

$Nu = 0.332\,(Re)^{1/2}\,(Pr)^{1/3}$

where, *Nu* (stands for Nusselt Number) = $\frac{h_{heat}d_p}{k_g}$

*Re* (stands for Reynold Number ) = $\frac{d_p\, v_g\, \rho_g}{\mu_g}$

and, *Pr* (stands for Prandtl Number) = $\frac{\mu_g\ c_{pg}}{k_g}$

here, $d_p$ is particle diameter (for cylindrical and spherical shaped) / particle length (for slab shaped)

and, $k_g$, $v_g$, $\rho_g$, $\mu_g$ and $c_{pg}$ are thermal conductivity, relative velocity, density, viscosity and heat capacity of surrounding gas, respectively.

The mass transfer coefficient for each species can be calculated using correlations available in Bird et al. (2007), which are similar analogies as that for heat transfer coefficients of given particles.

Like, for spherical particle

$Sh = 2 + 0.6\ (Re)^{1/2}\ (Sc)^{1/3}$

where, *Sh* (stands for Sherwood Number) = $\frac{h_{mass} d_p}{D_{eff}}$

and, *Sc* (stands for Schmidt Number ) = $\frac{\mu_g}{\rho_g\, D_{eff}}$

**A.8. Matlab code**

```
%-------------------------------------------------------------------------
%-------------------------------------------------------------------------
% Writing equations for mass  and energy balance inside a biomass particle
% during pyrolysis (considering both diffusion and convection term)
% PDEPE Solver is used for solving partial differential equations.
%Function is defined according to solver requirements
%-------------------------------------------------------------------------

function [c,f,s] =  Pyrolysis_model(r,t,m,DmDr)

P= m(1) ;  % Pressure at time t
T = m(2);  % Temperature at time t
m_B= m(3); % Solid Biomass weight at time t
```

```
m_C = m(4);% Char weight at time t
m_M = m(5);% Moisture weight at time t
Rho_B =  m(6); % Biomass density at time t
Rho_C =  m(7); % Char density at time t
Rho_M =  m(8); % Mositure density at time t
Rho_G =  m(9); % Non-condensable gases density at time t
Rho_T1 = m(10);% Primary tar density at time t
Rho_T2 = m(11);% Secondary tar density at time t
Rho_W = m(12); % Water vapor density at time t
Rho_I = m(13); % Inert gas density at time t
Velocity_v = m(14);%Vapor velocity inside particle at time t


global V0 Vf m_Cf m_B0 Rho_B0 Rho_Cf  omega epsilon
%-------------------------------------------------------------------
% Heat of reactions for given primary and secondary reactions
%-------------------------------------------------------------------

H1 = 64000;%heat of reaction for reaction 1
H2 = 64000;%heat of reaction for reaction 2
H3 = 64000;%heat of reaction for reaction 3
H4 = -42000;%heat of reaction for reaction 4
H5 = -42000;%heat of reaction for reaction 5
H6 = -42000;%heat of reaction for reaction 6
Hvap = 2440000;%heat of reaction for drying reaction


%-----------------------------------------------------------
% Specific heat of all components
%-----------------------------------------------------------
Cp_G = 1100; %Specific heat of non-condensable gas
Cp_T1 = 1100; %Specific heat of primary tar
Cp_T2 = 1100; %Specific heat of secondary tar
Cp_W = 2000; %Specific heat of water vapor
```

```
Cp_I = 1040; %Specific heat of inert gas
Cp_B = 2300; %Specific heat of biomass particle
Cp_C =1100; %Specific heat of char
Cp_M = 4180; %Specific heat of moisture

%--------------------------------
%Constants required
%--------------------------------
R = 8.314;% universal gas constant (required in kinetic constants)
SBC = 5.67*10^-8;%stefan-boltzmann constant (required in radiative term)
Cf = 0.55 ;% Dimensionless form drag constant (required for velocity calc.)
%-------------------------------------------------------------
% Volume of biomass particle at any time t, as function of biomass,
% moisture and char weight
V = V0 + (Vf-V0) * (m_B+m_M-m_B0)/(m_Cf-m_B0);
%-------------------------------------------------------------

%-----------------------------------------------------------
%Thermo-physical properties of biomass
%-----------------------------------------------------------

vis_v = 2.66*10^-5; % Average vapor phase viscosity
MW_v = 0.054; % Average vapor phase molecular weight

%porosity as function of biomass, moisture and char densities
epsilon = 0.4 + 0.51*((Rho_B + Rho_M) - Rho_B0)/(Rho_Cf-Rho_B0);

% permeability as function of biomass, moisture and char densities
beta = 5*10^-12 + 22.5*10^-12*((Rho_B + Rho_M) - Rho_B0)/(Rho_Cf-Rho_B0);

%pore diameter as function of biomass, moisture and char densities
d_pore = 0.00005 + 0.00005* ((Rho_B + Rho_M) - Rho_B0)/(Rho_Cf-Rho_B0);

%emissivity as function of biomass, moisture and char densities
```

```
omega = 0.6 + 0.4*((Rho_B + Rho_M) - Rho_B0)/(Rho_Cf-Rho_B0);

%solid phase component of thermal conductivity as function of biomass,
%moisture and char densities
k_solid = 0.1798 -0.0918*((Rho_B + Rho_M) - Rho_B0)/(Rho_Cf-Rho_B0);

%gas/vapor phase component of thermal conductivity
k_vapor = 0.02577;

%radiative component of thermal conductivity as function of temperature,
% porosity and pore diameter
k_rad = 4*epsilon*SBC*d_pore*T^4/T*(1-epsilon);

%effective thermal conductivity
k_eff = epsilon*k_vapor +k_solid +k_rad;

%effective diffusivity of vapor phase components
Di = 10^-6 ;% molecular diffusivity of components
D_eff = epsilon*Di;



%-------------------------------------------------------------------------
%Defining vapor phase density and its gradient for velocity calculation
%-------------------------------------------------------------------------
Rho_v = Rho_G + Rho_T1 + Rho_T2 + Rho_W +Rho_I; % Overall vapor phase
density
DRho_GDr = DmDr(9);
DRho_T1Dr = DmDr(10);
DRho_T2Dr = DmDr(11);
DRho_WDr = DmDr(12);
DRho_IDr = DmDr(13);
DRho_vDr = DRho_GDr+ DRho_T1Dr + DRho_T2Dr + DRho_WDr + DRho_IDr ;
% gradient of Overall vapor phase density
```

```
%--------------------------------------------------------------------
% Defining coefficient of accumulation term (function of time) of all
% dependent variables
%--------------------------------------------------------------------

c = [epsilon/T;
   epsilon*(Rho_G*Cp_G  +  Rho_T1*Cp_T1+  Rho_T2*Cp_T2+  Rho_W*Cp_W+
Rho_I*Cp_I)+(Rho_B*Cp_B + Rho_C*Cp_C+ Rho_M*Cp_M);
   1 ;
   1 ;
   1 ;
   V ;
   V ;
   V ;
   epsilon ;
   epsilon ;
   epsilon ;
   epsilon ;
   epsilon;
   0];

 %--------------------------------------------------------------------
% Defining Flux Term of all dependent variables
%--------------------------------------------------------------------
f = [0 ;
   k_eff ;
   0 ;
   0 ;
   0 ;
   0 ;
   0 ;
   0 ;
   epsilon*D_eff ;
```

```
   epsilon*D_eff ;
   epsilon*D_eff ;
   epsilon*D_eff ;
   epsilon*D_eff;
   0].*DmDr  +     [-epsilon*Velocity_v*P/T;
    -epsilon*(Rho_G*Cp_G  +  Rho_T1*Cp_T1+  Rho_T2*Cp_T2+
Rho_W*Cp_W)*Velocity_v*T ;
    0;
    0;
    0;
    0;
    0;
    0;
    -epsilon*Velocity_v*Rho_G;
    -epsilon*Velocity_v*Rho_T1;
    -epsilon*Velocity_v*Rho_T2;
    -epsilon*Velocity_v*Rho_W;
    0;
    0];
```

```
%-------------------------------------------------------------
%kinetic rate constants as function of temperature
%-------------------------------------------------------------

k1=4.38*10^9*exp(-152700/(8.314*T)); % Arrhenius equation for reaction 1
k2=1.08*10^10*exp(-148000/(8.314*T)); % Arrhenius equation for reaction 2
k3=3.27*10^6*exp(-111700/(8.314*T)); % Arrhenius equation for reaction 3
k4 = 1.48*10^6*exp(-144000/(8.314*T)); % Arrhenius equation for reaction 4
k5 = 1.48*10^6*exp(-144000/(8.314*T)); % Arrhenius equation for reaction 5
k6 = 1*10^5*exp(-108000/(8.314*T)); % Arrhenius equation for reaction 6
kvap = 5.13*10^10*exp(-88000/(8.314*T)); % Arrhenius equation for drying
reaction
```

```
%-----------------------------------------------------------------
% Defining  Source Term of all dependent variables
%-----------------------------------------------------------------

F1 = (R/MW_v)*(k1*Rho_B+ k2*Rho_B + kvap*Rho_M) + (epsilon* P/(V*T))*((Vf-V0)/(m_Cf-m_B0))*((k1+k2+k3)*m_B +kvap*m_M);

F2 =-((Rho_B*(k1*H1 + k2*H2 + k3*H3))+ (epsilon*Rho_T1*(k4*H4 + k5*H5))+ (epsilon*Rho_T2*(k6*H6)) + (Rho_M*(kvap*Hvap)))+ (T^2/T*V)*(epsilon*(Rho_G*Cp_G + Rho_T1*Cp_T1+ Rho_T2*Cp_T2+ Rho_W*Cp_W+ Rho_I*Cp_I)+ (Rho_B*Cp_B + Rho_C*Cp_C+ Rho_M*Cp_M))*((Vf-V0)/(m_Cf-m_B0))*(((k1+k2+k3)*m_B +kvap*m_M)) ;

F3 = -(k1+k2+k3)*m_B;

F4 = k3*m_B + epsilon*k6*Rho_T2*V;

F5= -kvap*m_M;

F6 = -(k1+k2+k3)*Rho_B* V;

F7 = k3*Rho_B*V + epsilon* k6* Rho_T2*V ;

F8 = -kvap*Rho_M*V ;

F9 =  k1*Rho_B + k4*0.78*Rho_T1 + (epsilon*Rho_G/V)*((Vf-V0)/(m_Cf-m_B0))*((k1+k2+k3)*m_B +kvap*m_M);

F10 = k2*Rho_B - (k4+k5)*Rho_T1 + (epsilon*Rho_T1/V)*((Vf-V0)/(m_Cf-m_B0))*((k1+k2+k3)*m_B +kvap*m_M);

F11 = k5*0.22*Rho_T1-k6*Rho_T2 + (epsilon*Rho_T2/V)*((Vf-V0)/(m_Cf-m_B0))*((k1+k2+k3)*m_B +kvap*m_M);

F12 = kvap*Rho_M + (epsilon*Rho_W/V)*((Vf-V0)/(m_Cf-m_B0))*((k1+k2+k3)*m_B +kvap*m_M);

F13 = (epsilon*Rho_I/V)*((Vf-V0)/(m_Cf-m_B0))*((k1+k2+k3)*m_B + kvap*m_M);

F14 =-(R/MW_v)*(T*DRho_vDr + Rho_v*DmDr(2))- vis_v*Velocity_v/beta - Cf*beta^-0.5* Rho_v* Velocity_v*abs(Velocity_v);


s = [F1; F2; F3; F4; F5; F6; F7; F8; F9; F10; F11; F12; F13;F14];


 %-------------------------------------------------------------------------
```

```
% Writing initial conditions for mass and energy balance equations defined
% in Pyrolysis_model function file (without convection and diffusion
% terms)
%-------------------------------------------------------------------------

function value =  Pyrolysis_modelic(r)
%  m(1) = Pressure
% m(2)= Temperature,
% m(3) = Biomass weight,
% m(4) =  Char weight,
% %m(5) =Moisture weight ,
% m(6) = Biomass density,
% m(7) = Char density,
% %m(8) = Moisture density,
% m(9) = Non-condensable gas density,
% m(10)= Primary  tar density,
% m(11) = Secondary tar density,
% m(12) =  Water vapor density,
% m(13)= Inert gas density,
%-------------------------
% Initial values
%-------------------------

T0 = 298.15; % initial particle temperature
P0 = 1.013*10^5;% initial particle pressure
I0 = 10^-7; %initial density of inert gas inside particle (assumed)
m_c0 = 0; %intial weight of char;
Rho_c0 = 0 ; %intial density of char;
Rho_G0 =10^-7; %intial density of non-condensable gas;
Rho_T10 = 10^-7; %intial density of primary tar;
Rho_T20 =10^-7; %intial density of secondary tar;
Rho_W0 =10^-7; %intial density of water vapor;

value = [ P0;
```

```
   T0;
   m_b0u ;
   m_c0 ;m_m0 ;Rho_b0u ;Rho_c0 ;Rho_m0 ; Rho_G0 ;Rho_T10; Rho_T20 ; Rho_W0; I0];


end

%-------------------------------------------------------------------------
% Writing boundary conditions for mass and energy balance equations defined
% in  Pyrolysis_model function file
%-------------------------------------------------------------------------

function [pl, ql, pr, qr] =  Pyrolysis_modelbc(rl, ml, rr, mr, t)
% m(1) = Biomass weight, m(2)= char weight, m(3) = moisture weight, m(4) = Biomass density
%m(5) =Char density , m(6) = Moisture density, m(7) = Temperature,
%m(8) = Non-condensable gas density, m(9) = Primary tar, m(10)= Secondary
%tar density,
%m(11) = Water vapor density, m(12) = Inert gas density,m(13)= Pressure,
%m(14) = Vapor velocity inside particle
global  w  p

h_mass = 2*10^-4; %mass transfer coefficient
h_heat = 20;%heat transfer coefficient
T_gas = 873;   %inert gas temperature (in Kelvin)
T_wall =873;  % reactor wall temperature (in Kelvin)
SBC = 5.67*10^-8;%stefan-boltzmann constant


pl = [0;0;0;0;0;0;0;0;0;0;0;0;0;0];

ql=  [ml(14)/ ml(1)*p;1;1;1;1;1;1;1;1;1;1;1;1;1];
```

```
pr = [mr(1)-1.013*10^5;0;0 ;0 ;0 ;0 ;0 ;-h_mass*mr(9) ;-h_mass*mr(10) ;-h_mass*mr(11) ;-h_mass*mr(12);-h_mass*(1.165-mr(13)) ;h_heat*(mr(14)-T_gas)+w*SBC*(mr(14)^4-T_wall^4)];


qr = [ 0;1 ; 1 ;1 ;1 ;1 ;1 ;1 ;-1 ;-1 ;-1 ; -1 ; -1; 1];

 %---------------------------------------------------------------------
%  Main (driver) file for solving overall mass and total energy
%  conservation equations for pyrolysis of biomass particle (considering
%  both diffusion and convection term)
%---------------------------------------------------------------------

global    m_B0 m_B0s m_Cf m_M0 Rho_B0 Rho_B0s Rho_M0 Rho_Cf Vf V0

% Input "Initial weight of total biomass(kg)"
m_B0 = 1;

% Input "Initial weight of  solid biomass(kg)(moisture-free)"
m_B0s = 1;

% Initial weight of moisture
m_M0 = m_B0 - m_B0s;

% Input "Final weight of char(kg)"
m_Cf = 0.1;

% Input "Initial total biomass density(kg/m3)"
Rho_B0 =630 ;

%Intial total volume of biomass
V0 = m_B0/Rho_B0;

% Input "Final char density(kg/m3)"
```

```
Rho_Cf = 200;

% Initial  solid biomass density (kg/m3)(moisture-free)
Rho_B0s = m_B0s/V0;

% Initial density of moisture
Rho_M0 = Rho_B0 - Rho_B0s;

% Final volume left (of char product)
Vf = m_Cf/ Rho_Cf;

% Input "Radius of particle (m)"
RD = 0.012;

% Input "Total pyrolysis time (sec)"
PT = 1000;


n = 2;%0 for flat, 1 for cylindrical, 2 for spherical particle

% Defining Step size for spatial discretization
r =linspace(0,RD,100);

% Defining Time step for solving DAEs after spatial discretization
t= linspace(0,PT,1000);

% Using PDEPE solver for solving defined PDEs (giving Pyrolysis_model
%function handle) with initial(giving Pyrolysis_modelic function handle)
% and boundary conditions (giving Pyrolysis_modelbc function handle)

options = odeset('AbsTol',1e-4);
sol
=pdepe(n,@Pyrolysis_model,@Pyrolysis_modelic,@Pyrolysis_modelbc,r,t,options);
```

```
pressure = sol(:,:,1);
Temp = sol(:,:,2);
m_biomass = sol(:,:,3);
m_char = sol(:,:,4);
m_moisture = sol(:,1,5);
Rho_biomass = sol(:,:,6);
Rho_char = sol(:,:,7);
Rho_moisture = sol(:,:,8);
Rho_noncgas = sol(:,:,9);
Rho_tar1 = sol(:,:,10);
Rho_tar2 = sol(:,:,11);
Rho_wvapor = sol(:,:,12);
Rho_inertgas = sol(:,:,13);
Velocity_v = sol(:,:,14);
```

**Appendix B**

(1) Gas phase stress-strain tensor

$$\bar{\tau}_g = \alpha_g \mu_g \left[ \nabla \vec{v}_g + \nabla \vec{v}_g{}^T \right] - \frac{2}{3} \alpha_g \mu_g \nabla . \vec{v}_g \bar{I}$$

where, $\mu_g$ is the gas-phase viscosity.

(2) Solid phase stress-strain tensor

$$\bar{\tau}_s = \alpha_s \mu_s \left[ \nabla \vec{v}_s + \nabla \vec{v}_s{}^T \right] + \alpha_s ( \lambda_s - \frac{2}{3} \mu_s) \nabla . \vec{v}_s \bar{I}$$

where $\mu_s$ is the shear viscosity of $s^{th}$ solid phase, and $\lambda_s$ is the bulk viscosity of $s^{th}$ solid phase.

(3) Solids Pressure

The solid pressure consists of a kinetic term (the first term) and other term due to particle collisions (Lun et al., 1984).

$$p_s = \alpha_s \rho_s \theta_s + 2\rho_s (1 + e_{ss}) \alpha_s{}^2 g_{0,ss} \theta_s$$

where $e_{ss}$ is the coefficient of restitution for particle collisions, and $g_{0,ss}$ is radial distribution function.

For a multi- phase system (N number of phases), this equation has been written by considering the presence of other phases as well.

$$p_l = \alpha_l \rho_l \theta_l + \sum_{l=1}^{N} 2 \frac{d_{ls}^3}{d_l^3} (1 + e_{ls}) g_{0,ls} \alpha_l \alpha_s \rho_l \theta_l$$

where $d_{ls}$ is the average diameter [ $(d_l + d_s)/2$] and $e_{ls}$ is the average value of restitution coefficient of $l^{th}$ fluid (gas) or solid phase and $s^{th}$ solid phase [$(e_l + e_s)/2$].

(4) Radial distribution function

This is a correction factor ($g_0$) that alters the probability of collisions between grains in dense solid granular phase. Its value varies from 1 for dilute solid phase to infinity for compact solid phase.

For solid phases, the function has been defined according to the relationship given by Iddir and Arastoopour (2005) as:

$$g_{0,ll} = \frac{1}{(1-\frac{\alpha_s}{\alpha_{s,max}})} + \frac{3}{2} d_l \sum_{k=1}^{M} \frac{\alpha_k}{d_k}$$

Here, $\alpha_s = \sum_{k=1}^{M} \alpha_k$ ( $k$ are solid phases only)

$\alpha_{s,max} = \sum_{k=1}^{M} \alpha_{k,max}$ ($\alpha_{k,max}$ = Maximum packing limit of $k^{th}$ solid = 0.63)

and, $M$ is the total number of solid phases,

whereas the equation at contact for mixtures ($l^{th}$ and $s^{th}$ solid phase) has been considered as:

$$g_{0,ls} = \frac{d_m g_{0,ll} + d_l g_{0,ss}}{d_s + d_l}$$

(5) Solid phase shear viscosity

This is made up of kinetic, collisional and frictional viscosity of the solid phase, discussed by Syamlal et al. (1993).

$$\mu_s = \mu_{s,kin} + \mu_{s,col} + \mu_{s,fr}$$

where $\mu_{s,kin} = \frac{\alpha_s d_s \rho_s \sqrt{\theta_s \pi}}{6(3-e_{ss})} [\, 1 + \frac{2}{5} (1 + e_{ss})(3e_{ss} - 1)\alpha_s g_{0,ss}]$

and $\mu_{s,col} = \frac{4}{5} \alpha_s d_s \rho_s g_{0,ss} \sqrt{\theta_s / \pi}\, (1 + e_{ss})\alpha_s$

For dense flow systems, where secondary volume fraction for solid phase is close to the packing limit (considered to be around 0.61), the generation of stress is majorly because of friction between particles and the instantaneous collision between

particles are less important. In such a case, frictional viscosity has to be included in solid phase shear viscosity expression.

$$\mu_{s,fr} = \frac{p_s sin\phi}{2\sqrt{I_{2D}}}$$

where $p_s$ is solid phase pressure (contribution due to kinetic pressure and frictional pressure as given by Johnson and Jackson (1987), ϕ is angle of internal friction($30^0$), $I_{2D}$ is second invariant of deviatoric stress tensor, and

$$P_{friction} = Fr\frac{(\alpha_s-\alpha_{s,min})^n}{(\alpha_{s,max}-\alpha_s)^p}$$

Here, $Fr$, *n* and *p* have the values of $0.1\alpha_s$, 2 and 5, respectively.

(6) Solid phase bulk viscosity

The resistance of the granular particles due to compression and expansion is described by Lun et al. (1984) as:

$$\lambda_s = \frac{4}{5}\alpha_s d_s \rho_s g_{0,ss}\sqrt{\theta_s/\pi}\,(1+e_{ss})\alpha_s$$

(7) Drag coefficient between fluid (gas) and solid phase

This drag coefficient, given by Gidaspow et al. (1991) is more appropriate for dense fluidized beds.

When $\alpha_g$ > 0.8, the fluid-solid momentum exchange coefficient is of the form:

$$K_{gs}(\text{ or } K_{ls}\text{for } l^{th}\text{ gas phase}) = \frac{3}{4}C_D\frac{\alpha_s\,\alpha_g\,\rho_g\,|\vec{v}_s-\vec{v}_g|}{d_s}\;\alpha_g{}^{-2.65}$$

where, $C_D = \frac{24}{\alpha_g Re_s}[1+0.15(\alpha_g Re_s)^{0.687}]$

Reynold's Number, $Re_s = \frac{\rho_g\,d_s\,|\vec{v}_s-\vec{v}_g|}{\mu_g}$

and, when $\alpha_g$ < 0.8,

$$K_{gs}(\text{ or } K_{ls}\text{for } l^{th} \text{ gas phase}) = 150\frac{\alpha_s(1-\alpha_g)\mu_g}{\alpha_g {d_s}^2} + 1.75\frac{\rho_g \alpha_s|\vec{v}_s - \vec{v}_g|}{d_s}$$

(8) Drag coefficient between solid and solid phase

This solid-solid drag coefficient, given by Syamlal (1987), is of the following form:

$$K_{ls} = \frac{3(1+e_{ls})\left(\frac{\pi}{2}+C_{fr,ls}\frac{\pi^2}{8}\right)\alpha_s\rho_s\,\alpha_l\rho_l(d_l+d_s)^2 g_{0,ls}}{2\pi(\rho_l {d_l}^3+\rho_s {d_s}^3)}\,|\vec{v}_l - \vec{v}_s|$$

where $C_{fr,ls}$ is the coefficient of friction between $l^{th}$ and $s^{th}$ solid phase-particles (the value considered here is 0).

(9) Diffusion coefficient of granular energy

This coefficient, given by Syamlal et al. (1993), contributes to the diffusive component of granular energy.

$$k_{\theta_s} = \frac{15 d_s\rho_s\,\alpha_s\sqrt{\theta_s\pi}}{4(41-33\eta)}\left[1+\frac{12}{5}\eta^2(4\eta-3)\,\alpha_s g_{0,ss}+\frac{16}{15\pi}(41-33\eta)\eta\,\alpha_s g_{0,ss}\right]$$

where $\eta = (1+e_{ss})/2$

(10) Collisional dissipation of energy

The energy dissipation rate within $s^{th}$ solid phase due to collision between particles (Lun et al., 1984), given as

$$\gamma_{\theta_s} = \frac{12(1-{e_{ss}}^2)g_{0,ss}}{d_s\sqrt{\pi}}\rho_s\,{\alpha_s}^2{\theta_s}^{3/2}$$

**Appendix C**

```
function GeneratFluentParticlesInjectionFile()
%
% file format of Fluent injection file:
%The file has the format that you write
%((x y z u v w diameter temperature mass-flow) injection0:ID )
%((# # # # # # # # # # #) injection0:0 ) ((# # # # # # # # # # #) injection0:1 ) ((# # # # # # # # # # #) injection0:2 ) … … … ((# # # # # # # # # # #) injection0:n )
%where # is a number under the unit that you are using.
%
% Input parameter: x, y, z and vel as init condition, only for XYZ coordination
%  Current implimentation :  rectangular seeding region and linear distribution,
%techniques for debug error:
% 1) always read fresh case and data file without injection
%    once reading the file, it will not read in next iteration
% 2) check if the mass-flow is bigger than 0,
% 3) check the injection time:  start time and stop time for unsteady flow
% 4) check if the particles  are in the domain
% 5) the InjectionName should match in fluent injection panel
% Total no. of  particles to be injected = 1274 (mass fr.% = 5.82 in mixture), with 3 particles in a parcel
%hence, total no. of parcels to inject = 10*4*10 = 400
x_start=0.0; x_end=0.0381;
x_count=10;
y_start=0.0; y_end=0.0207;
y_count=4;
z_start=0.0; z_end=0.0381;
z_count=10;
x_det=(x_end - x_start)/x_count;
y_det=(y_end - y_start)/y_count;
z_det=(z_end - z_start)/z_count;
x_vel=0;  % unit m/s
y_vel=0;
z_vel=0;
```

```
x_pos=x_start+x_det/2;
y_pos=y_start+y_det/2;
z_pos=z_start+z_det/2;
particle_diameter = 0.00154; % uint is meter
parcel_diameter=0.00225;  %unit is meter (calculated using parcel volume, which is equals to Min. cell volume/Scp)
time_step = 1e-8; % time for injection
temperature = 293; % unit  K   default 293
density=584;  % unit: kg/m3  this should be identical as flow to be track,
mass_flow =0;
injectionName='RectangleInjection0';
id=0;
f=fopen('RectangleInjection.inj','w');
% initial intro duction field
% fprintf(f,'((x y z u v w temperature diameter mass-flow) %s)\n',injectionName);
% fprintf(f,'n');
 for k=1:z_count
y_pos=y_start+y_det/2;
for j=1:y_count
x_pos=x_start+x_det/2;
for i=1:x_count
mass_flow = (pi*parcel_diameter*parcel_diameter*parcel_diameter*density)/(6*time_step); %mass of parcel in injection. This will be added for total counts (400 in this case) to give total mass for total injection time
fprintf(f,'((%e %e %e %f %f %f %f %f %e) %s)\n', x_pos ,y_pos ,z_pos ,x_vel,y_vel, z_vel,particle_diameter,temperature,mass_flow, injectionName);
% fprintf(f,'n');
x_pos=x_pos+x_det;
id=id+1;
end
y_pos=y_pos+y_det;
end
z_pos=z_pos+z_det;
end
```

```
disp(id);
disp(x_pos)
disp(y_pos)
disp(z_pos)
disp('particles has been seeded');
fclose(f);
```

# Bibliography


Abdullah, M. Z., Husain, Z.&Yin Pong, S. L. (2003). *Analysis of cold flow fluidization test results for various biomass fuels*. Biomass and Bioenergy, 24(6), 487-494.

Abu El-Rub, Z., Bramer, E. A.&Brem, G. (2008). *Experimental comparison of biomass chars with other catalysts for tar reduction*. Fuel, 87(10-11), 2243-2252.

Abu El-Rub, Z. Y. K. (2008). Biomass char as an in-situ catalyst for tar removal in gasification systems.

Adam, M., Ocone, R., Mohammad, J., Berruti, F.&Briens, C. (2013). *Kinetic Investigations of Kraft Lignin Pyrolysis*. Industrial & Engineering Chemistry Research.

Adjaye, J. D.&Bakhshi, N. N. (1995). *Catalytic conversion of a biomass-derived oil to fuels and chemicals II: Chemical kinetics, parameter estimation and model predictions*. Biomass and Bioenergy, 8(4), 265-277.

Agarwal, P. K. (1991). *Transport phenomena in multi-particle systems--IV. Heat transfer to a large freely moving particle in gas fluidized bed of smaller particles*. Chemical Engineering Science, 46(4), 1115-1127.

Agarwal, P. K., Genetti, W. E.&Lee, Y. Y. (1984). *Model for devolatilization of coal particles in fluidized beds*. Fuel, 63(8), 1157-1165.

Agrawal, R. K. (1988). *Kinetics of reactions involved in pyrolysis of cellulose I. The three reaction model*. The Canadian Journal of Chemical Engineering, 66(3), 403-412.

Alves, S. S.&Figueiredo, J. L. (1988). *Pyrolysis kinetics of lignocellulosic materials by multistage isothermal thermogravimetry*. Journal of Analytical and Applied Pyrolysis, 13(1-2), 123-134.

Alves, S. S.&Figueiredo, J. L. (1989). *A model for pyrolysis of wet wood*. Chemical Engineering Science, 44(12), 2861-2869.

ANSYS FLUENT "Release 14.0, Help System, Theory Guide, Ansys, Inc.".

Antal, M. J. (1982). *Biomass Pyrolysis: a Review of the Literature. Part I - Carbohydrate pyrolysis. In: Boer KW, Duffie JA, editors. Advances in Solar Energy* Boulder (CO): American Solar Energy, 1 61-111.

Antal, M. J.&Grønli, M. (2003). *The Art, Science, and Technology of Charcoal Production†*. Industrial & Engineering Chemistry Research, 42(8), 1619-1640.

Atutxa, A., Aguado, R., Gayubo, A. G., Olazar, M.&Bilbao, J. (2005). *Kinetic Description of the Catalytic Pyrolysis of Biomass in a Conical Spouted Bed Reactor*. Energy & Fuels, 19(3), 765-774.

Babu, B. V.&Chaurasia, A. S. (2003). *Modeling, simulation and estimation of optimum parameters in pyrolysis of biomass*. Energy Conversion and Management, 44(13), 2135-2158.

Babu, B. V.&Chaurasia, A. S. (2004a). *Heat transfer and kinetics in the pyrolysis of shrinking biomass particle*. Chemical Engineering Science, 59(10), 1999-2012.

Babu, B. V.&Chaurasia, A. S. (2004b). *Parametric study of thermal and thermodynamic properties on pyrolysis of biomass in thermally thick regime*. Energy Conversion and Management, 45(1), 53-72.

Balat, M., Balat, M., Kırtay, E.&Balat, H. (2009). *Main routes for the thermo-conversion of biomass into fuels and chemicals. Part 1: Pyrolysis systems*. Energy Conversion and Management, 50(12), 3147-3157.

Bamford, C. H., Crank, J.&Malan, D. H. (1946). *The combustion of wood. Part I*. Mathematical Proceedings of the Cambridge Philosophical Society, 42(02), 166-182.

Baumlin, S., Broust, F., Ferrer, M., Meunier, N., Marty, E.&Lédé, J. (2005). *The continuous self stirred tank reactor: measurement of the cracking kinetics of biomass pyrolysis vapours*. Chemical Engineering Science, 60(1), 41-55.

Becidan, M., Várhegyi, G., Hustad, J. E.&Skreiberg, Ø. (2007). *Thermal Decomposition of Biomass Wastes. A Kinetic Study*. Industrial & Engineering Chemistry Research, 46(8), 2428-2437.

Bird, R. B., Stewart, W. E.&Lightfoot, E. N. (2007). Transport Phenomena. New York, John Wiley and Sons.

Boemer, A., Qi, H.&Renz, U. (1998). *Verification of Eulerian simulation of spontaneous bubble formation in a fluidized bed*. Chemical Engineering Science, 53(10), 1835-1846.

Bokkers, G. A., Laverman, J. A., van Sint Annaland, M.&Kuipers, J. A. M. (2006). *Modelling of large-scale dense gas-solid bubbling fluidised beds using a novel discrete bubble model*. Chemical Engineering Science, 61(17), 5590-5602.

Boroson, M. L., Howard, J. B., Longwell, J. P.&Peters, W. A. (1989a). *Heterogeneous cracking of wood pyrolysis tars over fresh wood char surfaces*. Energy & Fuels, 3(6), 735-740.

Boroson, M. L., Howard, J. B., Longwell, J. P.&Peters, W. A. (1989b). *Product yields and kinetics from the vapor phase cracking of wood pyrolysis tars*. AIChE Journal, 35(1), 120-128.

Bradbury, A. G. W., Sakai, Y.&Shafizadeh, F. (1979). *A kinetic model for pyrolysis of cellulose*. Journal of Applied Polymer Science, 23(11), 3271-3280.

Branca, C., Albano, A.&Di Blasi, C. (2005). *Critical evaluation of global mechanisms of wood devolatilization*. Thermochimica Acta, 429(2), 133-141.

Branca, C.&Di Blasi, C. (2003). *Kinetics of the isothermal degradation of wood in the temperature range 528-708 K*. Journal of Analytical and Applied Pyrolysis, 67(2), 207-219.

Bridgwater, A. V. (1996). *Production of high grade fuels and chemicals from catalytic pyrolysis of biomass*. Catalysis Today, 29(1-4), 285-295.

Bridgwater, A. V., Meier, D.&Radlein, D. (1999). *An overview of fast pyrolysis of biomass*. Organic Geochemistry, 30(12), 1479-1493.

Broido, A.&Nelson, M. A. (1975). *Char yield on pyrolysis of cellulose*. Combustion and Flame, 24(0), 263-268.

Brown, A. L., Dayton, D. C., Nimlos, M. R.&Daily, J. W. (2001). *Design and Characterization of an Entrained Flow Reactor for the Study of Biomass Pyrolysis Chemistry at High Heating Rates*. Energy & Fuels, 15(5), 1276-1285.

Brown, R. (2009). *Biochar Production Technology.* Chapter 8 in J. Lehmann and S. Joseph (eds) Biochar for Environmental Management. Earthscan, London.

Brown, R. A., Kercher, A. K., Nguyen, T. H., Nagle, D. C.&Ball, W. P. (2006). *Production and characterization of synthetic wood chars for use as surrogates for natural sorbents*. Organic Geochemistry, 37(3), 321-333.

Brown, R. C. (2003). Biorenewable resources: Engineering new products from agriculture. Ames, IA, Blackwell Press.

Brownsort, P. A. (2009). *Biomass Pyrolysis Processes: Review of Scope, Control and Variability*. UKBRC Working Paper 5.

Bruchmüller, J., van Wachem, B. G. M., Gu, S., Luo, K. H.&Brown, R. C. (2011). *Modeling the thermochemical degradation of biomass inside a fast pyrolysis fluidized bed reactor*. AIChE Journal n/a-n/a.

Bruchmüller, J., van Wachem, B. G. M., Gu, S., Luo, K. H.&Brown, R. C. (2012). *Modeling the thermochemical degradation of biomass inside a fast pyrolysis fluidized bed reactor*. AIChE Journal, 58(10), 3030-3042.

Bryden, K. M.&Hagge, M. J. (2003). *Modeling the combined impact of moisture and char shrinkage on the pyrolysis of a biomass particle*. Fuel, 82(13), 1633-1644.

Bryden, K. M., Ragland, K. W.&Rutland, C. J. (2002). *Modeling thermally thick pyrolysis of wood*. Biomass and Bioenergy, 22(1), 41-53.

Caballero, J. A., Font, R., Marcilla, A.&Conesa, J. A. (1995). *New kinetic model for thermal decomposition of heterogeneous materials*. Industrial & Engineering Chemistry Research, 34(3), 806-812.

Chan, W.-C. R., Kelbon, M.&Krieger, B. B. (1985). *Modelling and experimental verification of physical and chemical processes during pyrolysis of a large biomass particle*. Fuel, 64(11), 1505-1513.

Chan, W. C. R., Kelbon, M.&Krieger-Brockett, B. (1988). *Single-particle biomass pyrolysis: correlations of reaction products with process conditions.* Industrial & Engineering Chemistry Research, 27(12), 2261-2275.

Chen, G., Andries, J.&Spliethoff, H. (2003). *Catalytic pyrolysis of biomass for hydrogen rich fuel gas production*. Energy Conversion and Management, 44(14), 2289-2296.

Chen, Y., Charpenay, S., Jensen, A., Wójtowicz, M. A.&Serio, M. A. (1998). *Modeling of biomass pyrolysis kinetics*. Symposium (International) on Combustion, 27(1), 1327-1334.

Chiba, S., Nienow, A. W., Chiba, T.&Kobayashi, H. (1980). *Fluidised binary mixtures in which the denser component may be flotsam*. Powder Technology, 26(1), 1-10.

Chitester, D. C., Kornosky, R. M., Fan, L. S.&Dankoo, J. P. (1984). *Characteristics of Fluidization at High Pressure*. ChemicalEngineering Science, 39.

Clarke, K. L., Pugsley, T.&Hill, G. A. (2005). *Fluidization of moist sawdust in binary particle systems in a gas–solid fluidized bed*. Chemical Engineering Science, 60(24), 6909-6918.

Cui, H.&Grace, J. R. (2007). *Fluidization of biomass particles: A review of experimental multiphase flow aspects*. Chemical Engineering Science, 62(1-2), 45-55.

Daizo, K.&Levenspiel, O. (1991). Fluidization engineering, 2nd edition.

Damartzis, T., Kostoglou, M.&Zabaniotou, A. (2009). *Simulation of the Agro-Biomass(Olive Kernel) Fast Pyrolysis in a Wire Mesh Reactor Considering Intra-Particle Radial and Temporal Distribution of Products*. International Journal of Chemical Reactor Engineering 7(1).

De Diego, L. F., García-Labiano, F., Abad, A., Gayán, P.&Adánez, J. (2002). *Modeling of the devolatilization of nonspherical wet pine wood particles in fluidized beds*. Industrial and Engineering Chemistry Research, 41(15), 3642-3650.

Demirbas, A. (2001). *Yields of hydrogen-rich gaseous products via pyrolysis from selected biomass samples*. Fuel, 80(13), 1885-1891.

Demirbas, A. (2004). *Combustion characteristics of different biomass fuels*. Progress in Energy and Combustion Science, 30(2), 219-230.

Demirbaş, A. (2006). *Global Renewable Energy Resources*. Energy Sources, Part A: Recovery, Utilization, and Environmental Effects, 28(8), 779-792.

Demirbas, A.&Arin, G. (2002). *An Overview of Biomass Pyrolysis*. Energy Sources, 24(5), 471-482.

Demirbas, M. F., Balat, M.&Balat, H. (2009). *Potential contribution of biomass to the sustainable energy development*. Energy Conversion and Management, 50(7), 1746-1760.

Di Blasi, C. (1993a). *Analysis of Convection and Secondary Reaction Effects Within Porous Solid Fuels Undergoing Pyrolysis*. Combustion Science and Technology, 90(5), 315 - 340.

Di Blasi, C. (1993b). *Modeling and simulation of combustion processes of charring and non-charring solid fuels*. Progress in Energy and Combustion Science, 19(1), 71-104.

Di Blasi, C. (1996a). *Heat, momentum and mass transport through a shrinking biomass particle exposed to thermal radiation*. Chemical Engineering Science, 51(7), 1121-1132.

Di Blasi, C. (1996b). *Kinetic and Heat Transfer Control in the Slow and Flash Pyrolysis of Solids*. Industrial & Engineering Chemistry Research, 35(1), 37-46.

Di Blasi, C. (1997). *Influences of physical properties on biomass devolatilization characteristics*. Fuel, 76(10), 957-964.

Di Blasi, C. (1998). *Physico-chemical processes occurring inside a degrading two-dimensional anisotropic porous medium*. International Journal of Heat and Mass Transfer, 41(24), 4139-4150.

Di Blasi, C. (2000). *Modelling the fast pyrolysis of cellulosic particles in fluid-bed reactors*. Chemical Engineering Science, 55(24), 5999-6013.

Di Blasi, C. (2002). *Modeling intra- and extra-particle processes of wood fast pyrolysis*. AIChE Journal, 48(10), 2386-2397.

Di Blasi, C. (2008). *Modeling chemical and physical processes of wood and biomass pyrolysis*. Progress in Energy and Combustion Science, 34(1), 47-90.

Di Blasi, C.&Branca, C. (2001). *Kinetics of Primary Product Formation from Wood Pyrolysis*. Industrial & Engineering Chemistry Research, 40(23), 5547-5556.

Di Blasi, C.&Branca, C. (2002). *Temperatures of Wood Particles in a Hot Sand Bed Fluidized by Nitrogen*. Energy & Fuels, 17(1), 247-254.

Di Blasi, C., Branca, C., Santoro, A.&Gonzalez Hernandez, E. (2001). *Pyrolytic behavior and products of some wood varieties*. Combustion and Flame, 124(1-2), 165-177.

Di Blasi, C., Branca, C.&Teislev, B. (2004). *Development of a novel reactor for the oxidative degradation of straw*. Bioresource Technology, 91(3), 263-271.

Di Blasi, C.&Lanzetta, M. (1997). *Intrinsic kinetics of isothermal xylan degradation in inert atmosphere*. Journal of Analytical and Applied Pyrolysis, 40-41 287-303.

Diebold, J. P. (1994). *A unified, global model for the pyrolysis of cellulose*. Biomass and Bioenergy, 7(1-6), 75-85.

Difelice, R., Coppola, G., Rapagna, S.&Jand, N. (1999). *Modeling of biomass devolatilization in a fluidized bed reactor*. The Canadian Journal of Chemical Engineering, 77(2), 325-332.

Ding, J.&Gidaspow, D. (1990). *A bubbling fluidization model using kinetic theory of granular flow*. AIChE Journal, 36(4), 523-538.

El-Rub, Z. A. (2008). Biomass char as an in-situ catalyst for tar removal in gasification, University of Twente [Host].

Fagbemi, L., Khezami, L.&Capart, R. (2001). *Pyrolysis products from different biomasses: application to the thermal cracking of tar*. Applied Energy, 69(4), 293-306.

Fan, R.&Fox, R. O. (2008). *Segregation in polydisperse fluidized beds: Validation of a multi-fluid model*. Chemical Engineering Science, 63(1), 272-285.

Fitz, H. C., DeBellevue, E. B., Costanza, R., Boumans, R., Maxwell, T., Wainger, L.&Sklar, F. H. (1996). *Development of a general ecosystem model for a range of scales and ecosystems*. Ecological Modelling, 88(1-3), 263-295.

Fletcher, D. F., Haynes, B. S., Chen, J.&Joseph, S. D. (1998). *Computational fluid dynamics modelling of an entrained flow biomass gasifier*. Applied Mathematical Modelling, 22(10), 747-757.

Fletcher, D. F., Haynes, B. S., Christo, F. C.&Joseph, S. D. (2000). *A CFD based combustion model of an entrained flow biomass gasifier*. Applied Mathematical Modelling, 24(3), 165-182.

Font, R., Marcilla, A., Verdu, E.&Devesa, J. (1990). *Kinetics of the pyrolysis of almond shells and almond shells impregnated with cobalt dichloride in a fluidized bed reactor and in a pyroprobe 100*. Industrial & Engineering Chemistry Research, 29(9), 1846-1855.

Formisani, B., Cristofaro, G. D.&Girimonte, R. (2001). *A fundamental approach to the phenomenology of fluidization of size segregating binary mixtures of solids*. Chemical Engineering Science, 56(1), 109-119.

French, R.&Czernik, S. (2010). *Catalytic pyrolysis of biomass for biofuels production*. Fuel Processing Technology, 91(1), 25-32.

Galgano, A.&Di Blasi, C. (2003). *Modeling Wood Degradation by the Unreacted-Core-Shrinking Approximation*. Industrial & Engineering Chemistry Research, 42(10), 2101-2111.

Galgano, A.&Di Blasi, C. (2004). *Modeling the propagation of drying and decomposition fronts in wood*. Combustion and Flame, 139(1–2), 16-27.

Gerber, S., Behrendt, F.&Oevermann, M. (2010). *An Eulerian modeling approach of wood gasification in a bubbling fluidized bed reactor using char as bed material*. Fuel, 89(10), 2903-2917.

Gidaspow, D., Bezburuah, R.&Ding, J. (1991). Hydrodynamics of circulating fluidized beds: Kinetic theory approach.

Gilbert, P., Ryu, C., Sharifi, V.&Swithenbank, J. (2009). *Tar reduction in pyrolysis vapours from biomass over a hot char bed*. Bioresource Technology, 100(23), 6045-6051.

Goldschmidt, M. J. V., Kuipers, J. A. M.&Swaaij van, W. P. M. (2000). Hydrodynamic modeling of dense gas-fluidised beds using the kinetic theory of granular flow: effect of coefficient of restitution on bed dynamics. ISCRE-16, Sixteenth International Symposium on Chemical Reaction Engineering. Krakow, Poland.

Goldschmidt, M. J. V., Link, J. M., Mellema, S.&Kuipers, J. A. M. (2003). *Digital image analysis measurements of bed expansion and segregation dynamics in dense gas-fluidised beds*. Powder Technology, 138(2-3), 135-159.

Grønli, M., Antal, M. J.&Várhegyi, G. (1999). *A Round-Robin Study of Cellulose Pyrolysis Kinetics by Thermogravimetry*. Industrial & Engineering Chemistry Research, 38(6), 2238-2244.

Grønli, M. G.&Melaaen, M. C. (2000). *Mathematical Model for Wood PyrolysisComparison of Experimental Measurements with Model Predictions*. Energy & Fuels, 14(4), 791-800.

Grønli, M. G., Várhegyi, G.&Di Blasi, C. (2002). *Thermogravimetric Analysis and Devolatilization Kinetics of Wood*. Industrial & Engineering Chemistry Research, 41(17), 4201-4208.

Gunn, D. J. (1978). *Transfer of heat or mass to particles in fixed and fluidised beds*. International Journal of Heat and Mass Transfer, 21(4), 467-476.

Hagge, M. J.&Bryden, K. M. (2002). *Modeling the impact of shrinkage on the pyrolysis of dry biomass*. Chemical Engineering Science, 57(14), 2811-2823.

Heidenreich, C. A., Yan, H. M.&Zhang, D. K. (1999a). *Mathematical modelling of pyrolysis of large coal particles—estimation of kinetic parameters for methane evolution*. Fuel, 78(5), 557-566.

Heidenreich, C. A., Yan, H. M.&Zhang, D. K. (1999b). *Mathematical Modelling of Temperature Response of Low-rank Coal Particles During Pyrolysis*. Developments in Chemical Engineering and Mineral Processing, 7(5-6), 593-610.

Hoomans, B. P. B., Kuipers, J. A. M., Briels, W. J.&van Swaaij, W. P. M. (1996). *Discrete particle simulation of bubble and slug formation in a two-dimensional gas-fluidised bed: A hard-sphere approach*. Chemical Engineering Science, 51(1), 99-118.

http://blogs.princeton.edu./chm333/f2006/biomass/bio_oil/02_chemistryprocessing_the_basics/02_processing/.

http://www.csudh.edu. /oliver/chemdata/woods.htm.

Huilin, L., Yunhua, Z., Ding, J., Gidaspow, D.&Wei, L. (2007). *Investigation of mixing/segregation of mixture particles in gas-solid fluidized beds*. Chemical Engineering Science, 62(1-2), 301-317.

Huilin, L., Yurong, H.&Gidaspow, D. (2003a). *Hydrodynamic modelling of binary mixture in a gas bubbling fluidized bed using the kinetic theory of granular flow*. Chemical Engineering Science, 58(7), 1197-1205.

Huilin, L., Yurong, H., Gidaspow, D., Lidan, Y.&Yukun, Q. (2003b). *Size segregation of binary mixture of solids in bubbling fluidized beds*. Powder Technology, 134(1-2), 86-97.

Hulme, I., Clavelle, E., van der Lee, L.&Kantzas, A. (2005). *CFD Modeling and Validation of Bubble Properties for a Bubbling Fluidized Bed*. Industrial & Engineering Chemistry Research, 44(12), 4254-4266.

Iddir, H.&Arastoopour, H. (2005). *Modeling of multitype particle flow using the kinetic theory approach*. AIChE Journal, 51(6), 1620-1632.

Jand, N.&Foscolo, P. U. (2005). *Decomposition of wood particles in fluidized beds*. Industrial and Engineering Chemistry Research, 44(14), 5079-5089.

Janse, A. M. C., Westerhout, R. W. J.&Prins, W. (2000). *Modelling of flash pyrolysis of a single wood particle*. Chemical Engineering and Processing, 39(3), 239-252.

Jin, G. (2013). *Multiscale Coupling Framework for Modeling of Large-Size Biomass Particle Gasification in Fluidized Beds*. Industrial & Engineering Chemistry Research.

Johnson, P. C.&Jackson, R. (1987). *Frictional–collisional constitutive relations for granular materials, with application to plane shearing*. Journal of Fluid Mechanics, 176 67-93.

Jones, J. M., Pourkashanian, M., Williams, A.&Hainsworth, D. (2000). *A comprehensive biomass combustion model*. Renewable Energy, 19(1–2), 229-234.

Joseph, D. D., Nield, D. A.&Papanicolaou, G. (1982). *Nonlinear equation governing flow in a saturated porous medium*. Water Resour. Res., 18(4), 1049-1052.

Kafui, K. D., Thornton, C.&Adams, M. J. (2002). *Discrete particle-continuum fluid modelling of gas-solid fluidised beds*. Chemical Engineering Science, 57(13), 2395-2410.

Kansa, E. J., Perlee, H. E.&Chaiken, R. F. (1977). *Mathematical model of wood pyrolysis including internal forced convection*. Combustion and Flame, 29 311-324.

Kanury, A. M.&Blackshear, P. L. (1970). *On the Combustion of Wood II: The Influence of Internal Convection on the Transient Pyrolysis of Cellulose*. Combustion Science and Technology, 2(1), 5 - 9.

Kaushal, P.&Abedi, J. (2010). *A simplified model for biomass pyrolysis in a fluidized bed reactor*. Journal of Industrial and Engineering Chemistry, 16(5), 748-755.

Kersten, S. R. A., Wang, X., Prins, W.&van Swaaij, W. P. M. (2005). *Biomass Pyrolysis in a Fluidized Bed Reactor. Part 1: Literature Review and Model Simulations*. Industrial & Engineering Chemistry Research, 44(23), 8773-8785.

Klose, W.&Wiest, W. (1999). *Experiments and mathematical modeling of maize pyrolysis in a rotary kiln*. Fuel, 78(1), 65-72.

Koufopanos, C. A., Lucchesi, A.&Maschio, G. (1989). *Kinetic modelling of the pyrolysis of biomass and biomass components*. The Canadian Journal of Chemical Engineering, 67(1), 75-84.

Koufopanos, C. A., Papayannakos, N., Maschio, G.&Lucchesi, A. (1991). *Modelling of the pyrolysis of biomass particles. Studies on kinetics, thermal and heat transfer effects*. The Canadian Journal of Chemical Engineering, 69(4), 907-915.

Kung, H.-C. (1972). *A mathematical model of wood pyrolysis*. Combustion and Flame, 18(2), 185-195.

Kunii, D.&Levenspiel, O. (1991). Fluidization Engineering. Massachusetts, Butterworth-Heinemann.

Lathouwers, D.&Bellan, J. (2001a). *Modeling of dense gas-solid reactive mixtures applied to biomass pyrolysis in a fluidized bed*. International Journal of Multiphase Flow, 27(12), 2155-2187.

Lathouwers, D.&Bellan, J. (2001b). *Yield Optimization and Scaling of Fluidized Beds for Tar Production from Biomass*. Energy & Fuels, 15(5), 1247-1262.

Leaper, M. C., Seville, J. P. K., Hilal, N., Kingman, S. W.&Burbidge, A. S. (2004). *Investigating the dynamics of segregation of high jetsam binary batch fluidised bed systems*. Chemical Engineering and Processing: Process Intensification, 43(2), 187-192.

Lehmann, J., Gaunt, J.&Rondon, M. (2006). *Bio-char Sequestration in Terrestrial Ecosystems – A Review*. Mitigation and Adaptation Strategies for Global Change, 11(2), 395-419.

Liden, A., Berruti, F.&Scott, D. S. (1988). *A kinetic model for the production of liquids from the flash pyrolysis of biomass*. Chemical Engineering Communications, 65(1), 207-221.

Lin, Y.-C., Cho, J., Tompsett, G. A., Westmoreland, P. R.&Huber, G. W. (2009). *Kinetics and Mechanism of Cellulose Pyrolysis*. The Journal of Physical Chemistry C, 113(46), 20097-20107.

Lu, C., Song, W.&Lin, W. (2009). *Kinetics of biomass catalytic pyrolysis*. Biotechnology Advances, 27(5), 583-587.

Lu, H., Ip, E., Scott, J., Foster, P., Vickers, M.&Baxter, L. L. (2010). *Effects of particle shape and size on devolatilization of biomass particle*. Fuel, 89(5), 1156-1168.

Lun, C. K. K., Savage, S. B., Jeffrey, D. J.&Chepurniy, N. (1984). *Kinetic theories for granular flow: inelastic particles in Couette flow and slightly inelastic particles in a general flow field*. Journal of Fluid Mechanics, 140 223-256.

Luo, Z., Wang, S.&Cen, K. (2005). *A model of wood flash pyrolysis in fluidized bed reactor*. Renewable Energy, 30(3), 377-392.

Luo, Z., Wang, S., Liao, Y., Zhou, J., Gu, Y.&Cen, K. (2004). *Research on biomass fast pyrolysis for liquid fuel*. Biomass and Bioenergy, 26(5), 455-462.

Lv, P., Chang, J., Wang, T., Wu, C.&Tsubaki, N. (2004). *A Kinetic Study on Biomass Fast Catalytic Pyrolysis*. Energy & Fuels, 18(6), 1865-1869.

Manyà, J. J., Velo, E.&Puigjaner, L. (2002). *Kinetics of Biomass Pyrolysis: a Reformulated Three-Parallel-Reactions Model*. Industrial & Engineering Chemistry Research, 42(3), 434-441.

Mészáros, E., Várhegyi, G., Jakab, E.&Marosvölgyi, B. (2004). *Thermogravimetric and Reaction Kinetic Analysis of Biomass Samples from an Energy Plantation*. Energy & Fuels, 18(2), 497-507.

Miller, R. S.&Bellan, J. (1997). *A Generalized Biomass Pyrolysis Model Based on Superimposed Cellulose, Hemicelluloseand Liqnin Kinetics*. Combustion Science and Technology, 126(1), 97 - 137.

Moghtaderi, B. (2006). *The state-of-the-art in pyrolysis modelling of lignocellulosic solid fuels*. Fire and Materials, 30(1), 1-34.

Mok, W. S. L.&Antal, M. J. (1983). *Effects of pressure on biomass pyrolysis. II. Heats of reaction of cellulose pyrolysis*. Thermochimica Acta, 68(2-3), 165-186.

Morf, P., Hasler, P.&Nussbaumer, T. (2002). *Mechanisms and kinetics of homogeneous secondary reactions of tar from continuous pyrolysis of wood chips*. Fuel, 81(7), 843-853.

Morf, P. O. (2001). Secondary Reactions of Tar During Thermochemical Biomass Conversion.

Nik-Azar, M., Hajaligol, M. R., Sohrabi, M.&Dabir, B. (1997). *Mineral matter effects in rapid pyrolysis of beech wood*. Fuel Processing Technology, 51(1-2), 7-17.

Niksa, S. (2000). *Predicting the rapid devolatilization of diverse forms of biomass with bio-flashchain*. Proceedings of the Combustion Institute, 28(2), 2727-2733.

Nunn, T. R., Howard, J. B., Longwell, J. P.&Peters, W. A. (1985). *Product compositions and kinetics in the rapid pyrolysis of sweet gum hardwood*. Industrial & Engineering Chemistry Process Design and Development, 24(3), 836-844.

Oevermann, M., Gerber, S.&Behrendt, F. (2009). *Euler-Lagrange/DEM simulation of wood gasification in a bubbling fluidized bed reactor*. Particuology, 7(4), 307-316.

Orfão, J. J. M., Antunes, F. J. A.&Figueiredo, J. L. (1999). *Pyrolysis kinetics of lignocellulosic materials—three independent reactions model*. Fuel, 78(3), 349-358.

Pain, C. C., Mansoorzadeh, S., Gomes, J. L. M.&de Oliveira, C. R. E. (2002). *A numerical investigation of bubbling gas-solid fluidized bed dynamics in 2-D geometries*. Powder Technology, 128(1), 56-77.

Papadikis, K., Bridgwater, A. V.&Gu, S. (2008). *CFD modelling of the fast pyrolysis of biomass in fluidised bed reactors, Part A: Eulerian computation of momentum transport in bubbling fluidised beds*. Chemical Engineering Science, 63(16), 4218-4227.

Papadikis, K., Gu, S.&Bridgwater, A. V. (2009a). *CFD modelling of the fast pyrolysis of biomass in fluidised bed reactors. Part B: Heat, momentum and mass transport in bubbling fluidised beds*. Chemical Engineering Science, 64(5), 1036-1045.

Papadikis, K., Gu, S.&Bridgwater, A. V. (2009b). *CFD modelling of the fast pyrolysis of biomass in fluidised bed reactors: Modelling the impact of biomass shrinkage*. Chemical Engineering Journal, 149(1-3), 417-427.

Papadikis, K., Gu, S.&Bridgwater, A. V. (2010a). *Computational modelling of the impact of particle size to the heat transfer coefficient between biomass particles and a fluidised bed*. Fuel Processing Technology, 91(1), 68-79.

Papadikis, K., Gu, S., Bridgwater, A. V.&Gerhauser, H. (2009c). *Application of CFD to model fast pyrolysis of biomass*. Fuel Processing Technology, 90(4), 504-512.

Papadikis, K., Gu, S., Fivga, A.&Bridgwater, A. V. (2010b). *Numerical Comparison of the Drag Models of Granular Flows Applied to the Fast Pyrolysis of Biomass*. Energy & Fuels, 24(3), 2133-2145.

Park, W. C., Atreya, A.&Baum, H. R. (2010). *Experimental and theoretical investigation of heat and mass transfer processes during wood pyrolysis*. Combustion and Flame, 157(3), 481-494.

Patil, D. J., van Sint Annaland, M.&Kuipers, J. A. M. (2005). *Critical comparison of hydrodynamic models for gas-solid fluidized beds--Part II: freely bubbling gas-solid fluidized beds*. Chemical Engineering Science, 60(1), 73-84.

Peters, B. (2011). *Validation of a numerical approach to model pyrolysis of biomass and assessment of kinetic data*. Fuel, 90(6), 2301-2314.

Pyle, D. L.&Zaror, C. A. (1984). *Heat transfer and kinetics in the low temperature pyrolysis of solids*. Chemical Engineering Science, 39(1), 147-158.

Qiaoqun, S., Huilin, L., Wentie, L., Yurong, H., Lidan, Y.&Gidaspow, D. (2005). *Simulation and experiment of segregating/mixing of rice husk-sand mixture in a bubbling fluidized bed*. Fuel, 84(14-15), 1739-1748.

Radmanesh, R., Courbariaux, Y., Chaouki, J.&Guy, C. (2006). *A unified lumped approach in kinetic modeling of biomass pyrolysis*. Fuel, 85(9), 1211-1220.

Ranade, V. V. (2002). Computational Flow Modeling for Chemical Reactor Engineering. Process Systems Engineering, Academic Press. Volume 5: 1-452.

Ranzi, E., Cuoci, A., Faravelli, T., Frassoldati, A., Migliavacca, G., Pierucci, S.&Sommariva, S. (2008). *Chemical Kinetics of Biomass Pyrolysis*. Energy & Fuels, 22(6), 4292-4300.

Rao, T. R.&Bheemarasetti, J. V. R. (2001). *Minimum fluidization velocities of mixtures of biomass and sands*. Energy, 26(6), 633-644.

Rath, J.&Staudinger, G. (2001). *Cracking reactions of tar from pyrolysis of spruce wood*. Fuel, 80(10), 1379-1389.

Raveendran, K., Ganesh, A.&Khilar, K. C. (1995). *Influence of mineral matter on biomass pyrolysis characteristics*. Fuel, 74(12), 1812-1822.

Roberts, A. F. (1971). *The heat of reaction during the pyrolysis of wood*. Combustion and Flame, 17(1), 79-86.

Rostami, A. A., Hajaligol, M. R.&Wrenn, S. E. (2004). *A biomass pyrolysis sub-model for CFD applications*. Fuel, 83(11-12), 1519-1525.

Ruiz, J. A., Juárez, M. C., Morales, M. P., Muñoz, P.&Mendívil, M. A. (2013). *Biomass gasification for electricity generation: Review of current technology barriers*. Renewable and Sustainable Energy Reviews, 18(0), 174-183.

Saastamoinen, J. J. (2006). *Simplified model for calculation of devolatilization in fluidized beds*. Fuel, 85(17-18), 2388-2395.

Sadhukhan, A. K., Gupta, P.&Saha, R. K. (2008). *Modelling and experimental studies on pyrolysis of biomass particles*. Journal of Analytical and Applied Pyrolysis, 81(2), 183-192.

Samolada, M. C.&Vasalos, I. A. (1991). *A kinetic approach to the flash pyrolysis of biomass in a fluidized bed reactor*. Fuel, 70(7), 883-889.

Saxena, R. C., Adhikari, D. K.&Goyal, H. B. (2009). *Biomass-based energy fuel through biochemical routes: A review*. Renewable and Sustainable Energy Reviews, 13(1), 167-178.

Scott, D. S., Majerski, P., Piskorz, J.&Radlein, D. (1999). *A second look at fast pyrolysis of biomass--the RTI process*. Journal of Analytical and Applied Pyrolysis, 51(1-2), 23-37.

Scott, D. S., Piskorz, J., Bergougnou, M. A., Graham, R.&Overend, R. P. (1988). *The role of temperature in the fast pyrolysis of cellulose and wood*. Industrial & Engineering Chemistry Research, 27(1), 8-15.

Shafizadeh, F.&Chin Peter P, S. (1977). Thermal Deterioration of Wood. Wood Technology: Chemical Aspects, AMERICAN CHEMICAL SOCIETY. 43: 57-81.

Shen, L.&Zhang, D.-K. (2003). *An experimental study of oil recovery from sewage sludge by low-temperature pyrolysis in a fluidised-bed*. Fuel, 82(4), 465-472.

Shen, L.&Zhang, D. K. (2001). *A CPD Modelling Study of Sewage Sludge Devolatilisation For Oil Production*. Proceedings of the 3rd Asia-Pacific Conference on Combustion, Seoul, Korea 437-440.

Shen, L.&Zhang, D. K. (2005). *Low-temperature pyrolysis of sewage sludge and putrescible garbage for fuel oil production*. Fuel, 84(7-8), 809-815.

Shen, L., Zhang, D. K., Yan, H. M., Roach, J. R.&Nguyen, Q. D. (2000). *Low Temperature Pyrolysis of an Australian Brown Coal in a Fluidised Bed Reactor*. Developments in Chemical Engineering and Mineral Processing, 8(3-4), 293-309.

Sheng, C.&Azevedo, J. L. T. (2002). *Modeling biomass devolatilization using the chemical percolation devolatilization model for the main components*. Proceedings of the Combustion Institute, 29(1), 407-414.

Sinclair, J. L.&Jackson, R. (1989). *Gas-particle flow in a vertical pipe with particle-particle interactions*. AIChE Journal, 35(9), 1473-1486.

Sonobe, T.&Worasuwannarak, N. (2008). *Kinetic analyses of biomass pyrolysis using the distributed activation energy model*. Fuel, 87(3), 414-421.

Sreekanth, M.&Kolar, A. K. (2009). *Progress of conversion in a shrinking wet cylindrical wood particle pyrolyzing in a hot fluidized bed*. Journal of Analytical and Applied Pyrolysis, 84(1), 53-67.

Srivastava, V. K., Sushil&Jalan, R. K. (1996). *Prediction of concentration in the pyrolysis of biomass material--II*. Energy Conversion and Management, 37(4), 473-483.

Sun, Z. Q., Wu, J., Haghighi, M.&Zhang, D. K. (2007). *Methane Cracking over a Bituminous Coal Char*. Energy and Fuels, 21(3), 1601 – 1605.

Syamlal, M. (1987). The particle–particle drag term in a multiparticle model of fludization, Topical Report.

Syamlal, M., Rogers, W.&O`Brien, T. J. (1993). MFIX documentation theory guide. Other Information: PBD: Dec 1993: Medium: ED; Size: 49 p.

Thurner, F.&Mann, U. (1981). *Kinetic investigation of wood pyrolysis*. Industrial & Engineering Chemistry Process Design and Development, 20(3), 482-488.

Toor, S. S., Rosendahl, L.&Rudolf, A. (2011). *Hydrothermal liquefaction of biomass: A review of subcritical water technologies*. Energy, 36(5), 2328-2342.

Tsuji, Y., Kawaguchi, T.&Tanaka, T. (1993). *Discrete particle simulation of two-dimensional fluidized bed*. Powder Technology, 77(1), 79-87.

van der Hoef, M. A., Annaland, M. V., Deen, N. G.&Kuipers, J. A. M. (2008). *Numerical simulation of dense gas-solid fluidized beds: A multiscale modeling strategy*. Annual Review of Fluid Mechanics, 40 47-70.

van Sint Annaland, M., Bokkers, G. A., Goldschmidt, M. J. V., Olaofe, O. O., van der Hoef, M. A.&Kuipers, J. A. M. (2009a). *Development of a multi-fluid model for poly-disperse dense gas-solid fluidised beds, Part I: Model derivation and numerical implementation*. Chemical Engineering Science, 64(20), 4222-4236.

van Sint Annaland, M., Bokkers, G. A., Goldschmidt, M. J. V., Olaofe, O. O., van der Hoef, M. A.&Kuipers, J. A. M. (2009b). *Development of a multi-fluid model for poly-disperse dense gas-solid fluidised beds, Part II: Segregation in binary particle mixtures*. Chemical Engineering Science, 64(20), 4237-4246.

van Wachem, B. G. M., Schouten, J. C., van den Bleek, C. M., Krishna, R.&Sinclair, J. L. (2001). *Comparative analysis of CFD models of dense gas–solid systems*. AIChE Journal, 47(5), 1035-1051.

Várhegyi, G. b., Bobály, B. z., Jakab, E.&Chen, H. (2010). *Thermogravimetric Study of Biomass Pyrolysis Kinetics. A Distributed Activation Energy Model with Prediction Tests*. Energy & Fuels, 25(1), 24-32.

Wagenaar, B. M., Prins, W.&van Swaaij, W. P. M. (1994). *Pyrolysis of biomass in the rotating cone reactor: modelling and experimental justification*. Chemical Engineering Science, 49(24, Part 2), 5109-5126.

Wang, X., Kersten, S. R. A., Prins, W.&van Swaaij, W. P. M. (2005). *Biomass Pyrolysis in a Fluidized Bed Reactor. Part 2: Experimental Validation of Model Results*. Industrial & Engineering Chemistry Research, 44(23), 8786-8795.

Williams, P. T.&Nugranad, N. (2000). *Comparison of products from the pyrolysis and catalytic pyrolysis of rice husks*. Energy, 25(6), 493-513.

Wu, J., Fang, Y., Wang, Y.&Zhang, D. K. (2005). *Combined coal gasification and methane reforming for production of syngas in a fluidised-bed reactor*. Energy and Fuels, 19 512-516.

Wu, Y., Zhang, Q., Yang, W.&Blasiak, W. (2013). *Two-Dimensional Computational Fluid Dynamics Simulation of Biomass Gasification in a Downdraft Fixed-Bed Gasifier with Highly Preheated Air and Steam*. Energy & Fuels, 27(6), 3274-3282.

Xue, Q., Dalluge, D., Heindel, T. J., Fox, R. O.&Brown, R. C. (2012). *Experimental validation and CFD modeling study of biomass fast pyrolysis in fluidized-bed reactors*. Fuel, 97(0), 757-769.

Xue, Q., Heindel, T. J.&Fox, R. O. (2011). *A CFD model for biomass fast pyrolysis in fluidized-bed reactors*. Chemical Engineering Science, 66(11), 2440-2452.

Yaman, S. (2004). *Pyrolysis of biomass to produce fuels and chemical feedstocks*. Energy Conversion and Management, 45(5), 651-671.

Yan, H.-m.&Lai, T.-p. (2006). *CFD Modeling of Biomass Combustion in Palm Oil Waste Boiler*. Developments in Chemical Engineering and Mineral Processing, 14(1-2), 259-276.

Yang, H., Yan, R., Chen, H., Lee, D. H.&Zheng, C. (2007a). *Characteristics of hemicellulose, cellulose and lignin pyrolysis*. Fuel, 86(12–13), 1781-1788.

Yang, Y. B., Phan, A. N., Ryu, C., Sharifi, V.&Swithenbank, J. (2007b). *Mathematical modelling of slow pyrolysis of segregated solid wastes in a packed-bed pyrolyser*. Fuel, 86(1-2), 169-180.

Yip, K., Wu, H.&Zhang, D.-k. (2007). *Effect of Inherent Moisture in Collie Coal during Pyrolysis Due to in-Situ Steam Gasification*. Energy & Fuels, 21(5), 2883-2891.

Yuen, R. K. K., Yeoh, G. H., de Vahl Davis, G.&Leonardi, E. (2007). *Modelling the pyrolysis of wet wood – I. Three-dimensional formulation and analysis*. International Journal of Heat and Mass Transfer, 50(21–22), 4371-4386.

Zabaniotou, A. A. (1999). *Pyrolysis of Forestry Biomass By-Products in Greece*. Energy Sources, Part A: Recovery, Utilization, and Environmental Effects, 21(5), 395 - 403.

Zhang, H., Xiao, R., Huang, H.&Xiao, G. (2009a). *Comparison of non-catalytic and catalytic fast pyrolysis of corncob in a fluidized bed reactor*. Bioresource Technology, 100(3), 1428-1434.

Zhang, H., Xiao, R., Wang, D., Zhong, Z., Song, M., Pan, Q.&He, G. (2009b). *Catalytic Fast Pyrolysis of Biomass in a Fluidized Bed with Fresh and Spent*

*Fluidized Catalytic Cracking (FCC) Catalysts*. Energy & Fuels, 23(12), 6199-6206.

Zhang, L., Xu, C.&Champagne, P. (2010). *Overview of recent advances in thermo-chemical conversion of biomass*. Energy Conversion and Management, 51(5), 969-982.

Zhang, Q., Chang, J., Wang, T.&Xu, Y. (2007). *Review of biomass pyrolysis oil properties and upgrading research*. Energy Conversion and Management, 48(1), 87-92.

Zhang, Y., Jin, B.&Zhong, W. (2009c). *Experimental investigation on mixing and segregation behavior of biomass particle in fluidized bed*. Chemical Engineering and Processing: Process Intensification, 48(3), 745-754.

Zhang, Y., Wu, J.-h.&Zhang, D. K. (2008a). *Cracking of Simulated Oil Refinery Off-Gas over a Coal Char, Petroleum Coke, and Quartz*. Energy & Fuels, 22(2), 1142-1147.

Zhang, Y., Wu, J.&Zhang, D. K. (2008b). *Ethane Cracking in Coal Char Bed and Quartz Sand Bed*. Petrochemical Technology 37(8), 770-775.

Zhong, H., Gao, J., Xu, C.&Lan, X. (2012). *CFD modeling the hydrodynamics of binary particle mixtures in bubbling fluidized beds: Effect of wall boundary condition*. Powder Technology, 230(0), 232-240.

Zhong, W., Jin, B., Zhang, Y., Wang, X.&Xiao, R. (2008). *Fluidization of Biomass Particles in a Gas−Solid Fluidized Bed*. Energy & Fuels, 22(6), 4170-4176.